Mechanisms of Epileptogenesis in a Mouse Model of Temporal Lobe Epilepsy

Dissertation

zur
Erlangung der naturwissenschaftlichen Doktorwürde
(Dr. sc. nat.)
vorgelegt der
Mathematisch-naturwissenschaftlichen Fakultät
der
Universität Zürich

von

Tilo Aurelio Gschwind

von

Grenchen, SO

Promotionskomitee:
Prof. Dr. Jean-Marc Fritschy (Vorsitz)
PD Dr. Irene Knuesel
Prof. Dr. Burkhard Becher
Prof. Dr. Hennric Jokeit

Zürich, 2017

ACKNOWLEDGEMENTS

During the course of my dissertation, I had the great fortune to be surrounded and supported by so many great supervisors, colleagues, friends and my family.

I would like to sincerely thank Prof. Dr. Jean-Marc Fritschy. He gave me the opportunity to perform my PhD thesis in his lab, be engaged in various projects and he supported me on various levels. Jean-Marc, despite your tremendous engagement in many different areas – as supervisor of many students, lecturer, EJN editor, vice dean of the medical faculty and many other things– you always found the time to support me with your excellent knowledge and expertise. Your advice and questions not only guided me through my thesis, but also shaped my way of approaching scientific problems. Your supervision granted me the scientific freedom to pursue many scientific questions, including establishing a collaboration with Prof. Ivan Soltesz. I am especially thankful for your support during the last part of my thesis. Being supportive and helpful allowed me to continue pursuing my goal of having a future in science despite those difficult times. The way of how you approach science, lead a group and supervise students is inspiring and I am grateful to have learned from you, worked with you and to be part of your group. Thank you.

I also like to thank PD. Dr. Irene Knuesel, who I first approached for a PhD position and who offered the position to work on the project linking Alzheimer's disease and epilepsy. I greatly enjoyed working with you and being a member of your group was a great experience. We had great discussions and your scientific input was always crucial, in particular from the Alzheimer field.

I would further like to express my gratitude to the other members of my thesis committee, Prof. Dr. Burkhard Becher and Prof. Dr. Hennric Jokeit for their guidance, scientific inputs and discussions about my project.

I would like to thank Prof. Dr. Ivan Soltesz. He welcomed me in his lab at Stanford and gave me the opportunity to work on different interesting projects. His support and scientific input not only heavily influenced the success of the project, but also opened my eyes for technical possibilities and conceptual frameworks beyond anything I had experienced so far.

I would like to thank Prof. Dr. Urs Meyer. His support and scientific input helped me with my project in the field of prenatal developmental models. In addition, providing me the opportunity to contribute to two papers helped me to progress in my scientific career.

At this point, I would like to thank our technicians Cornelia Schwerdel and Tatjana Haenggi for their help with processing large batches of IHC stainings and the genotyping of the transgenic

mice. Christina Koester and Giovanna Bosshard, I like to thank for their technical support and knowledge. Special thanks go to Romy Gisler for all her effort managing the administrative part of my stay in Stanford. I owe my profound gratitude to all the animal care takers, particularly Carmen Brazerol, Ana Hemmersbach and Dennis Boadum who did an excellent work in taking care of all the different mouse lines I used over time. Big thanks go to Nicole Wildner for her incredible organization skills, and for showing me how to organize and plan the breeding of my mouse lines for my experiments.

Very special and warm thanks go to Mariana Zaichuk (aka PhD bro) and Tina Notter, with whom I worked since the beginning of my PhD, and shared many projects and interests. Beyond the scientific input, your general support and our discussions were always of great value to me. Francine Deprez, Sandra Pfister, Claire de Groot, and Simon Früh - it was the greatest pleasure to work with all of you; it was a lot of fun! I hereby would like to thank the current members of the group(s): Kasifa Khalid, Yuan-Chen Tsai, and Lena Rubi – not only for joining the lunch group but also for all the discussions we had during and beyond lunch time. Special thanks go to Tim Gfeller, who did an incredible job during his masters. I am very grateful to have worked with you on the AD project. I also would like to thank Dr. Carlos Lafourcade and Dr. Lukas Rambousek, with whom I was not only working on various projects but also had some great time outside the lab.

I would like to thank all other people who helped me with the different projects. Roland Dürr, Harald Osswald and Stefan Weber, I would like to thank in particular for all their help setting up the video-EEG system. I would also like to thank Dr. Helge Johannssen for his help with the calcium imaging.

I would like to thank my past and present colleagues from the “Fritschy group” and also the members of the “Zeilhofer group” and “Weber group” for the unforgettable and inspiring time. I would have never been able to finish my dissertation without having such wonderful and helpful people around me.

Finally, I am deeply thankful to my mother Liliane, Christina and Heinrich for their support, encouragement and understanding over the years – without you it would not have been possible. Thank you!

TABLE OF CONTENTS

ZUSAMMENFASSUNG

Temporallappen Epilepsie (TLE) gehört zu den häufigsten Epilepsieformen und spricht oft nicht auf Pharmakotherapie an, insbesondere wenn TLE mit hippocampaler Sklerose (HS) assoziiert ist. TLE ist charakterisiert durch spontane rezidivierende Anfälle (SRS, Englisch: spontaous recurrent seizures), die im medialen Temporallappen ihren Ursprung nehmen. Solche Anfälle treten infolge einer initialen Hirnverletzung nach einer gewissen Latenzphase auf. Eine unilaterale Injektion von Kainate (KA) in den dorsalen Hippocampus einer ausgewachsenen Maus führt zu vielen Veränderungen, vergleichbar zu jenen, die dem Krankheitsbild von TLE zugeschrieben werden. Die intrahippocampale Kainate (IHK) Injektion löst einen Status epilepticus (SE) aus, der nach einer Latenzphase zur Entstehung von SRS führt. Ferner, kommt es nach dem IHK-induzierten SE zu einem progressiven Verlust von spezifischen Zellgruppen im Hippocampus, einer axonalen Reorganisation und der Dispersion von Körnerzellen im Gyrus Dentatus. Obwohl dieses TLE Modell histologisch und funktionell sehr gut charakterisiert ist, herrscht nach wie vor Unklarheit, welcher dieser vielen Veränderungen schlussendlich zur Epileptogenese beiträgt. Aus diesem Grund haben wir in der vorliegenden Studie den Einfluss der neuronalen Entzündung und früher epileptischer Aktivität während der Latenzphase auf die Epileptogenese in TLE untersucht. Ferner haben wir untersucht, wie sich frühe pathologische Veränderungen, die mit der Alzheimer Krankheit (AD, Englisch: Alzheimer's disease) einhergehen, auf die Entwicklung von Epilepsie im Kainate Model von TLE auswirken.

In der ersten Studie haben wir verschiedene Komponenten des Immunsystems untersucht, die mit der Epilepsie assoziiert sind und potentiell für die Entstehung eines epileptischen Fokus verantwortlich sind. Als erstes haben wir evaluiert, welchen Effekt eine chronische Störung des angeborenen Immunsystems, durch ein sogenanntes „priming", auf Epileptogenese und das Auftreten von SRS hat. Zu diesem Zweck haben wir Mäuse pränatal und/oder postnatal systemisch mit dem viralen Imitator PolyI:C injiziert, der das Immunsystem „primen" soll. Obwohl wir keinen Effekt nach vorausgeganger, systemischer Infizierung auf die Entwicklung der später induzierten Epilepsie beobachten konnten, sind die Resultate nicht eindeutig, insbesondere im Hinblick auf die Tatsache, dass es an einem unabhängigen Beleg gefehlt hat, der darauf hingewiesen hätte, dass das „primen" des Immune Systems funktioniert hat. Als nächstes haben wir intrazelluläre Sensoren untersucht, sogenannte Inflammasome, die in Mikroglia und Makrophagen die Produktion von Interleukin (IL)-1β verantwortlich ist. Wir haben evaluiert, welchen Auswirkungen das Fehlen von NLRP3 Inflammasome in Knockout Mäusen auf das

neurodegenerative Muster und die damit assoziierte Immunantwort hat während der Kainate-induzierten Epileptogenese. Da wir keine Unterschiede feststellen konnten zu Kontrollmäusen, gehen wir davon aus, dass die Produktion von IL-1β und das mit der Entzündung einhergehende Zellsterben im Kainate Model von TLE unabhängig von NLRP3 Inflammasomen sind. Schliesslich haben wir basierend auf den Schlussfolgerungen einer früheren Studie genauer untersucht, welche Rolle infiltrierende, periphere monozytische Phagozyten für das Überleben von Körnerzellen haben. Das Fehlen von C-C Chemokinen Rezeptor Typ 2 (CCR2) in Knockout Mäusen hatte jedoch keine Auswirkung auf das Überleben der Körnerzellen während der Kainate-induzierten Epileptogenese.

Bereits in einem frühen Krankheitsstadium weisen Patienten und Tiermodelle mit AD eine Dysfunktion des neuralen Netzwerkes und anomale epileptische Aktivität auf. Aus diesem Grund haben wir in der zweiten Studie untersucht, ob frühe Veränderungen, die mit AD assoziiert sind, das hippocampale Netzwerk empfänglich macht für die Entstehung von erworbener Epilepsie. Wir konnten nachweisen, dass unser AD Maus Modell noch vor dem Auftreten der für die AD charakteristischen amyloiden Plaque Ablagerungen eine erhöhte Anfälligkeit auf den SE und eine verfrühtes Auftreten von SRS zeigen. Elektrophysiologische Experimente in CA1 hippocampalen Neuronen haben erwiesen, dass diese drei Monate alten ArcticAβ Mäuse eine reduzierte synaptische Erregbarkeit, eine erhöhte KA-induzierte Langzeit Potenzierung (LTP, Englisch: long-term potentiation) und reduzierte Frequenz von spontanen inhibitorischen Strömen besitzen. Das neurodegenerative Muster, die Entzündungsreaktion, die axonale Reorganisation oder die adulte Neurogenese hat sich nach der IHK-induzierten Epileptogenese zwischen ArcticAβ und Kontrollmäusen nicht unterschieden. Im Gegensatz dazu, wurde jedoch eine Abschwächung der SE-assoziierten Erhöhung von Neuropeptide Y (NPY) in Moosfasern und Körnerzellen im AD Model beobachtet. Obwohl eine Beeinträchtigung in der NPY Signalkaskade direkte zum verfrühten Auftreten von SRS beitragen könnte, konnte der übererregbare Phänotyp und die verfrüht auftretenden SRS unterbunden werden, wenn vor der IHK-induzierten Epileptogenese die löslichen Aβ Spezimen in ArcticAβ Mäusen mit Hilfe eines intrazerebral applizierten anti-Aβ spezifischen Antikörpers entfernt wurden.

Schliesslich haben wir in der dritten Studie untersucht, welche Rolle der frühen epileptiformen Aktivität während der Latenzphase zukommt und wie diese den Entwicklung von SRS beeinflusst. Zusammen mit diesen kurzen epileptischen Entladungen treten viele andere Veränderungen während der Latenzphase auf, wie zum Beispiel das Zellsterben oder die Schaffung von zurückprojizierenden, erregenden Kreisläufen. Eine optogenetische Intervention

im geschlossenen Kreislauf (COI, Englisch: closed-loop optogenetic intervention) während der zwei Wochen langen Anfallsfreien Latenzzeit wurde verwendet, um herauszufinden ob diese frühe epileptische Aktivität die der Epileptogenese zugrunde liegende Netzwerk Reorganisation begünstigt. Wir haben erfolgreich einen Algorithmus entwickelt, der es ermöglicht schnell (innerhalb von weniger als 40ms) online kurze epileptische Aktivität zu detektieren. Unsere vorläufigen Daten zeigen eine Reduktion in der SRS Frequenz vier Monate nachdem während der IHK-induzierte Epileptogenese mit Hilfe von COI anomale Aktivität inhibiert wurde.

Unsere Resultate weisen darauf hin, dass frühe epileptiforme Aktivität während der Latenzphase mit hoher Wahrscheinlichkeit direkt die Entstehung von SRS beeinflusst. Ferner ist während der Latenzphase die Entzündungsreaktion als Antwort auf die Neurodegeneration und insbesondere das angeborene Immunsystem involviert in die Netzwerkreorganisation und Bildung eines epileptischen Fokus im IHK Model von TLE. Jedoch sollte die Aktivierung des angeborenen Immunsystems als ein Teil einer breiteren Immunantwort verstanden werden, in welcher bestimmte Prozesse höchstwahrscheinlich von anderen Immunzellen kompensiert werden können ohne dabei den Verlauf der Epileptogenes zu beeinflussen. In einem AD Mausmodell konnten wir das Auftreten von SRS während der Latenzphase auf das Vorhandensein von löslichen Aβ Spezimen zurückführen, die sehr wahrscheinlich die synaptische Funktion beeinflussen. Obwohl wir zeigen konnten, dass die Anfallspathologie durch eine Intervention während der Latenzphase beeinflusst werden kann, deuten diese Resultate darauf hin, dass das Netzwerk bereits früh nach dem SE sich so verändert hat um die Entstehung von SRS zu ermöglichen.

ABSTRACT

Temporal lobe epilepsy (TLE) is one of the most common form of adult seizure disorders, and when associated with hippocampal sclerosis (HS) often resistant to pharmacotherapy. Electrographically, TLE is defined by the occurrence of spontaneous recurrent seizures (SRS) originating from the medial temporal lobe after latent period following a precipitating brain insult. The unilateral injection of kainic acid (KA) into the dorsal hippocampus in adult mice mirrors many characteristics of TLE and induces a status epilepticus (SE), which is followed by a two-week latent period and subsequently the onset of SRS. Histologically, intrahippocampal kainic acid (IHK) injection causes a progressive loss of specific groups of hippocampal cells, axonal reorganization and dispersion of granule cells (GC) in the dentate gyrus (DG), similar to TLE. Although this model of TLE is well characterized histologically and functionally, it still remains unknown which of these multiple alterations contribute to epileptogenesis. Therefore, we evaluated the contribution of neuroinflammation and early epileptiform activity to epileptogenesis in TLE, as well as the impact of early pathophysiological alterations related to Alzheimer's disease (AD) on the development of epilepsy in the IHK model of TLE.

In the first study, we investigated the role of different components of the epileptogenesis-associated immune reaction to the formation of an epileptic focus. First, we assessed the effect of chronically perturbing innate immunity, 'priming', on epileptogenesis and SRS occurrence by prenatally and/or postnatally exposing mice to the viral mimic PolyI:C. Although no effect of these systemic immune challenges was observed on the development of epilepsy, we lacked independent evidence that the immune system was primed as expected at the time of IHK-induced SE. Therefore, these results remain inconclusive. Second, mice devoid of NLRP3 inflammasomes were examined to determine if these intracellular sensors involved in the interleukin (IL)-1β production of microglia and macrophages affect the pathogenesis of a pro-epileptic lesion. The IHK-induced neurodegenerative pattern and associated immune response was not altered, suggesting that the production of IL-1β and inflammation-associated neurodegeneration are independent of NLRP3 inflammasomes in the IHK model of TLE. Finally, as proposed by an earlier study, we examined whether preventing infiltration of peripheral monocytic phagocytes is essential for GC survival in the DG. Selectively interfering with their recruitment, the absence of infiltrating peripheral phagocytes in C-C chemokine receptor type 2 (CCR2)-KO mice had no effect on the survival of GC during IHK-induced epileptogenesis.

Already at early disease stages, neuronal network dysfunction and aberrant epileptic activity are detected in both patients and animal models of AD. We determined in the second study whether early AD-associated alterations render the hippocampal network more susceptible to development of acquired epilepsy. We found an increased susceptibility to IHK-induced SE and early onset of SRS in an AD mouse model, ArcticAβ mice, characterized by delayed amyloid deposition in the brain. In 3-months-old ArcticAβ mice, prior to plaque formation, electrophysiological recordings in CA1 hippocampal neurons revealed a decreased synaptic strength, increased KA-induced long-term potentiation (LTP), and reduced frequency of spontaneous inhibitory currents. While ArcticAβ mice and wildtype littermates did not differ in the IHK-induced pattern of neurodegeneration, neuroinflammation, axonal reorganization or adult neurogenesis, the elevated expression of neuropeptide Y (NPY) in mossy fibers and GC induced by IHK was attenuated in mutants. While impaired NPY signaling might directly contribute to the early seizure onset, the hyperexcitable phenotype and the SRS pathology early during epileptogenesis in ArcticAβ mice were prevented by clearing soluble Aβ species by an Aβ-specific antibody applied intracerebrally prior to induction of acquired epilepsy.

Finally, the third study examined the role of early epileptiform activity occurring during the latent period for the development of SRS. Together with these brief epileptic discharges, multiple alterations, including neurodegeneration and the formation of new recurrent excitatory circuits, precede the first occurrence of SRS. Closed-loop optogenetic intervention (COI) was used for the first two weeks after IHK injection to curtail brief epileptic discharges and determine whether this early aberrant activity drives epileptogenesis-associated network reorganization. We succeeded to develop an algorithm for fast (<40ms) on line detection of brief discharges. Our preliminary data reveal a reduction in SRS frequency four months after interfering with IHK-induced epileptogenesis by COI.

Our results suggest that early epileptiform activity during the latent period most likely affects the development of SRS directly, while the neurodegeneration-associated immune responses, in particular of the innate immune system, are involved in concomitant network reorganization and the formation of an epileptic focus in the IHK model of TLE. However, as part of a broader immune response, certain processes might be compensated by other immune cells, without affecting epileptogenesis per se. In the AD-mouse model, the early onset of SRS during the latent period is mediated primarily by soluble Aβ specimen, probably by affecting synaptic function. Although seizure pathology can be influenced later on, our findings suggest that alterations occurring early after SE render the network highly susceptible to the generation of SR

I. GENERAL INTRODUCTION

Epilepsy and seizure classification

Epilepsy is a group of chronic neurological disorder with 65 million people being affected worldwide. The International League Against Epilepsy (ILAE) formulated two definitions for seizure and epilepsy. The conceptual definitions were formulated by Fisher et al. (2014):

- "An epileptic seizure is a transient occurrence of signs and/or symptoms due to abnormal excessive or synchronous neuronal activity in the brain."
- "Epilepsy is a disorder of the brain characterized by an enduring predisposition to generate epileptic seizures, and by the neurobiologic, cognitive, psychological, and social consequences of this condition. The definition of epilepsy requires the occurrence of at least one epileptic seizure."

Practical clinical definition of epilepsy, however, demands two unprovoked or reflex seizures, which are more than twenty-four hours apart (Fisher et al., 2014). The classification of seizures is based on different categorize and summarized in the ILAE 2017 seizure classification (Fisher et al., 2017b; Fisher et al., 2017a). Seizures of focal, generalized and unknown onset can be distinguished. While focal seizures are limited to one hemisphere and are often originate in subcortical structures, generalized seizures rapidly spread bilaterally. Seizures of unknown onset still can feature certain characteristics and serves as a placeholder for future reclassification (Fisher et al., 2017b). The other levels of classification are optional and in some cases specific for one of the categorize mentioned above (Table 1).

Table 1 The basic ILAE 2017 operational classification of seizure types (Fisher et al., 2017b; Fisher et al., 2017a)

Focal Onset	**Generalized Onset**	**Unknown Onset**
Aware/Impaired Awareness	Motor	Motor
	(Tonic-clonic/other motor)	(Tonic-clonic/other motor)
	Nonmotor (Absence)	Nonmotor (Absence)
Focal to bilateral tonic-clonic		Unclassified

Temporal lobe epilepsy (TLE) and different animal models

Temporal lobe epilepsy (TLE) is a group disorders that involves the generation of focal seizures originating from the temporal lobe of one hemisphere. Two main categories can be distinguished: mesial (MTLE) and lateral temporal lobe epilepsy (LTLE). While seizures in MTLE arise from the inner aspect of the temporal lobe, including the hippocampus, parahippocampal gyrus and the amygdala, LTLE seizures originate from neocortex at the outer surface of the temporal lobe.

MTLE (which we from now on refer to as TLE) is often associated with hippocampal sclerosis (HS), delineating the epileptic focus. Typical HS features a loss of neurons in the cornu ammonis (CA) region 1 (CA1) and in the polymorphic layer - the so-called hilus of the dentate gyrus (DG) (Thom, 2004). Occasionally, a dispersion of granule cells (GC) can be found in the DG, and only in a few cases GC loss is observed (Houser, 1990). In TLE patients, mossy fibers, GC axons that project into the hilus of the DG and stratum lucidum of CA3, were shown to target GC dendrites in the inner molecular layer of the DG (Scheibel et al., 1974), in a process termed mossy fiber sprouting.

Although it still not entirely resolved what mechanisms underlie the induction of these multiple alterations in humans, several animal models exist mirroring certain aspects of the histological and electrographic hallmarks of TLE. Experimentally, traumatic brain injury, different pharmacologic agents or electrical stimulation can induce a status epilepticus (SE), which is defined as continuous seizure activity lasting for more than 30 min (for tonic-clonic SE) or 60 min (for focal SE) (Trinka et al., 2015). Common pharmacological models of SE are pilocarpine or kainic acid (KA). Pilocarpine is a cholinergic agonist and induces after systemic administration brain damage in hippocampal and extrahippocampal regions, including olfactory cortex, amygdala, thalamus, neocortex, and substantia nigra (Turski et al., 1983; Curia et al., 2008). Since KA can be injected on different ways (intracerebroventricular, intracerebral, or systemically), different lesion patterns are observed. Systemic injection of KA causes damage in the hippocampus, entorhinal cortex, amygdala, pyriform cortex, septum and medial thalamus, whereas in the hippocampus, the ventral area seems particularly vulnerable (Lothman and Collins, 1981). Even within the brain, intrahippocampal KA (IHK) injection (described below) differed from the intracerebroventricular (icv) injection of KA, showing hippocampal damage most consistently in CA3 (Nadler et al., 1978).

Histopathology during TLE epileptogenesis in the IHK model

Neurodegeneration and granule cell dispersion

Some of the first cells that disappear after a IHK injection are calretinin (CR)-positive hilar mossy neurons in the ipsilateral hippocampus, as evident in Nissl-stained sections 24 hours after the injection (Bouilleret et al., 2000b). At the same time, pyknotic pyramidal cells are found in CA1 and in CA3, proximal between the blades of the DG (CA3c), while CA2 and CA3a,b cell are generally spared (Figure 1) (Bouilleret et al., 2000b; Bouilleret et al., 2000a). The pattern remains the same at about 600-800 µm both anterior and posterior from the injection side, while gradually diminishing posteriorly thereafter (personal observation). Although the entire CA1-3 can be affected at the injection side, the IHK-induced lesion can presumably be conceived as a uniform focus. The following days, cell loss in the pyramidal layers and dispersion of GC becomes evident (Suzuki et al., 1995b; Bouilleret et al., 1999). The dispersion of GC was found to be a result of reelin deficiency (Heinrich et al., 2006) and could be locally prevented by an infusion of exogenous reelin (Müller et al., 2009). Duveau et al. (2011) revealed that reelin secretion from Cajal-Retzius, located in the hippocampal fissure, is impaired due to abnormal proteolytic processing and the production of truncated reelin. After 4 months, the dispersed DG enlarged and covered almost the entire hippocampal formation, while CA3 was reduced and CA1

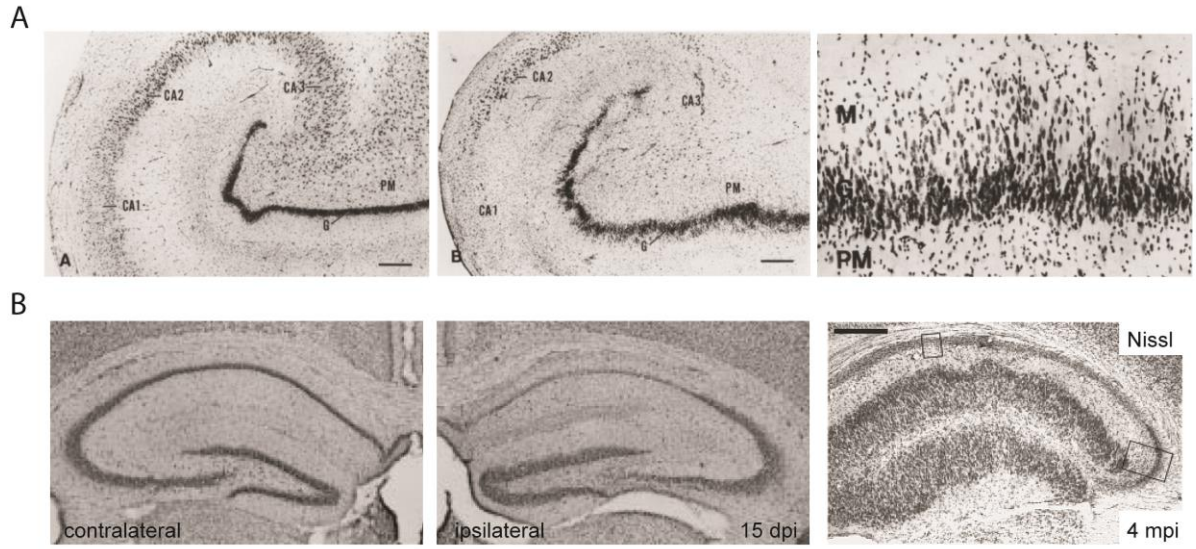

Figure 1 Characteristic changes in the epileptic focus in patients with TLE and the IHK model of TLE. A. Cresyl violet-stained (Nissl) section of a control (*left*) and an epilepsy (*middle*) specimen, showing the hippocampal formation. Cell loss is apparent in CA1, parts of CA3 and the hilus. The dentate gyrus shows a dispersion of granule cell (see also higher magnification on the *right*). B. Similar neuropathological alterations can be seen in adult mice 15 days post IHK injection (dpi) in the ipsilateral (*middle*), but not in the contralateral hippocampus (*left*). The dispersion of granule cells progressively increases, as seen 4 months post injection (*right*). Images are modified from Houser (1990) for A and Bouilleret et al. (1999; 2000b) for B.

almost completely disappeared (Bouilleret et al., 2000b). Strikingly, Bouilleret et al. (2000b) observed that GC dispersion at 7 or 15 days post injection (dpi) was only evident in mice displaying a severe degeneration of CA1. This was later confirmed by simultaneously alleviating cell loss in CA1 and GC dispersion after an intrahippocampal application of botulinum neurotoxin E (BoNT/E) 3 hours after IHK-induced SE (Antonucci et al., 2008), in a process shown to involve brain derived neurotrophic factor (BDNF)-tropomyosin receptor kinase B (TrkB) signaling (Duveau et al., 2011).

Reelin-and CR-positive Cajal-Retzius are one of the few interneurons that survive in the epileptic focus. In contrast, parvalbumin (PV)-, calbindin (CB)-, somatostatin (SOM)-, neuropeptide Y (NPY)- and other reelin-positive interneurons disappear in CA1, DG and to some extent in CA3, while CR-positive interneurons were mostly spared (Bouilleret et al., 2000b; Bouilleret et al., 2000a; Duveau et al., 2011). The loss of interneurons happens within the first 24 hours and was confirmed to be not just a loss of staining of a particular protein (e.g. calcium-binding protein) by observing a simultaneous disappearance of GABAA-receptor α1 subunit-immunoreactivity (IR) (Bouilleret et al., 2000b; Bouilleret et al., 2000a), which is expressed by all hippocampal PV-positive interneurons (Gao and Fritschy, 1994).

Synaptic reorganization

Different forms of sprouting were reported, however mainly involving the DG. For example, mossy fibers and axons of GC projecting to CA3 were found to sprout and innervate GC dendrites in the inner molecular layer after epileptic activity. As also noticeable after chronic synchronous activation of the perforant path, mild sprouting can be detected by the high Zn2+ content of mossy fibers (Sutula et al., 1988), and severe epileptic discharges as for example IHK- or pilocarpine-induced SE are able to cause a strong (Okazaki et al., 1995; Bouilleret et al., 1999). Interestingly, rapamycin was able to suppress mossy fiber sprouting and reduce the hypertrophy of dentate GC, however, without having any effect on seizure frequency, granule cell proliferation, the occurrence of ectopic cells and the loss of hilar neurons (Buckmaster and Lew, 2011). At the same time, ablating mossy cells by an adeno-associated virus (AAV)-mediated cell-specific diphtheria toxin (DT) expression did not cause mossy fiber sprouting or spontaneous seizures (Jinde et al., 2012).

Ectopic expression of NPY

Under physiological conditions, NPY is selectively expressed in interneurons, while epileptic activity induces an ectopic expression of NPY in various animal models and patients suffering

from TLE. Seizures induced by systemic or intrahippocampal KA (Sperk et al., 1992; Gruber et al., 1994; Makiura et al., 1999; Bouilleret et al., 2000b), pilocarpine (Lurton and Cavalheiro, 1997) or a hilar lesion (White and Gall, 1987) lead to a transient increase in NPY levels in NPY-positive interneurons, granule cells and mossy fibers (Figure 2). An early study in NPY-deficient mice reported an increase in seizure susceptibility, severity and a shortened latency to behavioral seizures upon injection of the GABAergic antagonist pentylenetetrazole (PTZ) (Erickson et al., 1996). While both NPY-deficient mice and mice deficient of the NPY Y5 receptor (Y5R) showed more severe behavioral seizures and seizure-associated deaths, similar frequency and duration of pure electrographic seizures were reported in NPY-deficient mice (Baraban et al., 1997; Marsh et al., 1999). As a result, many studies examined the effect of NPY supplementation through direct NPY injection (Woldbye et al., 1996; Baraban et al., 1997; Woldbye et al., 1997; Vezzani et al., 1999a) or local AAV-mediated overexpression of NPY and Y2R or Y5R in the hippocampus (Richichi et al., 2004; Sorensen et al., 2009; Woldbye et al., 2010; Gotzsche et al., 2012). Summarized in Table 2, the stimulation of the NPY pathway particularly affected seizure severity and mortality.

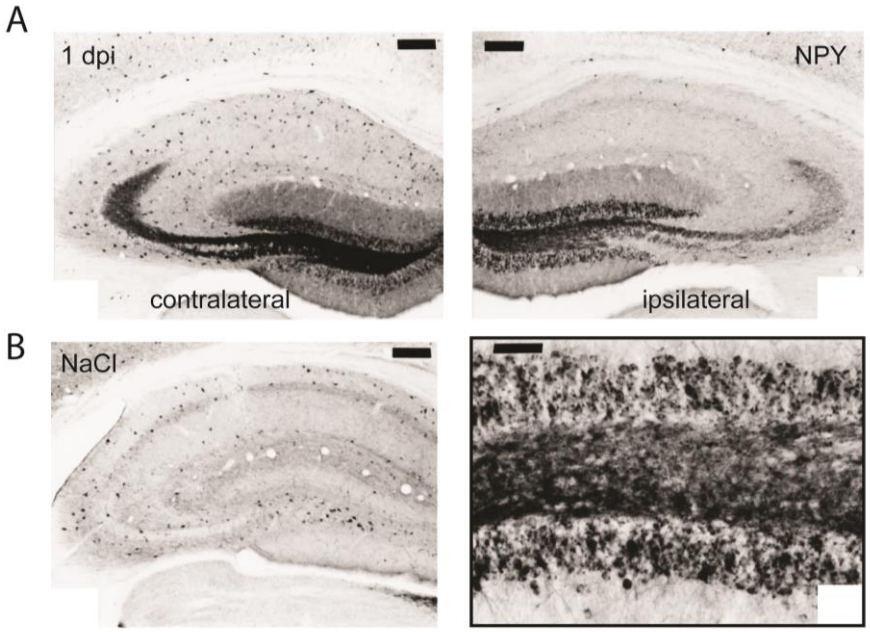

Figure 2 Ectopic NPY-IR. A. NPY-IR appears already 24 hours after IHK injection in both hemispheres. While NPY interneurons are spared in the contralateral hippocampus, the cells are lost on the ipsilateral side. Ectopic NPY-IR can be detected in mossy fibers and granule cells of the dentate gyrus (compare also magnification of the ipsilateral dentate gyrus). B. In NaCl (or naïve) mice, NPY is almost solely detected in interneurons. Images are modified from Bouilleret et al. (2000b).

Table 2 Literature about the seizure leviating effect of NPY

Ref.	Treatment/model		Model	Acute/ chronic	Animals	latency			number		Seizure freq	duration		Time in seizure	score (modified Racine scale)	survival	AD duration	Seizure grade over progression of stimulation	Number of seizures	Number of stimulations for seizure induction	Number of second ADs	AD threshold
	overexpr	area				SE (contin.; >10/30 min)	1st MS	non-conv	conv	non-conv		conv	nonconv									
Gotzsche et al., 2012	NPY	H bilat.; dorsal	KA (s.c.)	acute	Male Wistar rats	↑	↑		-					↓	↓							
	YR5					-	-		-					-	-							
	NPY/YR5					↑↑↑	↑↑↑		↓					↓↓↓	↓↓↓							
Woldbye et al., 2010	YR2	H bilat. dorsal and ventral	rapid kindl.	acute	Male Sprang. Dawley rats												↓	↓	↓ (for Grade 4-5)	↑ (for Grade 3-5 of 5)		-
			re-kindl.															↓	↓ (for Grade 4-5)	↑ (for Grade 2-5 of 5)	↓↓	
			KA (s.c.)		Male Wistar rats	↑	↑							↓		↑ (from 25% to 100%)						
	NPY/YR2		rapid kindl.		Male Sprang. Dawley rats																	↑
Lendri et al., 2016	NPY/YR2	H unilat. dorsal and ventral	IHK (unilat.)	chronic	Male Wistar rats				steady (before/after treatment; unlike increase in control)		↓	↓ (before/after treatment; unlike steady in control)		steady (before/ after treatment; unlike increase in control)								
Vezzani et al., 2002	NPY	trans. mice	KA (i.c.v.)	acute	Sprang. Dawley rats	-			↓					↓	↓ (stage 5 for 30 min)							
			kindling														↓ (2nd, not 1st; for Grade 2)			↑ (for Grade 4-5 of 5)		-
Richichi et al., 2004	NPY	H bilat. dorsal	IHK (unilateral)	acute	Male Sprang. Dawley rats		↑↑		↓					↓								
			KA (i.c.v.)			↑			-	-				↓↓	↓ (stage 5 for 30 min)							
			rapid kindling														↓ (sum of all AD after stimulation)			↑ (for Grade 3-5 of 5)		↑
Sorensen et al., 2009	NPY	H bilat. dorsal and ventral	rapid kindling	acute	Male Sprang. Dawley rats												↓ (at thr and Gr1-4, not Gr5)			-		-

Epileptogenesis-associated neuroinflammation in TLE

Over the past years, neuroinflammation has received increasing attention in epilepsy research, as both clinical (Crespel et al., 2002; Wu et al., 2008; Choi et al., 2009; Varella et al., 2011) and experimental studies (Voutsinos-Porche et al., 2004; Fabene et al., 2008; Ravizza et al., 2008a; Zattoni et al., 2011) indicate that inflammatory processes are involved in seizure pathology. Especially during the early stages of epileptogenesis, the activation of the immune system triggered by a brain insult and the subsequent inflammatory reactions can contribute to seizures and hence the development of epilepsy (Pitkänen and Sutula, 2002; Vezzani et al., 2011). Research in both patients and animal models of TLE revealed that not only local but also peripheral immune cells are present in the epileptic focus and potentially involved in epileptogenesis (Fabene et al., 2008; Ravizza et al., 2008b; Deprez et al., 2011; Zattoni et al., 2011). Hence, several different immune cells are accompanying the development of TLE, interacting with each other and supposedly shaping the course of the disease.

Microglia and peripheral macrophages

Microglia, resident macrophages of the CNS, form the frontline defense of the innate immune system and play an important role in several neurological diseases (Glass et al., 2010). Neurodegeneration associated with a brain insult causes an immediate and sustained activation of microglia in many diseases, including epilepsy. For example, activated microglia engulfing fragmented DNA were significantly increased in patients with chronic intractable epilepsy (Choi et al., 2009). In several animal models of TLE, the activation of microglia closely reflects the neurodegenerative pattern and can thereby be used to assess the severity of the lesion. During the first two weeks of the IHK-induced epileptogenesis, an activation of microglia is already evident after 24 hours and progressively increases over the next days, while reaching a plateau between 3-6 dpi (Zattoni et al., 2011; Gfeller, 2015a). However, not only resident macrophages, but also peripheral mononuclear phagocytes were detected in the ipsilateral dentate gyrus, specifically in the molecular layer and to a lesser extent in the granule cell layer (Zattoni et al., 2011). Between 1-3 days after the IHK-injection, the peripheral mononuclear phagocytes infiltrate into the dentate gyrus and also need until day 3-6 to reach their maximum (Gfeller, 2015a). Spatial and temporal specificity suggested that these macrophages might be involved in the dispersion of dentate GC. Therefore, Zattoni et al. (2011) were depleting peripheral mononuclear phagocytes using repeated systemic injections of clodronate liposomes, overall resulting in a reduced dispersion with areas containing pyknotic GCs. In these areas of extensive degeneration of GCs,

activated microglia were evident. Two recent studies using the systemic KA or pilocarpine model of TLE found that the lesion in CA3 recruits peripheral mononuclear phagocytes within 24 hours through chemokine C-C motif ligand 2 (CCL2), however, only transiently for about one week (Varvel et al., 2016; Tian et al., 2017). In contrast to the IHK model, a depletion of peripheral mononuclear phagocytes in CCR2-KO mice lead to a reduction of Iba1+ microglia in CA3 and, in one of these studies, to reduced neuronal loss, anxiety, memory decline and SRS two weeks after systemic KA. Although there seem to be differences between models of TLE, the influence of peripheral on resident monocytes, in particular on their state of activation and signal transducer and activator of transcription 3 (STAT3)-mediated interleukin (IL)-1β production, are potentially universal and might affect epileptogenesis in the IHK model of TLE.

Leukocytes and the role of lympocytes

Previous findings in hippocampal tissue sections of TLE patients and animal models revealed intraparenchymal migration of T lymphocytes (Fabene et al., 2008; Zattoni et al., 2011). In the IHK model, cluster of differentiation 3 (CD3)-positive T cells were first found in large blood vessels between 1-3 dpi, in particular in the hippocampal fissure, and then they start to enter the parenchyma in large numbers between 6-10 dpi (Zattoni et al., 2011; Gfeller, 2015a). The expression of vascular cell adhesion molecules (intercellular adhesion molecule-1 [ICAM-1], vascular cell adhesion molecule-1 [VCAM-1], E-selectin, and P-selectin) was elevated after systemic administration of pilocarpine, enabling the rolling and arrest of leukocytes in brain vessels near the lesion by their leukocyte counterparts mucin P-selectin glycoprotein ligand-1 (PSGL-1) and integrins α4β1 and αLβ2 (Fabene et al., 2008). Interestingly, Fabene et al. (2008) were able to markedly reduce acute seizures, block the onset of SRS, blood-brain barrier (BBB) leakage and reduced neuronal loss by inhibiting leukocyte-vascular interactions or neutrophil depletion. In line with these findings, recombination activating gene-1 (RAG1)-knockout (KO) mice, devoid of B and T lymphocytes, exhibited severe neurodegeneration and early onset of SRS between 2-3 days after IHK injection (Zattoni et al., 2011). The exacerbated neurodegeneration in mice lacking B and T lymphocytes was caused by an infiltration of Gr-1+ neutrophils, which could be rescued by a systemic injection of anti-Gr-1 antibodies (Zattoni et al., 2011). While adoptive transfer of specific T lymphocyte populations to immune deficient mice had no influence on the seizure onset, they blocked the infiltration of macrophages and abolished GC dispersion in mice lacking CD4+ T cells (MHCII-KO) and, in contrast, enhanced recruitment of macrophages and increased GC dispersion in mice lacking CD8+ T cells (b2-microgloblin-KO) (Deprez et al., 2011). Based on these observations, the formation of an

epileptic focus and the development of SRS strongly relies on the interplay between innate and adaptive immune cells, which are recruited and activated in defined stages during epileptogenesis.

Cytokines, inflammasomes and priming

Along with the neuroinflammation, specific cytokines and chemokines are detected in epileptic patients. Increased levels of IL-1β, IL-8, IL-12p70 and macrophage inflammatory protein (MIP)-1β were found in postmortem tissue of patients with intractable seizures in childhood epilepsy (Choi et al., 2009). Similarly, surgical specimens of TLE patients with hippocampal sclerosis revealed a significant increase in IL-1β and tumor necrosis factor TNFα in the hippocampus (Varella et al., 2011). In both the IHK and the pilocarpine model, IL-1β and α (TNFα) were immediately upregulated after SE, while the expression slowly declined towards the chronic phase ((Benson et al., 2015); collaboration Dr. Rambousek). Besides a direct (chemokines) or indirect (cytokines) involvement in the recruitment of peripheral immune cells, cytokines (directly) and chemokines (indirectly) were shown to affect neuronal excitability ((Manley et al., 2007; Fabene et al., 2008; Ravizza et al., 2008b; Fabene et al., 2010; Riazi et al., 2010; Deprez et al., 2011; Zattoni et al., 2011; Galic et al., 2012; Balosso et al., 2013; Liimatainen et al., 2013; Arisi et al., 2015; Vezzani and Viviani, 2015; Varvel et al., 2016). For example, TNFα increases synaptic activity at perforant path-granule cell synapses through release of glutamate by astrocytic processes in the proximity of presynaptic NR2B+ NMDARs (Santello et al., 2011). IL-1β, however, was shown to modulate synaptic transmission through phosphorylation of the NMDA NR2A/B subunit (Vezzani et al., 1999c; Viviani et al., 2003). Recent findings revealed that damage-associated molecular patterns (DAMPs) from necrotic or distressed cells, while causing in glial cells an increased production of IL-1β (Saijo and Glass, 2011), lead to the expression and release of high-mobility group box-1 (HMGB1) in neurons (and macrophages (Jiang et al., 2007)), which in turn activates toll-like receptor 4 (TLR4) and like IL-1β, and mediates, through NR2A/B phosphorylation, a rapid increase in NMDA calcium conduction (Maroso et al., 2010; Balosso et al., 2013).

Several recent findings discovered that inflammasomes, multimeric protein complexes in the cytosol, are mediating the production and release of IL-1β and HMGB1 and are important in different neurological diseases such as Alzheimer's disease (Lamkanfi and Kanneganti, 2010; Lu et al., 2012; Heneka et al., 2014). Inflammasomes consist of different pattern-recognition receptors (PRRs), such as nucleotide-binding domain, leucine-rich repeat containing proteins (also known as NOD-like receptors, NLRs) or the absent in melanoma 2 (AIM2)-like receptors

(ALRs). After sensing DAMPs, NLRs or AIM2 oligomerize to activate caspase-1, which in turn cleaves pro-IL-1β and pro-IL-18 into the bioactive form IL-1β and IL-18 (reviewed in (Latz et al., 2013; Walsh et al., 2014; Heneka et al., 2015)). Interestingly, NLRP3 inflammasomes, for example in innate immune cells, are activated by various stimuli and can be primed for example by lipopolysaccharide (LPS)-induced activation of TLR4 or an activation of TLR3 by polyinosinic:polycytidylic acid (PolyI:C), a double-stranded RNA (dsRNA) mimetic (Lu et al., 2012; Guo et al., 2015).

Various neurodevelopmental changes are associated with maternal infections during pregnancy (Knuesel et al., 2014; Meyer, 2014). Prenatal exposure to systemic PolyI:C at gestation day 17 was shown to cause sustained increase in proinflammatory cytokine levels, especially of plasma IL-1β, cortical IL-10 and TNFα (Meyer et al., 2006; Krstic et al., 2012). In addition, Krstic et al. (2012) found that a second immune challenge at 12 months of age ("double hit") exacerbated inflammatory response in the CNS of 15-months old wildtype mice. In the "double hit" study, prenatally 'priming' microglia was sufficient to cause a chronic inflammation and an AD-like phenotype, comprising increased levels of hippocampal amyloid precursor protein (APP) and its fragments, hyperphosphorylated Tau, and an impairment in working memory (Knuesel et al., 2009; Krstic et al., 2012; Krstic and Knuesel, 2013). Interestingly, prenatal or acute peripheral immune stimulation was shown to affect the seizure threshold and the development of epilepsy. An acute systemic immune challenge hours or days prior to a pro-convulsive or electrical kindling increased the severity of subsequent seizures (Auvin et al., 2007; Galic et al., 2008; Kwon et al., 2010; Kirschman et al., 2011; Lee et al., 2012; Michalovicz and Konat, 2014). Maternal immune activation by prenatal immune challenges with PolyI:C during gestation day (GD)12-16 increased hippocampal excitability and lowered the seizure threshold, while being dependent on IL-1β and IL-6 (Pineda et al., 2013). Moreover, febrile seizures induced by LPS and KA were exacerbated and IL-1β levels elevated after maternal restraint stress at GD14 (Qulu et al., 2012). Therefore, maternal immune challenge potentially affects the fetal development long-term.

Alzheimer disease and hyperexcitability

The pathogenesis of Alzheimer disease (AD) is still an enigma and remains a topic of lively debate. AD is characterized by the progressive loss of cognitive abilities, network abnormalities, severe neurodegeneration and prominent neuroinflammation (Castellani et al., 2010; Palop and Mucke, 2016). The neuropathological hallmarks of AD include the formation of senile plaques,

containing aggregated amyloid-β (Aβ) peptides, and neurofibrillary tangles (NFTs) consisting of hyperphosphorylated tau (Alzheimer et al., 1995; Serrano-Pozo et al., 2011). Several lines of evidence support the hypothesis that the dysfunction of the APP and the accumulation of amyloid β play a causal role in the development of AD (Huang and Mucke, 2012; Krstic and Knuesel, 2013; De Strooper and Karran, 2016). Various mutations in APP, the catalytic γ-secretase subunit presinilin-1 (PS1) or PS2 were shown to alter the production of Aβ towards aggregation-prone species and held responsible for autosomal dominant, early-onset familial AD (FAD) (Karran et al., 2011). In this 'amyloid cascade hypothesis', a shift towards proteolytic cleavage of APP by β-site APP-cleaving enzyme 1 (BACE1 or β-secretase) and γ-secretase leads to an increase in Aβ production and Aβ1-42/Aβ1-40 ratio, which in turn promote the assembly of monomers to oligomers, fibrils and amyloid plaques (Hardy and Higgins, 1992; Benilova et al., 2012b). Moreover, a specific mutation in APP (A673T) associated with reduced β-secretase-mediated cleavage was shown to decrease the risk for late-onset sporadic AD (LOAD) (Jonsson et al., 2012; Maloney et al., 2014). Although it remains controversial to which extent the pathogenesis of LOAD and FAD overlay (Krstic and Knuesel, 2013), the functional alterations remain largely the same (McKhann et al., 1984). Interestingly, both transgenic mice with a mutation in the apolipoprotein E4 (APOE4), a risk factor for LOAD (Corder et al., 1993), and animal models of FAD display alterations in network activity prior to the occurrence of other AD characteristic alterations (reviewed in (Palop and Mucke, 2016). This early time window, before the predicted onset of clinical disease when cellular reactions gradually fail to maintain homeostasis (De Strooper and Karran, 2016), is important for a mechanistic understanding of the impairment and the selection of therapeutic strategies in AD patients.

The network abnormalities reported in AD comprise abnormal rhythmic activity and network hyperactivity, which bear close resemblance with pathological activity seen in epilepsy (Palop and Mucke, 2009, 2010). In mice overexpressing human APP (hAPP) with a mutation found in a familial form of AD in Sweden (Swe; K670N, M671L), the Tg2576 mouse model, large amplitude potentials were found at 5 weeks of age, which had remarkable similarities to interictal spikes (Kam et al., 2016). At a later stage, spontaneous seizures were recorded in 7-months old Tg2576 mice (Kam et al., 2016), at a time when Aβ deposits start to occur (at around 6 months) (Kawarabayashi et al., 2001). Similarly, in mice overexpressing hAPP carrying the Swe and Indiana (Ind; V717F) mutations, the J20 mouse line, frequent, sharp, synchronous discharges and intermittent nonconvulsive seizures were found at an age of 3 to 7 months (Palop et al., 2007). In 65% of APdE9 mice carrying the hAPP with the Swe mutation cointegrated with

human presenilin-1 with a deletion in exon 9 (PS1dE9) at least one seizure was reported during 3 weeks of continuous video-EEG (vEEG) recording at an age of 3 to 4.5 months (Minkeviciene et al., 2008). The hyperexcitable phenotype was associated with an ectopic expression of NPY in mossy fibers and axons sprouting into the outer molecular layer (Palop et al., 2007; Roberson et al., 2007; Roberson et al., 2011). Interestingly, tau reduction had an antiepileptogenic effect by preventing the occurrence of SRS, reducing the severity of PTZ-induced seizures, inhibiting bicuculline-induced epileptiform bursting, and normalizing miniature inhibitory postsynaptic potentials (mIPSCs) (reducing), miniature excitatory postsynaptic potentials (mEPSCs) (increasing), spontanous inhibitory postsynaptic potentials (sIPSCs) (increasing), and sEPSCs (decreasing) in dentate granule cells of hAPPJ20 mice (Roberson et al., 2011). In this study, they revealed further that a normalization of the excitatory/inhibitory balance is accompanied by a lack of ectopic NPY-IR in mossy fibers or the dentate molecular layer. In the same hAPPJ20 mice, spontaneous epileptiform discharges were primarily found to occur during reduced gamma oscillatory activity, which in turn was attributed to a dysfunction of PV-positive interneurons caused by the reduced expression of interneuron-specific and PV-cell-predominant voltage-gated sodium channel subunit Nav1.1 (Verret et al., 2012). Strikingly, learning and memory impairment in knockin mice for human apoE4 (apoE4-KI) could be linked to a disruption in slow gamma oscillations during hippocampal sharp-wave ripples (SWR), while a selective elimination of apoE4 in GABAergic interneurons prevented cognitive sequelae, the deficit in SWR-associated slow gamma but not the overall decline in SWRs of aged apoE4-KI mice (Knoferle et al., 2014; Gillespie et al., 2016). During awake immobility and slow-wave sleep, the local field potential (LFP) in CA1 of freely moving mice revealed that these short bursts of a high-frequency oscillation (150-250 Hz), the SWRs, mark the firing of pyramidal cell ensembles in a time-compressed manner to encode past experiences in so-called replay (Buzsaki et al., 1992; Skaggs and McNaughton, 1996; Lee and Wilson, 2002; Buzsaki et al., 2003; Buzsáki, 2015). Slow gamma oscillation (20-40 Hz) during SWRs is thought to promote the coordination of ensemble activity across CA3 and CA1 from both hemispheres, preserving the sequential activity in the SWR (Carr et al., 2012; Colgin, 2012, 2016), which in turn is important for memory consolidation and retrieval (Buzsaki, 1989, 1996; Kudrimoti et al., 1999). In regard to the similar network abnormalities seen in both AD and epilepsy, GABAergic interneurons, especially NPY- and SOM-expressing hilar cells, were shown to be important as they are particularly vulnerable in different rodent models of AD (Ramos et al., 2006; Mahar et al., 2016) and epilepsy (Sperk et al., 1992; Bouilleret et al., 2000a). For example, in 6- to 7-months-old hAPPJ20 mice, decreased CB-IR in the granular and molecular layer of the DG was correlating with behavioral deficits in

these mice (Palop et al., 2003). Interestingly, CB-IR in the DG showed a similar pattern 30 days after IHK injection, in particular the contralateral side, with a reduced but highly variable staining intensity between individual cells (Bouilleret et al., 2000b). As in models of TLE (Vezzani et al., 1999c; Vezzani et al., 1999a), NPY is ectopically expressed in CA3 pyramidal cells, mossy fibers and the molecular layer of the dentate gyrus in J20 mice (Palop et al., 2007). In the same study, it was shown that sprouting axons in the molecular layer are double-immunoreactive for NPY and SOM, with presumably a hilar origin (Palop et al., 2007). However, a recent study reports that fibers of SOM-positive oriens lacunosum-moleculare (O-LM) cells, which solely project to the striatum lacunosum-moleculare (SLM), start to sprout aberrantly after a pilocarpine injection into the outer molecular layer and to innervate granule cells of the dentate gyrus (Peng et al., 2013). As pyramidal cells are the main excitatory input to O-LM cells (Blasco-Ibanez and Freund, 1995), this aberrant circuit between CA1 pyramidal cells, O-LM cells and DG granule cells might lead to an interference with the normal inhibitory feedback circuit in the dentate gyrus (Peng et al., 2013). Although its functional implication remains to be determined, it might serve as an explanation for the reduced expression of the immediate early gene c-Fos detected in dentate GC (Palop et al., 2003), at an age when circuit reorganization is already detectable in a mouse model of AD (Palop et al., 2007).

Neurogenesis

Adult neurogenesis is the process of generating neurons from neural stem cells (NSCs). Two specific neurogenic areas – "niches" – can be distinguished: the subventricular zone (SVZ) of the lateral ventricles and the subgranular zone (SGZ) in the DG of the hippocampus (Gage, 2000). Neurogenesis is involved in many brain functions from neuronal development, structural plasticity and disease progression (Ming and Song, 2011). Therefore, it is no wonder that adult neurogenesis is affected in both AD and TLE. For example, some AD transgenics (e.g. pPDGF-APPSw,Ind) were shown to have increased hippocampal neurogenesis prior to any neuronal loss or amyloid deposition, however augmenting with a progress in Aβ pathology (Jin et al., 2004; Gan et al., 2008). However, in other AD models (e.g. APP/PS1 mice) the proliferation was not affected, but the survival of newborn cells later on was (Verret et al., 2012). In a model featuring both (hAPP-J20 mice), the accelerated early development and impaired maturation of adult-born granule cells was linked to an increased GABAergic input to these cells and ultimately to synaptic reorganization present in these mice (Sun et al., 2009). Interestingly, a selective depletion of the APP in GABAergic neurons also lead to an increased progenitor cells

proliferation and reduced dendritic length in newborn granule cells (Wang et al., 2014). Recent studies revealed that tonic GABA activation maintains NSCs quiescence (Song et al., 2012) and promotes the dendritic development of newborn neurons (Ge et al., 2006). Taken together, this suggests that a malfunction of local GABAergic circuits is detrimental for adult neurogenesis and affected early by the AD pathology (e.g. through Aβ toxicity or APP dysfunction). Similar observations were made in other studies and these mechanisms might underlie alterations seen in animal models of TLE (Parent et al., 1997; Jessberger et al., 2005). IHK-induced SE lead to a massive activation of NSCs, which after symmetrical division cause both mother and daughter cells to convert into reactive astrocytes in the ipsilateral hippocampus (Sierra et al., 2015). This distinct self-renewal mode exhausts the NSC pool and eventually impairs neurogenesis long term (Hattiangady et al., 2004; Kralic et al., 2005; Ledergerber et al., 2006; Sierra et al., 2015). While a large body of literature report a direct effect of aberrant excitability on adult neurogenesis, recent studies suggest that neurogenesis directly affects the development of seizures, with findings showing reduced SRS 5 to 7 weeks after pilocarpine injection due to genetic ablation of adult-generated granule cells (Cho et al., 2015) and another group reporting an increased susceptibility to KA-induced SE after reducing neurogenesis by X-irradiation (Iyengar et al., 2015).

II. AIM OF THE THESIS

The overall objective of this thesis was to evaluate the role of neuroinflammation and early epileptiform activity in epileptogenesis of TLE, as well as the impact of early pathophysiological changes associated with Alzheimer's disease (AD) on the development of acquired epilepsy, using IHK injection as TLE model in wildtype mice and different transgenic mouse lines.

Study I **Effects of chronic and acute inflammatory responses on epileptogenesis in the intrahippocampal kainic acid model of temporal lobe epilepsy**

In this study, we aimed to characterize the effects of either chronic inflammation (prenatal immune challenge) or acute epileptogenesis-associated immune reactions on the formation of an epileptic focus in the IHK mouse model of TLE. We used three different approaches in order to determine

- the effect of chronic inflammation on the pathogenesis of TLE,
- the role of NLRP3 inflammasomes in the activation and recruitment of different immune cells during epileptogenesis, and
- the contribution of infiltrating macrophages to the formation of an epileptic focus.

We used IHK injection in either wildtype mice prenatally infected with a viral mimic, NLRP3-KO mice or CCR2-KO mice. To assess the effect of chronic inflammation on epileptogenesis, intrahippocampal EEG recordings were acquired and analyzed for occurrence of SRS. We performed histological stainings to visualize neurodegenerative patterns at different time points during epileptogenesis. We used different antibodies against various immune cells, glial cells and markers of axonal reorganization for immunohistochemistry (IHC) to evaluate histopathological changes and associated immune response in the developing epileptic focus.

Study II **Contribution of early Alzheimer-related pathophysiology to the development of acquired epilepsy**

Here, we aimed to elucidate the significance of early pathophysiological changes in a mouse model of AD for the development of IHK-induced epilepsy. Based on various reports about hyperexcitability phenotypes in mouse models of AD, we thereby aimed to answer the following questions:

- Are hippocampal circuits in AD transgenic mice already affected prior to the occurrence of amyloid β plaques and more prone to excitatory-inhibitory imbalance?
- Do early changes associated with an AD predisposition, in particular soluble Aβ species, render the hippocampal formation more susceptible to the development of acquired epilepsy?
- Does early AD pathology affect neuronal survival, neuroinflammation, axonal reorganization, or adult neurogenesis either prior to or following IHK-induced epileptogenesis?

To address these questions, we compared wildtype mice to ArcticAβ mice, overexpressing mutated human APP transgene, employing field and patch-clamp recordings in vitro, 24/7 video-EEG recordings, histological and IHC measures in naive or IHK-injected mice. Focusing on the course of epileptogenesis, we captured changes at different time points during development of epilepsy, in particular electrographically and immunohistochemically. To test the contribution of Aβ oligomers, an early manifestation of AD pathology, to the development of acquired seizures, we injected intracerebrally a neutralizing antibody prior to IHK-induced epileptogenesis.

Study III **Contribution of early aberrant activity to the development of acquired epilepsy**

We aimed to understand the contribution of early aberrant activity during the latent period following status epilepticus (SE) to the development of spontaneous recurrent seizures (SRS) in the IHK mouse model of TLE. To this end, we adapted state-of-the-art closed-loop optogenetic intervention (COI) techniques to inhibit brief epileptiform discharges occurring spontaneously during early epileptogenesis. Establishing a detection method for fast online COI and an offline approach for post-analysis of large data sets, we determined the effect of early, transient COI on the emergence of SRS in the long-term, exemplified in a subsample analyzsed four months after IHK injection. Further, by applying hippocampal COI through either a brief activation of parvalbumin (PV)-expressing interneurons or repeated inhibition of pyramidal cells, we determined the role of either cell type for the generation of early epileptiform activity.

III. RESULTS

STUDY I: EFFECT OF CHRONIC AND ACUTE INFLAMMATORY RESPONSES ON EPILEPTOGENESIS IN THE INTRAHIPPOCAMPAL KAINIC ACID MODEL OF TEMPORAL LOBE EPILEPSY

Tilo Gschwind[1,2], Tina Notter[1,2], Mariana Zaichuk[1,2], Tim Gfeller[1], Irene Knuesel[1,3] and Jean-Marc Fritschy[1,2]

[1] Institute of Pharmacology and Toxicology, University of Zurich, Switzerland

[2]Neuroscience Center Zurich, University of Zurich and ETH Zurich, Winterthurerstrasse 190, CH-8057 Zurich, Switzerland

[3] Present address: Roche Pharmaceutical Research and Early Development, NORD Discovery & Translational Area, Roche Innovation Center Basel, Grenzacherstrasse 124, Basel, Switzerland

unpublished data

Author's contribution

All the experimental procedures were carried out by TG. PolyI:C injections were performed with TN, MZ and IK. TG and JMF wrote the manuscript. Authors have no conflict of interest to declare.

Abstract

Research in animal models of temporal lobe epilepsy (TLE) revealed that most histopathological features of TLE form early, during the pathogenesis, and render the neuronal network susceptible to seizure generation. Neuroinflammation accompanies the early network reorganization, directly affects the formation of an epileptic focus and lowers the seizure threshold. The activation of innate immune cells can modulate neuronal excitability, in particular, through the release of pro-inflammatory cytokines (e.g. IL-1β). To investigate the contribution of the immune response in establishing an epileptic focus, adult mice received a single, intrahippocampal injection of kainic acid (IHK). Different components of the epileptogenesis-associated immune reaction were examined more closely. First, the effect of a chronic perturbation of innate immunity, 'priming', on epileptogenesis was studied in mice exposed either prenatally and/or postnatally to a viral mimic. Although the results remained inconclusive, they underline the relationship between the innate immune response and neuronal excitability. Second, for a better understanding of the molecular basis underlying the innate immune response, the pathogenesis of a pro-epileptic lesion was examined in mice devoid of NLRP3 inflammasomes. These intracellular sensors were shown to be involved in IL-1β production in microglia and macrophages. The neurodegenerative pattern and immune response caused by IHK was not affected by the lack of the NLRP3 inflammasome suggesting an NLRP3-independent production of IL-1β. Finally, we tested whether recruitment of peripheral macrophages is pivotal for the survival of granule cells in the dentate gyrus, as suggested in an earlier study. Selective interference with macrophage recruitment in C-C chemokine receptor type 2 (CCR2)-KO mice revealed that infiltrating macrophages are not directly responsible for the granule cell survival after IHK.

We conclude that the immune response mediated by activated microglia and infiltrating macrophages contribute to the formation of an epileptic focus. However, both are integrated in a broader immune response and certain processes might be compensated for by other immune cells, as shown in other models of TLE.

Introduction

Epilepsy affects 65 million people worldwide. Mesial temporal lobe epilepsy (TLE) is one of the most common adult seizure disorders and, when associated with hippocampal sclerosis, is the most refractory to pharmacotherapy (Engel, 1998; Semah et al., 1998; Browne and Holmes, 2001; England et al., 2012). Overall, treatment options for epilepsy remain inadequate for many patients who suffer from uncontrolled seizures. The pathogenesis of TLE and seizure etiology remain unknown, in particular the relationship between histological changes and neuronal mechanisms underlying the generation and persistence of spontaneous recurrent seizures (SRS).

Several neuropathological features of TLE can be replicated in a mouse model receiving a single intra-hippocampal injection of kainic acid (IHK). In this model, the IHK-induced status epilepticus (SE) causes a focal lesion in the dorsal hippocampus, which in turn leads within two weeks to the onset of SRS lasting for the life time of the animal (Suzuki et al., 1995a; Riban et al., 2002b). After this latent phase, mice show a high frequency of non-convulsive SRS, which are restricted to the dorsal hippocampus (Riban et al., 2002b; Arabadzisz et al., 2005; Dugladze et al., 2007). These animals also display pathological high frequency oscillations and, albeit at a much lower frequency, secondarily generalized convulsive behavioral seizures (Engel et al., 2009; Krook-Magnuson et al., 2013). The neuropathological alterations include the degeneration of pyramidal cells in CA1, CA3c and the loss of hilar mossy cells in the dentate gyrus (Suzuki et al., 1995a; Bouilleret et al., 1999). Impaired Reelin signaling leads in the injected hemisphere to a gradual but pronounced dispersion of dentate granule cells through to a point where most of the space originally filled by the hippocampal formation is occupied by the dentate gyrus (Bouilleret et al., 1999; Heinrich et al., 2006; Müller et al., 2009; Duveau et al., 2011). In addition, various hippocampal interneurons are differently affected by IHK, with parvalbumin (PV)-positive interneurons (including axo-axonic and basket cells) being the most vulnerable (Bouilleret et al., 2000b; Bouilleret et al., 2000a). These changes are accompanied by an increased expression of neuropeptide Y (NPY), a peptide with anticonvulsive properties (Richichi et al., 2004; Noè et al., 2012). NPY is expressed in interneurons, where it is often co-localized with GABA and/or somatostatin, in mossy fibers and ectopically in dentate granule cells (Vezzani and Sperk, 2004). Interestingly, during the latent phase, mossy fibers start sprouting in the dentate gyrus and in CA3, which is expected to be involved in formation of an aberrant, recurrent, excitatory circuit (Buckmaster, 2012). Despite the knowledge about all these multiple alterations, which are shared by different models of TLE, it is unknown if they contribute directly to development of seizures.

Increasing evidence from both clinical and experimental studies indicates a link between seizures and the concomitant neuroinflammation, in particular during the early stages of epileptogenesis. A local inflammatory reaction, which is triggered by a brain insult such as neurotrauma, stroke, infection or SE, are associated with acute symptomatic seizures and often followed by the development of epilepsy (Pitkänen and Sutula, 2002). The activation of the innate immune system and associated inflammatory reactions in the brain have been proposed to contribute to the pathogenesis of epilepsy (Vezzani et al., 2011). In the IHK model, the emerging hippocampal sclerosis is accompanied by a local inflammation, disruption of the blood brain barrier, infiltration of leukocytes, and - in areas of neurodegeneration - a sustained endothelial and microglial activation (Deprez et al., 2011; Zattoni et al., 2011). The importance of innate and adaptive immunity in epileptogenesis is further corroborated by observations suggesting macrophage depletion causes granule cell degeneration, whereas elimination of lymphocytes in a mouse model called RAG1-KO curtails the latent period prior to SRS onset (Zattoni et al., 2011).

To elucidate the role of inflammation, in particular the response of microglia and macrophages, in the pathogenesis of TLE, we used three different approaches in the IHK model of TLE. First, to study the effect of chronic inflammation on the pathogenesis of TLE, by priming microglia and peripheral macrophages, mice were prenatally injected with the viral mimic polyriboinosinic-polyribocytidilic acid (PolyI:C) during late gestation prior to the IHK-induced epileptogenesis during adulthood. When injected at gestation day (GD) 17, PolyI:C causes an acute rise in fetal brain cytokine levels (Meyer et al., 2006), a chronic increase of plasma IL-1β postnatally, and leads to an increased microglia activation in older mice (Krstic et al., 2012). Second, we studied the involvement of NLRP3 (NLR family, pyrin domain containing 3) inflammasomes in the activation and recruitment of different immune cells during epileptogenesis. NLRP3 inflammasomes are expressed by the innate immune system, important for sensing cellular molecules exposed after damaged-induced necrosis and involved in the release of IL-1β (Walsh et al., 2014). To examine the role of these intracellular sensors in establishing an epileptic focus, NLRP3-KO were injected with IHK. Finally, the role of infiltrating macrophages during epileptogenesis was investigated. It was recently shown that depleting peripheral macrophages with clodronate causes a degeneration of dentate granule cell (Zattoni et al., 2011). However, as clodronate might affect other cells types, the IHK-induced lesion was examined in mice lacking the C-C chemokine receptor type 2 (CCR2), which is pivotal for monocyte recruitment.

Materials and Methods

Animals

All experiments performed for this study were carried out in accordance with the Swiss law on animal experimentation and approved by the Cantonal Veterinary Office of Zurich.
Experiments were performed with C57Bl6/JOla (Harlan Laboratories, Horst, the Netherlands), NLRP3-KO (Jackson), and CCR2-KO mice (compare table 1). For experiments involving prenatal treatment, time-pregnant dams were shipped on gestational day (GD) 14 and injected with PolyI:C at GD17. All animals were housed in an in-house hygiene area (Institute of Pharmacology and Toxicology, University of Zurich, Switzerland) under a 12-hour light/dark cycle, with access to food and water *ad libitum.*

Polyriboinosinic-polyribocytidilic acid (PolyI:C) injections

As described by Notter (2015), 5 mg/kg PolyI:C potassium salt (P9582, 50 mg; Sigma-Aldrich Chemie GmbH, Buchs, Switzerland) was dissolved in 0.9% sterile, pyrogen-free NaCl. For both the prenatal and postnatal treatment, a single intravenous injection (i.v.) of either PolyI:C or NaCl were given at an injection volume of 5 mL/kg body weight to pregnant mouse dams at GD17 or 22-weeks old adult mice, respectively.

Intrahippocampal kainic acid (IHK) injection and electrode implantation

At the age of 12-weeks or 36-weeks, mice anaesthetized by inhalation of 2.5-3% isoflurane (Baxter) in oxygen were injected with 70 nL kainic acid (5mM in NaCl; Tocris biosciences) or an equivalent volume of NaCl into the right dorsal hippocampus (anteroposterior -1.8 mm, mediolateral -1.6 mm, dorsoventral -1.9 mm relative to Bregma) as described by Bouilleret et al. (2000).

Particular groups of mice were implanted with electrodes for electroencephalographic recordings. To this end, a bipolar electrode was implanted immediately after stereotactic injection into the same coordinates and a monopolar reference electrode was inserted into the cerebellum. The bipolar electrode consisted of two twisted enamel insulated stainless steel wires connected to a male connector (for details see (Arabadzisz et al., 2005)). Electrodes were fixed to the scull by Prime&Bond (Dentsply) in combination with Tetric EvoFlow® (Ivoclar vivadent) while the electrode shaft entering the hole was sheathed by Kwik-Cast™ Silicone Elastomer (World Precision Instruments). After surgery, all mice were i.p. injected with 1 mg/kg

buprenorphine (Temgesic®, Reckitt Benckiser AG, Switzerland) and placed on a warm pad for recovery.

Table 1 Animals used in this study.

Genetic background	Age (months)	Prenatal treatment (i.v.)	Postnatal treatments (i.v.)	Hippocampal injection	EEG recordings	Group abbreviation
C57BL/6J	3	-	-	NaCl	No	-
(n=3-6/gr)				KA	No	-
C57BL/6J	3	NaCl	-	NaCl	Yes	NN
(n=6-8/gr)		PolyI:C	-	NaCl	Yes	PN
		NaCl	-	KA	Yes	NK
		PolyI:C	-	KA	Yes	PK
C57BL/6J	9	NaCl	NaCl	NaCl	No	NNN
(n=6-12/gr)		NaCl	PolyI:C	NaCl	No	NPN
		PolyI:C	NaCl	NaCl	No	PNN
		PolyI:C	PolyI:C	NaCl	No	PPN
		NaCl	NaCl	KA	No	NNK
		NaCl	PolyI:C	KA	No	NPK
		PolyI:C	NaCl	KA	No	PNK
		PolyI:C	PolyI:C	KA	No	PPK
NLRP-3 KO	3	-	-	KA	No	-
(n=3/gr)						
CCR-2 KO	3	-	-	KA	No	-
(n=3)						

Acute seizures monitoring and electroencephalographic (EEG) recordings

To assess the acute response to IHK, video recordings were taken during the recovery from surgery. During a period of 2 hours, mice were recorded in individual cages before they were returned to their home cage. For the analysis, the severity of behavioral seizures was categorized according to the Racine, Pinel and Rover scale (table 2) (Racine, 1972; Pinel and Rovner, 1978).

Intrahippocampal EEG activity was recorded at 7 and 21 days post-injection (dpi). Freely moving mice were placed in a Faraday cage and connected via a swivel to an amplifier and digitizer (AcqKnowledge MP100; Biopac Systems). Mice were first habituated for 30 min. Subsequently, EEG activity was recorded for 3 hours were taken at a sampling rate of 200 Hz. Recordings were always taken between 11 am and 3 pm to minimize potential circadian variations. Seizures were defined as paroxysmal events lasting longer than 10 s and only if they were separated by intervals of at least 1 s. The average frequency and duration of SRS was calculated for each mouse.

Table 2 Modified Racine scale for behavioral seizures. Adapted from (Pinel and Rovner, 1978)

Scale	**Stage**	**Behavior**
Racine behavioral scale	1	Oroalimentary movements
	2	Head nodding
	3	Anterior limb clonus
	4	Dorsal extension (rearing)
	5	Loss of balance and falling
Pinel and Rovner behavioral scale	6	Repeated falling
	7	Strong jumping and running
	8	Stage 7 with tonic period

Tissue preparation for immunohistochemistry

Tissue preparation was performed as described by Notter et al. (2014). In brief, anesthetized mice (Nembutal; 50 mg/kg; i.p.) were perfused intracardially with 15–20 mL ice-cold, oxygenated aCSF [containing (mM) NaCl 125, KCl 2.5, $CaCl_2$, 3.7, $MgCl_2$ 2, $NaHCO_3$ 26, NaH_2PO_4 1.25, glucose 25], pH 7.4, at a flow rate of 10–15 mL/min. The brain was immediately extracted from the skull and divided into 3 blocks: rostral, medial and caudal part. All three parts were immediately immersion-fixed for 3 hours in ice-cold fixative [4% paraformaldehyde dissolved in 0.15 M sodium phosphate buffer], pH 7.4, then rinsed with PBS (pH = 7.4) and cryoprotected overnight in 30% sucrose in PBS at 4°C.

The fixed tissue was cut into 40-µm thick serial coronal sections collected in ice-cold PBS using a sliding microtome. The sections were transferred to a cryoprotectant solution (50 mM sodium phosphate buffer, pH 7.4, containing 15% glucose and 30% ethylene glycol; Sigma-Aldrich) for storage at -20°C until they were used for immunohistochemistry.

Immunohistochemistry

Immunoperoxidase staining was preformed as described earlier (Zattoni et al., 2011). Sections were incubated overnight at 4°C under constant agitation with primary antibodies (see table 3) diluted in Tris buffer, pH 7.4, containing 0.2% Triton X-100 and 2% normal serum. After washing 3 x 10 min in Tris buffer, sections were incubated for 30 min at room temperature in biotinylated secondary antibodies (Jackson ImmunoResearch Laboratories Inc., West Grove, PA, USA) diluted 1:300 in Tris buffer containing 2% normal serum, followed by 3 washes in Tris-buffer and an incubation for 30 min in ABC solution (Vectastain Elite kit; Vector Laboratories, Burlingham, CA, USA). After washing them again, sections were stained by the immunoperoxidase reaction combining 3,3-diaminobenzidine (DAB; Sigma–Aldrich Inc.) in Tris, pH 7.7, with hydrogen peroxide for 5-15 min. Finally, sections were washed 3 x 10 min in PBS, mounted onto gelatinized glass slides, air-dried overnight, dehydrated through ethanol, cleared in xylene and coverslipped with resinous (Eukitt™; Sigma-Aldrich) mounting medium.

Nissl Staining

To determine the pattern of degeneration in response to IHK and the placement of EEG electrodes, a 1:12 series of sections were Nissl-stained with Cresyl violet. The slides were dipped successively in the following solutions: 5 min in dH_2O, 5 min in filtered Cresyl violet solution ($C_{18}H_{15}N_3O_3$, M 321.34, Fluka BioChemika, Cat. no. 10510-54-0), 30 sec in dH_2O and cleared in 96% ethanol containing 0.5% acetic acid until the desired coloration was obtained, 5 min in isopropanol, 5 min in isopropanol:Xylene (1:2) and 4 times dehydrated in xylene for 2 min. Finally, the slides were coverslipped with Eukitt.

Visual scoring and image acquisition

An Axioscop 2 microscope (Carl Zeiss AG, Jena, Germany) with bright-field illumination and either a 10x, 20x objective or 40x oil immersion objective was used for visual scoring and acquiring images for display. Digital images were taken with a color digital camera (AxioCam MRc5) and the corresponding software AxioVision 4.5 (Carl Zeiss AG, Jena, Germany).

Merging and cropping of images, adjustments of brightness and contrast were performed using Adobe Lightroom CC, Photoshop CC and Illustrator CC. All adjustments made were identical for each staining.

Table 3 List of primary antibodies.

Target	Distributor	Description, Ref. no.	Dilution	Marker of
CD3ε	BD Biosciences Pharmingen	Armenian hamster, 145-2C11, 01081D	1:1000	CD3+ T-cells
CD4	BD Biosciences Pharmingen	Rat, L3T4, 09421D	1:1000	CD4+ T-cells
CD8a	BD Biosciences Pharmingen	Rat, monoclonal, 01041D	1:1000	Cytotoxic CD8+ T-cells
CD68	AbD Serotec Ltd, Oxford, UK	Rat, monoclonal, clone FA11, MCA1957GA	1:2000	(Activated) microglia
F4/80	Abcam, UK	Rat, monoclonal, b6640	1:1000	Monocytic lineage (tissue macrophages, microglia)
GFAP	Dako Schweiz AG, Baar, Switzerland	Rabbit, polyclonal, Z334	1:20’000	(Activated) astrocytes
Iba1	Wako	Rabbit, polyclonal, 019-19741	1:3000	Microglia
Neuropeptid Y (NPY)	Peninsula Lab.	Rabbit, serum, T-4069	1:1000	NPY+ interneurons and mossy fiber tract
Parvalbumin (PV)	Incstar	Rabbit, serum, 24428	1:5000	PV+ interneurons
ZnT3	Synaptic Systems	Rabbit, polyclonal, 197002	1:1000	Mossy fiber tract (focus)

Densitometry analysis

Densitometry analyses of immunoperoxidase staining intensity were performed using the MCID software (MCID Elite 6.0, InterFocus Imaging Ltd., Cambridge, UK). Images were digitized using a precision illuminator (Nothern light Model B95, Imaging Research Inc., Brock University, St.Catharines, Canada) and CoolSnap cf photo-camera (Photometrics, Tuscon, AZ, USA) with a Micro-Nikkor (55 mm + 12 mm) objective (Nikon Corporation). After grey values

were calibrated (Kodak step tablet no. 310ST607), the intensity values in the different regions of interest acquired. Each intensity value was normalized to the intensity of the whole section to correct for variations in background staining.

Stereological analysis

The number of F4/80+ macrophage-like cells was determined stereologically using an Axioplan 2 bright-field microscope (Carl Zeiss AG, Feldbach, Switzerland) with 20x (air, NA 0.75) objective and an integrated digital camera (MicroFIRE, Optronics AG, Goldach, Switzerland). The granule cell layer and molecular layer of the dentate gyrus were outlined and the number of macrophage-like cells within these regions were counted with Mercator software (Mercator Pro rev. 7.8.2, Explora Nova, La Rochelle, France). The thickness of each layer was estimated by dividing the length of the area by its perimeter. For each mouse, the number of macrophage-like cells and the estimated thickness was averaged over all sections.

Statistical Analyses

Data are presented as mean ± standard error of the mean (SEM). Statistical analyses for multiple group comparison was performed by a one-way or two-way ANOVA with a Bonferroni *post-hoc* test. An unpaired *t* test, two-tailed, was use to compare two groups (Prism software, GraphPad version6). Statistical significance was set at $p < 0.05$ for all data shown.

Results

Characterization of histological changes in the epileptic focus and associated immune response in wildtype mice after IHK-induced epileptogenesis

For a better understanding of the histopathological changes during epileptogenesis and to confirm earlier observations emphasizing the importance of concomitant immune reactions, adult wildtype mice were injected unilaterally into the dorsal hippocampus with kainic acid (or NaCl as control), and histologically characterized at different time points after injection. Two weeks after IHK injection, when the first spontaneous recurrent seizures occur (Riban et al., 2002b), several neuropathological changes can be observed when comparing NaCl- (figure 1A) and IHK-injected mice (figure 1B). In the injected hemisphere, pyramidal cells in CA1 and CA3c, as well as hilar mossy cells are lost and dentate granule cells dispersed (figure 1B, red and black boxes), while the contralateral hemisphere appears similar to both hemispheres of the NaCl-injected control. Already 24 hours after IHK, pyramidal cells in CA1 become pyknotic (figure 1A'), whereas hilar mossy cells and most cells of CA3c already disappeared (figure 1B'). As described earlier (Bouilleret et al., 2000b; Bouilleret et al., 2000a), IHK injection also causes a focal degeneration of different interneurons. For example, PV+ interneurons are only spared in the CA3a,b of the ipsilateral dorsal hippocampus (figure 1C) whereas the rest are lost at 1 dpi (figure 1C'). A similar pattern can be observed for NPY+ interneurons. However, as a result of the IHK-induce lesion, NPY is also expressed in mossy fibers of both dorsal hippocampi (figure 1D). In addition, dentate granule cells, axons and dendrites in the molecular layer show an increased NPY-IR after IHK with a peak between 1 and 3 dpi (figure 1D'). Also in the dentate gyrus, granule cell axons (i.e. mossy fibers) synapse with granule cell dendrites in the inner molecular layer in a process called mossy fiber sprouting (figure 1E). This synaptic reorganization, which is assumed to be a consequence of neuronal loss, in particular of hilar interneurons, is gradually established and clearly evident at 10 dpi (figure 1E'). The IHK-induced neuronal loss and synaptic reorganization is accompanied by a distinct astroglial (Gouder et al., 2004; Ledergerber et al., 2006) and immune response (Zattoni et al., 2011). A local astrogliosis emerges over the progression of epileptogenesis and is visible at 14 dpi by reactive astrocytes in the ipsilateral hippocampus (figure 1F). Similarly, a strong microgliosis can be observed ipsilaterally (figure 1G), which was reported to form gradually over two weeks in CA1, in contrary to the temporary peak at 6 dpi in the dentate gyrus and CA3 (Gfeller, 2015b). The distribution of reactive microglia cells with their distinct morphological shape (figure 1G') closely reflects the

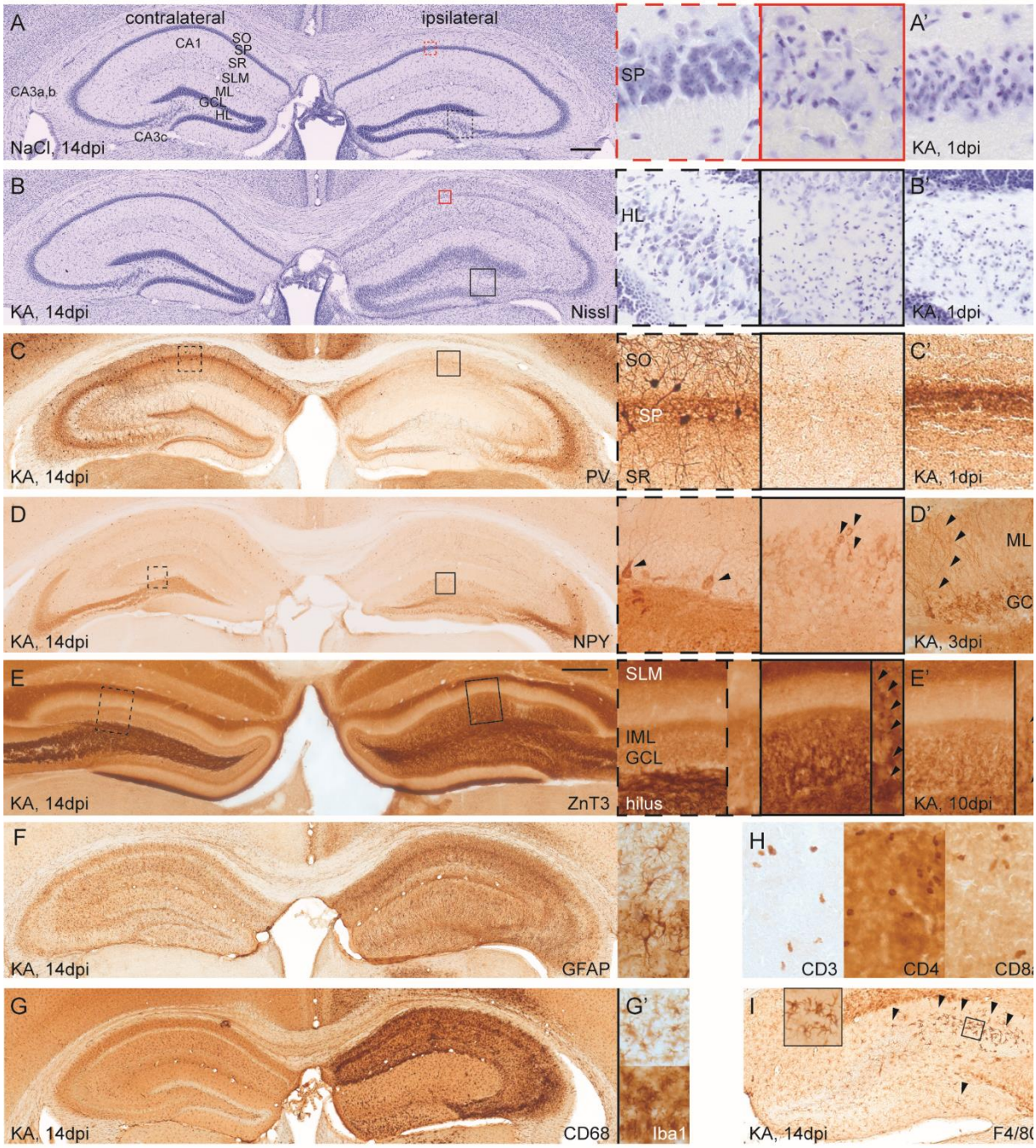

Figure 1 Characteristic changes in the epileptic focus induced by an intrahippocampal IHK injection. Nissl staining of the ipsi- and contralateral hippocampus 14 dpi after NaCl (**A**) or IHK injection (**B**). Higher magnification views showing the CA1 pyramidal cell layer (red) and the hilus-CA3c area (black) of the ipsilateral hippocampus after NaCl (dashed boxes) and IHK injection (solid boxes). Similarly, the CA1 pyramidal cell layer (**A'**) and the hilus-CA3c area (**B'**) is shown at 1 dpi after IHK. **C.** PV+ staining of a IHK injected animal at 14 dpi including a higher magnification of the contra- (dashed box) and ipsilateral (solid box) hippocampi. For direct comparison, PV-IR within the CA1 pyramidal cell layer is shown at 1 dpi (**C'**). **D.** NPY-IR marks interneurons, mossy fibers and depict in higher magnification (arrowheads), single dentate granule cells after 14 dpi. At 3 dpi, a strong NPY-IR is seen in dendrites of granule cells reaching into the molecular layer (arrowheads in **D'**). **E.** At 14 dpi, mossy fiber sprout into the inner molecular layer passing through granule cell layer (arrowheads). This process is already clearly visible at 10 dpi (**E'**). **F.** At 14 dpi, an astrogliosis is evident ipsilaterally by an increased GFAP-IR in astrocytes. **G.** The ipsilateral hippocampus shows a local microgliosis at 14 dpi. These microglia cells show an upregulation of Iba1-IR (**G'**), which is characteristic for the activated state of microglia cells. **H.** At 14 dpi, leukocytes that are positive for CD3, CD4, and CD8a migrate into the dorsal ipsilateral hippocampus (image of CA1 SR/SLM). **I.** Macrophages selectively occur in the molecular layer and the granule cell layer. Macrophage have a high F4/80-IR and can be distinguished from resident microglia cells by their shape. Scale bars, 150 µm.

neurodegenerative pattern (figure 1B). Besides the response of resident immune cells, peripheral immune cells migrate into the epileptic focus (Zattoni et al., 2011). CD3/4/8a+ leukocytes migrate into the ipsilateral hippocampus (figure 1H), first accumulating in large blood vessels (at 3 dpi), and then at 10 dpi reaching a peak intraparenchymal (Gfeller, 2015b). Peripheral macrophages, on the other side, selectively appear in the molecular layer and granule cell layer of the dentate gyrus (figure 1I), where they reached their maximum number already at 6 dpi (Gfeller, 2015b). The very high concordance between our results and previous studies underscores the reproducibility of the model and allow us to test novel specific hypotheses. The fact that during epileptogenesis different neuropathological alterations and certain immune responses share a specific temporal and spatial pattern raises the question how individual immune responses affect the formation of the epileptic focus.

Effect of prenatal immune stimulation with PolyI:C during late gestation on the pathogenesis of IHK-induced TLE in early adulthood

Maternal infections during pregnancy can cause various neurodevelopmental alterations (Knuesel et al., 2014; Meyer, 2014). Unlike many other changes, including alterations in Reelin processing and behavioral performance (Knuesel et al., 2009), a sustained increase in pro-inflammatory cytokine levels, in particular in plasma IL-1β levels, was already reported in 3-months old mice prenatally exposed to PolyI:C at GD17 (Krstic et al., 2012). To test whether a chronic rise in inflammatory cytokines affects epileptogenesis, 3-month-old wildtype mice prenatally immune challenged with PolyI:C were unilaterally injected with kainic acid into the dorsal hippocampus. The pattern and extent of neurodegeneration induced by IHK was similar between mice prenatally exposed to PolyI:C (PK) or NaCl (NK) (figure 2A). However, the accompanied microgliosis was less pronounced in the regions undergoing neurodegeneration in PolyI:C compared to saline-pretreated mice (figure 2B and B'). Comparing both intrahippocampal controls injected with saline revealed that there is no difference in microglial

Figure 2 IHK-induced epileptogenesis in prenatal immune challenged, 3-month old mice. **A.** Representative images of Nissl-stained sections to compare the neurodegenerative pattern after IHK-induced epileptogenesis in mice pretreated with PolyI:C or NaCl at 21 dpi. **B**. Pattern of CD68-IR showing the microgliosis in ipsilateral hippocampus of both groups. **B'.** Corresponding densitometry analysis of the CD68-IR in 9 hippocampal regions comparing different injection groups to each other (i.v.-intrahippocampal): NaCl-NaCl (NN), PolyI:C-NaCl (PN), NaCl-KA (NK), PolyI:C-KA (PK). **C.** Infiltration of peripheral macrophages into the ipsilateral dentate gyrus depicted by the F4/80 staining. **C'**. Corresponding stereological and volumetric analysis quantifying the number of macrophages and thickness of the granule cell layer (GCL) and molecular layer (ML). **D.** Quantitative analysis of behavioral seizures during status epilepticus (0 dpi) including (from left to right) percentage of convulsive seizures with severity 2-8, number of seizures, latency to first convulsive seizure with a severity grater or equal to 6, and duration of seizures. E. Electroencephalographic analysis of the early chronic phase (21 dpi) quantifying number and duration of seizures. Statistical significance was set at $p < 0.05$ (lines). Scale bars, 150 μm.

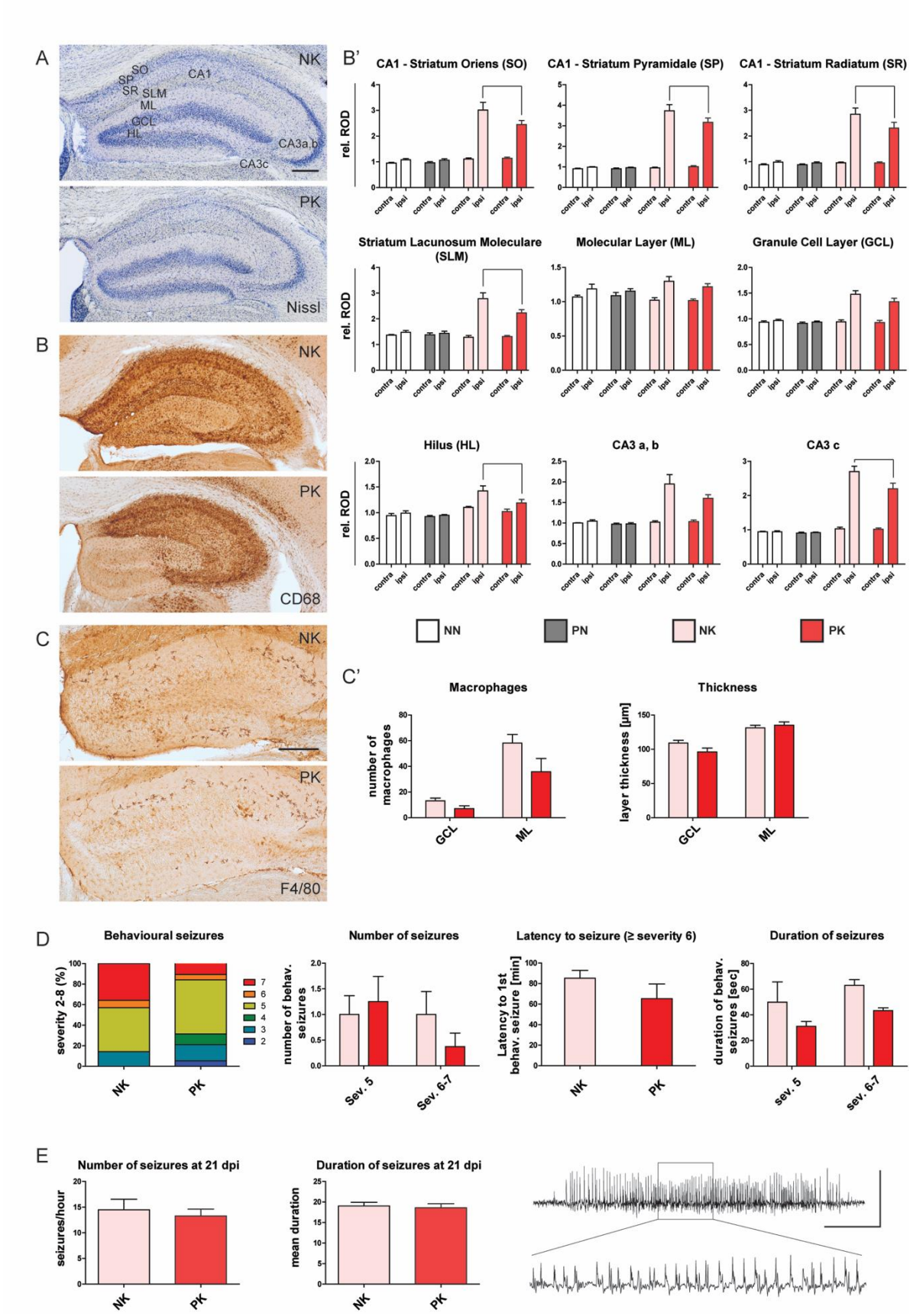
A
NK
SO
SP
SR
SLM
ML
GCL
HL
CA1
CA3a,b
CA3c
PK
Nissl
B
NK
PK
CD68
C
NK
PK
F4/80
B'
CA1 - Striatum Oriens (SO)
CA1 - Striatum Pyramidale (SP)
CA1 - Striatum Radiatum (SR)
Striatum Lacunosum Moleculare (SLM)
Molecular Layer (ML)
Granule Cell Layer (GCL)
Hilus (HL)
CA3 a, b
CA3 c
rel. ROD
contra
ipsi
NN
PN
NK
PK
C'
Macrophages
number of macrophages
GCL
ML
Thickness
layer thickness [µm]
D
Behavioural seizures
severity 2-8 (%)
Number of seizures
number of behav. seizures
Sev. 5
Sev. 6-7
Latency to seizure (≥ severity 6)
Latency to 1st behav. seizure [min]
Duration of seizures
duration of behav. seizures [sec]
sev. 5
sev. 6-7
E
Number of seizures at 21 dpi
seizures/hour
Duration of seizures at 21 dpi
mean duration

activation in 3-months old mice either prenatally immune challenged or not (NN vs. PN in figure 2B'). The recruitment of peripheral macrophages, which was previously reported to correlated with the thickness of the granule cell layer and the survival of granule cells in the dentate gyrus (Zattoni et al., 2011), was reduced in mice prenatally exposed to PolyI:C (figure 2C and C'), albeit not significantly. Interestingly, PolyI:C-pretreated mice showed fewer behavioral seizures in the range of severity 6-7 directly after IHK during SE (figure 2D). However, there was no statistical difference in the number, latency, or duration of seizures compared to NaCl-pretreated controls during the acute phase (figure 2D). EEG recordings at 7 dpi during the latent period revealed that mice prenatally exposed to PolyI:C did not show any early onset of seizures (data not shown) as reported in other immune disturbed mice (Zattoni et al., 2011). In the chronic period, when spontaneous recurrent seizures (SRS) occur (Riban et al., 2002b), the number and duration of seizures were the same in PolyI:C- and saline-pretreated mice (figure 2E). Altogether, it seems that prenatal exposure to PolyI:C during late gestation has almost no effect on the seizure pathology in the IHK model of TLE, except for fewer behavioral seizures of high severity during SE. However, a prenatal exposure to a viral mimic at GD17 seems to affect the innate immune response to an IHK-induced lesion during early adulthood.

Effect of prenatal and/or postnatal immune stimulation with PolyI:C during late gestation on the pathogenesis of acquired epilepsy in middle aged mice

To evaluate whether the effect of a previous exposure to PolyI:C on the innate immune response during IHK-induced epileptogenesis is dependent on the time-point of PolyI:C injection (prenatal vs. postnatal) or rather on the interval between the two events (3 vs. 9 months), mice either prenatally or postnatally exposed to PolyI:C or NaCl were injected with IHK at an age of 9 months. In addition, it was reported that a second immune challenge at the age of 12 months ("double hit") exacerbated central inflammatory responses in 15-months old wildtype mice prenatally injected with PolyI:C (Krstic et al., 2012). As this "double hit" model was not only associated with an increased microgliosis and astrogliosis, but also with changes related to Alzheimer's disease (AD) (Knuesel et al., 2009; Krstic et al., 2012), the postnatal PolyI:C injection was performed at the age of 6 months, whereas the IHK-induced epileptogenesis was kept 3 months apart from the PolyI:C injection, similar to the previous experiment, and was therefore conducted at an age of 9 months (for the groups compare table 1 and section *Material and Methods*).

At 21 dpi, 9-months old mice showed a similar pattern of neurodegeneration in response to IHK as 3-months old mice (figure 3A). Cresyl violet staining of hippocampal sections of IHK-treated

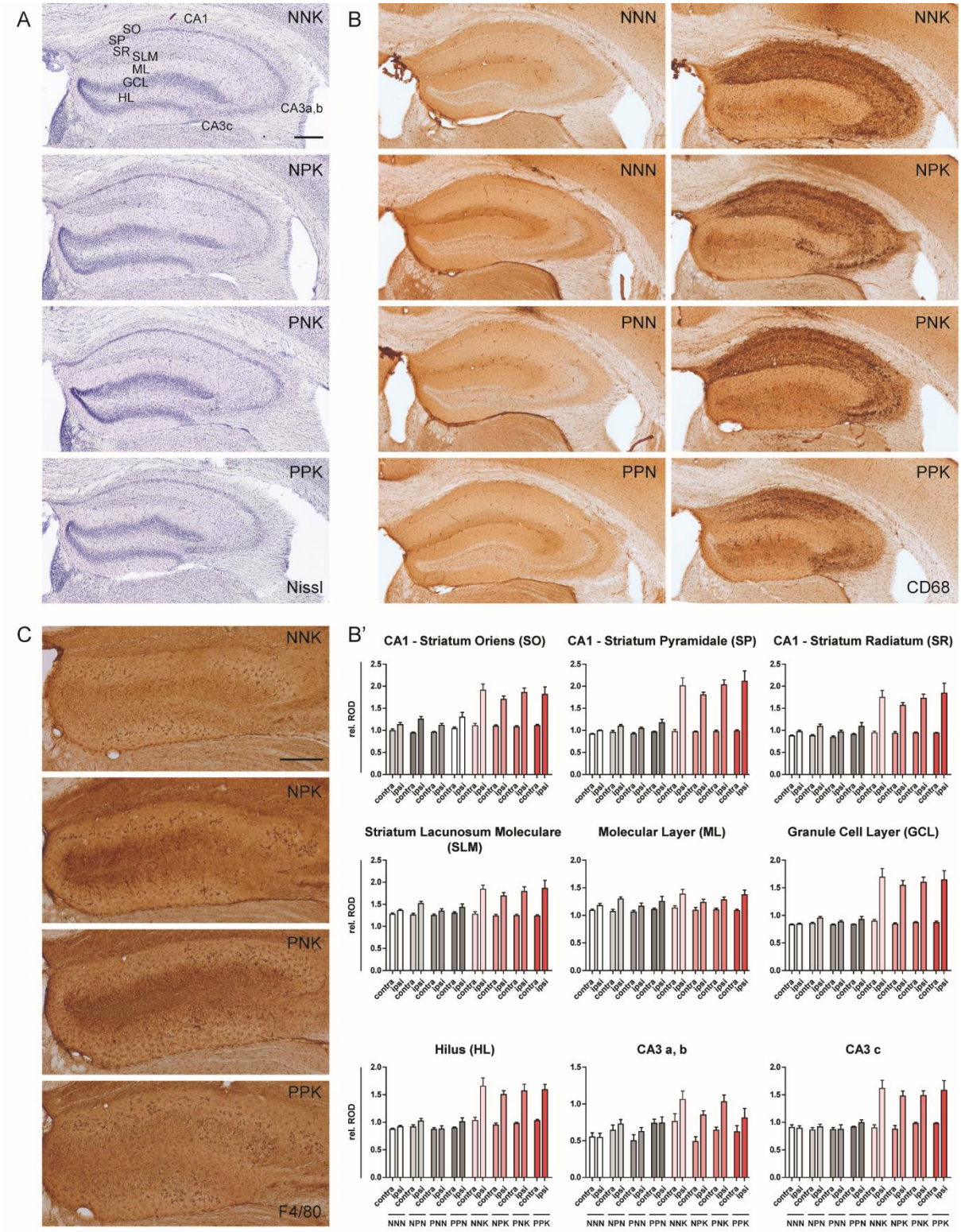

Figure 3 IHK-induced lesion and associated immune response at 21 dpi in prenatal and/or postnatal immune challenged, 9-month old mice. **A.** Bright-field microscopy images of Nissl-stained sections comparing the IHK-induced lesion in mice prenatally and/or postnatally exposed to either PolyI:C or NaCl. **B**. Microglial activity in the ipsilateral hippocampus depict by CD68-IR. **B'.** Corresponding densitometry analysis of the CD68-IR in 9 hippocampal regions comparing different injection groups to each other (prenatal i.v. – postnatal i.v. -intrahippocampal): NaCl-NaCl-NaCl (NNN), NaCl-PolyI:C-NaCl (NPN), PolyI:C-NaCl-NaCl (PNN), PolyI:C-PolyI:C-NaCl (PPN), NaCl-NaCl-KA (NNK), NaCl-PolyI:C-KA (NPK), PolyI:C-NaCl-KA (PNK), PolyI:C-PolyI:C-KA (PPK). Two-way ANOVA revealed no significant differences between intrahippocampal NaCl injected groups or between IHK injected groups (compare text). **C.** F4/80 staining visualizing infiltrating macrophages in the ipsilateral dentate gyrus of IHK injected mice. Scale bars, 150 μm.

mice revealed that the extent of both neuronal loss and granule cell dispersion was independent from a previous exposure to a viral mimic at GD17, at the age of 6 months or both. In controls intrahippocampally injected with saline, no obvious change was visible in the hippocampal and cortical cytoarchitecture (data not shown). Similarly, these control groups did not show any difference in accompanied microglial activation (figure 3B and 3B'). Therefore, the 9-months old control mice of this study, which were immune challenged with PolyI:C both at GD17 and at an age of 6 months, did not show an increase in microglia activation as it would have been expected from previous findings in 15-months old mice exposed to the "double hit" model (Krstic et al., 2012). However, IHK-induced neurodegeneration caused a massive microgliosis in the ipsilateral hippocampus of all mice (figure 3B). Two-way ANOVA revealed a significant difference in CD68-IR between IHK- and saline-treated mice (in SO, SP, SR, SLM, GCL, HL, and CA3c) and between hemispheres of IHK injected mice (in SO, SP, SR, SLM, GCL, HL, and CA3c). However, the reactive microgliosis was independent of the history of previously experienced immune challenges. Therefore, unlike in the 3-months old cohort, previous exposure to PolyI:C had no effect on IHK-induced microgliosis in 9-months old mice (figure 3B).

Visual analysis of F4/80 staining revealed no change in the invasion of peripheral macrophages (figure 3C). Macrophages were found exclusively in the ipsilateral dentate gyrus, and the number of cells were comparable between the different groups. In line with observations made in Nissl stained sections (figure 3A), the survival of dentate granule cell, which was suggested to rely on invading macrophages (Zattoni et al., 2011), was affected neither by previous immune challenges nor the age of the animal.

All groups showed a comparable sprouting of zinc-containing mossy fibers in the inner molecular layer and the pyramidal layer of CA3 (figure 4A). Both areas exhibited a clear staining for the zinc transporter ZnT3. However, in contrast to naïve 3-month-old wildtype mice at 14 dpi (figure 1E), all 9-month-old mice at 21 dpi showed a reduced ZnT3-IR in the ipsilateral hilus (figure 4A). In comparison, NPY-IR was strongly increased on the ipsilateral side, in mossy fibers and dentate granule cell layer (figure 4B). In some sections, an increased NPY-IR was found contralaterally in the most dorsal part of the lucidum, next to CA2. However, unlike the ZnT3-IR, the NPY staining was unable to reveal mossy fiber sprouting in IML and CA3, despite its presence in mossy fibers otherwise. The focal loss of NPY+ interneurons in the ipsilateral CA1 and dentate gyrus was comparable between all groups.

Altogether, the pattern of neurodegeneration, microglial activation and the extent of macrophage invasion, mossy fiber sprouting as well as NPY expression after IHK was unaffected by either a prenatal, postnatal or double immune challenge in 9-month old mice.

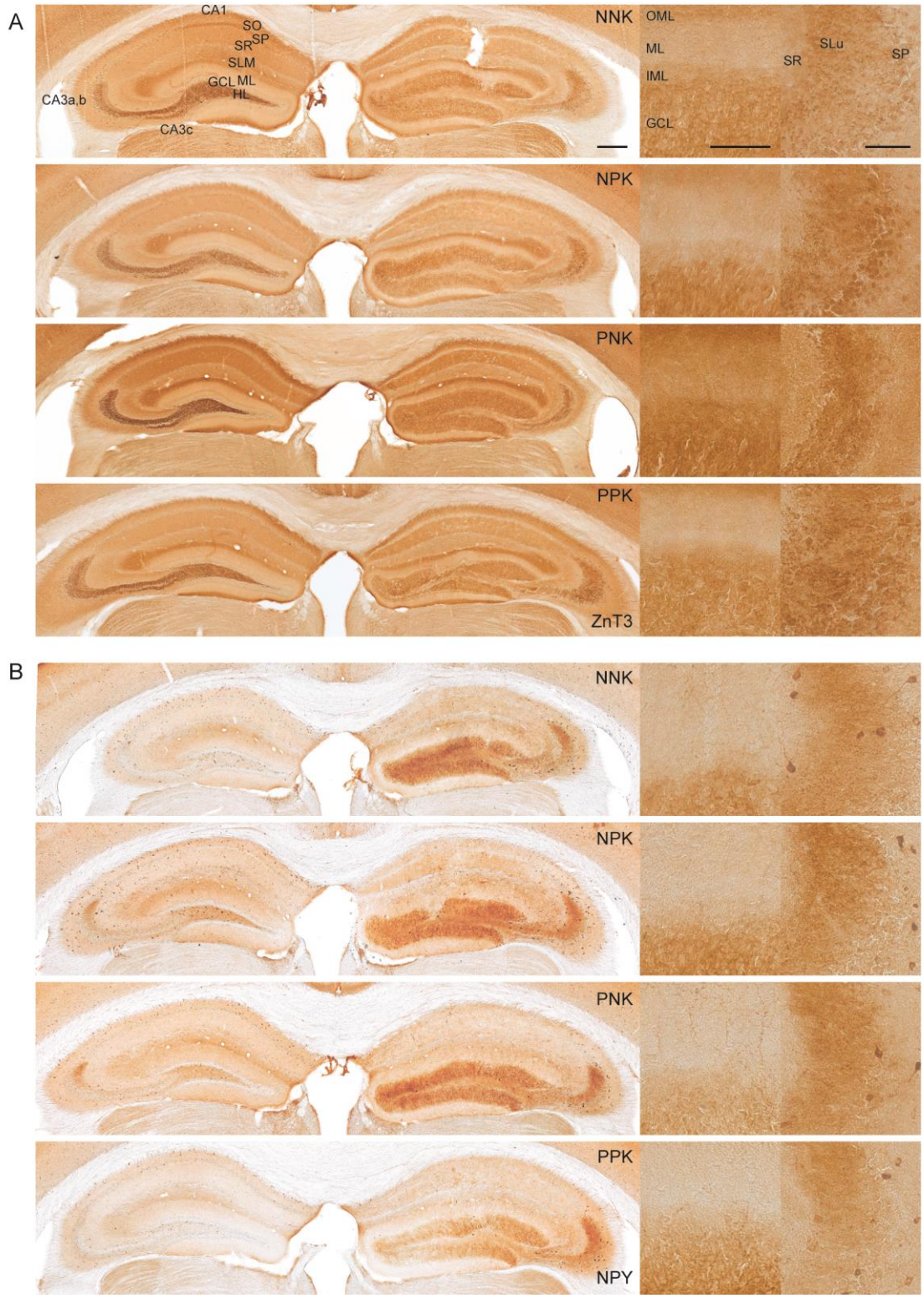

Figure 4 Axonal reorganization and NPY-expression in prenatal and/or postnatal immune challenged, 9-month old mice at 21 dpi after IHK injection. A. Axonal sprouting of zinc-containing mossy fibers in the inner molecular layer (left box) and in the pyramidal cell layer (SP) of CA3 (right box) using the zinc transporter ZnT3. All groups show a comparable extend of sprouting at 21 dpi. B. NPY-expression after IHK-induced epileptogenesis in mossy fibers and the granule cell layer. All mice show a focal loss of NPY+ interneurons in ipsilateral CA1 and dentate gyrus. Scale bars, 150 µm.

Role of NLRP3 inflammasomes during IHK-induced epileptogenesis

Inflammasomes are part of the signaling cascade involved in sensing various types of danger-signals, including the toll like receptor (TLR)-mediated response to the viral mimic PolyI:C (Latz et al., 2013; Walsh et al., 2014). Moreover, inflammasomes were shown to contribute to the activation of the innate immune system after sensing damage-signals released by cells undergoing necroptosis in different neurological diseases (Heneka et al., 2014; Walsh et al., 2014). To investigate the role of NLRP3 inflammasomes, one of the best characterized inflammasomes, in mediating the immune response after IHK-induced cell death, NLRP3-KO mice were injected with IHK. The histopathological outcome was analyzed at three different time-points: (1) at 5 dpi, when most immune cells are already present and activated, but the immune response not yet reached its maximum (figure 1; (Gfeller, 2015b)), (2) at 14 dpi, around the onset of SRS (Riban et al., 2002b), and (3) at 30dpi, when apart from the ongoing granule cell dispersion many histopathological changes already reached their final state (Bouilleret et al., 1999; Bouilleret et al., 2000b).

The histopathological changes after IHK followed the same pattern in wildtype and NLRP3-KO mice, corresponding to those described in previous studies (Bouilleret et al., 1999; Zattoni et al., 2011). In particular, a profound loss of cells in the hilus and CA3c, as well as pyknotic cells in CA1 was evident at 5 dpi, followed by a loss of CA1 pyramidal cells and progressive aggravation of the dispersion of dentate granule cells at 14 dpi and 30 dpi (figure 5A-E).

In both genotypes, the IHK-induced neurodegeneration resulted in a similar astrogliosis (figure 5A'-E'). The difference between ipsi- and contralateral side became more evident at 14 dpi and persisted until 30 dpi (contralateral not shown). GFAP-IR was primarily increased in the stratum oriens, pyramidale, radiatum and lacunosum moleculare of CA1, in the lucidum, CA3c and the hilus. In some sections, near the injection side CA3a,b was also affected. Interestingly, at 5 dpi, the pyramidal cell layer did not show any astrogliosis (figure 5A'), which is in line with earlier observations (Gfeller, 2015b).

In comparison, the pattern of microglial activation remained the same comparing the different time points (figure 5A''-E''). Increased CD68-IR was found in areas undergoing neurodegeneration including CA1, parts of CA3 and the hilus. However, no difference was found between wildtype and NLRP3-KO mice.

Peripheral immune cells were infiltrating the ipsilateral hippocampus in both wildtype and NLRP3-KO mice. Peripheral macrophages were present from day 5 until day 30 after the IHK

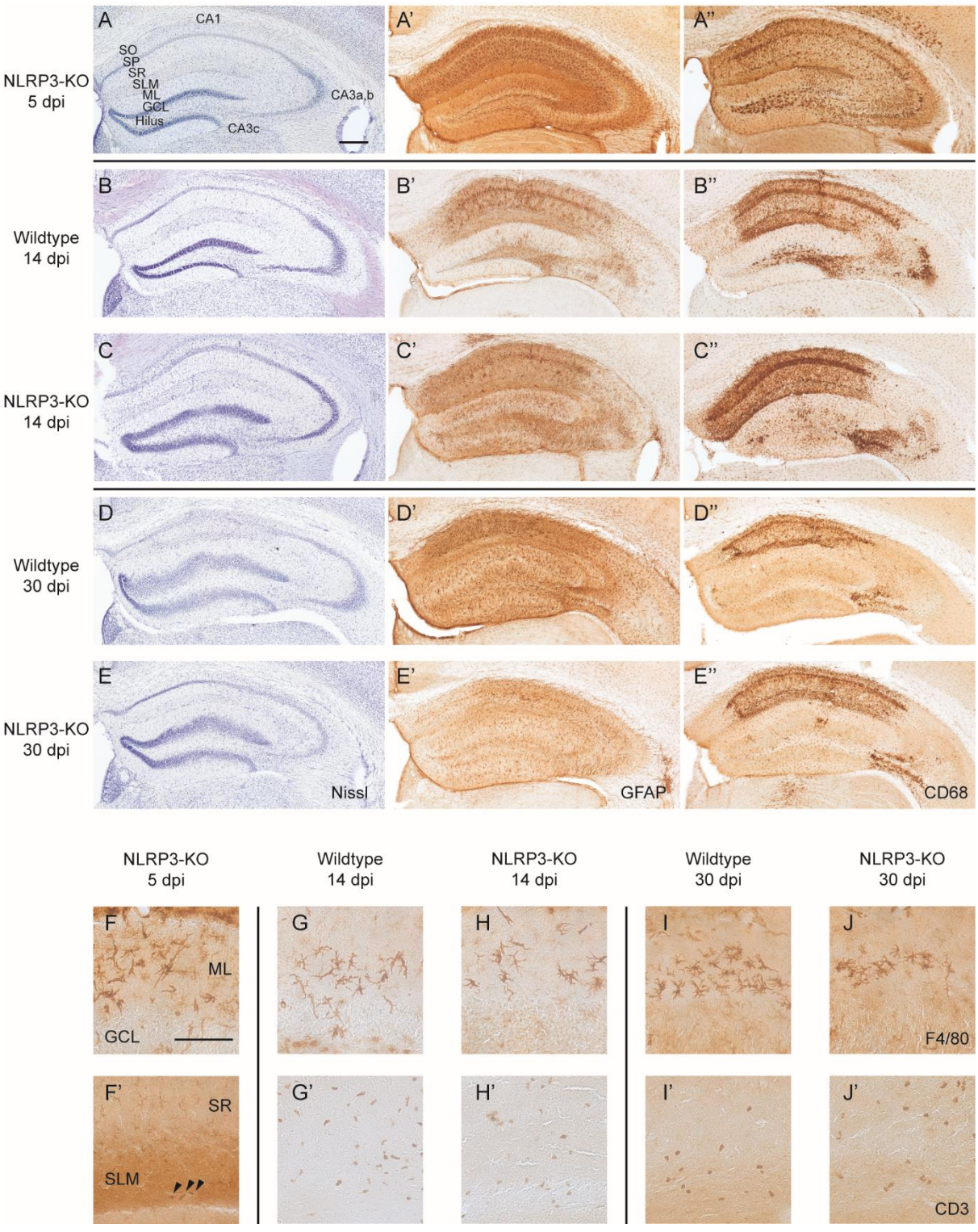

Figure 5 Neurodegenerative pattern and immune response after IHK in NLRP3-KO mice compared to wildtype mice. Nissl staining of the IHK-lesion (**A-E**), astrogliosis (**A'-E'**) and microglial activation (**A''-E''**) is depicted at 5 dpi, 14 dpi, and 30 dpi. The progression of neuronal loss, granule cell dispersion and the associated activation of astrocytes and microglia is comparable between the genotypes. The infiltration of peripheral macrophages into the dentate gyrus **(F-J**) and of CD3+ leukocytes into the ipsilateral hippocampus, shown here in CA1, (**F'-J'**) is similar between NLRP-KO and wiltype mice. Scale bars, 150 µm.

injection (figure 5F-J). In all animals, their distribution was restricted to the dentate gyrus, whereas most of the F4/80+ macrophages were found in the molecular layer. There was no obvious difference in the number of invading peripheral macrophages between the two genotypes. Similarly, the number of infiltrating CD3+ T cells did not differ between wildtype and NLRP3-KO mice (figure 5F'-J'). At 5 dpi, unlike peripheral macrophages, most CD3+ T cells were found in large blood vessels particularly of the hippocampal fissure, which is in accordance with previous findings (Zattoni et al., 2011; Gfeller, 2015b).

In conclusion, there was no difference between wildtype and NLRP3-KO mice in the pattern of neurodegeneration, astrogliosis, microglial activation, the infiltration of peripheral macrophages and of CD3+ T cells.

Role of macrophage infiltration for hippocampal granule cell survival

The lesion induced by IHK causes a local activation of the innate immune system, in particular of microglia, CNS resident monocytes. In addition, peripheral macrophages are recruited into the ipsilateral dentate gyrus and can be visualized together with microglia cells by F4/80 staining (Zattoni et al., 2011). Macrophages can be distinguished from microglia by their stronger expression of the F4/80 antigen, their larger, often elongated cell bodies, as well as having fewer and thicker processes (Andersson et al., 1991). As previously shown (Zattoni et al., 2011), both the blockage of leukocyte infiltration by anti-α4-integrin treatment and the peripheral ablation of macrophages by the toxic bisphosphonate clodronate lead to a reduced macrophage infiltration and are correlated with the presence of pyknotic cells in the granule cell layer. However, both approaches do not affect only infiltrating macrophages. To unravel the contribution of peripheral macrophages to the IHK-induced lesion, CCR2-KO mice were used, which selectively lack a chemokine receptor required for recruitment of peripheral macrophages.

As assumed, CCR2-KO mice did not show any infiltration of peripheral macrophages after IHK (figure 6A). In the dentate gyrus, F4/80 staining only revealed resident microglia. The distribution and morphology of F4/80+ microglia were similar to those of wildtype mice at 14 dpi (figure 1I; (Andersson et al., 1991; Zattoni et al., 2011)). However, in contrast to previous findings (Zattoni et al., 2011), the lack of peripheral macrophages had no effect on granule cell survival. IHK-induced granule cell dispersion in CCR2-KO mice was similar to wildtype mice, with no evidence for pyknotic cells in the dentate granule cell layer (figure 6B). Similarly, the activation of microglia cells did not differ between the two genotypes (figure 6C). Moreover, there was no clear effect on the number or distribution of infiltrating CD3+ T cells (figure 6D).

Altogether, CCR2-KO mice show no obvious difference in the IHK-induced lesion despite the lack of infiltrating macrophages.

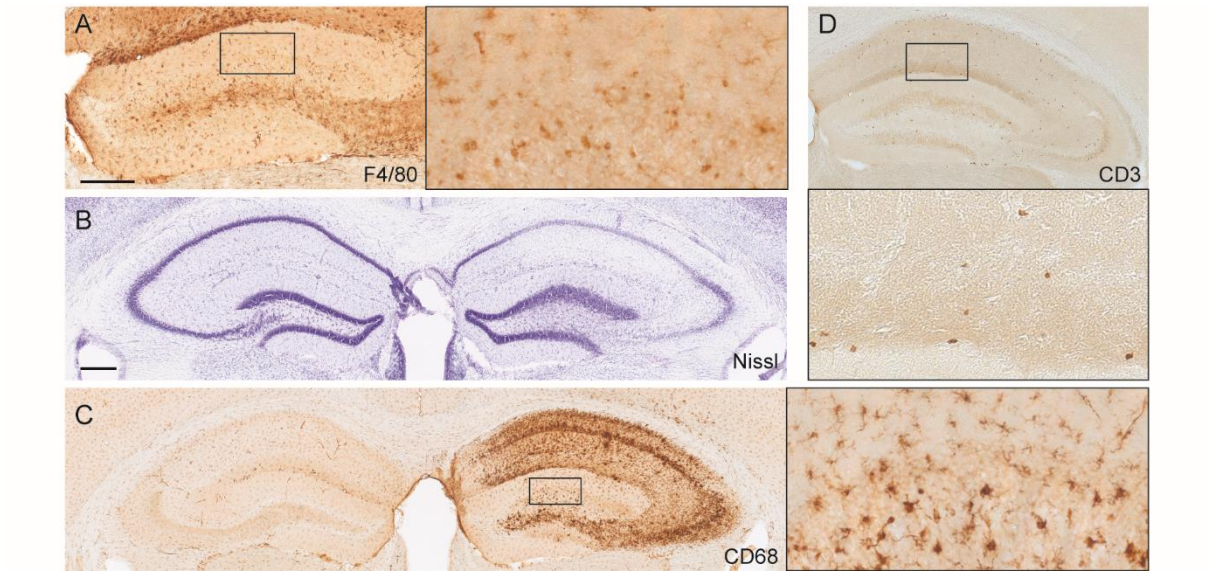

Figure 6 The role of infiltrating peripheral macrophages in the IHK-induced epileptogenesis. A. Representative image of the ipsilateral dentate gyrus stained with anti-F4/80 antibodies. Note the lack of peripheral macrophages in dentate gyrus of CCR2-KO mice at 14 dpi. **B.** CCR2-KO mice show a similar granule cell dispersion and pattern of neuronal loss as wildtype mice at 14 dpi. **C.** Lack of peripheral macrophages does not cause an excessive microglial activation in CCR2-KO mice, however, activated microglia are occasionally detected in the granule cell layer. D. CD3+ leukocytes infiltrating the ipsilateral hippocampus of CCR2-KO similar as in wiltype mice. Scale bars, 150 µm.

Discussion

The present study highlights the importance of innate immune responses during epileptogenesis and reveals their contribution in the formation of an epileptic focus in a model of TLE. Firstly, the course of epileptogenesis was examined in a mouse model of chronic inflammation. Chronic inflammation was induced by systemic PolyI:C, prenatally and/or postnatally, shown to 'prime' microglia (Krstic et al., 2012; Krstic and Knuesel, 2013; Perry and Holmes, 2014). Unexpectedly, a prenatal immune challenge had no effect on the development of IHK-induced seizures (figure 2). Except fewer behavioral seizures of high severity during SE and a slightly reduced microglial activation during the chronic phase, prenatally immune challenged mice showed a similar histopathology and number of seizures after IHK injection. Even multiple systemic challenges with PolyI:C had no effect on the neurodegenerative pattern and the associated axonal reorganization in the IHK model of TLE (figure 3 and 4). A major caveat of this study, though, is the lack of independent evidence that the PolyI:C treatment induced the expected effect, as published, on immune system activation, precluding any definitive conclusion from our negative results. Secondly, the role of NLRP3 inflammasomes during epileptogenesis was investigated, in particular their contribution to the inflammatory response following IHK-induced SE. As part of the signaling cascade sensing foreign and host-derived danger signals, inflammasomes mediate the microglial production of pro-inflammatory cytokines and are most likely involved in microglial priming (Latz et al., 2013; Heneka et al., 2014; Walsh et al., 2014). However, the lack of NLRP3 did not affect the IHK-induced lesion (figure 5). NLRP3-KO mice showed a similar activation and infiltration of innate and adaptive immune cells as wildtype mice. Thus, NLRP3 seems not pivotal for the inflammation-associated neurodegeneration following the IHK-induced SE. Finally, it was never explicitly confirmed whether the presence of infiltrating macrophages in the dentate gyrus is responsible for the survival of dentate granule cells. Previous findings showed that peripheral depletion of infiltrating macrophages using clodronate liposomes leads to a degeneration of dentate granule cell in the IHK model of TLE (Zattoni et al., 2011). However, clodronate depletes circulating monocytes (Van Rooijen and Sanders, 1994; Tacke et al., 2007) and not only affects the focal infiltration of F4/80+ macrophages into the ipsilateral dentate gyrus. Hence, CCR2-KO mice were injected with IHK to investigate the pathogenesis of TLE in mouse a model selectively missing an important chemokine receptor for the recruitment of macrophages (Boring et al., 1997; Mack et al., 2001). Surprisingly, the lack of infiltrating macrophages in CCR2-KO mice did not cause a

degeneration of dentate granule cells (figure 6) as previously reported (Zattoni et al., 2011). Therefore, the early infiltration of peripheral macrophages selectively into the ipsilateral dentate gyrus seems not responsible for the granule cell survival.

Contribution of peripheral inflammation to seizure susceptibility and its effect on the pathogenesis of acquired epilepsy

Several studies reported that peripheral immune stimulation lowers the seizure threshold and affects the pathogenesis of epilepsy. Most studies focussed on the acute effect of a systemic immune challenge on the development of evoked seizures, preceding the application of pro-convulsives or electrical kindling by several hours up to a couple of days (Auvin et al., 2007; Galic et al., 2008; Kwon et al., 2010; Kirschman et al., 2011; Lee et al., 2012; Michalovicz and Konat, 2014). However, very little research examined the effect of chronic elevation of pro-inflammatory cytokines on the generation of seizures (Qulu et al., 2012; Pineda et al., 2013). In this respect, infectious exposure during pregnancy is of major interest. Clinical and preclinical evidence suggest that maternal immune activation, in particular through microglial priming, pose a risk for the development of epilepsy (Knuesel et al., 2014). For example, Pineda et al. (2013) reported that repeated prenatal immune challenge with PolyI:C from GD12 to 16 increases hippocampal excitability, accelerates kindling rate, and prolongs increased seizure susceptibility for a few weeks. Moreover, this PolyI:C-induced pro-epileptic phenotype was dependent on IL-1β and IL-6. Similarly, maternal restraint stress at GD14 exacerbated febrile seizures induced by postnatal injection of lipopolysaccharide (LPS) and kainic acid, as well as lead to an increased expression of IL-1β (Qulu et al., 2012). In contrast, prenatal stimulation with PolyI:C at GD17 did not affect the development of acquired epilepsy in the present study. The seizure susceptibility and the innate immune response was rather reduced in mice pre-exposed to PolyI:C contradicting previous observations made during a pilot study (data not shown). A comparable discrepancy was found in 9-month-old mice prenatally and postnatally exposed to PolyI:C. While a similar ‘double hit’ with PolyI:C evoked an increased microglial activation in previous experiments conducted in our lab (Krstic et al., 2012), there was no effect of PolyI:C found in the present study.

Our observations after a PolyI:C ‘double hit’ are in line with those of another recent study from our lab (Notter, 2015), which used a similar cohort of mice as the present study. The inability to replicate previous findings made by our lab raised questions how the PolyI:C-treated cohorts in the recent studies differ from our earlier once (Krstic et al., 2012). Notter (2015) addressed those differences focusing on the mouse strain, the stress exposure of pregnant dams, and a possible

litter effect. In brief, the recently used C57Bl/6JOla strain differs from the earlier used C57Bl/6JRcc strain (Krstic et al., 2012) in particular by carrying a spontaneous mutation associated with a suppressed α-synuclein expression. Changes in α-synuclein, which were shown to be involved in the assembly of the SNARE complex (Burré et al., 2010) and associated with glucocorticoid-induced apoptosis in patients with Parkinson's disease (Kim et al., 2004), might be responsible for the different results. Moreover, Notter (2015) indicated that in previous experiments (Krstic et al., 2012) time pregnant mice were mated in-house compared to the shipment of pregnant dams at GD14 in the present experiment. It was pointed out that a potential stress-induced raise in corticosterone levels at GD14, which together with other sequelae can be detected for several days after arrival (Landi et al., 1982; Tuli et al., 1995), might interfere with the response of a maternal infection at GD17.

As described above, 3 month-old mice prenatally exposed to PolyI:C showed a trend towards a reduced immune activation and neuronal excitability after IHK (figure 2). Although, the effect of a previous immune challenge tends in different direction as suspected, the relationship between immune activation and neuronal excitability is in line with previous findings. Thus, the present study was unable to replicate the increase immune response after pre-exposure to PolyI:C (Krstic et al., 2012), probably due to the differences mentioned earlier. However, our results support a synchronous mode of behavior between immune activation and neuronal excitability.

Inflammatory cytokines, neuronal excitability and the role of inflammasomes

The immune response following IHK is associated with a change in the cytokine profile and the release of pro-inflammatory cytokines (Benson et al., 2015). Beside their role in orchestrating the inflammatory response, pro-inflammatory cytokines were shown to modulate neuronal excitability (reviewed in (Fabene et al., 2010; Riazi et al., 2010; Galic et al., 2012; Balosso et al., 2013; Liimatainen et al., 2013; Vezzani and Viviani, 2015)). For example, it was shown that microglia, astrocytes and endothelial cells in the epileptic focus show an acute increase in the pro-inflammatory cytokine IL-1β during seizures (Vezzani et al., 1999b; De Simoni et al., 2000; Ravizza et al., 2008b; Ravizza et al., 2008a). Together with other inflammatory cytokines, including TNF-α and IL-6, which are also upregulated, IL-1β has neuromodulatory properties affecting synaptic transmission and neuronal excitability (Viviani et al., 2003; Yang et al., 2005; Gardoni et al., 2011a). The pathway underlying IL-1β-mediated increase in neuronal excitability depends on the myeloid differentiation primary response protein (MyD88), which can also be recruited by TRLs (Vezzani et al., 1999b; Viviani et al., 2003; Balosso et al., 2013). In neurons, the activation of TLR4 through molecules released by necrotic cells or distressed cells, so-called

damage-associated molecular patterns (DAMPs), in particular high-mobility group box-1 (HMGB1), leads to an increased excitability, which is partially mediated by NMDA receptors (Maroso et al., 2010). However, in microglia, the DAMP signaling contributes to a change in the activation state of the cell accompanied by an upregulation of the production of IL-1β (Saijo and Glass, 2011).

Recent studies revealed that the production of IL-1β is mediated by inflammasomes (Latz et al., 2013). However, the lack of NLRP3 inflammasomes, which were shown to be important for an excess expression of microglial IL-1β in different neurological disorders (Heneka et al., 2014; Walsh et al., 2014), had no effect on the development of a pro-epileptic lesion in the present study (figure 5). The lack of a phenotype in IHK-injected NLRP3-KO mice might be explained by the complex molecular pathway underlying microglial activation and expression of IL-1β. For example in an ischemic brain injury model, Denes et al. (2015) showed that AIM2 (absent in melanoma 2) and NLRC4 (NLR family, CARD domain containing 4) inflammasomes, but not the NLRP3 inflammasome, are involved in inflammation and injury after middle cerebral artery occlusion (MCAo). Interestingly, while the number of IL-1β+ microglia was similar in all genotypes, only AIM2-KO mice and NLRC4-KO mice showed a reduced microglial activation, leukocyte recruitment, and infarct size. Thus, in the MCAo model of ischemic brain injury, both neurodegeneration and inflammation were found to be independent from the IL-1β production and the activation of the NLR3 inflammasome (Denes et al., 2015). Similar to these findings, the lesion and inflammation during IHK-induced epileptogenesis were not dependent on the NLRP3 inflammasome as described in the present study. Although, without following the course of epileptogenesis electroencephalographically, no explicit conclusions can be drawn about putative changes in neuronal excitability caused by a knockout of NLRP3. Nevertheless, the comparable pattern of neurodegeneration and immune activation as well as similar behavioral response during SE (data not shown) in NLRP3-KO mice provide evidence that these mice follow the same disease progression as wildtype mice after IHK. The comparable histopathology in wildtype and NLRP3-KO mice suggest further that NLRP3 signaling is not essential for the IL-1β production after IHK-induced lesion. This is supported by observations that increased IL-1β levels exacerbate the initial neuronal loss (Noè et al., 2012) and are involved in the recruitment of leukocytes during epileptogenesis (Ravizza et al., 2008b; Zattoni et al., 2011). Together with the large body of literature emphasizing the role of IL-1β in establishing an epileptic focus, an NLRP3-independent production of IL-1β in the IHK model of TLE seems likely and would need to be confirmed by measuring IL-1β levels in epileptic NLRP-KO mice.

Recruitment of peripheral immune cells and the role of infiltrating macrophages

The injury-induced release of cytokines and chemokines is involved in the recruitment of peripheral immune cells, which in turn were shown to be pivotal for the course of epileptogenesis (Manley et al., 2007; Fabene et al., 2008; Ravizza et al., 2008b; Deprez et al., 2011; Zattoni et al., 2011; Arisi et al., 2015; Varvel et al., 2016). The contribution of infiltrating immune cells in the formation of an epileptic lesion and the occurrence of SRS were studied in different animal models of TLE. The anti-α_4-integrin treatment reduced the infiltration of CD3+ T cells and F4/80+ macrophages, while causing a more severe neuronal loss in CA3 and the dentate gyrus of IHK-injected wildtype mice (Zattoni et al., 2011). In the same TLE model, macrophage depletion by clodronate liposomes was associated with the exact same neurodegenerative sequelae. However, Zattoni et al. (2011) showed that both treatments have a positive effect on the exacerbated IHK-induced neurodegeneration in a mouse model lacking B and T cells, the RAG1-KO strain. In these immune deficient mice, both treatments interfered with the invasion of neutrophils into the ipsilateral hippocampus, immune cells which are not present in IHK-injected wildtype mice (Zattoni et al., 2011). Similarly, in the pilocarpine model of TLE, where wildtype mice exhibit invading neutrophils in areas undergoing neurodegeneration, an interference with infiltrating leukocytes or a specific depletion of neutrophils reduced both the occurrence of SRS and the neuronal loss (Fabene et al., 2008). Apart from the aggravating nature of invading neutrophils, these findings suggested a possible protective role of lymphocytes, which is missing in RAG1-KO mice and seems to be responsible for the early seizure onset in those mice (Zattoni et al., 2011). More generally, these results highlight the importance of a strong interaction between the innate and the adaptive immune system during epileptogenesis.

So far, all treatments or mouse models, which did include a change in macrophage infiltration, also influenced the survival and dispersion of dentate granule cells during IHK-induced epileptogenesis (Deprez et al., 2011; Zattoni et al., 2011). While none of these approaches solely affected the recruitment of macrophages, mice devoid of the chemokine receptor CCR2 were used in the present study. Unlike previous findings, the selective interference with macrophage recruitment did not affect granule cell dispersion or survival in the IHK model of TLE. There was no increase in microglial activation. However, CCR2-KO mice showed a rather low number of infiltrating CD3+ T cells compared to wildtype mice 14 days after IHK injection. Although, the difference was not unambiguous, it might be interesting to examine the ratio of CD4+ to CD8+ T cells in those mice. This might be especially interesting, as Deprez et al. (2011) showed

that the adoptive transfer of T lymphocytes in immune deficient mice strongly influenced the infiltration of F4/80+ macrophages. Grafting of the missing T cell population blocked the macrophage infiltration and abolished the granule cell dispersion in mice lacking CD4+ T cells (MHCII-KO), while in mice lacking CD8+ T cells (β2-microgloblin-KO) it caused an enhanced recruitment of macrophages and an increased dispersion of dentate granule cells (Deprez et al., 2011). Therefore, positive signals provided by CD8+ T cells and negative signal emanating from CD4+ T cells might not only affect the macrophage infiltration as earlier suggested (Deprez et al., 2011), but rather could have a direct influence on the survival and dispersion of granule cells, for example through regulation of microglial activation or secretion of neurotrophic factors like BDNF (Kerschensteiner et al., 1999; Duveau et al., 2011; Chan et al., 2015).

Varvel and colleagues (2016) recently investigated the contribution of CCR2+ monocytes in two models of TLE. They showed that systemic kainic acid-induced SE, which causes a lesion in CA3, leads to the recruitment of CCR2+ monocytes through the expression of CCL2 by microglia and perivascular macrophages. In contrast to the IHK model, these infiltrating macrophages were only detected transiently, at 3 dpi, and were missing later on, at 14 dpi. Similarly, CCR2+ monocytes were infiltrating regions undergoing neurodegeneration in the pilocarpine model. In both TLE models, CCR2-KO mice showed a similar seizure severity sore during SE as wildtype mice. However, CCR2-KO mice showed a reduction in the number of Iba1+ microglia in CA3 compared to wildtype mice after systemic kainic acid. While no obvious difference in microglial activation between genotypes was noticed in the IHK model (figure 6), these discrepancies delineate the peculiarities of the different TLE models. Unlike for the systemic application of a pro-convulsive (Varvel et al., 2016), IHK-induced infiltration of peripheral macrophages is restricted to the dentate gyrus, an area not affected by conspicuous neuronal loss. Despite discrepancies between different models of TLE, the interaction between different immune cells seems to be important for the coordination of various processes (e.g. neuronal protection or phagocytosis) involved in formation of the epileptic focus.

Conclusions

Despite the absence of chronic neuroinflammation after pre-exposure to PolyI:C, our data concur with previous findings highlighting the importance of the innate immune response for neuronal excitability. Further, we uncovered that the NLRP3 inflammasome, which was proposed to be pivotal for the IL-1β-mediated increase in neuronal loss and excitability, does not affect the

IHK-induced lesion. Finally, we show that the survival and dispersion of dentate granule cells are independent of the infiltration of peripheral macrophages.

STUDY II: CONTRIBUTION OF EARLY ALZHEIMER-RELATED PATHOPHYSIOLOGY ON THE DEVELOPMENT OF ACQUIRED EPILEPSY

Tilo Gschwind[1,2], Carlos Lafourcade[1,3], Tim Gfeller[1], Mariana Zaichuk[1,2], Lukas Rambousek[4], Irene Knuesel[1,5] and Jean-Marc Fritschy[1,2]

[1]Institute of Pharmacology and Toxicology, University of Zurich, Winterthurerstrasse 190, 8057 Zurich, Switzerland,

[2]Neuroscience Center Zurich, University of Zurich and ETH Zurich, 8057 Zurich, Switzerland,

[3]Laboratorio de Neurociencias, Universidad de los Andes, Santiago, Chile,

[4]Institute of Experimental Immunology, University of Zurich, Winterthurerstrasse 190, 8057 Zurich, Switzerland,

[5]Roche Pharmaceutical Research and Early Development, NORD Discovery & Translational Area, Roche Innovation Center Basel, Grenzacherstrasse 124, Basel, Switzerland

submitted

Author's contribution

All IHK experiments were carried out by TGs and TGe. Electrophysiology experiments were performed by CL and TGs. BrdU and eGFP experiments were carried out by MZ. Histology and qPCR experiments in naïve mice were conducted by TGs and LR. TGs and JMF wrote the manuscript. Authors have no conflict of interest to declare.

Abstract

Neuronal network dysfunction is frequently associated with Alzheimer's disease (AD). In patients and in animal models of AD, aberrant epileptic activity is detectable already at early disease stages. However, it is unknown whether AD-pathology renders neuronal networks more susceptible to development of acquired epilepsy. Here, we report that 3-months-old ArcticAβ mice, an AD mouse model without any amyloid deposition at this age, are more susceptible to seizures induced by unilateral intrahippocampal injection of kainic acid (IHK). In this temporal lobe epilepsy model, IHK-induced status epilepticus is followed by occurrence of spontaneous recurrent seizures (SRS) after two weeks. ArcticAβ mice exhibited more severe status epilepticus and early onset of SRS. The electrophysiological signature of this hyperexcitable phenotype was characterized in CA1 neurons by decreased synaptic strength, increased kainic acid-induced LTP, and reduced frequency of spontaneous inhibitory currents. However, ArcticAβ mice did not display any major difference in neurodegeneration, neuroinflammation, axonal reorganization or adult neurogenesis compared to wildtype littermates, either prior to or following IHK-induced epileptogenesis. Expression of neuropeptide Y (NPY) was reduced at baseline and its IHK-induced elevation in mossy fibers and granule cells was attenuated in 3-months-old ArcticAβ mice. However, although alteration in NPY signaling might underlie premature seizure onset, neutralization of soluble Aβ species by Aβ-specific antibody (6E10) ameliorated the hyperexcitable phenotype of ArcticAβ mice and prevented early SRS onset. These results suggest that development of seizures at early stages of AD is mediated primarily by Aβ species causing widespread changes in synaptic function.

Significance statement

Although Alzheimer's disease (AD) and epilepsy are separate syndromes, the pathogenesis of AD is associated with a high incidence of aberrant network activity, including unprovoked limbic seizures. To unravel the contribution of AD-like pathology to the development of a pro-epileptogenic environment, we analyzed ArticAβ transgenic mice in a model of temporal lobe epilepsy, induced by intra-hippocampal kainic acid injection. We observed that these AD-transgenic mice are more susceptible than wildtype littermates to the effects of kainate and exhibit early onset of spontaneous recurrent seizures. Ameliorating the hyperexcitable phenotype of AD-transgenic mice with an antibody against Aβ delayed seizure onset, suggesting that soluble Aβ species alter network functions prior to plaque formation, contributing to the occurrence of unprovoked seizures.

Introduction

Alzheimer's disease (AD) is the most prevalent age-related dementia, characterized by progressive neuronal dysfunctions. Early stages of AD and other age-related dementia are associated with aberrant network activity, including a high incidence of unprovoked epileptic seizures (Hesdorffer et al., 1996; Amatniek et al., 2006; Scarmeas et al., 2009; Vossel et al., 2013; Vossel et al., 2016). Early neurochemical alterations render neuronal networks susceptible to seizure generation (Palop and Mucke, 2016). Indeed, different AD mouse models exhibit neuronal hyperactivity and even interictal spikes long before the occurrence of plaques (Busche et al., 2012; Kam et al., 2016). While hyperexcitability reduces seizure threshold in AD-transgenic mice (Palop et al., 2007; Roberson et al., 2007; Westmark et al., 2008; Born et al., 2014), it is unknown whether it is causally related to onset of spontaneous recurrent seizures (SRS).

AD and epilepsy, in particular temporal lobe epilepsy (TLE), share major pathogenic mechanisms, including neurodegeneration, synaptic dysfunction, inflammation, and altered adult neurogenesis. In mouse TLE models, loss of parvalbumin- (PV), calbindin- (CB), somatostatin- (SOM) and neuropeptide Y (NPY) -expressing interneurons occurs in CA1 and dentate gyrus early during epileptogenesis (Bouilleret et al., 2000b; Bouilleret et al., 2000a; Andre et al., 2001). Similarly, different AD mouse models show reduced numbers of interneurons in these regions (Ramos et al., 2006; Mahar et al., 2016); and functional impairments of PV interneurons were directly related to network hypersynchrony in parietal cortex (Verret et al., 2012). In dentate gyrus granule cells (GC), calbindin expression is disease stage-dependently reduced in AD mouse models and AD patients (Palop et al., 2003; Stefanits et al., 2014). Moreover, TLE is characterized by recurrent sprouting of mossy fiber collaterals (Buckmaster, 2012) and by ectopic expression of NPY in GCs (Marksteiner et al., 1990; Tonder et al., 1994; Vezzani et al., 1999c). AD-transgenic mice revealed a similar adaptation to a hyperexcitable network, including mossy fibers sprouting onto GABAergic basket cells and hilar interneurons (Palop et al., 2007). In both TLE and AD, activation of innate immunity is an important pathogenic feature. For instance, in TLE, secreted cytokines render the neuronal network hyperexcitable and thereby more susceptible to seizures (Viviani et al., 2003; Maroso et al., 2010; Gardoni et al., 2011b). Likewise, amyloid β recruits microglia (Alzheimer et al., 1995; Meyer-Luehmann et al., 2008; Wang et al., 2015) and thus triggers inflammatory cytokine release, causing various sequelae associated with AD (Heneka et al., 2013). Finally, neurogenesis is altered in both TLE and AD.

Prolonged seizure activity transiently increases precursor cell proliferation (Parent et al., 1997; Jessberger et al., 2005), followed by neurogenic niche destruction and impaired hippocampal neurogenesis (Kralic et al., 2005; Ledergerber et al., 2006; Sierra et al., 2015). In AD, survival of newborn neurons is impaired in mice with plaque-burden (Verret et al., 2007), while in young AD transgenic, accelerated development of newborn GC leads to impaired dendritic maturation (Sun et al., 2009).

It is difficult to disentangle which AD-related changes directly contribute to seizure development and which are by-products of a hyperexcitable environment. Therefore, we investigated TLE-related epileptogenesis in ArcticAβ mice (Knobloch et al., 2007), overexpressing human APP transgene containing the Swedish and Arctic mutations. Since neuronal dysfunctions associated with Aβ pathology occur prior to plaque deposits (Billings et al., 2005; Busche et al., 2012; Kam et al., 2016), it is possible to separate the two phenomena. We monitored the clinical course of epileptogenesis induced by intrahippocampal injection of kainic acid (IHK) in young adult ArcticAβ mice and wildtype littermates. IHK induces a status epilepticus followed by a seizure-free 2-week latent period preceding SRS onset (Suzuki et al., 1995b; Bouilleret et al., 1999; Riban et al., 2002a), allowing to causally determine the role of early AD-related neurochemical alterations for epileptogenesis and TLE development, as assessed by chronic EEG recordings and immunohistochemical analysis. Finally, we tested the possible role of soluble Aβ species (Benilova et al., 2012a) by inactivating them intracerebrally with a neutralizing antibody.

Materials and Methods

Animals

All experiments performed for this study were carried out in accordance with the Swiss law on animal experimentation and approved by the Cantonal Veterinary Office of Zurich.

Experiments were performed with arcAβ transgenic mice (Knobloch et al., 2007) and age-matched wildtype (wt) littermates, bred at the Laboratory Animal Sciences Center of the University of Zurich. They were genotyped by PCR analysis from ear biopsies. All animals were housed at standard conditions (20-24℃; minimum 40% relative humidity) under a 12-hour light/dark cycle, with access to food and water *ad libitum*. Experiments were performed in males unless indicated otherwise and all group sizes are reported with the statistical analyses.

Stereotactic injection

Intrahippocampal kainic acid (IHK) injection

At the age of 12-to-15-weeks, mice anaesthetized by inhalation of 2.5-3% isoflurane (Baxter) in oxygen were injected (Nanoject II, Drummond Scientific) with 70 nL kainic acid (5 mM in NaCl; Tocris biosciences) or an equivalent volume of NaCl into the right dorsal hippocampus (anteroposterior [AP] -1.8 mm, mediolateral [ML] -1.6 mm, dorsoventral [DV] -1.9 mm relative to Bregma) as described by (Bouilleret et al., 2000b). For analgesia, mice were i.p. injected with 1 mg/kg buprenorphine (Temgesic®, Reckitt Benckiser AG, Switzerland) prior and after surgery.

Intrahippocampal retrovirus injection

Adult mice (2 months old) were anesthetized as described above. Retrovirus encoding enhanced green-fluorescent protein (eGFP; 1 μL) was bilaterally injected into the hilus of the dentate gyrus (AP -2.0 mm, ML +/- 1.5 mm, DV -2.3 mm relative to Bregma) and the tissue was collected at 21 or 42 days post injection (dpi). eGFP-encoding retrovirus was produced "in house", as described in (Deprez et al., 2016). HEK 293T cells were transfected with three different plasmids containing the capsid (CMV-vsvg), viral proteins (CMV-gag/pol) and the transgene (CAG-eGFP) under the control of the CAG promoter (including the CMV CMS enhancer and chicken β-actin promoter).

Antibody injection

A subset of mice was intracerebroventricularly injected with purified mouse anti-Aβ antibody (6E10, Aβ3–8, IgG1; Covance) or control immunoglobulin G (IgG; 4 mg/mL; kindly provided by Britta Engelhardt, Theodor Kocher Institute, University of Bern) for a local neutralization of soluble Aβ species (Sudduth et al., 2013). A bilateral infusion (5 µL each, 500 nL/min, 10 min wait prior to retraction) into the lateral ventricles (AP -1.8 mm, ML +/-2.75 mm, DV -2.5 mm relative to Bregma) was performed under general anesthesia 3 days prior to the IHK injection. The tissue was collected at 18 dpi (IHK injection) for histological analysis.

5′-bromo-2′-deoxyuridine (BrdU) treatment

Three weeks prior BrdU treatment adult female mice were housed together (5 per cage) and bedding containing male mouse urine was introduced to the cages to induce Lee-Boot and Whitten cycle-synchronizing effects. At the age of two months mice received two intraperitoneal injections of 90 mg/kg BrdU (Sigma-Aldrich, #B5002, dissolved in 0.9% NaCl) on two consecutive days. The tissue was collected at 1 dpi to assess cell proliferation and at 28 dpi to evaluate cell survival and cell fate.

Electroencephalographic (EEG) recordings

Electrode implantation

For EEG recordings, mice were implanted immediately after stereotactic injection of KA with a bipolar electrode into the same coordinates as the injection and a monopolar reference electrode was placed into the cerebellum of the left hemisphere. Two enamel insulated stainless steel wires were connected to a male connector and twisted to a bipolar electrode for EEG recordings (for details see (Arabadzisz et al., 2005)), while two gold wires were inserted into the neck muscles for EMG recordings (for details see (Palchykova et al., 2010)). Electrodes were connected through a board-to-board connector (M52-5050545, Harwin) and fixed to the skull by a combination of Prime&Bond (Dentsply) and Tetric EvoFlow (Ivoclar vivadent) while the entering electrode shaft was sheathed by Kwik-CastTM Silicone Elastomer (World Precision Instruments).

Data acquisition and analysis

Continuous video-EEG (vEEG) recordings were acquired after the injection until 18 days post-injection (dpi) or once at 21 dpi. To this end, mice were placed into custom-made recording cages within a Faraday cage. A custom-made vEEG system was used for continuous

synchronous video and EEG recordings, consisting of a custom-made swivel, an amplifier and digitizer (AcqKnowledge MP100; Biopac Systems), infrared-switchable video cameras (Vivotek Inc., New Tapei City, Taiwan), NAS server (Synology), and a custom-made timer for synchronization (BASIC Stamp 2, Parallax Inc, Rocklin, CA, USA). EEG and EMG data was acquired at a sampling rate of 200 Hz. To assess the acute response to IHK, vEEG recordings of the first 4 hours were manually analyzed (open source software Polyman, EDF+). The severity of behavioral seizures was categorized according to the Racine, Pinel and Rovner scale (Table 1) (Racine, 1972; Pinel and Rovner, 1978). For each day, one hour was analyzed during the activity phase (around 1 AM) and during the resting phase (around 1 PM). For seizure quantification during the chronic phase, a three-hour recording (11 am to 2 pm) was analyzed. Seizures were defined as paroxysmal events lasting longer than 20 s that were separated by intervals of at least 1 s. The average frequency and duration of SRS was calculated for each mouse.

Table 1 Modified Racine scale for behavioral seizures. Adapted from (Pinel and Rovner, 1978)

Scale	**Stage**	**Behavior**
Racine behavioral scale	1	Oroalimentary movements
	2	Head nodding
	3	Anterior limb clonus
	4	Dorsal extension (rearing)
	5	Loss of balance and falling
Pinel and Rovner behavioral scale	6	Repeated falling
	7	Strong jumping and running
	8	Stage 7 with tonic period

Electrophysiology

Acute brain slice preparation

Mice were anesthetized with sodium pentobarbital (Nembutal®; 50 mg/kg; i.p.) and decapitated. 300 µm – thick sagittal slices were cut on a vibratome (Leica VT 1200 S) in ice-cold cutting solution and then stored in ACSF at room temperature in an interface type holding chamber for at least 1 h. Cutting solution contained (in mM) NaCl 87, KCl 2.5, $CaCl_2$ 0.5, MgCl 7, NaH_2PO_4

1.25, $NaHCO_3$ 25, glucose 10 and sucrose 75. ACSF contained (in mM) NaCl 120, KCl 3, $CaCl_2$ 2.5, $MgSO_4$ 2, NaH_2PO_4 1, $NaHCO_3$ 25, and glucose 20, and was bubbled with 95% O_2, 5% CO_2 (pH 7.4).

Field recordings

For the recording of extracellular population spikes glass microelectrodes of approx. 1.5 MΩ were filled with saline and placed near the border of CA1 stratum radiatum. Population spikes were evoked at 0.05 Hz with two pulses (50 ms apart) through a bipolar stimulating electrode positioned in CA3. A 15 min stable baseline was acquired before the application of 1µM KA for 10 min. The amplitudes of the population spikes were measured using Clampfit 10 (Molecular Devices, LCC, Sunnyvale, California, United States). To evaluate changes induced by kainic acid (KA) application, mean baseline values (mean of all amplitudes 5 min before the application of KA, i.e. 15 consecutive responses) were compared to those elicited 30 min after the washout of KA (mean of 15 consecutive responses).

Patch clamp recordings

For whole cell patch clamp recordings CA3 area was cut away. CA1 hippocampal cells were visualized with an upright microscope (Axioscope Examiner.A1, Carl Zeiss; 63x water immersion objective). Whole-cell pipettes were pulled from thin wall glass capillaries (1.5 O.D. X 1.17 I.D., Harvard Apparatus, Massachusetts, USA) using a Zeitz DMZ Puller (Martinsried, Germany). Electrode resistances in the bath were 3–6 mV. Series resistance was monitored by a –5mV step, and cells were discarded if this changed significantly (~20%). The intracellular solution consisted of (in mM) CsCl 140, HEPES 10, EGTA 10, MgATP 2, Na3GTP 0.3, pH 7.3, 290 mOsM. Cells were clamped at a holding potential of –70 mV to register spontaneous postsynaptic currents (sPSC). Currents were recorded with a multiclamp 700B (Molecular Devices, Pennsylvania, USA), and digitized at 10 kHz using a Digidata 1550 digitizer (Molecular Devices) and Clampex 10.0 (MolecularDevices). Traces were recorded with pClamp 10 and analysis of sPSCs frequencies and amplitudes were performed with MiniAnalysis (Synaptosoft, New Jersey, USA). KA (250 nM) was added for 5 min. For each condition (i.e. before the addition of KA and in the presence of KA) traces of one-minute duration were used for statistical analysis. The one-minute period where the effect of KA was maximal, was chosen for the statistical analysis.

RNA isolation and quantitative real-time PCR

Adult mice were anesthetized, decapitated, brains were extracted rapidly on ice and hippocampus dissected. Whole cell RNA from brain tissue was extracted using NucleoSpin RNA kit (Macherey-Nagel). cDNA was prepared using random hexamer primer (Thermo Scientific) and MuLV Reverse Transcriptase (Thermo Scientific). 1 µg of total RNA was amplified in CFX384 Touch™ Real Time PCR detection system (Biorad) using the SYBRgreen PrecisionPLUS qPCR Mastermix (Primerdesign). The relative levels of each RNA sample were calculated by the 2-ΔΔCT method using Biogazelle, qBase plus software (Livak KJ, 2001) and were normalized to that of HPRT and eEF1a1 mRNA. Each CT value used for these calculations was the mean of triplicates of the same reaction. All primers were synthesized by Eurofins genomics. Sequences of all primers are listed in Table 2.

Table 2 List of primers for RT-qPCR.

Target	**Forward sequence 5' → 3'**	**Reverse sequence 5' → 3'**
Y1 receptor	CAAGATATACATTCGCTTGA	AGATTGTGGTTGCAGG
Y2 receptor	CCATCTTCCGGGAATAC	TGACGTGGTTCCTCAG
Y5 receptor	TCAAGCGTTCCCTCAC	ACAACAGGACATCATGC
NPY	TGGACTGACCCTCGCTCTAT	TGTCTCAGGGCTGGATCTCT
IL-10	GGGAAGAGAAACCAGGGAGAT	GCCACAGTTTTCAGGGATGA
IL-6	TCCATCCAGTTGCCTTCTTG	GGTCTGTTGGGAGTGGTATC
TNFα	AGCCAGGAGGGAGAACAGA	CAGTGAGTGAAAGGGACAGAAC
SCN1a	CTCGTTCCTGATCGTGTTCC	ATCCTGTCCACAGCAATCTG
BDNF	TGCAGGGGCATAGACAAAAGG	CTTATGAATCGCCAGCCAATT
IL-1β	CAACCAACAAGTGATATTCTCCAT	GGGTGTGCCGTCTTTCATTA
Eef1a1	AAGCCCATGTGTGTTGAGAG	CTCCAGCAGCCTTCTTGTC
HPRT1	TCCTCCTCAGACCGCTTTT	AGGTATACAAAACAAATCTAGGTCAT

Tissue preparation for immunohistochemistry

Tissue was collected and prepared similar to the protocol of Notter et al. (2014). In brief, mice were anesthetized (Nembutal®; 50 mg/kg; i.p.) and perfused intracardially with 15–20 mL ice-cold, oxygenated aCSF [containing (mM) NaCl 125, KCl 2.5, $CaCl_2$ 3.7, $MgCl_2$ 2, $NaHCO_3$ 26,

NaH_2PO_4 1.25, glucose 25], pH 7.4, at a flow rate of 10–15 mL/min. The brain was extracted and divided into 3 blocks: rostral, medial and caudal part. All three parts were immediately immersion-fixed for 3 hours in ice-cold fixative [4% paraformaldehyde dissolved in 0.15 M sodium phosphate buffer], pH 7.4, then rinsed with PBS (pH = 7.4) and cryoprotected overnight in 30% sucrose in PBS at 4°C.

The fixed tissue was cut into 70-µm (dendritic morphology) or 40-µm (rest) thick serial coronal sections using a sliding microtome and collected in ice-cold PBS. For storage, sections were transferred to a cryoprotectant solution (50 mM sodium phosphate buffer, pH 7.4, containing 15% glucose and 30% ethylene glycol; Sigma-Aldrich) and kept at -20°C.

Immunohistochemistry

Sections were washed three times in Tris buffer (50 mM Tris, 150 mM NaCl, 0.05% Triton X-100, pH 7.4) for 10 min each and incubated overnight at 4 ℃ under continuous agitation with primary antibodies (Table 3) diluted in Tris buffer containing 2% normal goat serum (NGS) and 0.2% Triton X-100. Sections were rinsed three times in Tris buffer and incubated with the secondary antibody solution (2% NGS, Tris buffer) for 30 min at room temperature with secondary antibodies raised in goat. For immunofluorescence, secondary antibodies conjugated to AlexaFluor-488 (Invitrogen) were diluted to 1:1000 and those conjugated to Cy3 or Cy5 (Jackson ImmunoResearch Laboratories) to 1:500. After washing three times in PBS, sections were mounted to gelatin-coated glass slides and cover-slipped using Fluorescence Mounting Medium (Dako). For immunoperoxidase staining, biotinylated secondary antibodies (Jackson ImmunoResearch Laboratories) were diluted 1:300 and after washing three times in Tris buffer, incubated with avidin-peroxidase-complex solution (Vectastain Elite kit, Vector Labs) at room temperature. After washing them again three times in Tris buffer, sections were stained by combining 3,3-diaminobenzidine (DAB; Sigma–Aldrich Inc.) in Tris buffer (pH 7.7) with hydrogen peroxide for 5-15 min. Sections were immediately transferred to ice-cold PBS and washed three times. Finally, sections were mounted onto gelatinized glass slides, air-dried overnight, dehydrated through ethanol, cleared in xylene and coverslipped with resinous (Eukitt™; Sigma-Aldrich) mounting medium.

Table 3 List of primary antibodies (IF, immunofluorescence; IP, immunoperoxidase)

Target	Distributor	Description, Ref. no.	Dilution	Marker of
BrdU	Oxford Biotech	Rat, OBT0030	1:1000	IP
CD68	AbD Serotec	Rat, MCA1957GA	1:2000	IP/IF
DCX	Chemicon	Guinea pig, AB2253	1:2000	IF
F4/80	Abcam	Rat, b6640	1:1000	IP
GFAP	Dako	Rabbit, Z334	1:20'000	IF
Neuropeptide Y	Peninsula Lab.	Rabbit, T-4069	1:1000	IP
ZnT3	Synaptic Systems	Rabbit, 197002	1:1000	IP

Nissl staining

The IHK-induced pattern of degeneration and the placement of EEG electrodes was determined by Nissl staining with Cresyl violet. To this end, slides with air-dried sections were dipped in the following solutions: 5 min in dH_2O, 5 min in filtered Cresyl violet solution ($C_{18}H_{15}N_3O_3$, M 321.34, Fluka BioChemika, Cat. no. 10510-54-0), 30 sec in dH_2O and cleared in 96% ethanol containing 0.5% acetic acid until the desired coloration was obtained, 5 min in isopropanol, 5 min in isopropanol:Xylene (1:2) and 4 times dehydrated in xylene for 2 min. Finally, the slides were coverslipped with Eukitt.

Image acquisition and analysis

Visual scoring and image acquisition

For visual scoring of the neurodegenerative pattern (Nissl), 3-4 sections per mouse were examined using an Axioscop 2 microscope (Carl Zeiss) with bright-field illumination and either a 10x, 20x objective or 40x oil immersion objective. All images for display were acquired with a color digital camera (AxioCam MRc5) and the corresponding software AxioVision 4.5 (Zeiss).

Densitometry analysis

Immunoperoxidase staining (CD68, NPY) intensity was assessed by densitometry analysis (3-4 sections per mouse) using the MCID software (MCID Elite 6.0, InterFocus Imaging Ltd., Cambridge, UK). First, images were digitized using a precision illuminator (Northern light Model B95, Imaging Research Inc., Brock University, St.Catharines, Canada) and CoolSnap cf photo-camera (Photometrics, Tuscon, AZ, USA) with a Micro-Nikkor (55 mm + 12 mm) objective (Nikon Corp.). Then, the grey values were calibrated (Kodak step tablet no. 310ST607)

and the intensity was measured in the different regions of interest. To correct for variations in background staining, the intensity value was normalized to the intensity of the whole section.

Stereological analysis

The number of immunoreactive cells (F4/80+ macrophage-like cells) was determined stereologically in 3-4 sections per mouse using an Axioplan 2 bright-field microscope (Carl Zeiss AG, Feldbach, Switzerland) with 20x (air, NA 0.75) objective and an integrated digital camera (MicroFIRE, Optronics AG, Goldach, Switzerland). The size of the granule cell layer and molecular layer of the dentate gyrus as well as the number of macrophage-like cells within these outlined regions were estimated using the Mercator software (Mercator Pro rev. 7.8.2, Explora Nova, La Rochelle, France). For each mouse, the number of macrophage-like cells and the estimated thickness was averaged over three to four equidistant coronal sections.

Quantification of cell proliferation and survival

BrdU+ cells in the subgranular zone (SGZ) and granule cell layer (GCL) of the dentate gyrus were counted in 4-5 sections per mouse in dorsal hippocampus using the Axioscop 2 (Carl Zeiss; 40x oil-immersion lens, NA 1.3). Dorsal hippocampal volume was estimated using Mercator software (compare above).

Sholl analysis

Fluorescent Z-stacks (spaced by 0.7 µm) throughout the entire thickness of the section were acquired with a confocal microscope (LSM710) using a 40x oil immersion objective (NA, 1.4) and ZEN 2012 black edition (Carl Zeis MicroImaging GmbH, Goettingen, Germany) software. Images were analyzed with ImageJ (version 1.49o; Java 1.6.0_12 (Wayne Rusband, National Institutes of Health, USA). Sholl analysis (Sholl, 1953) (concentric circles spaced at 10 µm intervals, centered on the cell body) was used to analyze the complexity of the dendritic trees. First, neurons were traced using NeuronJ plugin (NIH ImageJ; (Meijering et al., 2004)). Further Sholl analysis plugin (Anirvan Ghosh Laboratory, University of California, San Diego, La Jolla, CA, USA) was used to calculate the number of intersections between dendrites and concentric circles. For the number of intersections as a function of distance from the soma, area-under the curve (AUC) was calculated and used for further statistical analysis. Dendritic morphometry (primary dendrite length, total dendrite length) was assessed with the NeuronJ plugin. In total 14-36 cells from the groups of 5 to 8 mice per time point were quantified.

Spine density

Z-stacks for spine density morphology analysis of randomly selected eGFP-positive dendritic segments were obtained with a 40x oil immersion objective using a 2.7 digital zoom. Spines density quantification and spine type classification were performed using CellCounter (ImageJ). The length of each segment was measured and the number of spines/µm was quantified.

Statistical analysis

Data are presented as mean ± standard error of the mean (SEM). Statistical analyses for multiple group comparison was performed by a one-way or two-way ANOVA with a Bonferroni post-hoc test. An unpaired t test, two-tailed, was used to compare two groups (Prism software, GraphPad version6). For KA-induced LTP a two-way repeated measure ANOVA was performed with a Sidak´s multiple comparisons test. To compare the distribution of spontaneous currents (inter-event interval and amplitude) a Kolmogorov–Smirnov test was used (differences were considered significant if $p<0.01$).

Results

Acquired epilepsy and increased seizure-associated mortality in ArcticAβ mice

To determine whether an AD-like predisposition prior to detectable plaque pathology renders the limbic neuronal network more vulnerable to excitotoxicity and affects the development of acquired epilepsy, 3-months-old ArcticAβ mice and wildtype littermates were injected with IHK (Fig. 1A). Both genotypes exhibited the characteristic neurodegenerative pattern 3 weeks after IHK: loss of pyramidal cells in CA1 and CA3c as well as loss of hilar mossy cells in the dentate gyrus (Fig. 1B) as previously described (Bouilleret et al., 2000b; Bouilleret et al., 2000a). The severity and region-specificity of the cell loss were not different between the genotypes. IHK-induced GC dispersion in the dentate gyrus was similar in ArcticAβ and wildtype littermates, as determined by measuring the thickness of the GC layer (GCL; t_{20} = 1.13, P = 0.27) and the molecular layer (ML; t_{20} = 1.4, P = 0.18; unpaired two-tailed t-test) (Fig. 1C). The number of invading macrophages, which was shown to correlate with the extent of GC dispersion (Zattoni et al., 2011), did not differ between genotypes (ML: t_{20} = 1.9, P = 0.07; GCL: t_{20} = 0.2, P = 0.85; unpaired two-tailed t-test). In line with observations about the neurodegenerative pattern induced by IHK, microglial activation was not altered by the ArcticAβ transgene in the injected hemisphere (Fig. 1D).

IHK led to the development of acquired epilepsy in both genotypes, with mice exhibiting similar seizure frequency three weeks after the injection (t_7 = 0.04, P = 0.97; unpaired two-tailed t-test) (Fig. 1E). Unexpectedly, however, mortality of ArcticAβ mice was observed acutely (χ2(1) = 13.4, P = 0.0003; Mantel-Cox test), due to strong convulsive seizures during status epilepticus as well as during the transition from the latent to the chronic period, when SRS start to appear (Fig. 1F). Thus, the AD-like predisposition in 3-months-old ArcticAβ mice increases seizure severity possibly by altering the response to excitotoxicity and causing aberrant activity during early epileptogenesis, while having no effect on the frequency of SRS and associated histopathological changes in surviving mutant mice.

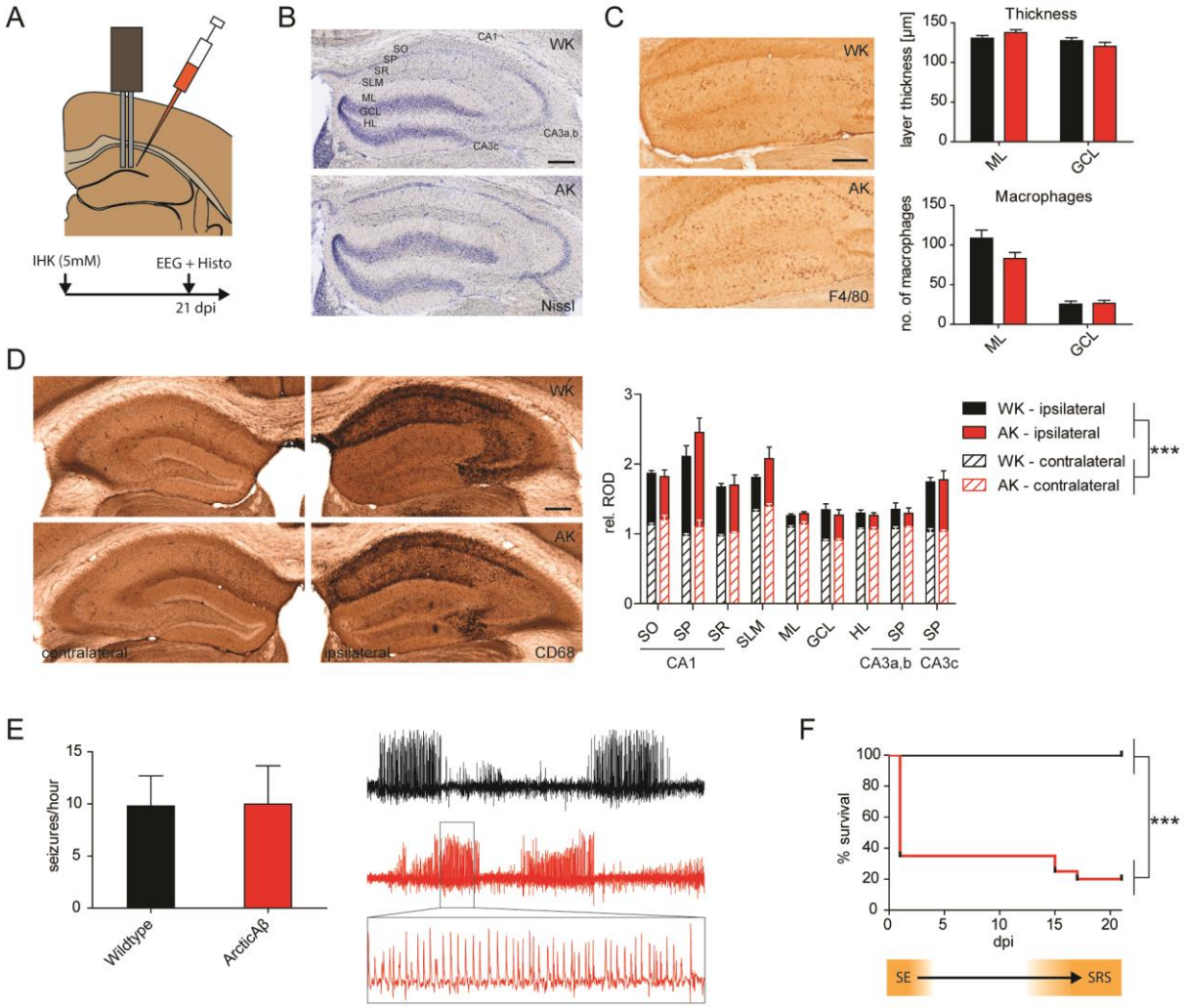

Figure 1 Increased response of ArcticAβ mice to IHK-induced epilepsy. . A, Schematic representation of the experimental design to assess acquired epilepsy. Kainic acid injection and electrode implantation were performed in the right dorsal hippocampus, while EEGs were recorded and tissue was collected for histological analysis at 21 dpi. B, Cresyl violet staining of the ipsilateral hippocampus. Neurodegeneration in CA1, CA3c, and the hilus, along with the dispersion of dentate granule cells, show a similar pattern in both IHK-injected wildtype (WK) and ArcticAβ mice (AK) (SO, stratum oriens; SP, stratum pyramidale; SR, stratum radiatum; SLM, stratum lacunosum moleculare; ML, molecular layer; GCL, granule cell layer; HL, hilus). C, F4/80+ macrophages invading the ipsilateral dentate gyrus and the dispersion of dentate GC. Stereological quantification of F4/80+ macrophages and measuring the layer thickness of GCL and ML revealed no differences between genotypes (n = 6/genotype; unpaired t-tests). D, Densitometric analysis of CD68 staining. Microglial activation was increased 3 weeks after IHK injection in the ipsilateral hemisphere of both genotypes (n = 6/genotype; *** $p < 0.0001$, two-way ANOVA). E, Frequency of SRS. Both genotypes show a similar number of seizures three weeks after IHK. Representative traces of intrahippocampal recordings reveal a high frequency of SRS in the IHK model of acquired epilepsy (box outlines 10 s and 15 mV). F, Survival curve during epileptogenesis. ArcticAβ mice (n = 20) exhibit an increased mortality rate during the status epilepticus and during the transition from the latent to the chronic period with SRS in comparison to their wildtype littermates (n = 8) (*** P = 0.0003, Mantel-Cox test). Quantitative data represent mean ± SEM. Scale bars, 150 µm.

Increased response to excitatory stimulation in the hippocampal network

To study the differential impact of IHK-induced status epilepticus on the hippocampal neuronal network of ArcticAβ mice, we recorded field population spikes (PS) in the main hippocampal output region, CA1, in tissue slices (Fig. 2A). A current-voltage plot illustrates the significantly different slope ($p < 0.01$) of recorded PS as a function of stimulus intensity in wildtype compared to ArcticAβ mice (Fig. 2B). This difference suggests that the strength of synaptic transmission in CA1 is reduced in ArcticAβ mice, which is consistent with previous findings in other AD transgenic mice (Palop et al., 2007).

KA has recently been shown to induce an NMDA-independent form of long term potentiation (LTP) (Petrovic et al., 2017). Similarly, we observed that a 10-min application of KA (1 µM) produces a stable potentiation of CA1 PS, which remained unchanged for at least 30 min after the drug had been washed out, in both wildtype (98.7 % ± 0.9 before KA to 116.7 % ± 7.4 after 30 min washout, 9 slices from n = 7 different animals) and ArcticAβ mice (101.1% ± 3,36 before KA to 177.7 % ± 26.10 after 30 min washout, 6 slices from n = 5 different animals) (Fig. 2C). The KA-induced potentiation was significantly higher in ArcticAβ mice compared to wildtype littermates (Fig. 2D) (two-way ANOVA repeated measure ANOVA; significant effect of treatment 30 min after wash-in, $F_{(1, 10)} = 8.6$, $p < 0.01$, and genotype, $F_{(1, 10)} = 8.6$, $p < 0.05$). The latter difference was due to the stronger effect of KA in slices of ArcticAβ mice (Sidak´s multiple comparison post-hoc test). Although not significant, we observed a tendency towards reduced paired pulse ratio after KA in ArcticAβ mice (Fig. 2E), suggesting some degree of presynaptic involvement in their enhanced response to KA.

Impairment of the inhibitory circuit in CA1

In order to examine the response of the inhibitory CA1 microcircuit to KA application without interfering pharmacologically with KA receptors, we isolated the CA1 region from CA3 by cutting out the latter with a scalpel and performed whole cell patch clamp recordings of CA1 pyramidal cells (Fig. 3A). To measure predominantly GABA currents, we used an intracellular solution consisting of a high Cl^- concentration (see *Materials and Methods*). Most spontaneous events recorded were inhibitory (sIPSCs), as the addition of ionotropic glutamate receptor blockers did not change the frequency of baseline activity, whereas the application of 20 µM bicuculline blocked most spontaneous activity (data not shown). Therefore, we will henceforth refer to the recorded spontaneous events as sIPSCs.

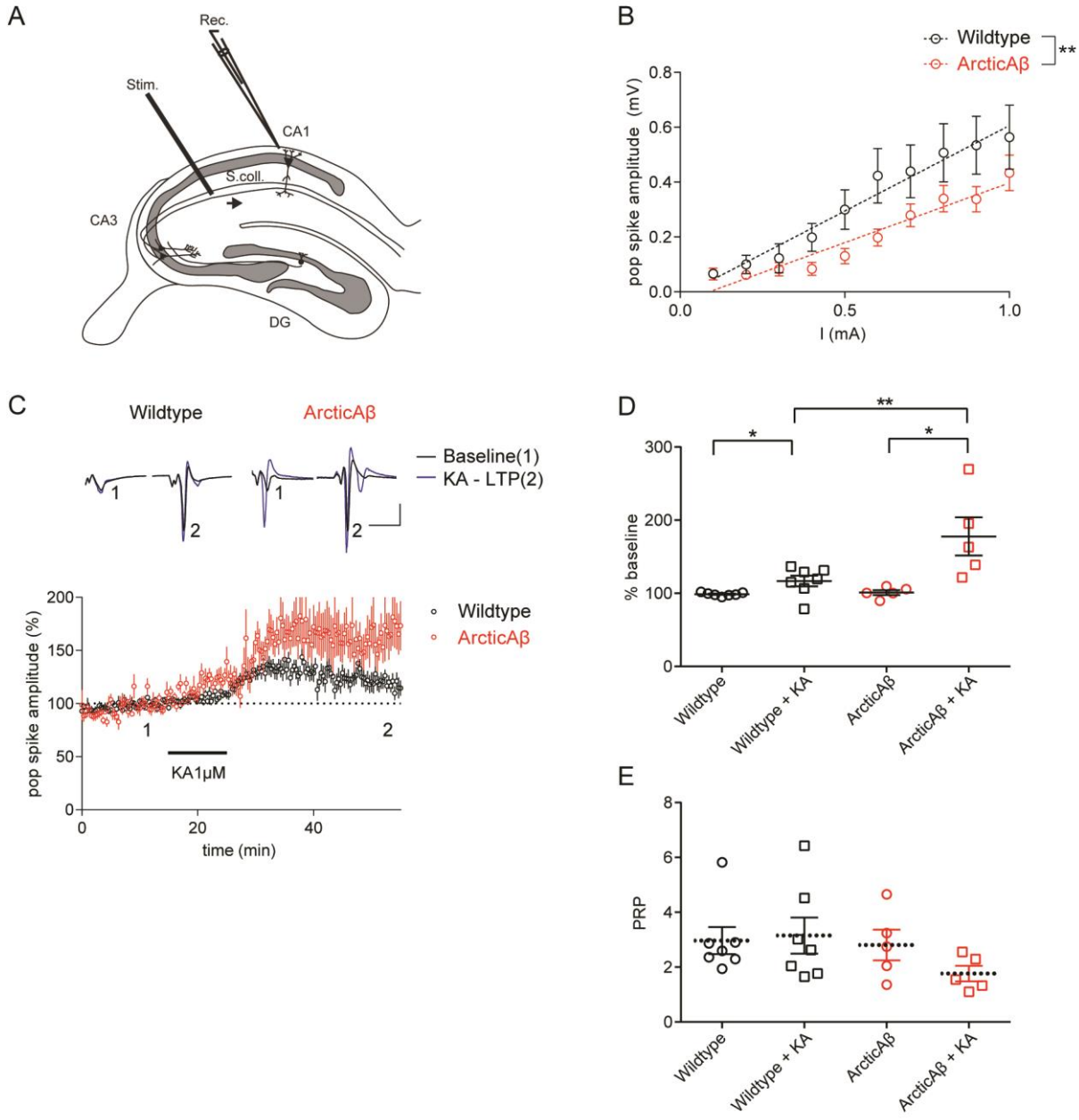

Figure 2 Decreased synaptic strength and increased KA-induced LTP in slices of ArcticAβ mice. A, Schematic diagram showing electrode placement (Stim = bipolar stimulation electrode, Rec = recording electrode) and hippocampal regions (S. coll = Schaffer collateral, DG = dentate gyrus, CA1 and 3 = areas Cornu Ammonis 1 and 3 respectively). B, Current - voltage relationship. ArcticAβ mice show a decreased synaptic strength compared to wildtype littermates (** $p < 0.01$). Linear regression lines used for statistical comparison are dashed. C, KA-induced LTP is more pronounced in ArcticAβ mice. Upper inset: representative traces of population spikes before (black traces) and 30 mins after (blue trace) a 10-min application of 1 µM KA. Paired pulses were given 50 msec apart. Stimulation artifacts were removed for visual clarity. D, Percent change per cell before and 30 mins after a 10-min application of 1 µM KA. The increase in PS amplitude is significant for both groups after application of 1µM KA ($P = 0.02$, two-way repeated measure ANOVA), and between wildtype and ArcticAβ mice in the degree of potentiation after a 30-min washout period ($P = 0.01$, two-way repeated measure ANOVA). E, Paired-pulse ratio before and 30 min after a 10-min application of 1 µM KA. Quantitative data represent mean ± SEM.

Hippocampal network hyperactivity is an early symptom in AD (Palop and Mucke, 2016), and an increase in inhibitory activity in the dentate gyrus of $hAPP_{FAD}$ mice has been postulated as a compensatory mechanism (Palop et al., 2007). We observed no difference in baseline frequency of sIPSCs between wildtype and ArcticAβ mice in CA1 cells. However, the application of 250 nM KA significantly diminished the frequency of events in the mutant (Fig. 3B). In slices from wildtype mice, KA increased the frequency of sIPSCs (data not shown), as shown previously (Fisher and Alger, 1984). In line with this finding, we observed that the clustering of these events before and after KA application differed between genotypes. To quantify this phenomenon, clusters of activity were defined as groups of sIPSCs occurring within less than 100 ms from each other, and binned them into four main groups, containing up to 3 events, 4-6 events, 7-9 events or >10 events (Fig. 3C). ArcticAβ mice showed more clusters with a higher number of events during baseline, which disappeared in the presence of KA, whereas the opposite occurred for wildtype mice.

We also explored how KA affects oscillations in these mice, since inhibitory networks generate gamma and theta rhythms that regulate and shape hippocampal oscillatory patterns (Whittington et al., 2000; Reich et al., 2005). Although, we did not find any significant difference in gamma or theta power, the KA-induced increase in gamma oscillations (relative gamma power of 0.2 ± 0.07 in baseline vs 0.6 ± 0.24 in KA) seemed attenuated in ArcticAβ mice (relative gamma power of 0.19 ± 0.07 in baseline vs 0.2 ± 0.12 in KA; two-way ANOVA, interaction: $F_{(1, 7)} = 2.0$, $p = 0.2$) (Fig. 3D-E).

Severe status epilepticus and early seizure onset during epileptogenesis

Having observed an increased mortality in ArcticAβ mice during early stages of epileptogenesis (Fig. 1F), we used video-EEG (vEEG) monitoring to determine whether ArcticAβ mice suffer from more severe seizures during status epilepticus and die from convulsive seizures during the latent phase (Fig. 4A). During the first four hours of status epilepticus, ArcticAβ mice had more severe behavioral seizures (stage 6-7 of the Racine-Pinel-Rovner scale; Table 1) than wildtype littermates even after reducing the dose of KA by half to 2.5 mM (Fig. 4B; left panel). Tonic-clonic seizures (stage 8) were only observed in ArcticAβ mice (Fig. 1F), and were lethal in some cases (data not shown). However, neither the number (Fig. 4C) nor the duration (Fig. 4D) of

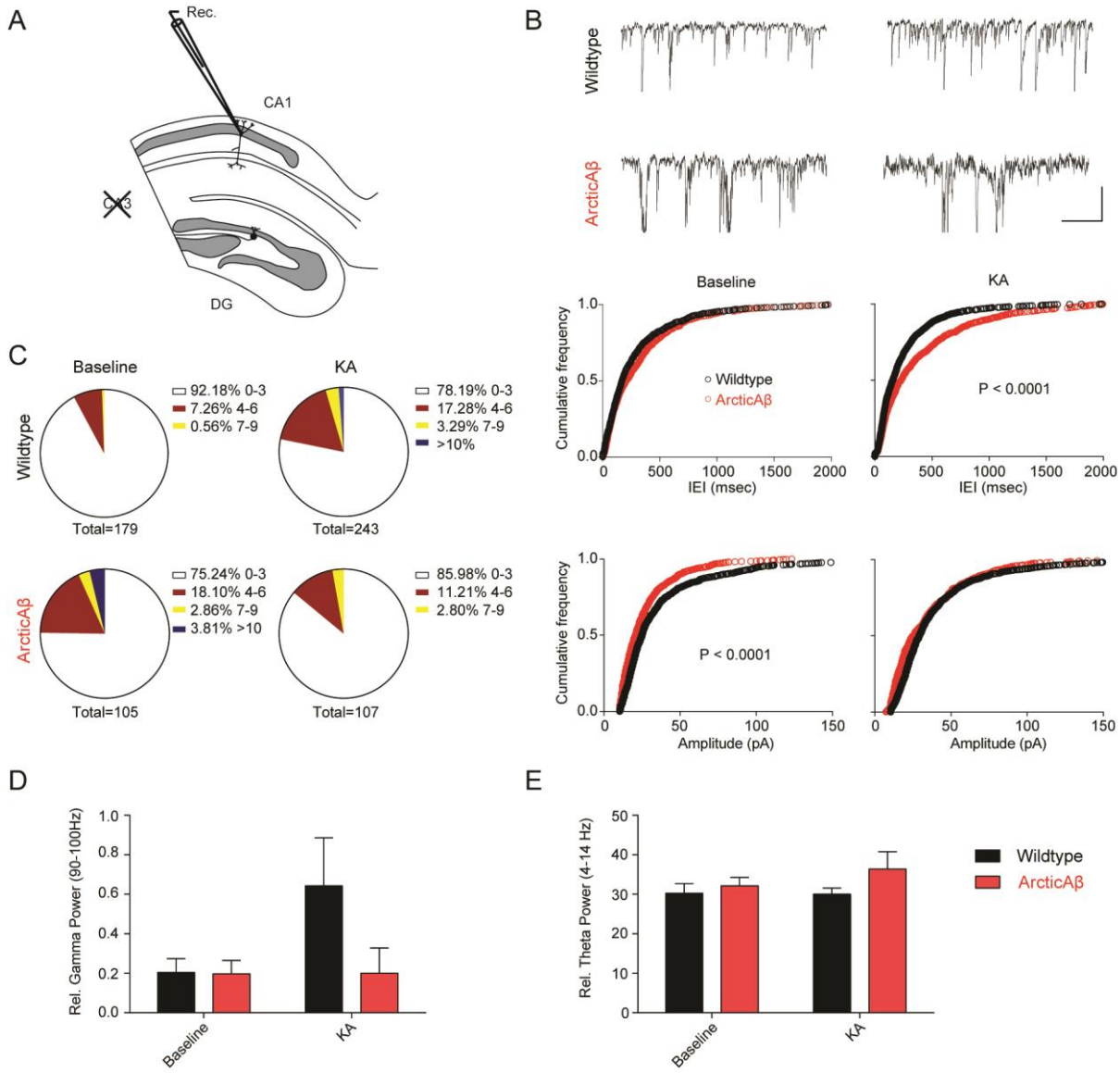

Figure 3 Reduced frequency of spontaneous inhibitory currents after KA application in slices of ArcticAβ mice. A, Schematic diagram of a hippocampal slice after removal of the CA3 area. B, Top inset: representative traces. Bottom graphs: Cumulative frequency distribution plots illustrating the frequency and amplitude of sIPSCs. Frequency of events is similar in wildtype and ArcticAβ mice, but a 5-min application of KA decreases the inter-event interval in ArcticAβ mice significantly ($p < 0.0001$, Kolmogorov–Smirnoff test). The sIPSC amplitude is higher in ArcticAβ mice under baseline conditions ($p < 0.0001$, Kolmogorov–Smirnoff test), but not after KA application. C, Distribution of clustered activity, consisting of events that are separated by <100 ms. KA uncovers clusters with a higher number of events in wildtype mice, whereas the opposite is found in ArcticAβ mice. D, Relative fast gamma (90-100 Hz) power. There is a tendency for impaired upregulation of gamma power in ArcticAβ mice in the presence of KA. E, Relative theta (4-14 Hz) power. Wildtype (n = 5), ArcticAβ mice (n = 4).

seizures differed between genotypes. In addition, mortality of ArcticAβ mice was not associated with reduced latency to the first seizure (data not shown). Mortality was a major confounding factor in our study, because it implied that ArcticAβ mice that survived the status epilepticus might have only mild lesions induced by KA. Therefore, we decided to administer all mice a protective dose of diazepam (5 mg/kg) immediately after the end of IHK injection (Fig. 4A). As

expected, diazepam treatment strongly reduced seizure severity (stage 2-3 of the Racine-Pinel-Rovner scale; Fig. 4B; right panel) and frequency (convulsive: $F_1 = 52.94$, $P < 0.0001$; non-convulsive: $F_1 = 6.16$, $P = 0.025$; Fig. 4C), while having no effect on seizure duration (Fig. 4D). Moreover, diazepam treatment after IHK injection averted status epilepticus-associated mortality, but not mortality occurring during the latent phase (Fig. 4F). Thus, increased susceptibility to severe behavioral seizures can not only be evoked by a proconvulsant, but also by spontaneous aberrant network activity in a later stage of epileptogenesis.

To determine whether abnormal EEG activity during early epileptogenesis is associated with mortality during the latent phase, we acquired continuous vEEG recordings during the progress of epileptogenesis. As reported (Riban et al., 2002a; Arabadzisz et al., 2005), wildtype mice exhibit initially low voltage spikes or sharp waves (200-800 μV, 1-3 Hz), whereas SRS (800-1500 μV, 3-5 Hz, duration > 20 s) appear two weeks after IHK injection (Fig. 4E). ArcticAβ mice, however, showed a mixture of low voltage spikes and sharp waves (200-800 μV, 1-3 Hz) up to 3-4 dpi, with a subsequent early onset of SRS-like events (800-1500 μV, 3-5 Hz, duration 10 - 20 s) at 4-5 dpi (Fig. 4E). These early short SRS were progressively replaced by regular SRS (duration > 20 s) from 12 dpi on. Interestingly, mortality of ArcticAβ mice during the latent phase (Fig. 4F) was associated with early onset of SRS at 3 dpi (Fig. 4E). Thus, ArcticAβ mice are more susceptible to the development of seizures, even when they are "protected" with diazepam during the IHK-induced status epilepticus. These findings suggest that early onset of SRS in ArcticAβ mice is due either to a missing anticonvulsive protection or a premature proconvulsive environment during the otherwise seizure-free latent period.

Figure 4 Severe status epilepticus and early onset of SRS in ArcticAβ mice. A, Schematic representation of the experimental design to monitor EEG activity during early epileptogenesis. Continuous vEEG recordings were performed for 18 days after IHK injection. B, Percentage of convulsive seizures with severity 2-8 according to the Racine-Pinel-Rovner scale during status epilepticus (Table 1). While ArcticAβ mice had more severe seizures than wildtype mice after IHK injection (left), both genotypes had seizures with severity 2-3 when treated with diazepam immediately after IHK injection (right). C, Total number of convulsive (left) and non-convulsive (right) seizures during status epilepticus. Diazepam significantly reduced the number of seizures (n = 4-6 mice/genotype; * $p < 0.05$, **** $p < 0.0001$, two-way ANOVA). D, Duration of convulsive behavioral seizures of severity 2-8. There was no difference between genotypes (unpaired t-test). E, Characterization of EEG pattern during the latent phase and beginning of chronic phase. An early onset of short SRS-like events (defined as seizures with a duration of 10-20 s) occurred in ArcticAβ mice at 5-8 dpi, while regular SRS were detected already at 3 dpi in the two mice that died later on. Bottom traces depict representative examples of an SRS-like event ($10 \text{ s} < \Delta t < 20 \text{ s}$), a regular SRS ($\geq 20$ s), and a tonic-clonic seizure leading to the death of the animal. The spectrogram in the bottom left corner depicts the increase power in the frequency range of 20-100 Hz that is characteristic for seizures. F, Mortality rate for mice receiving diazepam after IHK injection. With diazepam, status epilepticus-associated mortality in ArcticAβ mice is abrogated, but some transgenic mice still died during the transition from the latent to the chronic phase. Quantitative data represent mean ± SEM.

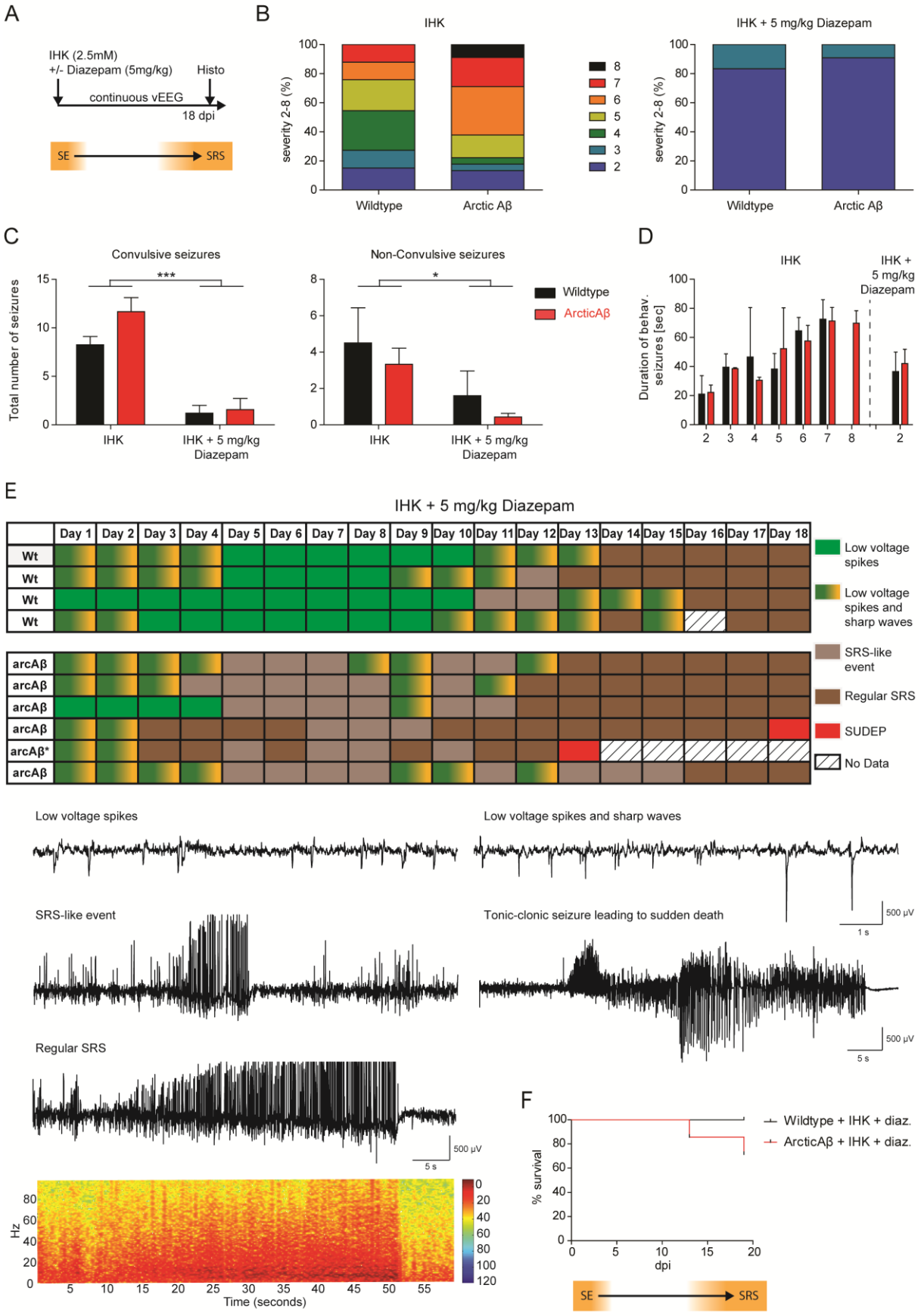
A
IHK (2.5mM)
+/- Diazepam (5mg/kg)
Histo
continuous vEEG
18 dpi
SE
SRS
B
IHK
IHK + 5 mg/kg Diazepam
severity 2-8 (%)
Wildtype
Arctic Aβ
8
7
6
5
4
3
2
C
Convulsive seizures
Non-Convulsive seizures
Total number of seizures
***
*
IHK
IHK + 5 mg/kg Diazepam
Wildtype
ArcticAβ
D
IHK
IHK + 5 mg/kg Diazepam
Duration of behav. seizures [sec]
E
IHK + 5 mg/kg Diazepam
Day 1
Day 2
Day 3
Day 4
Day 5
Day 6
Day 7
Day 8
Day 9
Day 10
Day 11
Day 12
Day 13
Day 14
Day 15
Day 16
Day 17
Day 18
Wt
arcAβ
arcAβ*
Low voltage spikes
Low voltage spikes and sharp waves
SRS-like event
Regular SRS
SUDEP
No Data
Low voltage spikes
Low voltage spikes and sharp waves
SRS-like event
Tonic-clonic seizure leading to sudden death
Regular SRS
500 µV
1 s
5 s
Hz
Time (seconds)
F
% survival
dpi
Wildtype + IHK + diaz.
ArcticAβ + IHK + diaz.
SE
SRS

Gradual progression of neurodegeneration and microgliosis during epileptogenesis

Neurodegeneration and inflammation play an important role in the pathogenesis of both AD (Heppner et al., 2015) and TLE (Vezzani and Viviani, 2015). To test whether the hyperexcitable phenotype observed in ArcticAβ mice accelerates the development of a pro-epileptogenic lesion, we determined the course of neurodegeneration and microglial activation (CD68 immunoreactivity) in the dorsal hippocampus at different time-points (1, 3, 6, 14 dpi) of epileptogenesis (Fig. 5). Cresyl violet staining was used to assess the neurodegenerative pattern (data not shown). As expected (Bouilleret et al., 1999), hilar cells in the dentate gyrus were lost and pyramidal cells in CA1 became pyknotic within 24 h. During the progression of epileptogenesis, pyramidal cells in CA1 and in CA3c gradually degenerated, starting at 3 dpi up to an almost complete disappearance at 14 dpi. Dentate gyrus GC dispersion was clearly evident at 14 dpi (data not shown) and progressed further at 21 dpi (Fig. 1B). Similarly for microglial activation, both genotypes showed a gradual increase of CD68-IR compared to control animals over a two-week period in the ipsilateral hippocampus (in all layers of CA1, the stratum lacunosum moleculare, CA3c and the strati pyramidale and radium of CA3 a,b; Fig. 5 and Table 3). Microgliosis peaked between 1 and 6 dpi in the hilus and the stratum lucidum, while being very low in the molecular layer and GC layer (besides a minor peak at 3 and 6 dpi; Fig. 5B). Interestingly, ArcticAβ mice exhibited a less enhanced CD68-IR compared to wildtype mice in the stratum oriens of CA3a,b at 1 dpi, and at 6 dpi in the hilus of the ipsilateral hippocampus. The contralateral hemisphere showed increased CD68-IR except in stratum pyramidale of CA1, the stratum lacunosum-moleculare, or CA3c (Fig. 5B and Table 3).

In addition, tissue of ArcticAβ mice that died during status epilepticus (~45 min after injection; Fig. 1F) was compared to a group of wildtype littermates perfused 45 min post-injection ("SE group"). We evaluated whether these ArcticAβ mice belonged to a subgroup with particularly pronounced sequelae associated with the AD pathology (including ectopic cell death and aggravated inflammation). Cresyl violet (data not shown) and CD68 (Fig. 5B) immunoreactivity revealed no difference between genotypes or between hemispheres suggesting that neither an AD-like predisposition nor the IHK injection affected cellular integrity or microglial activation during early status epilepticus. Thus, the general progression of neurodegeneration and microgliosis does not reflect increased vulnerability to aberrant excitation and does not predict early onset of SRS in AD transgenic mice during IHK-induced epileptogenesis.

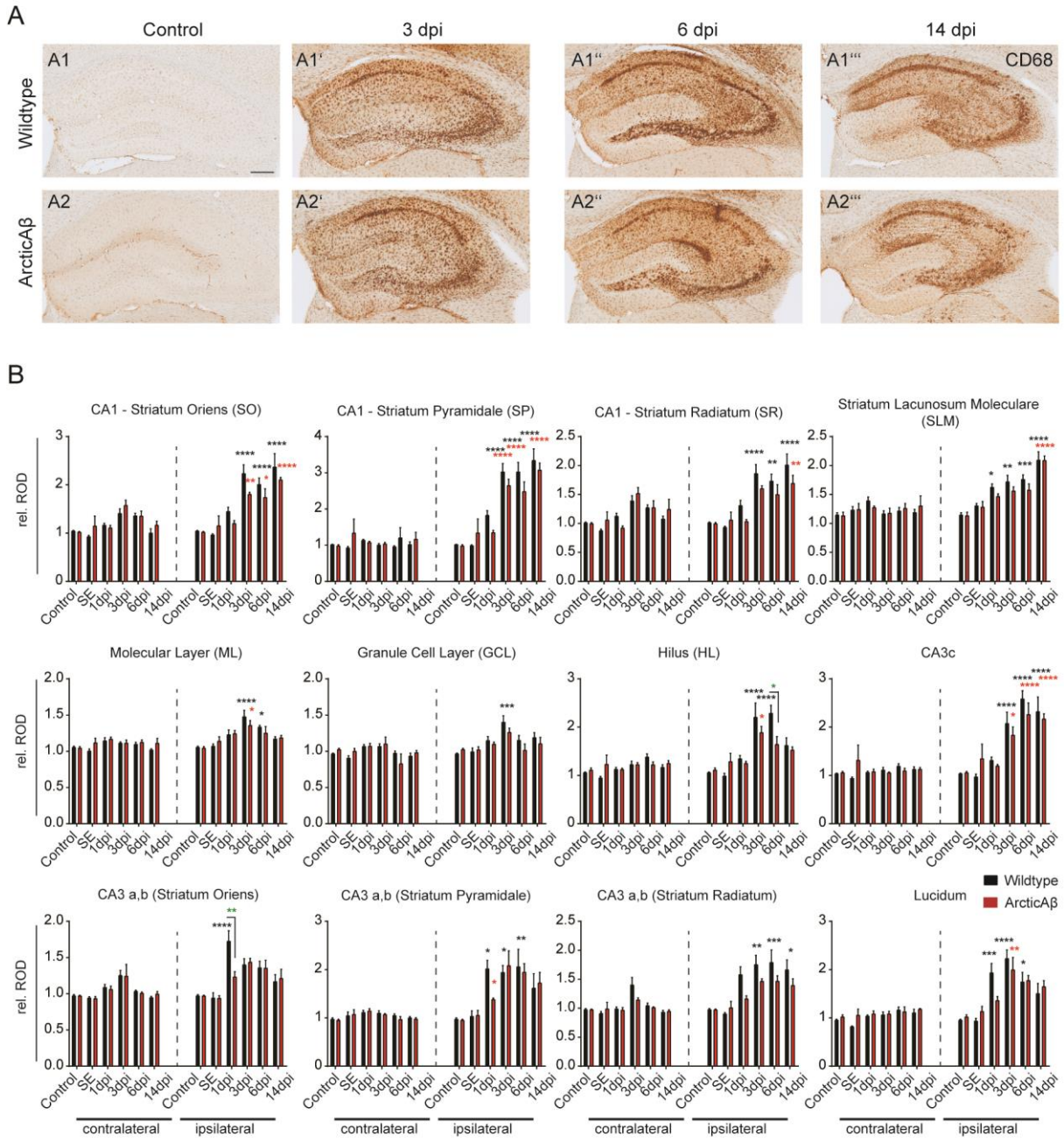

Figure 5 Reduced microgliosis in ArcticAβ mice during epileptogenesis. A, Representative images of a marker for microglial activation (CD68) at 3, 6 and 14 dpi compared to control levels. Scale bar, 250 µm. B, Densitometric analysis of CD68-IR in controls, as well as at 1, 3, 6, and 14 dpi. Both ArcticAβ mice (n = 4-5/ time point; red stars) and wildtype littermates (n = 5-7/ time point; black stars) showed an increased CD68-IR compared to baseline control over the time course of early epileptogenesis in all layers of the ipsilateral and in some layers of the contralateral hippocampus (* $p < 0.05$, ** $p < 0.01$, *** $p < 0.001$, **** $p < 0.0001$; two-way ANOVA, Bonferroni post-hoc test). Analysis revealed a significant group difference in the SO of CA3a,b and the hilus (green stars; compare Table S1 for details). Data represent mean ± SEM normalized to control for each region.

Genotype-specific differences and epileptogenesis-associated changes in hippocampal adult neurogenesis

A large body of literature suggests a direct link between aberrant excitability and adult neurogenesis (Jessberger et al., 2005; Kralic et al., 2005; Ledergerber et al., 2006; Song et al., 2012; Sierra et al., 2015). We explored the hypothesis that ArcticAβ mice, like other AD-transgenic mice (Sun et al., 2009), show impaired neurogenesis, which has been reported to exacerbate KA-induced status epilepticus (Iyengar et al., 2015). In order to assess proliferation and survival rate of newborn cells in the subgranular zone (SGZ) of the dentate gyrus, mice were injected with BrdU and tissue was collected at 1 and 28 dpi to assess proliferation and cell survival, respectively (Fig. 6A). At 1 dpi, ArcticAβ mice showed significantly more BrdU+ cells in the SGZ compared to wildtype littermates (14039 ± 1243 cells/mm^3, N = 8; 10415 ± 728 cells/mm^3, N = 8; data shown as mean ± SEM; P = 0.03, paired, two-tailed Student's t-test), while there was no difference between genotypes at 28 dpi (ArcticAβ: 2663 ± 261.8 cells/mm^3, N = 9; wild-type: 3384 ± 491 cells/mm^3, N = 9; data shown as mean ± SEM; P = 0.21, paired, two-tailed Student's t-test) (Fig. 6B). To determine the fate of BrdU+ cells at 28 dpi, we used neuronal (NeuN+) or astroglial (GFAP+) markers. In both genotypes a similar proportion of neuronal (NeuN/BrdU; wildtype: 89.4% ± 2.6%, N = 9; ArcticAβ: 91.5% ± 3.5%, N=7) and astroglial (GFAP/BrdU; wildtype: 7.5% ± 2.5%, N = 9; ArcticAβ: 5.9% ± 3.1%, N=7) progenitors were observed. Further, we examined the morphological development of immature (21 dpi) and mature (42 dpi) newborn neurons infected with a retrovirus expressing eGFP (Fig. 6C). Sholl analysis of adult-born GC at 21 and 42 dpi revealed a tendency towards a reduced

Figure 6 Increased proliferation of newborn cells and reduced spine density in ArcticAβ mice. A, Schematic representation of the experimental design to quantify newborn neurons. Mice received BrdU injections of two consecutive days and brain tissue was collected at day 1 and 28 post-BrdU injection to evaluate cell proliferation and survival rate, respectively. B, Quantification and representative images of BrdU immunostaining 1 and 28 days after the last BrdU treatment. BrdU+ cells were located in the inner part of the GCL. Higher density of BrdU+ cells was common in ArcticAβ mice at 1 dpi, but there were no differences at 28 dpi (* p > 0.05, unpaired t-test). Scale bar, 160 µm. C, Schematic representation of the experimental design to assess the dendritic arborization and spine density in adult-born neurons. Brain tissue of both genotypes was collected 21 and 42 days after the intrahippocampal injection of eGFP retrovirus. Quantification of dendritic arborization was done by Sholl analysis measuring the number of intersections between eGFP+ dendrites and virtual concentric circles centered on the cell body and spaced by 10 µm (bottom). D, Fluorescent images of representative examples of eGFP+ cells in each genotype at 21 and 42 dpi. Quantitative result of Sholl analysis showed no significant difference, but a trend towards a reduced dendritic arborization in ArcticAβ compared to wildtype mice at 21 dpi. There were no differences between genotypes at 42 dpi. Scale bar, 50 µm. E, Dendritic spine classification analysis. Representative images of dendritic segments from eGFP expressing GCs of wild-type and ArcticAβ mice at 21 and 42 dpi (Scale bar, 5µm). Quantification of mushroom, stubby, thin and overall spine density. ArcticAβ mice had significantly reduced overall spine density and specifically thin spine density at 21 dpi and a reduced stubby spine density at 42 dpi with no difference in the overall spine density (* p > 0.05, unpaired t-test). There were no genotype differences for the proportion of the three types of spines. Quantitative data represent mean ± SEM.

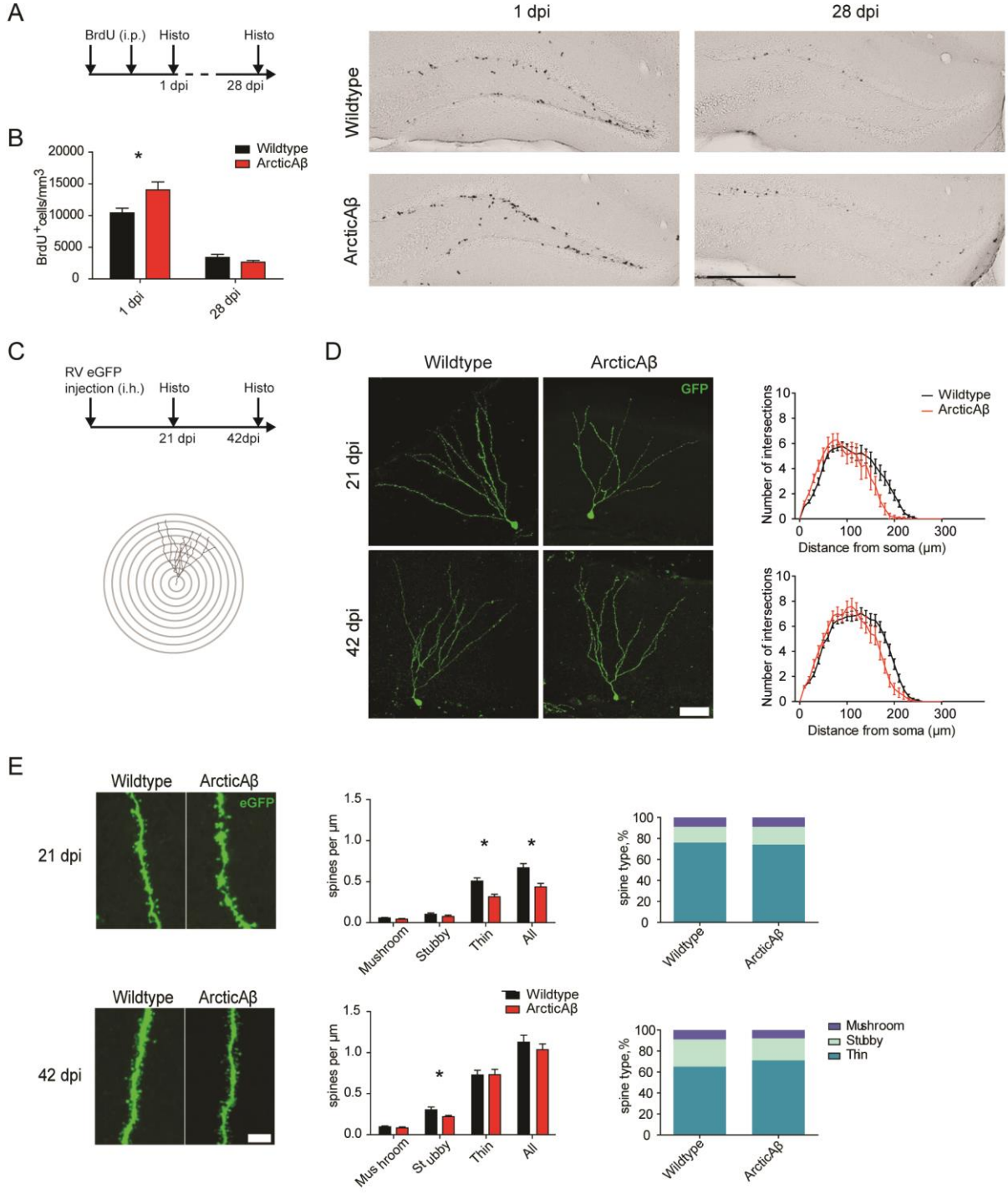

dendritic arborization between genotypes (Fig. 6D). However, further away from the soma, starting from 150µm, this difference was statistically significant at both 21 dpi (wildtype: 197.4 ± 31, N = 27; ArcticAβ at 21 dpi: 70 ± 23, N = 14; P = 0.0094) and 42 dpi (wildtype: 359 ± 25, N=36; ArcticAβ: 258 ± 34, N=17; P = 0.0221; data displayed as area under the curve (AUC), mean ± SEM, paired, two-tailed Student's t-test). Moreover, dendritic spine density was assessed and spines were classified in three subgroups (Fig. 6E). Overall spine density was significantly

reduced in ArcticAβ mice at 21 dpi, with a specific reduction in thin spines. At 42 dpi, adult-born GC of ArcticAβ mice had significantly fewer stubby spines, while overall spine density was normalized. At both time-points, the proportion of spine types did not differ between animals. Although ArcticAβ mice had increased cell proliferation, the survival of both neuronal and glial progenitors seems to be reduced. Together with the reduced spine density in adult-born GC, these findings point towards a slight impairment of neurogenesis in 3-months-old ArcticAβ mice.

Neuronal stem cells (NSCs) divide into reactive astrocytes after IHK-induced status epilepticus, which ultimately leads to depletion of the NSCs pool and thereby, long-term impairment of adult neurogenesis (Sierra et al., 2015). To evaluate whether the alterations in proliferation and survival of progenitor cells in ArcticAβ mice accelerates the disruption of neurogenesis during epileptogenesis, we analyzed DCX+ neuronal precursor cells at different time points (1, 3 , 6, 14 dpi) after IHK-induced status epilepticus (Fig. 7). DCX-IR decreased over time in both genotypes ($F_{(4, 40)}$ = 38.9, $p < 0.0001$, two-way ANOVA) , and at a similar rate (Fig. 7A), as previously described in wildtype mice (Ledergerber et al., 2006). In controls, DCX+ cells, which are located close to the SGZ, send their dendrites into the molecular layer (Fig. 7A). Ipsilaterally, DCX+ processes disappear within 1 dpi, followed by a gradual disappearance of most cell bodies until 14 dpi. Contralaterally, DCX-IR remained unchanged until 6 dpi, and increased at 14 dpi. However, there was no difference between ArcticAβ mice and wildtype littermates. Similarly, both genotypes exhibited a comparable number of ectopic cells in the hilus ($F_{(11, 96)}$ = 1.20, p = 0.2964, two-way ANOVA; Fig. 7B). In addition, ArcticAβ mice that died during status epilepticus did not differ from wiltype mice at 45 min post-injection with regard to DCX-IR or number of ectopic cells in the ipsilateral hilus (Fig. 7B). Taken together, the decline of neuronal progenitors after IHK-induced epileptogenesis follows a similar course in both genotypes.

Impairment in status epilepticus-induced upregulation of neuropeptide Y in ArcticAβ mice

Neuropeptide Y has anticonvulsive properties and is immediately upregulated in mossy fibers after increased excitation (Guo et al., 2002; Tu et al., 2005; Gotzsche et al., 2012). Reduced NPY expression has been reported in patients (Beal et al., 1986; Minthon et al., 1990) and animal models of AD (Ramos et al., 2006). Therefore, we determined whether AD-like pathology in 3-months-old ArcticAβ mice interferes with seizure-induced upregulation of NPY during early epileptogenesis (Fig. 8 and Table 3). In wildtype mice, NPY-IR was increased bilaterally, reaching significance in a region- and time-dependent manner across the various regions of the hippocampal formation (Fig. 8B). The increase was seen in both the GC and mossy fibers, as well as in interneurons contralaterally in CA1 and CA3. In comparison, ArcticAβ mice only

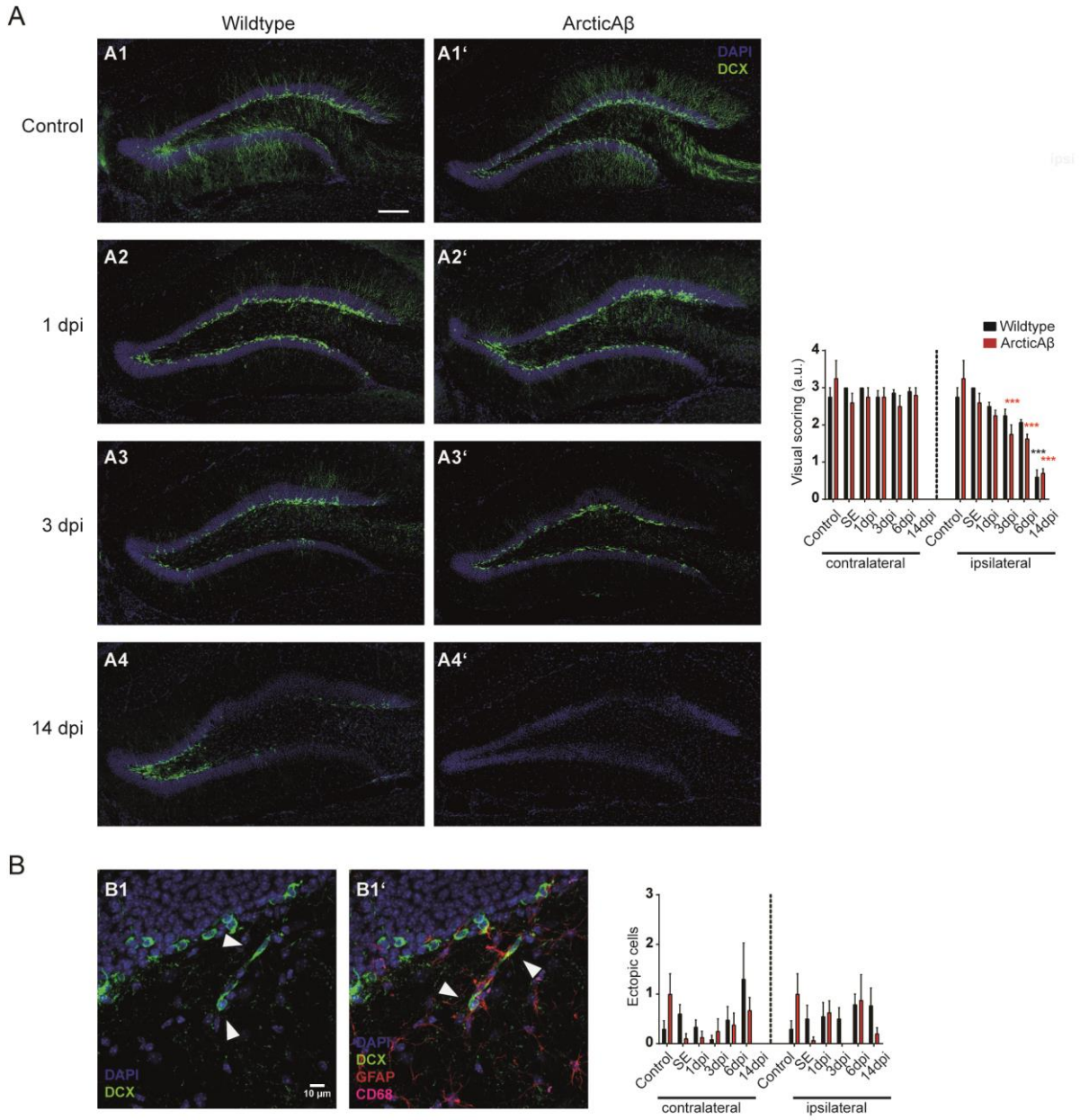

Figure 7 Gradual decrease of DCX+ progenitor cells in the ipsilateral SGZ during epileptogenesis. A, Representative images of the neurogenic niche in the dentate gyrus of wildtype and ArcticAβ mice. Over the course of epileptogenesis, DCX-IR in the SGZ of the ipsilateral dentate gyrus gradually decreases in both genotypes up to almost complete disappearance at 14 dpi, while it remains unchanged on the contralateral side (*** $p < 0.001$, **** $p < 0.0001$; two-way ANOVA). Scale bar, 200 µm. B, Ectopic cell in the hilus. The number of ectopic cells in the hilus is similar between ArcticAβ mice and wildtype littermates. Triple immunofluorescence labeling for glial and early neuronal markers ensured that ectopic cells are indeed newly born neurons. Quantitative data represent mean ± SEM.

displayed a moderate increase of NPY-IR at 1-3 dpi ipsilaterally and at 1-14 dpi contralaterally in the hilus and CA3c (Fig. 8 and Table 3). In the early SE group, there was no difference between wildtype mice perfused 45 min after injection and ArcticAβ mice that died due to a severe status epilepticus (Fig. 8B). Thus, while status epilepticus provokes a transient increase in NPY in dorsal hippocampus of wildtype mice, peaking after 24 hours and gradually declining

over two weeks, this mechanism seems to be partially impaired in ArcticAβ mice. SE group, there was no difference between wildtype mice perfused 45 min after injection and ArcticAβ mice that died due to a severe SE (Figure S5). Thus, while status epilepticus provokes a transient increase in NPY in dorsal hippocampus of wildtype mice, peaking after 24 hours and gradually declining over two weeks, this mechanism seem to be, at least partially, impaired in ArcticAβ mice.

Impairment of NPY expression as an early sequelae of AD pathology

To determine whether differences in microglial activation and NPY levels during epileptogenesis in ArcticAβ mice rest upon sequelae and immune system activation associated with AD pathology, we examined 3-months- and 9-months-old naive ArcticAβ mice (Fig. 9). While intracellular Aβ deposits have been reported in 3-months-old ArcticAβ mice (Knobloch et al. (2007), plaques appear between 7 and 9 months of age (Fig. 9A) with a progressive increase thereafter. Aβ plaques are surrounded by reactive microglia, but up to the age of 9 months, there is no general microglia activation, as seen by CD68-IR (two-ANOVA; Table 5; Fig. 9B). qPCR analysis of inflammatory cytokines in hippocampal samples revealed a decreased expression of IL-10 over time in both genotypes (one-way ANOVA, $F_{(1,16)} = 11$, $P = 0.004$; Fig. 9C) and a different expression of IL-1β between genotypes (one-way ANOVA, $F_{(1,16)} = 4.7$, $P = 0.047$; Fig. 9D). No difference was detected in TNF expression between wildtype and ArcticAβ mice at the age of 3 and 9 months ($F_{(1,16)} = 1.19$, $P = 0.291$; two-way ANOVA; Fig. 9E), whereas the expression of triggering receptor expressed on myeloid cells 2 (Trem2) – a cell surface receptor expressed on microglia cells that was proposed to be important for phagocytosis and removal of apoptotic cells and β-amyloid without being accompanied by inflammation (Colonna and Wang, 2016) – was increased concomitant with the appearance of Aβ plaques in 9-months old ArcticAβ mice ($F_{(1,16)} = 6.8$, $P = 0.02$; two-way ANOVA, Bonferroni post-hoc test; Fig. 9F). Interestingly, when we determined the hippocampal expression of markers involved in NPY signaling, ArcticAβ mice showed a significantly reduced expression of NPY at both 3 and 9 months of age ($F_{(1,16)} = 4.7$, $P = 0.047$; two-way ANOVA, Bonferroni post-hoc test; Fig. 9G). The NPY receptor 1 (YR1) expression was not affected ($F_{(1,16)} = 1.12$, $P = 0.3064$; two-way ANOVA; Fig. 9H), but ArcticAβ mice exhibited an increase in YR2 expression at 9 months ($F_{(1,16)} = 1.12$, $P = 0.3064$; two-way ANOVA; Fig. 9H) and a reduced YR5 expression at 3-months of age ($F_{(1,16)} = 1.12$, $P = 0.3064$; two-way ANOVA; Fig. 9G).

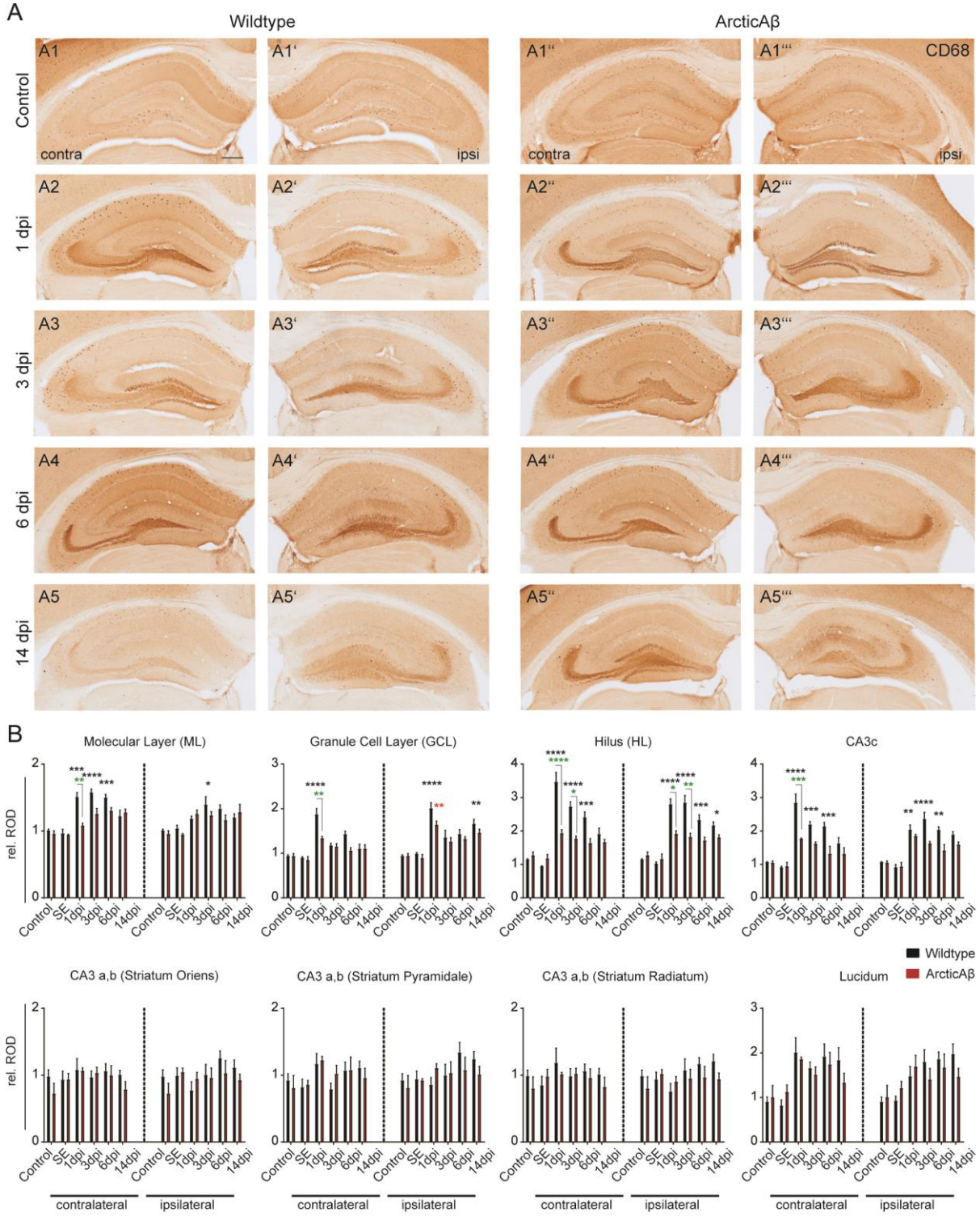

Figure 8 Impaired epileptogenesis-associated increase of neuropeptide Y in ArcticAβ mice. A, Representative images of NPY staining at different time points during epileptogenesis. NPY-IR increases bilaterally particularly in mossy fibers in the hilus and CA3 at 1 dpi and declines thereafter gradually until 14 dpi. B, Densitometric analysis of NPY-IR. IHK-injected mice show a significant increase in NPY levels in the ML, GCL, HL and CA3c. A comparison of both genotypes (green) reveals a significantly higher NPY-IR in the contralateral ML, HL, and CA3c as well as ipsilateral hilus of wildtype mice compared to ArcticAβ mice at 1 and 3 dpi (* $p < 0.05$, ** $p < 0.01$, *** $p < 0.001$, **** $p < 0.0001$; two-way ANOVA, Bonferroni post-hoc test). Quantitative data represent mean ± SEM.

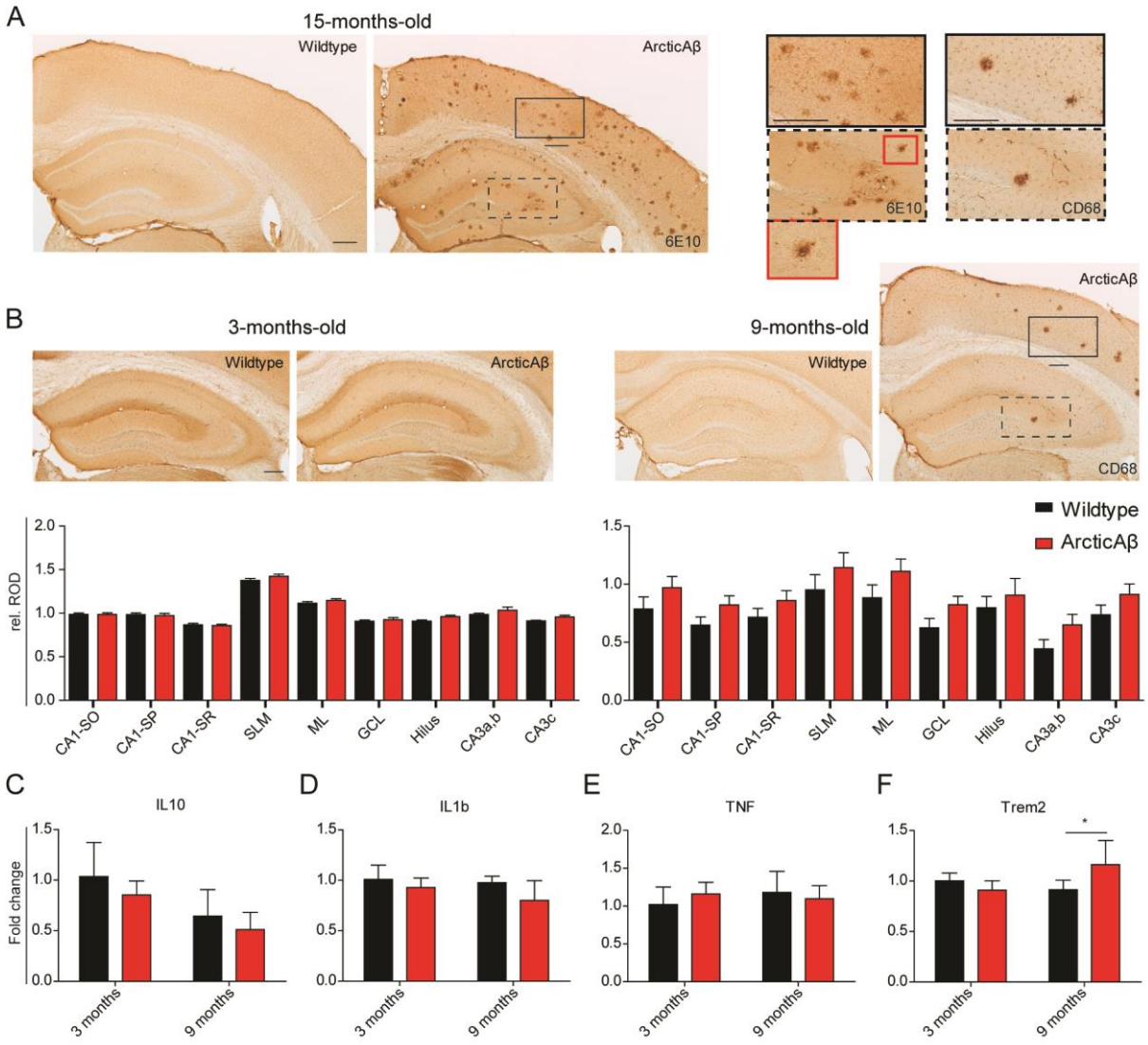

Figure 9 Reduced NPY expression is an early, pre-plaque sequelae of AD pathology. A, Representative images of tissue section stained for β-amyloid (6E10-IR) from 15-months-old ArcticAβ and wildtype mice. Only transgenic mice show plaques with their characteristic dense core morphology (red and black boxes). B, Representative images and densitometric analysis of CD68-IR in hippocampal sections from 3- and 9-months-old ArcticAβ and wildtype mice. From their appearance in ArcticAβ mice at 9 months of age, plaques are surrounded by activated microglia (black box). Densitometric analysis revealed no difference between genotypes at both the pre-plaque (3 months) and the early-plaque (9 months) stage (n = 6/group; one-way ANOVA). C-E, Hippocampal expression of cytokines IL10, IL1β, and TNF. While the expression of IL10 decreased over time ($F(1,16) = 10.96$, $P = 0.0044$) and IL1β differed between genotypes ($F(1,16) = 4.655$, $P = 0.0465$), TNF expression did not change. F, The expression of Trem2, a marker for microglial phagocytosis of β-amyloid peptides and apoptotic neurons without inflammation. ArcticAβ mice show a significant increase in Trem2 expression at 9 months of age, when β-amyloid plaques start to appear (n = 4-7; * $p < 0.05$, ** $p < 0.01$; two-way ANOVA, Bonferroni post-hoc test). Quantitative data represent mean ± SEM. Scale bars, 250 μm.

Previous studies in hAPP-J20 mice reported sprouting of NPY+ axons in the molecular layer, ectopic expression of NPY in mossy fibers, increased recurrent sprouting of mossy fiber collaterals (Timm staining or zinc transporter ZnT3-IR) and depletion of calbindin (CB) in GC (Palop et al., 2003; Palop et al., 2007). Increased levels of neuropeptides, most notably NPY in areas with high plaque burden, might reflect an attempt to counteract degeneration

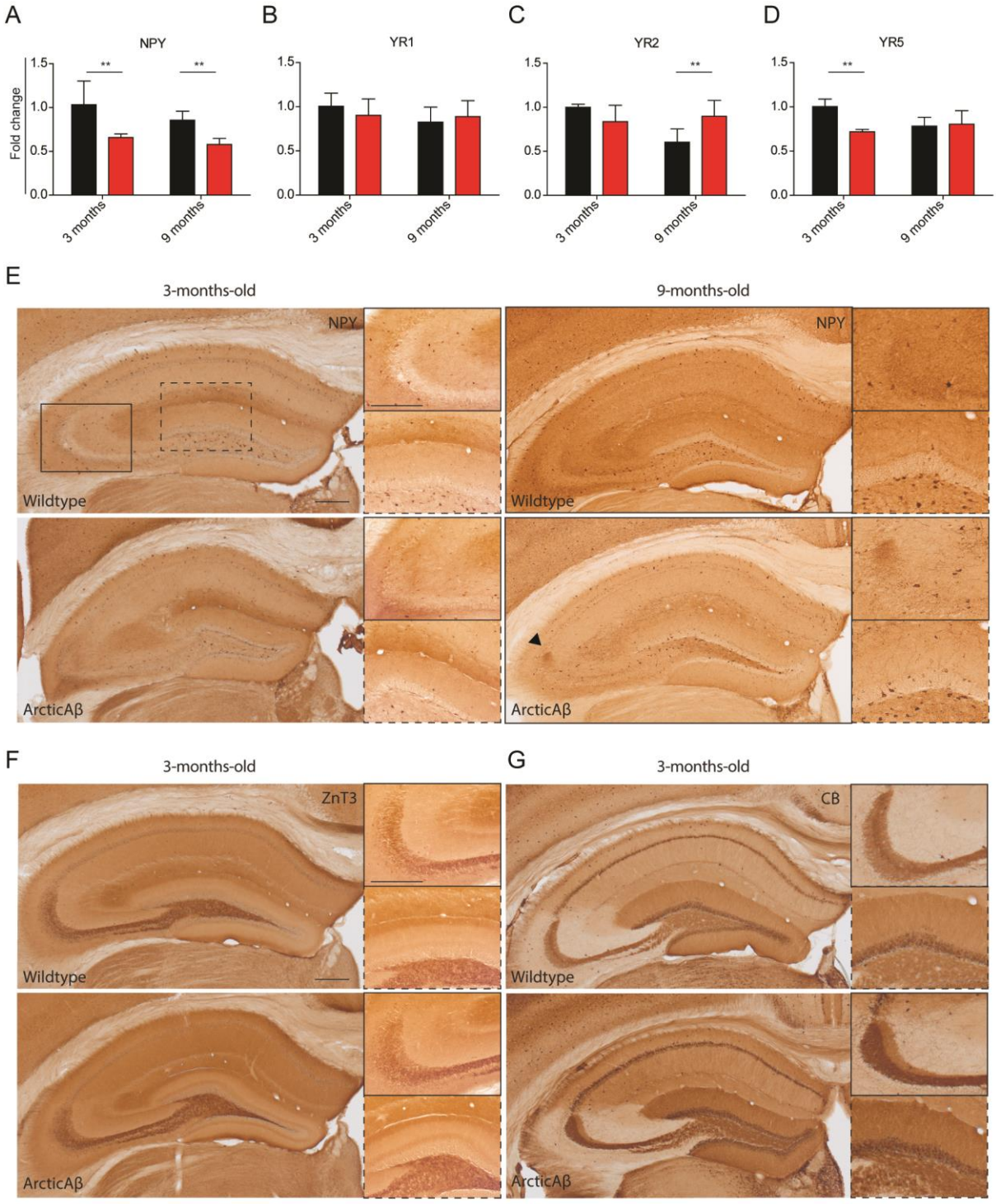

Figure 10 Neuropeptide Y, zinc transporter 3 and calbindin immunoreactivity in naive ArcticAβ mice during early AD pathology. A-D. Hippocampal expression of genes related to NPY signaling. The expression of NPY is reduced in both 3- and 9-months-old ArcticAβ mice. Regarding NPY receptors, YR1 expression does not change, while the expression of YR2 is increased at 9 months and YR5 decreased at 3 months in ArcticAβ mice (n = 4-7; * $p < 0.05$, ** $p < 0.01$; two-way ANOVA, Bonferroni post-hoc test). Quantitative data represent mean ± SEM.. E. Representative images of NPY-IR from 3-months and 9-months-old wildtype and ArcticAβ mice. Both genotypes reveal a similar NPY-IR at both time points. However, at 9 months, three of seven ArcticAβ mice reveal weak ectopic NPY-IR in mossy fibers visible in the hilus and CA3a,b (arrowhead). F, Representative images of ZnT3-IR in 3-months-old wildtype and ArcticAβ mice. There is no obvious axonal sprouting in the molecular layer in either genotype (dashed box). G, Representative images of CB-IR in ArcticAβ mice and wildtype littermates at 3 months. CB-IR in mossy fibers of CA3 (solid box) and in the granule cell layer of the dentate gyrus (dashed box) are comparable between genotypes. Scale bars, 250 µm.

(Diez et al., 2003). Therefore, we determined whether NPY, ZnT3 and CB were changed in naive ArcticAβ mice before (3 months) or after (9 months) occurrence of Aβ plaques (Fig. 10). Compared to wildtype littermates (n = 6-8 / time point) no difference in NPY-IR in the hilus and molecular layer of the dentate gyrus (Fig. 10A). Similarly, qualitative assessment of ZnT3-IR and CB-IR in GCs and in CA3 showed no difference between genotypes (Fig. 10B). Together, these observations suggest that gene expression involved in NPY signaling, specifically the expression of NPY and YR5, is impaired prior to occurrence of Aβ plaques and associated inflammatory reactions, but the presence of the transgene does not influence NPY-IR in 9-months-old mutants.

Soluble Aβ species contribute to the early onset of SRS during IHK-induced epileptogenesis

Given that 3-months-old ArcticAβ mice do not show any plaques while constitutively overexpressing Aβ (Knobloch et al., 2007), we aimed to determine whether a clearance of soluble Aβ species might prevent the early onset of SRS in these mice. Three days prior to the IHK-induced status epilepticus, a mouse anti-Aβ antibody (6E10) or a control IgG were bilaterally injected into the lateral ventricles on the anterio-posterior plane of the IHK-injection side (Fig. 11A). Mice were then subjected to continuous vEEG during the next three weeks and seizure-like events were analyzed. Interestingly, injection of Aβ antibody alleviated the epileptic phenotype in comparison to an IgG injection in ArcticAβ mice (Fig. 11B). While three out of four IgG-injected ArcticAβ mice exhibited regular SRS from 3-4 dpi, as shown above (Fig. 4E), and one died from convulsive seizures at 12 dpi, the four mice treated with Aβ antibody only had a few SRS-like events and did not develop SRS during the first 14 days post-IHK. In addition, several mice injected with IgG showed tonic-clonic seizures whereas only one of the ArcticAβ mice injected with Aβ antibody had a convulsive seizure. One IgG-injected animal exhibited multiple short clusters of spikes that were considered to be SRS-like events (B1 in Fig. 11B). In contrast, one mice injected with Aβ antibody had a transient phenotype, with only two short SRS-like events at 3 dpi, while otherwise the EEG pattern was characterized by short clusters of spikes (B2 in Fig. 11B). Noteworthy, this mouse (C3 in Fig. 11C), like the others, revealed the normal neurodegenerative pattern of the IHK-model (Bouilleret et al., 1999): degeneration of pyramidal cells in CA1 and C3c, as well as of hilar cells in the dentate gyrus (Fig. 11C). In the eight mice administered with IgG or Aβ antibodies, no GC dispersion was seen, suggesting a potential interference between the two processes. Taken together, antibody-mediated neutralization of soluble Aβ species prevented the occurrence of SRS during the latent phase in

3-months-old ArcticAβ mice, suggesting that Aβ overexpression promotes epileptogenesis in these mice.

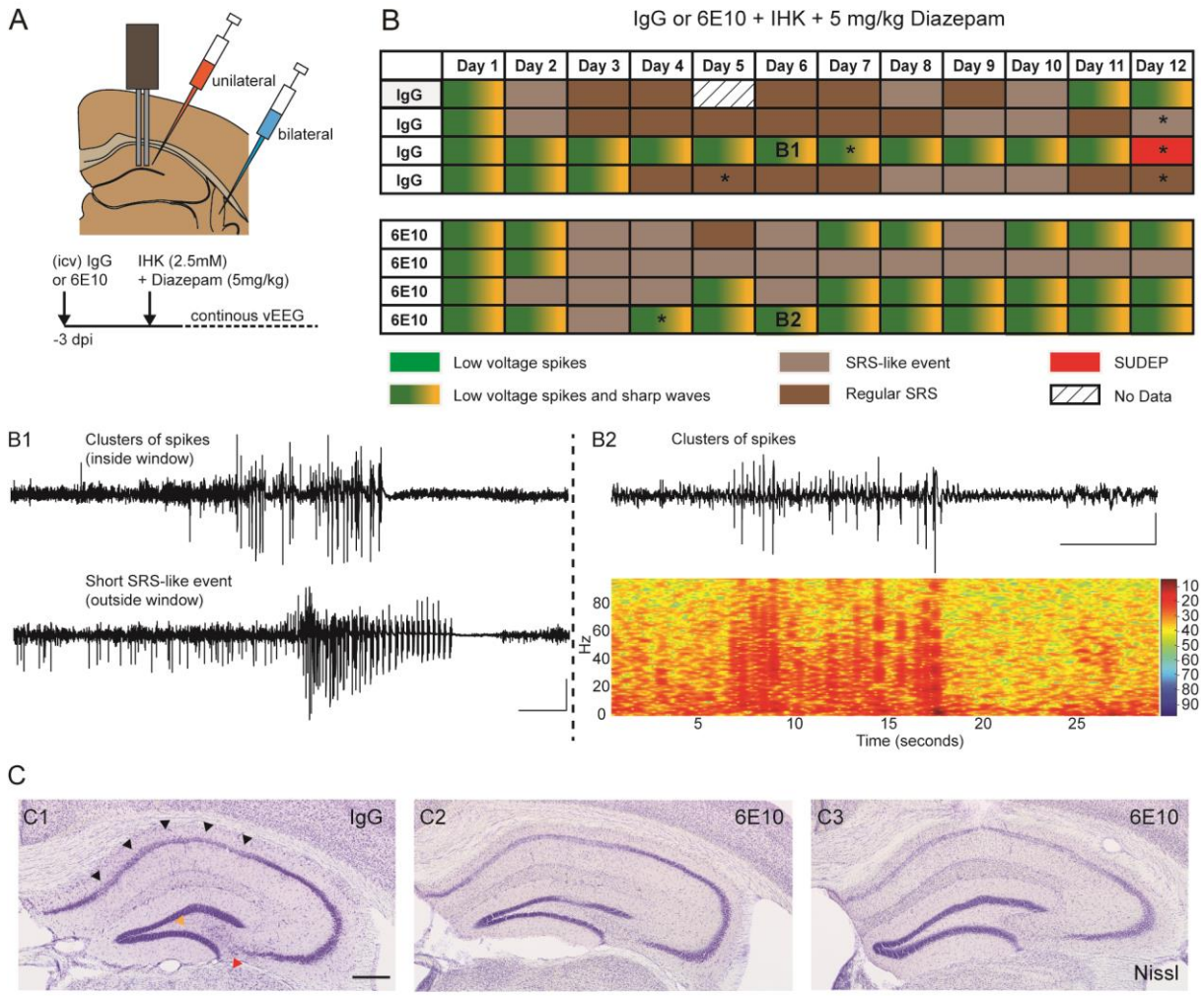

Figure 10 Clearance of soluble Aβ species ameliorates epileptic phenotype in 3-months-old ArcticAβ mice during early epileptogenesis. A, Schematic representation of the experimental design using the anti-Aβ antibody, 6E10. Three days before the unilateral IHK injection, ArcticAβ mice were intracerebroventricularly (icv) injected with either 6E10 or control IgG into both hemispheres near the dorsal hippocampus. After injecting IHK, mice were monitored by vEEG to assess early onset of seizures in ArcticAβ mice. B, Characterization of EEG pattern during the latent period. IgG-treated ArcticAβ mice exhibited multiple SRS-like events and regular SRS, whereas mice injected with 6E10 showed only a few SRS-like events and short single or grouped spikes. B1, Example of IgG-injected mouse that had few SRS-like events within the analysis window; this animal had a high number of spikes clusters that were sometimes followed by a SRS-like event occurring outside of the window chosen for analysis. B2, This 6E10-injected mouse showed almost exclusively single or grouped spikes with typical frequency and power characteristics (spectrogram below). Scale bars, 500 µV, 5 s. C, Cresyl violet staining of the ipsilateral hippocampus. Both IgG and 6E10 pre-treated animals showed the characteristic neurodegenerative pattern seen after IHK injection, including degeneration of pyramidal cells in CA1 (black arrowheads), CA3c (red arrowhead), and the cells in the hilus (yellow arrowheads). The mouse illustrated in (B2) shared these typical histopathological hallmarks (C3). Note the absence of GC dispersion in both groups. Scale bars, 150 µm.

Discussion

The results indicate that transgenic expression of mutant APP in ArcticAβ mice leads to increased susceptibility towards KA-induced hyperexcitability long before the stage of plaque formation. In these mice, the strength of GABAergic inhibition in the CA1 region is reduced, facilitating LTP and altering the power of gamma oscillations. Hyperexcitability in ArcticAβ mice leads to lethal convulsions during status epilepticus, which can be prevented by diazepam. In addition, it leads to the premature onset of SRS, and in some mice, to lethal convulsive seizures during the first three weeks post-IHK. This increased seizure susceptibility does not correlate with aggravated neurodegeneration, altered synaptic reorganization, immune responses or adult neurogenesis, but is paralleled by a reduced basal expression and upregulation of NPY in dentate gyrus GC, a neuropeptide with anti-convulsant properties. Importantly, hyperexcitability could be reversed upon neutralization of soluble Aβ species, arguing against constitutive adaptation mechanisms and in favor of a direct effect on synaptic, in particular GABAergic, transmission in the hippocampal formation.

Hyperexcitability and epileptogenesis in AD mouse models

AD is associated with network abnormalities, characterized by hypersynchrony and altered oscillatory activity that precede clinical disease onset (Palop and Mucke, 2016). Epileptiform activity has been reported in AD patients, in particular at early stages (Amatniek et al., 2006; Scarmeas et al., 2009; Vossel et al., 2013; Vossel et al., 2016) and with a higher incidence during sleep (Horvath et al., 2017; Lam et al., 2017). Recent studies confirmed that hyperexcitability in AD mouse models appears prior to plaque and tangle pathology. For example, 25% CA1 pyramidal cells are hyperactive in mice overexpressing human APP with a Swedish mutation and mutant human presinilin 1 (APP/PS1) already at an age of 1.5 months (Busche et al., 2012). This neuronal dysfunction was rescued by acute treatment with a ɣ-secretase inhibitor and neuronal hyperexcitability was induced in wildtype mice by applying soluble Aβ. Although which cell types are most vulnerable and therefore first affected by Aβ is not fully clarified, interneurons are among the earliest cells affected. Axonal loss of SOM+ interneurons in CA1 was reported in APP/PS1 mice at pre-plaque stage, and at later stages correlating with proximity to Aβ plaques (Schmid et al., 2016), suggesting that GABAergic boutons are affected early by soluble Aβ species. In line with these findings, we found in young ArcticAβ mice that decreased synaptic strength and increased KA-induced LTP are associated with changes in sIPSCs in CA1

pyramidal cells. Unlike previous studies using mice overexpressing human APP with a Swedish mutation (hAPP-J20) at plaque-bearing stage (Palop et al., 2007), we did not find any increase in inhibitory activity at baseline. As suggested by Palop et al. (2007), increased inhibitory activity might be a compensatory response to an hyperexcitable phenotype. Such compensatory mechanism might explain clustered sIPSCs at baseline in ArcticAβ mice (Fig. 3). Ectopic expression of NPY and sprouting of GABAergic axons has been reported in different AD mouse models (Chin et al., 2004; Palop et al., 2007; Roberson et al., 2007). Our results indicate that these effects differ between models, especially in the timing of their appearance. Nevertheless, plaque-independent Aβ toxicity appears as a predominant feature altering local inhibitory circuits and increasing network excitability during early stages of the AD pathogenesis.

Increased susceptibility to induced seizures have been reported in different mouse models of AD (Palop et al., 2007; Roberson et al., 2007; Roberson et al., 2011; Sanchez et al., 2012; Verret et al., 2012; Kam et al., 2016). AD transgenic mice show age-dependent, and therefore disease-stage-dependent, occurrence of SRS with hippocampal origin (Palop et al., 2007; Minkeviciene et al., 2008; Kam et al., 2016). In our model, it is unclear which mechanisms underlie the development of SRS. We have shown previously in mutant mice lacking lymphocytes (RAG1-knockout), which exhibit SRS within 24 h of IHK, that the latent period can be massively curtailed (Zattoni et al., 2011; Deprez et al., 2011). Our present results indicate a key role for soluble Aβ species, but the reduced overexpression of NPY in mutant mice compared to their wildtype littermates might also be an important contributing factor, along with the differential regulation of cytokines seen in our qPCR analysis.

The role of NPY during epileptogenesis

A body of literature examined the effect of NPY on modulating excitatory transmission and its role during different stages of epileptogenesis (Baraban, 2002; El Bahh et al., 2005). Erickson et al. (1996) reported that NPY-deficient mice are more susceptible to seizures induced by the GABAergic antagonist pentylenetetrazole (PTZ). Moreover, status epilepticus induced by repeated intraperitoneal injection of low dose kainic acid led to convulsive seizures in both genotypes at a similar concentration and within the same latency, but being lethal for 90% NPY-deficient mice compared to 22% wildtype littermates (Baraban et al., 1997). Similarly, Y5R-deficient mice are more susceptible to KA, having more severe seizures and increased mortality (Marsh et al., 1999). Here, we found a similar phenotype after IHK in young ArcticAβ mice accompanied by weaker expression of NPY and Y5R at the age of injection (Fig. 9). In contrast, NPY application (Woldbye et al., 1996; Baraban et al., 1997; Woldbye et al., 1997; Vezzani et

al., 1999c) or hippocampal overexpression of NPY and Y2R or Y5R using rAAV vectors (Richichi et al., 2004; Sorensen et al., 2009; Woldbye et al., 2010; Gotzsche et al., 2012) were shown to have an alleviating effect on electrically or chemically induced acute seizures. In particular, seizures of higher severity and seizure-associated death were reduced upon activation of NPY signaling, while mild seizures remained unchanged. We likewise found no difference in the latency, number or duration of non-convulsive seizures in ArcticAβ mice during IHK-induced status epilepticus (Fig. 4). Moreover, at 9 months of age, hippocampal Y2R expression is increased in ArcticAβ mice, similar to plaque-bearing hAPP-J20 mice (Palop et al., 2007), suggesting a compensatory mechanism after months of increased excitability.

Although, the similarities between NPY-deficient animals and ArcticAβ mice are compelling, additional experiments are needed to evaluate if the decrease in NPY expression is directly responsible for the hyperexcitable phenotype of the AD model. To this end, it would be interesting to test whether neutralization of soluble Aβ species (e.g. with the 6E10 antibody) would restore NPY expression and signaling in ArcticAβ mice, and thereby ameliorate the excitability in vivo and in slices.

The role of inflammation during epileptogenesis

Perhaps the least expected finding of this study is that inflammation that accompanies neurodegeneration in the dorsal hippocampus after IHK was not more severe in ArticAβ mice, despite on-going stimulation of innate immunity by increased Aβ species and their accumulation in the brain (Knobloch et al., 2007). In our previous work in RAG1-KO mice (Zattoni et al., 2011), we showed that in the absence of adaptive immunity by T and B lymphocytes, IHK causes a stimulation of innate immunity mediated by neutrophils, leading to extensive neurodegeneration in CA1-CA3 and eventually complete atrophy of the injected hippocampus. We also observed that this phenotype is accompanied by a dramatic shortening of the seizure-free latent phase that follows IHK, with RAG1-KO mice exhibiting SRS at 1-2 dpi (Zattoni et al., 2011). Therefore, the disrupted balance between adaptive and innate immunity induces a condition in the brain of IHK-treated mice that favors SRS onset, presumably mediated by inflammation-related secreted or blood-born factors. Our present results show that the AD-like predisposition in ArticAβ mice also induces a condition that favors the occurrence of SRS during the latent phase, which is due, at least in large part to Aβ overexpression in the brain, and which does not stimulate further inflammatory mechanisms that would aggravate neurodegeneration. Both studies relativize the importance of neuronal circuit reorganization that takes place during the latent phase for SRS onset. Rather, they favor the view that the latent phase is seizure-free

because of unknown protective mechanisms preventing seizure onset. These mechanisms can be overruled by immune factors or by hyperexcitability.

Therefore, despite the fact that temporal lobe epilepsy and AD share common pathogenic mechanisms and exhibit comparable alterations in inhibitory neuronal networks in the hippocampal formation, as outlined in the Introduction, there appears to be little cross-over between the two disease conditions. In AD patients, like in mice subject to IHK, epileptogenic activity and unprovoked seizures are most likely related to toxic Aβ species affecting synaptic transmission and favoring a state of chronic hyperexcitability.

Supplementary Information

Table S1 Results of statistical tests performed for immunohistochemical stainings (1)

CD68 (Figure 5)				**NPY** (Figure 8)			
Area	Source of Variation	F (DFn, DFd)	P value	Area	Source of Variation	F (DFn, DFd)	P value
CA1 - SO	Interaction	F (9, 80) = 1.486	P=0.1674	ML	Interaction	F (9, 78) = 3.062	P=0.0034
	Genotype	F (1, 80) = 3.723	P=0.0572		Genotype	F (1, 78) = 13.97	P=0.0004
	Time	F (9, 80) = 28.97	P<0.0001		Time	F (9, 78) = 8.029	P<0.0001
CA1 - SP	Interaction	F (9, 80) = 1.282	P=0.2598	GCL	Interaction	F (9, 78) = 1.757	P=0.0901
	Genotype	F (1, 80) = 3.237	P=0.0758		Genotype	F (1, 78) = 13.6	P=0.0004
	Time	F (9, 80) = 56.68	P<0.0001		Time	F (9, 78) = 15.85	P<0.0001
CA1 - SR	Interaction	F (9, 80) = 1.338	P=0.2309	HL	Interaction	F (9, 78) = 4.85	P<0.0001
	Genotype	F (1, 80) = 4.28	P=0.0418		Genotype	F (1, 78) = 67.47	P<0.0001
	Time	F (9, 80) = 16.5	P<0.0001		Time	F (9, 78) = 15.52	P<0.0001
SLM	Interaction	F (9, 80) = 0.7	P=0.7070	CA3c	Interaction	F (9, 78) = 2.584	P=0.0116
	Genotype	F (1, 80) = 1.492	P=0.2256		Genotype	F (1, 78) = 44.9	P<0.0001
	Time	F (9, 80) = 25.7	P<0.0001		Time	F (9, 78) = 12.48	P<0.0001
ML	Interaction	F (9, 80) = 0.7915	P=0.6249	CA3a,b - SO	Interaction	F (9, 77) = 0.6358	P=0.7631
	Genotype	F (1, 80) = 0.06475	P=0.7998		Genotype	F (1, 77) = 2.937	P=0.0906
	Time	F (9, 80) = 12.13	P<0.0001		Time	F (9, 77) = 1.16	P=0.3322
GCL	Interaction	F (9, 79) = 1.006	P=0.4425	CA3a,b - SP	Interaction	F (9, 77) = 0.7915	P=0.6250
	Genotype	F (1, 79) = 1.653	P=0.2023		Genotype	F (1, 77) = 0.1921	P=0.6624
	Time	F (9, 79) = 8.004	P<0.0001		Time	F (9, 77) = 1.48	P=0.1703
HL	Interaction	F (9, 79) = 1.738	P=0.0940	CA3a,b - SR	Interaction	F (9, 77) = 0.4054	P=0.9286
	Genotype	F (1, 79) = 4.389	P=0.0394		Genotype	F (1, 77) = 3.654	P=0.0597
	Time	F (9, 79) = 17.29	P<0.0001		Time	F (9, 77) = 0.8237	P=0.5963
CA3c	Interaction	F (9, 80) = 0.4201	P=0.9208	Lucidum	Interaction	F (9, 77) = 0.5332	P=0.8461
	Genotype	F (1, 80) = 2.593	P=0.1112		Genotype	F (1, 77) = 2.248	P=0.1379
	Time	F (9, 80) = 36.45	P<0.0001		Time	F (9, 77) = 3.357	P=0.0016
CA3a,b - SO	Interaction	F (9, 77) = 2.006	P=0.0498				
	Genotype	F (1, 77) = 1.286	P=0.2602				
	Time	F (9, 77) = 11.22	P<0.0001				
CA3a,b - SP	Interaction	F (9, 77) = 0.7629	P=0.6506				
	Genotype	F (1, 77) = 0.6179	P=0.4342				
	Time	F (9, 77) = 11.91	P<0.0001				
CA3a,b - SR	Interaction	F (9, 77) = 0.9621	P=0.4777				
	Genotype	F (1, 77) = 8.415	P=0.0048				
	Time	F (9, 77) = 11.61	P<0.0001				
Lucidum	Interaction	F (9, 77) = 1.263	P=0.2707				
	Genotype	F (1, 77) = 0.3842	P=0.5372				
	Time	F (9, 77) = 16.16	P<0.0001				

The results of two-way ANOVA tests assessing changes in CD68- and NPY-IR in ArticAb mice and wildtype littermates. Source of variation includes interaction (Int), genotype (Geno) and time. The degrees of freedom numerator (Dfn) and denominator (Dfd) of the F distribution are indicated in brackets. SO, stratum oriens; SP, stratum pyramidale; SR, stratum radiatum; SLM, stratum lacunosum moleculare; ML, molecular layer; GCL, granule cell layer; HL, hilus.

Table S2 Results of statistical tests performed for immunohistochemical stainings (2)

CD68 (Figure 9)			
Area	Source of Variation	F (DFn, DFd)	P value
CA1 - SO	Inter	F (1, 20) = 2.40	P=0.1369
	Geno	F (1, 20) = 2.34	P=0.1417
	Age	F (1, 20) = 3.08	P=0.0943
CA1 - SP	Inter	F (1, 20) = 2.55	P=0.1259
	Geno	F (1, 20) = 2.07	P=0.1652
	Age	F (1, 20) = 18.05	P=0.0004
CA1 - SR	Inter	F (1, 20) = 1.60	P=0.2206
	Geno	F (1, 20) = 1.26	P=0.2756
	Age	F (1, 20) = 1.51	P=0.2334
SLM	Inter	F (1, 20) = 0.60	P=0.4485
	Geno	F (1, 20) = 1.61	P=0.2195
	Age	F (1, 20) = 14.00	P=0.0013
ML	Inter	F (1, 20) = 1.49	P=0.2362
	Geno	F (1, 20) = 2.68	P=0.1174
	Age	F (1, 20) = 2.84	P=0.1073
GCL	Inter	F (1, 20) = 2.61	P=0.1217
	Geno	F (1, 20) = 3.69	P=0.0692
	Age	F (1, 20) = 11.83	P=0.0026
HL	Inter	F (1, 20) = 0.09	P=0.7701
	Geno	F (1, 20) = 0.68	P=0.4192
	Age	F (1, 20) = 0.77	P=0.3921
CA3c	Inter	F (1, 20) = 1.03	P=0.3229
	Geno	F (1, 20) = 2.98	P=0.0995
	Age	F (1, 20) = 2.89	P=0.1044
CA3a,b	Inter	F (1, 20) = 1.41	P=0.2483
	Geno	F (1, 20) = 3.77	P=0.0664
	Age	F (1, 20) = 49.70	P<0.0001

The results of one-way ANOVA tests assessing changes in CD68-IR in ArticAb mice and wildtype littermates. Source of variation includes interaction (Int), genotype (Geno) and time. The degrees of freedom numerator (Dfn) and denominator (Dfd) of the F distribution are indicated in brackets. SO, stratum oriens; SP, stratum pyramidale; SR, stratum radiatum; SLM, stratum lacunosum moleculare; ML, molecular layer; GCL, granule cell layer; HL, hilus.

STUDY III: CONTRIBUTION OF EARLY ABERRANT ACTIVITY TO THE DEVELOPMENT OF ACQUIRED EPILEPSY

Tilo Gschwind[1,2], Mikko Ojala[3,4], Darren Reed[5,6], Jean-Marc Fritschy[1,2] and Ivan Soltesz[3]

[1] Institute of Pharmacology and Toxicology, University of Zurich, Switzerland

[2]Neuroscience Center Zurich, University of Zurich and ETH Zurich, Winterthurerstrasse 190, CH-8057 Zurich, Switzerland

[3] Department of Neurosurgery, Stanford University, Stanford, CA 94305, USA

[4] Department of Anatomy and Neurobiology, University of California, Irvine, Irvine, CA 92697, USA.

[5] Institute for Computational Science, University of Zurich, Winterthurerstrasse 190, 8057 Zurich, Switzerland

[6] S3IT, University of Zurich, Winterthurerstrasse 190, 8057 Zurich, Switzerland

In preparation for publication

Author's contribution

All experiments were carried out by TG. The program for fast intervention and post analysis were written by TG and MO, while the analysis program was implemented on a HPC cluster in collaboration with DR. The study was conceptualized by TG, IS and JMF. TGs and JMF wrote the manuscript. Authors have no conflict of interest to declare.

Abstract

Temporal lobe epilepsy (TLE) is one of the most common forms of epilepsy in adults and often medically refractory. The development of TLE is associated with multiple alterations, like neurodegeneration and the formation of new recurrent excitatory circuits, rendering the network susceptible for the generation of spontaneous recurrent seizures (SRS). Many of these features can be replicated by inducing status epilepticus (SE) in mice through a single intrahippocampal kainic acid (IHK) injection. While this and other animal models of TLE are well suited to study different facets of epileptogenesis, it remains difficult to identify the mechanisms that directly contribute to the formation of an epileptic focus. Interestingly, however, during the latent, seizure-free period directly following SE, when most of these processes occur, brief epileptic discharges precede the first occurrence of SRS. In order to determine whether this early epileptiform activity drives network reorganization during epileptogenesis, we used closed-loop optogenetic intervention (COI) in the IHK model during the first two weeks post-injection, prior to the onset of SRS. Our preliminary data suggest that early epileptic discharges during the latent period contribute to the development of SRS.

Introduction

Temporal lobe epilepsy (TLE) belongs to one of the most common adult partial seizure disorders and is often refractory to current anti-epileptic drugs (Engel, 1998; Semah et al., 1998; Browne and Holmes, 2001). Traditionally, epilepsy research focused on seizure control and reduction in chronic, already established epilepsy. However, a major research interest resides in elucidating the mechanisms underlying the development of epilepsy and uncovering possibilities to interfere early on during the process of epileptogenesis, by disrupting processes that lead to the emergence of spontaneous recurrent seizures (SRS) after a brain insult. While there have been notable recent advances in this field, e.g., by applying agents that alter various signaling pathways like BDNF (McNamara and Scharfman, 2012), mTOR (Lasarge and Danzer, 2014) or NRSF (McClelland et al., 2014), the etiology and pathogenesis of the histological changes and their relationship with neuronal network alterations underlying the generation and the persistence of recurrent seizures in TLE remain unknown.

Several lines of evidence indicate that "seizures beget seizures" in TLE (reviewed in (Ben-Ari et al., 2008)). Severity and frequency of seizure can be directly linked to neuronal loss in certain limbic areas (e.g. (Buckmaster et al., 2017)). Moreover, selective cell loss, for example of interneurons (Antonucci et al., 2012; Spampanato and Dudek, 2017) or hilar mossy cells in the dentate gyrus (Jinde et al., 2012), is associated with aberrant neuronal discharges and substantial neuronal reorganization. In animal models of acquired epilepsy, such short epileptic discharges are characteristic for the latent period (Riban et al., 2002a), the phase between a precipitating brain insult and the onset of SRS. As a consequence of a chemically or electrically induced status epilepticus (SE), neuronal loss, synaptic reorganization and other neuropathological changes can be observed, notably during the latent period (Suzuki et al., 1995b; Bouilleret et al., 1999; Bouilleret et al., 2000b; Bouilleret et al., 2000a; Duveau et al., 2011). However, it still remains to be determined whether epileptiform activity during this period, prior to onset of SRS, is a mere manifestation of functional alterations or a driver of epileptogenesis.

Hence, rather than investigating different pathways potentially contributing to epileptogenesis, we determined whether control of aberrant neuronal activity during the initial phases of epileptogenesis is able to significantly decrease seizure frequency and prevent the structural and functional changes associated with epilepsy. To this end, a closed-loop optogenetic approach had to be designed to intervene selectively upon brief aberrant activity and curtailing these epileptiform events. In the intrahippocampal kainic acid (IHK) mouse model of TLE, a multi-

algorithm based detection software was previously used for on-demand seizure suppression during the chronic phase, starting 2 weeks after IHK injection (Armstrong et al., 2013; Krook-Magnuson et al., 2013; Krook-Magnuson et al., 2014; Ewell et al., 2015; Krook-Magnuson et al., 2015) The existing system was adapted for closed-loop optogenetic intervention (COI) to inhibit low-voltage spikes, spike-and-wave events and bursts of high frequency that were previously found to be characteristic for the latent period, which lasts for approximately two weeks after an IHK-induced SE (Riban et al., 2002a). Preliminary results of this early COI suggest that activity-dependent pathological plasticity processes contribute to the emergence and frequency of SRS.

Materials and Methods

Animals

All procedures were approved by the Stanford University's Animal Care and Use Committee. The molecular Cre-lox system was enabled the selective expression of the excitatory channelrhodopsin (ChR2) and the inhibitory halorhodopsin (HR) into specific cell populations. To this end, mice expressing Cre either in PV-containing GABAergic interneurons (PV-Cre;B6;129P2-Pvalbtm1(Cre)Arbr/J; stock 008069 from Jackson labs (Hippenmeyer et al., 2005)) or in principal cells (CamK-Cre; B6.Cg-Tg(Camk2a-cre)T29-1Stl/J; stock 005359 from Jackson labs (Tsien et al., 1996)) were crossed with either floxed-STOP ChR mice (Ai32; Rosa-CAG-LSLChR2H134R-EYFP-deltaNeo; Jackson labs, stock 012569 (Madisen et al., 2012)) or floxed-STOP HR mice (Ai39; B6;129S-Gt(ROSA)26Sortm39(CAGHOP/EYFP)Hze/J; Jackson labs, stock 014539 (Madisen et al., 2012)), respectively. Similar to Krook-Magnuson et al. (2013), all experiments were performed with these two cohorts, mice expressing ChR in all PV+ cells (PV-ChR) and mice expressing HR in principal cells (Cam-HR). Littermates that do not express the opsin were used as controls. All animals were housed at standard conditions (20-24℃; minimum 40% relative humidity) under a 12-hour light/dark cycle, with access to food and water ad libitum.

Intrahippocampal kainic acid (IHK) injection and implantation of optrodes and electrodes

The stereotactic surgeries were performed similar to Krook-Magnuson et al. (2013), however, including minor adjustments to investigate epileptogenesis. Mice were anaesthetized with 2.5-3% isoflurane in oxygen and 70 nL kainic acid (5mM in NaCl; Tocris biosciences) was injected into the right dorsal hippocampus (anteroposterior [AP] -1.8 mm, mediolateral [ML] -1.6 mm, dorsoventral [DV] -1.9 mm relative to Bregma) as described by Bouilleret et al. (2000b). A bipolar depth electrode (PlasticsOne) was inserted at the same location. Optrodes, optic fibers (0.37NA, Low OH, 200 μm diameter, ThorLabs) attached to ceramic ferrulas (Kientec Systems, Inc.), were build as described in Armstrong et al. (2013) and placed into the striatum oriens of CA1 to provide light to the hippocampal formation. In PV-ChR mice, optrodes were implanted ipsilaterally (AP -2.3 mm, ML 1.75 mm, DV -1.25 mm), posterior to the epileptic focus, and contralaterally (AP -1.8 mm, ML -1.75 mm, DV -1.25 mm) on the same plane as the IHK injection. In Cam-HR mice, optrodes were placed near the IHK injection on the ipsilateral side (AP -2.3 mm, ML 1.75 mm, DV -1.25 mm). Two screws were used for additional support and

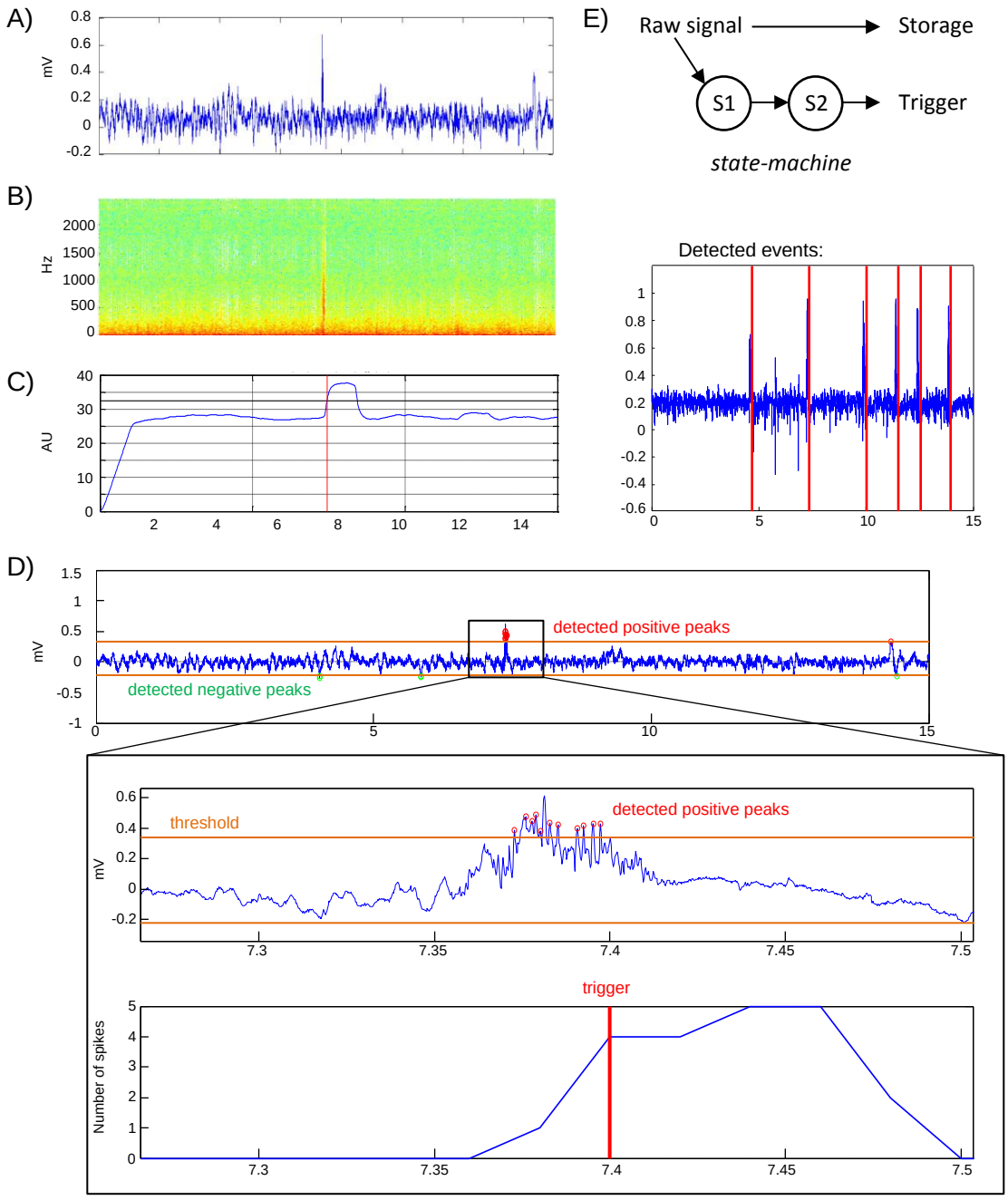

Figure 1 Online, fast detection of short epileptic events and close-loop optogenetic intervention (COI). (A) The signal was sampled at 5 kHz, buffered and one frame of 100 samples (20 ms) was processed at a time. In order to detect epileptic activity online, gain factors for thresholds of different signal properties were selected by the user. Thresholds were obtained by calculating the standard deviation of the signal and two first order unit gain IIR-filter integrators (Slow and Fast integrator). These integrators were used to threshold the different signal properties by specifying the rate of change over time. (B) Changes in energy of different frequency bands are characteristic for epileptic activity. Therefore, their contribution to the frequency spectrum of the signal was tracked by computing an FFT (Fast Fourier Transform). The different frequency bands could be selected and their ratio was compared to a predefined threshold. (C) As the signal of most spikes are of high amplitude and high frequency, the sum of distances between consecutives data points, the coastline, was calculated. (D) During early epileptogenesis, spikes were often characterized by an initial raise in amplitude followed by a small spike-train-like, high frequency activity. Predefining the width and distance between these small spikes, peaks were detected above a specific threshold. (E) The raw signal is saved for post-analysis and processed online for COI. A state-machine approach was used to define the trigger conditions. A first state (S1) consisting of a sum of different criteria (i.e. defined signal features) had to be met and followed by a second state (S2) with different conditions before the laser was triggered.

together with optrodes and electrodes fix to the skull by a combination of Prime&Bond (Dentsply) and Tetric EvoFlow® (Ivoclar vivadent).

Electroencephalographic (EEG) recordings and online closed-loop intervention (COI)

Directly after surgeries, mice were placed into a recording cage for EEG monitoring and later closed-loop optogenetic intervention. As earlier described (Armstrong et al., 2013; Krook-Magnuson et al., 2013), an electric commutator (PlasticsOne) connected the mouse to the amplifier (NeuroPhase 440) and signals sampled at 5 kHz were digitized (NI USB-6229 M Series DAQ) and analyzed in real-time by a custom-made MATLAB program (see below). Up to 8 animals could be recorded in parallel, while hourly files were saved (i.e. a recording file). After 24 hours, when the status epilepticus ended and the latent period began (Riban et al., 2002a), the closed-loop optogenetic intervention was conducted for 12 days to curtail short clusters of spikes. The light was applied by different fiber-coupled diode lasers (Shanghai Laser & Optics Century Co., Ltd), which each were connected to the implanted optrode of an animal by a ceramic split sleeve (Precision Fibre Products, Inc.), optical patch cords (Thorlabs, Doric lenses) and optical commutator (Doric lenses). Lasers with a wavelength of 473 nm were used for PV-ChR mice, while Cam-HR mice were connected to lasers with a wavelength of 589 nm. As the laser power at the source differed between different diode lasers (20-50 mW), optrodes were selected prior the implantation to provide a laser power at the tips of the optical fiber of approximate 10 mW.

For a fast intervention upon short epileptic events, the online seizure detection software used for closed-loop optogenetic seizure intervention (Armstrong et al., 2013; Krook-Magnuson et al., 2013; Krook-Magnuson et al., 2015) was modified. A state-machine approach, where several conditions have to be true in sequential manner, enabled a fast online detection of epileptic activity within approximately 40 ms (Figure 1) to detect and inhibit during single or small clusters of spikes. Thresholds for several signal features were selected, including power (magnitude and rate of change), spike (amplitude and width) and frequency (changes in energy within different frequency bands) properties (for details compare (White et al., 2006; Krook-Magnuson et al., 2013)). Inclusion or exclusion criteria were formulated for each animal individually by combining these features using Boolean operators and defining their sequential appearance in order to maximize sensitivity and specificity of the detection. Once the specific criteria were met, the program triggered the activation of the laser for an immediate intervention. Short light pulses (50 ms on, 100 ms off) were applied for 2 s. To avoid constant triggering over

a long period of time, an intermission of 5s to the next trigger was implemented and in only 50% of detected events (in a random sequence), the laser was actually triggered.

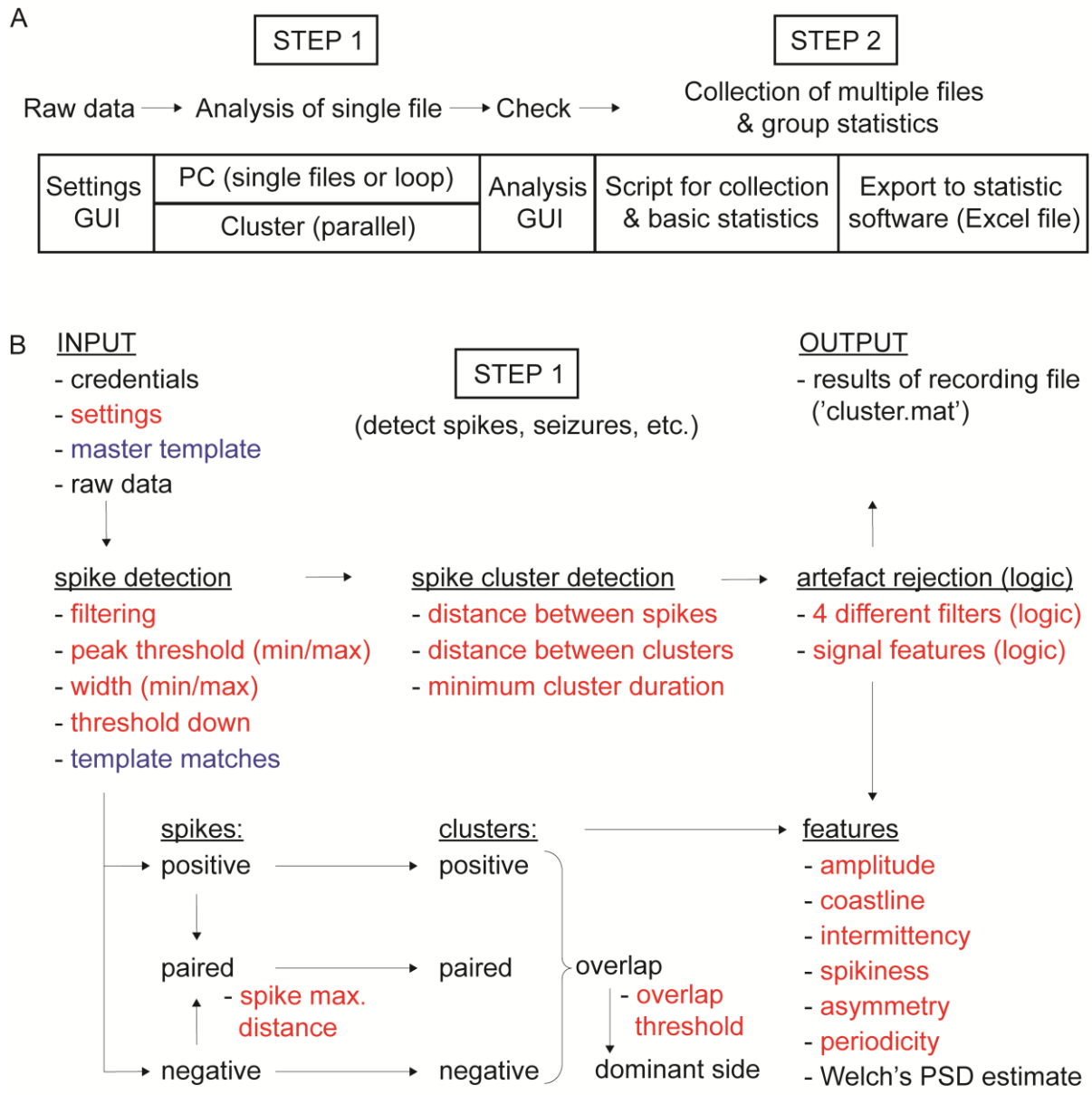

Figure 2 Analysis pipeline and software for offline detection of single spikes, short spike clusters and seizures. (A) The offline analysis pipeline is divided into two main steps: analyzing single files (step 1) and combining the result of an individual animal over a specific time period and form (treatment) groups for statistical analysis (step 2). (B) Step 1 of the analysis software is subdivided into three main steps: the detection of spikes, the formation of clusters, and the delimitation from artefacts. Inputs of step 1 comprise the credentials of an animal (ID, recording date, etc.), the settings for the analysis (examples in red), a master template with up to 8 spike templates and the raw data. After the analysis (compare text for details), a output file is saved containing the results of almost every interim step, as for example the number of positive, negative and paired clusters before and after artefact rejection.

Offline data analysis

While we used the online spike and cluster spike detection for fast optogenetic intervention, we established an offline analysis pipeline to accurately detect spikes, short clusters of spikes and seizures in order to enable validation of our online detection and quantification of different forms of epileptic activity during the development of epilepsy. In contrast to the online spike (or cluster spike) detection described in the previous paragraph, offline analysis described in this paragraph is different in many regards, in particular concerning the available options to filter. While we had to use infinite impulse response (IIR) filters for the online detection, for the offline analysis here, the more stable finite impulse response (FIR) filters could be implemented. During offline analysis, we used for many applications zero-phase digital filtering, processing the input data in both the forward and reverse directions, to minimize distortion (Oppenheim et al., 1999). Besides filtering, the processing time during offline analysis is of lower priority, enabling a more elaborate analysis. The analysis pipeline (Figure 2A) can be divided into two main steps: the analysis of a single recording file (step 1) and the collection of the results for statistical analysis (step 2). In step 1, key information (i.e. credentials) about the animals together with a range of settings for the analysis is selected using a custom-made settings GUI. The settings for spike detection included a second-order bandpass Butterworth filter with a lower (typically at 2 Hz) and a higher cutoff frequency (typically at 500 Hz) (Figure 2B). In order to exclude baseline and large amplitude artefacts, a minimum and maximum threshold was specified for peak detection (Figure 2B and 3A). Adapted from Quiroga et al. (2004), thresholds were semi-automatically set to

$$Thr = k\sigma_n; \qquad \sigma_n = median\left\{\frac{|x|}{0.6745}\right\}, \tag{3.1}$$

where k is a constant scale factor selected separately for a positive and negative threshold, x is the filtered signal and the standard deviation of the background noise is estimated by σ_n (Donoho and Johnstone, 1994). Spikes were defined when the width in a certain distance (threshold down) below the peak was within the range of preset thresholds (i.e. minimum and maximum width) similar to the online detection (Krook-Magnuson et al., 2013). In addition to a threshold-guided spike detection, a pattern matching approach was used to find spikes that were otherwise hard to identify. To this end, up to 8 templates, i.e. short pieces of data, could be selected by hand and saved in a master template to detect matching patterns (Figure 3B). The positive and negative spikes from both sources were pooled. As many spikes had a positive and a negative peak, we formed pairs (Figure 3C). We found that the distance between the negative and positive peak of a

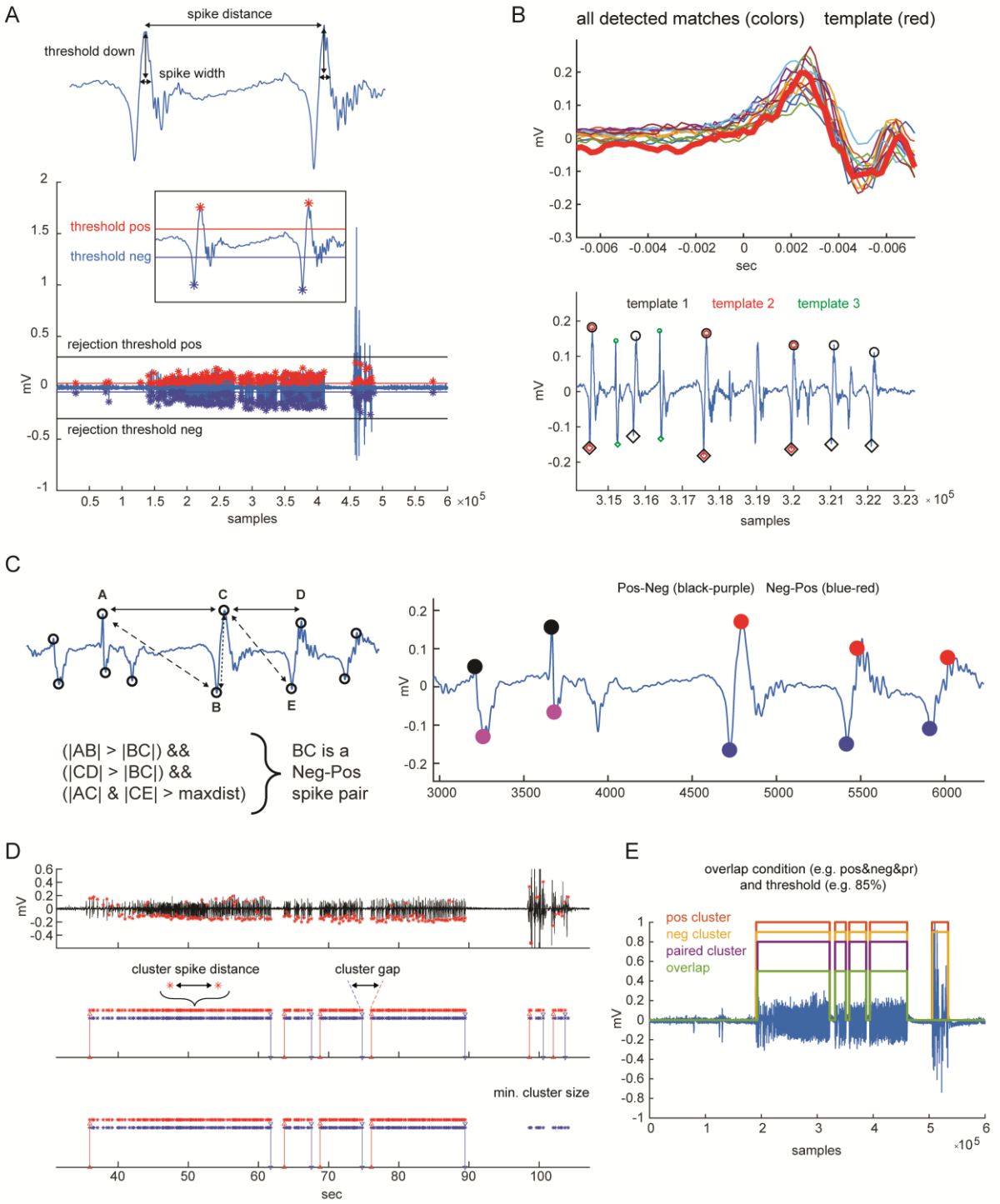

Figure 3 Spike and spike cluster detection with the offline analysis software. (A) For offline spike detection, local extrema (peaks) were identified using a positive (red) and negative (blue) threshold (inset). A rejection threshold (black) was specified to exclude artefacts of high amplitude. Spikes were defined by the width of the waveform at a specific distance from the peak (threshold down). (B) Another approach for spike detection was using pattern matching. *Top:* a predefined template of a spike (red) was run through the entire signal and the locations of matches (colors) were saved. Bottom: different templates could be run in parallel and single or joint matches were marked. (C) Most spikes featured a pair of peaks. Calculating the distance between peaks and specifying a maximum distance between peaks enabled the identification of these pairs. (D) Spikes (blue asterisk) were classed as cluster spikes (red) defining a minimal distance between spikes (compare also spike distance in A), while starts and stops of clusters were determined by the minimal cluster gap. (E) The overlap of clusters that were detected using either positive, negative or paired spikes were compared to exclude artefacts and identify true clusters for each type (i.e. positive, negative and paired clusters).

spike pair was in most cases smaller than to the previous or next peak of the respective other sign. This pertains particularly for clusters of spikes, where spikes often have a highly uniform appearance. Separately for each of the three groups of spikes (i.e. positive, negative and paired), clusters were defined by specifying the distance between spikes and a maximal cluster gap, with the option to exclude short clusters by specifying a minimal cluster size (Figure 2B and 3D). While paired clusters were detected with high precision (i.e. identifying an actual cluster), the accuracy to detect the actual start and stop of a cluster and include all spikes within this time window was rather low. Therefore, a logical condition and threshold specifying the overlap of clusters from different groups was used to identify true spike clusters in all groups (Figure 2B and 3E). In addition, within this overlap, positive and negative peaks were compared to determine the dominant side.

The settings for spike and cluster detection, albeit harboring great potential for artefact rejection, were rather selected in a manner to increase the sensitivity of the detection (i.e. avoiding false negatives). A second approach included different filters and determined various signal properties to increase the specificity (i.e. avoiding false positives) of the spike cluster detection (Figure 4A). Based on an algorithm written in Tcl (Tool Command Language) and Pascal by Open Source Instruments (http://alignment.hep.brandeis.edu/Software/Sources/), we implemented in our MATLAB code an assessment of different signal properties including amplitude, coastline, intermittency, spikiness, asymmetry, periodicity and frequency (Figure 4B). The amplitude,

Figure 4 Signal features and artefact rejection for offline analysis. (A) Artefact rejection is collaterally handled in the analysis pipeline. Signal features and four different filters were combined through a logic conjunction to specify areas in the signal that should be excluded from the analysis. In addition, in a later step, clusters could be selectively removed by determine more restrictive criteria using the same signal properties (compare text for details). (B) The signal properties encompassed amplitude, coastline, intermittency, spikiness, asymmetry, periodicity, and frequency. (C) For each of these signal properties (magenta; normalized) thresholds (red) could be selected as shown here for asymmetry and intermittency. A logical conjunction of these different conditions could be used to distinguish areas of interest with clusters (magenta) from artefacts and the baseline. (D) A band-pass filter could be used to select areas predominated by a certain frequency band. Specifying the filter center frequency, the bandwidth and the stopband limit determined filtered signal (black). A threshold number of standard deviations for the envelope (magenta) was prescribed to define the active areas (orange). Up to four filters could be combined by logical conjunction to highlight different frequency bands and thereby select areas of interest.

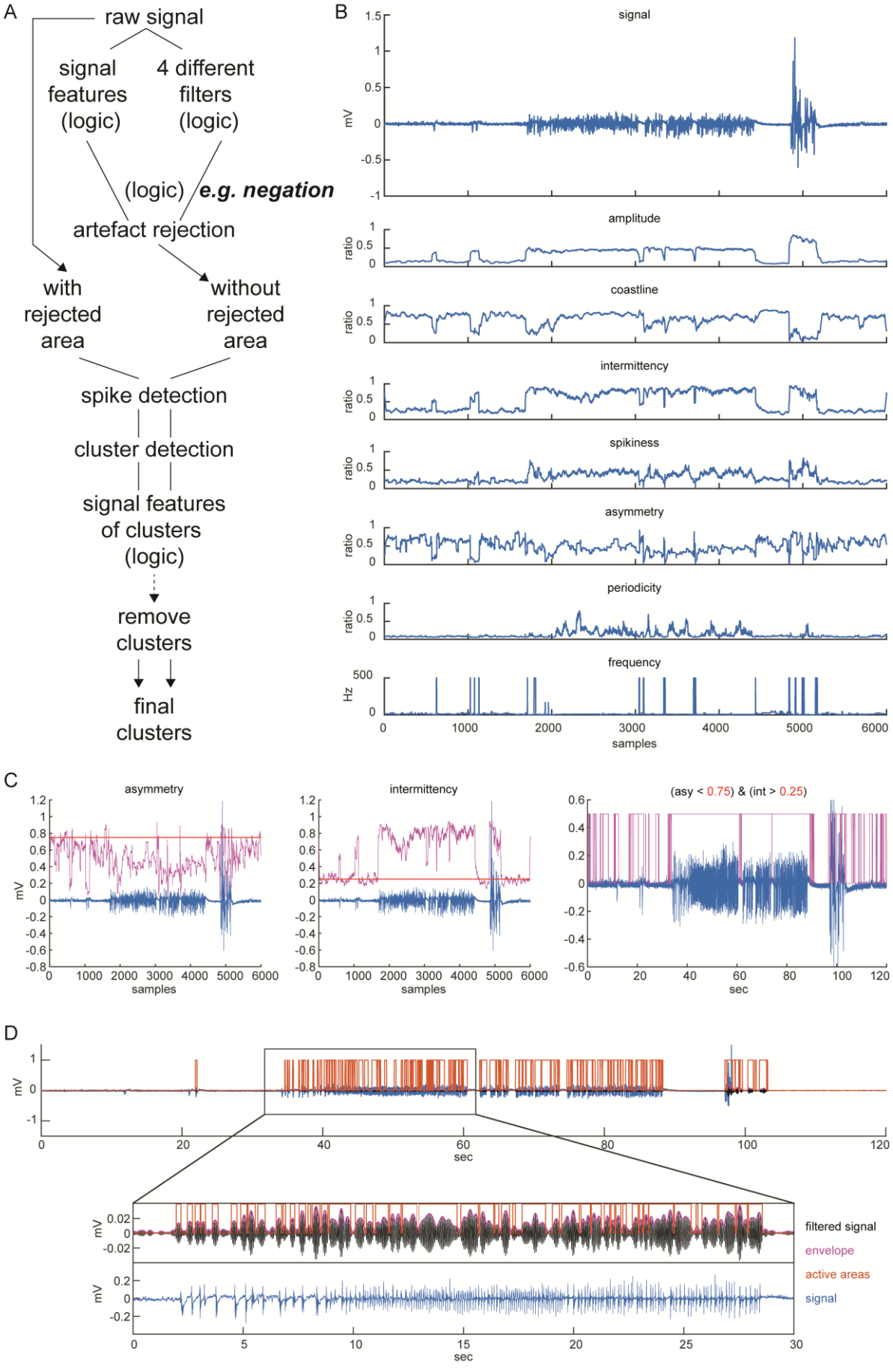
A
raw signal
signal features (logic)
4 different filters (logic)
(logic) e.g. negation
artefact rejection
with rejected area
without rejected area
spike detection
cluster detection
signal features of clusters (logic)
remove clusters
final clusters
B
signal
amplitude
coastline
intermittency
spikiness
asymmetry
periodicity
frequency
mV
ratio
Hz
samples
C
asymmetry
intermittency
(asy < 0.75) & (int > 0.25)
mV
samples
sec
D
mV
sec
filtered signal
envelope
active areas
signal

coastline, intermittency and asymmetry were calculated as follows:

$$Amp = \sqrt{\frac{1}{N}\left(\sum_{i=1}^{N} x^2 - \frac{1}{N}\left(\sum_{i=1}^{N} x\right)^2\right)} \tag{3.2}$$

$$Coast = \sum_{i=1}^{N} |x_{i+1} - x_i| \tag{3.3}$$

$$Inter = \frac{\sum_{i=1}^{N} x_i}{\sum_{i=1}^{N} |x_{i+1} - x_i|} \tag{3.4}$$

$$Asy = \frac{\max(x) - \frac{\sum_{i=1}^{N} x_i}{N}}{\frac{\sum_{i=1}^{N} x_i}{N} - \min(x)}, \tag{3.5}$$

where x is the filtered signal and N the number of samples. While the coastline describes the absolute change in signal value over time, the intermittency defines how concentrated the coastline is at specific points in time. Similar to frequency variation (called frequency in Figure 4), the asymmetry metric highlights sudden fluctuations in the signal. For periodicity, a measure of the oscillatory fraction of the signal, and spikiness, a metric of the variation in amplitude of local extrema, minima and maxima greater than the mean absolute deviation of signal are assessed. Thresholds for the different properties could be specified and a logic condition was formulated to distinguish periods with spike clusters from those with artefacts and baseline activity (Figure 4C). In a similar incentive, up to four different filters could be selected to identify changes in frequency bands (Figure 4D). Through a logical conjunction, these two different approaches of signal classification were combined to define periods that should not be considered (i.e. rejected areas) for spike and cluster detection (Figure 4A). Although a selection of artefact-specific signal properties would in principle be possible, in our hands it turned out that defining spike cluster-specific signal properties and specifying exclusion criteria *ex negativo* were more effective for artefact rejection. An example of the necessity of artefact rejection for cluster detection is shown in Figure 5.

However, under certain circumstances, when many artefacts appear within spike clusters, this rejection approach interfered with cluster detection by rejecting many correctly identified clusters. Therefore, we implemented an additional step after the detection of clusters to define more restrictive cluster-specific signal properties and remove falsely identified clusters in retrospect (Figure 4A). The results of each individual step were saved separately (e.g., positive clusters with and without the rejected area). This is particularly important, when analyzing (in step 1) several hundred files in parallel on a high performance computing (HPC) cluster. In this case, settings can be chosen for a few recording files, while the other are analyzed with settings

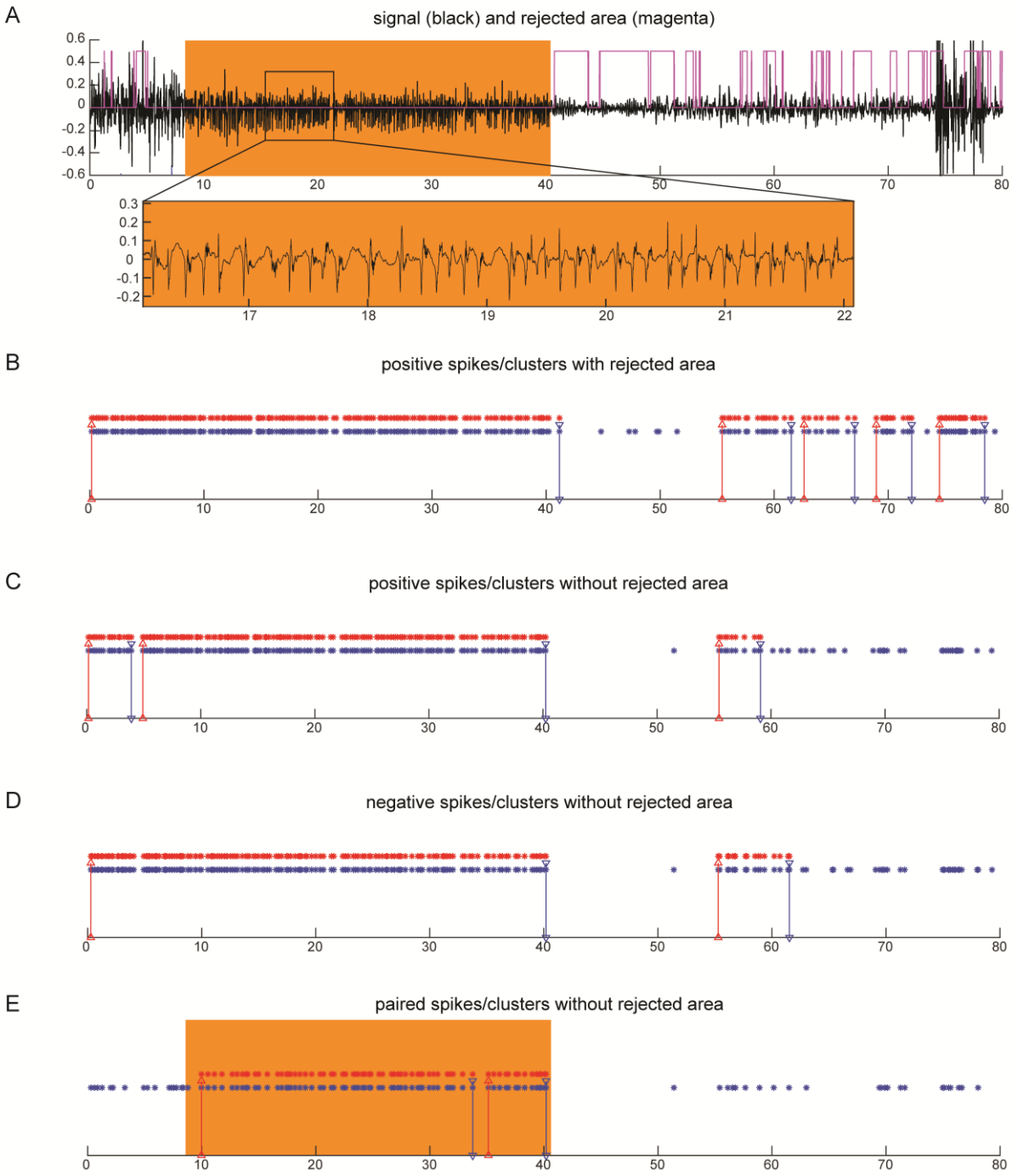

Figure 5 An example of detecting a cluster of spikes using the custom-made MATLAB algorithm of step 1 for offline analysis. (A) A LFP signal (black) of a mouse 4 months after IHK injection was analyzed. Manual scoring of the signal with the aid of the corresponding video revealed that a spike cluster (highlighted in orange) is following a movement artefact. Signal properties and filters were selected to determine the rejection area (magenta). (B-E) After spike (blue asterisk) detection and cluster spike (red asterisk) classification, clusters were formed (red and blue lines). (B) Spikes with positive peaks formed five clusters. (C) Using the rejection area, some of the falsely detected clusters (in B) were removed. (D) As for positive clusters, the algorithm detects negative clusters (i.e. clusters formed using negative spikes) that either entirely or partially comprise of artefacts. (E) Only clusters of paired spikes in combination with the rejected area represent an accurate approximation of the manual scoring.

of the file that match closest their own date of acquisition. A custom-made Python script using GC3Pie (http://gc3pie.readthedocs.io/en/master/) was written to submit and control batch jobs to HPC clusters in order to analyze several files (i.e. run step 1) in parallel, while each job created an output file containing all the results of one channel of a particular recording file (typically an hour long recording of one animal). These results can be checked and clusters if necessary manually corrected using a custom-made analysis GUI (Figure 2A). After this verification, all results can be collected and grouped for statistical analysis using another custom-made MATLAB script (step 2).

Results and Discussion

Several clinical features of TLE can be reproduced through IHK injection in adult mice. In the course of the first two weeks after injection, a progressive cell loss in the ipsilateral CA1, CA3c and hilus, occurs, which is associated with reactive gliosis, a strong granule cell dispersion in the dentate gyrus, and mossy fiber sprouting (Bouilleret et al., 1999). As reported earlier (Riban et al., 2002a), hippocampal activity during early epileptogenesis can be divided into three phases (Figure 6A). Immediately after injection, EEG activity was characterized by an almost continuous train of spikes (approx. 3-7 Hz), while the amplitude increased (200-900 µV) as the animal recovered from anesthesia. This SE lasted several hours, and gradually phased into the latent period, which in turn is characterized by the loss of theta activity and the occurrence of isolated or grouped low voltage spikes and spikes-and-waves (500-1000 µV) (Figure 6A). After approximately two weeks, progressively more and longer clusters of spikes emerged, eventually resulting in the appearance of spontaneous recurrent non-convulsive seizures (SRS; 1200-4800 µV) lasting for tens of seconds (Figure 6A), and thereby heralding the beginning of the chronic phase. During SE and the chronic period, mice showed occasionally behavioral seizures of different severity, including behavioral arrest, mastication, vocalisation, clonic limb movements right up to jumping and running with tonic periods (data not shown). The progressive course of emerging aberrant activity towards the end of the latent period suggests that epileptogenesis is a continuous process with a gradual increase in seizure probability. Although the end of the latent period and the occurrence of the first clinical seizure might not be the final milestone of the epileptogenesis process (Williams et al., 2009), the latent period probably corresponds to an important phase and promising target to prevent the development of acquired epilepsy.

Despite meticulous research into different aspects of epileptogenesis in TLE, the mechanisms underlying the development of SRS still remain unknown. However, the fact that overexcitation during SE triggers a series of reactions culminating in the development of seizures suggest that similar excitatory-inhibitory imbalance during the latent period is not just a manifestation of a yet complete pathogenesis. Rather, it might be an active constituent of the epileptogenic process. Therefore, we took advantage of recent advances in optogenetics to inhibit epileptiform activity selectively during the latent period to unravel its contribution to the formation of an epileptic focus (Figure 6B). While closed-loop optogenetic intervention (COI) was already used previously to inhibit long-lasting seizures in chronic models of thalamocortical (Paz et al., 2013) and temporal lobe epilepsy (Armstrong et al., 2013; Krook-Magnuson et al., 2013; Krook-

Magnuson et al., 2014; Ewell et al., 2015; Krook-Magnuson et al., 2015), we implemented a system for fast inhibition of epileptiform activity occurring during the latent period in the IHK model of TLE (Figure 1). Exemplified by the analysis of a randomly selected hourly recording (at 4 dpi), a brief laser stimulation (for 2 s, in 50% of the cases) reduced the number of spikes detected in this 2-second time window (10000 samples) in a mouse expressing the opsin compared to its opsin-negative littermate (Figure 6C). However, for an adequate evaluation of COI during the latent period (i.e. determining accuracy and precision of the online detection) and assessing if it has any long term effect on seizure pathology, a much larger sample of data (animals and recording hours) will have to be analyzed at different time points during the latent phase. This holds particularly true as any early and continuous intervention might have an effect already within the period of intervention; for example when, similar to Figure 6C, the number of spikes is used to assess the efficacy of COI during the late latent period, the absolute number or (potentially) form of shape activity might have been changed. Therefore, we developed an offline analysis program to support the handling of a larger amount of data (Figure 2). Selecting settings for spike and spike cluster detection (Figure 3), as well as signal features and artefact rejection (Figure 4) enabled a reasonably accurate detection of clusters even within noisy signal (Figure 5). Hence, we analyzed a 24-hour window four months after the injection to test the program, selecting settings for each animal individually without knowledge about their group affiliation (Figure 6D). While these preliminary results have to be verified manually using the analysis GUI (Figure 2A), they indicated that Cam-HR mice, where COI was delivered through inhibition of pyramidal cells, showed a reduction in the number of spikes four months after the injection compared non-opsin expressing controls or PV-ChR mice, where COI was delivered through activation of PV+ interneurons. If these results hold true, it would suggest that early epileptiform activity in the surviving CA1 pyramidal cells during the latent phase directly contributes to the development of

Figure 6 Closed-loop optogenetic intervention (COI) during early epileptogenesis. (A) Early epileptogenesis is characterized by an initial status epilepticus with continuous high frequency activity (30 s, inset 3 s), followed by a latent period with single or short clusters of spikes (30 s, inset 6 s), and finally the occurrence of spontaneous recurrent seizures during the chronic period (60 s, inset 3 s). (B) Experimental design of COI during early epileptogenesis. Mice are injected with kainic acid and both an optrode and an electrode were implanted into the dorsal hippocampus. After 24 hours, closed-loop optogenetic intervention was started for the next 12 days. Thereafter, EEG recordings were continued for another week and once again four months later. (C) Proximate effect of COI on spike clusters. The number of spikes (normalized and binned) in the 2-s window after triggering the laser is reduced in an opsin-expressing mouse compared to a control animal. (D) Preliminary results of the long-term effect of COI during the latent period on the number of seizures four months after injection. Recordings in a 24 hour window of PV-ChR (n = 5), Cam-HR (n = 3) and opsin negative littermate controls (n = 4) were analyzed (blinded and without manual correction) on the cluster computer. This preliminary analysis reveals an ameliorating effect of inhibiting pyramidal cells during the latent period on the number of electrographic seizures during the chronic phase.

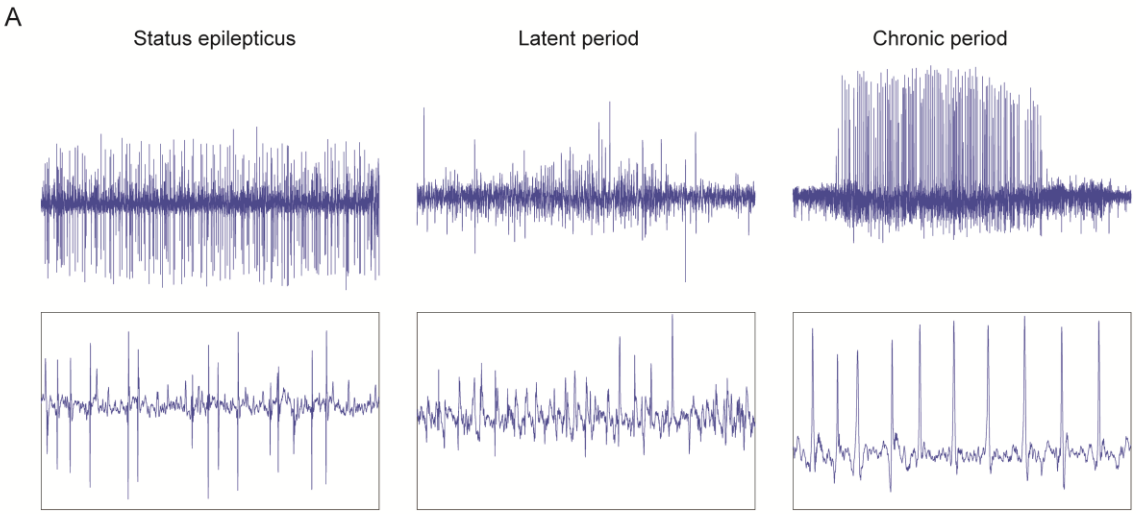
A
Status epilepticus
Latent period
Chronic period

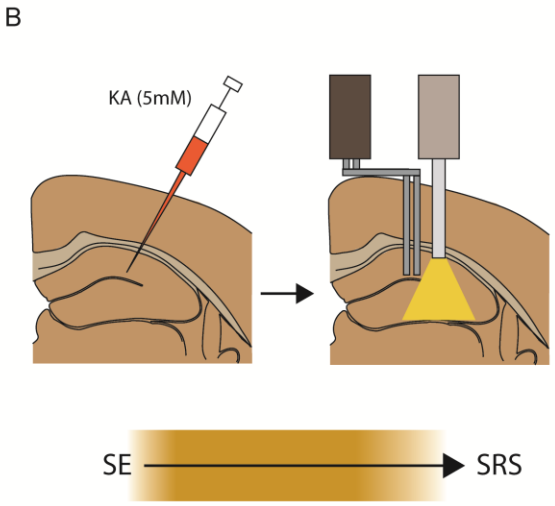
B
KA (5mM)
SE
SRS

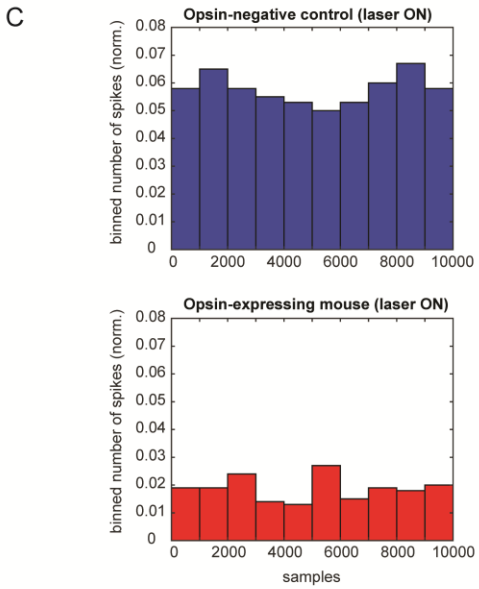
C
Opsin-negative control (laser ON)
Opsin-expressing mouse (laser ON)
binned number of spikes (norm.)
samples

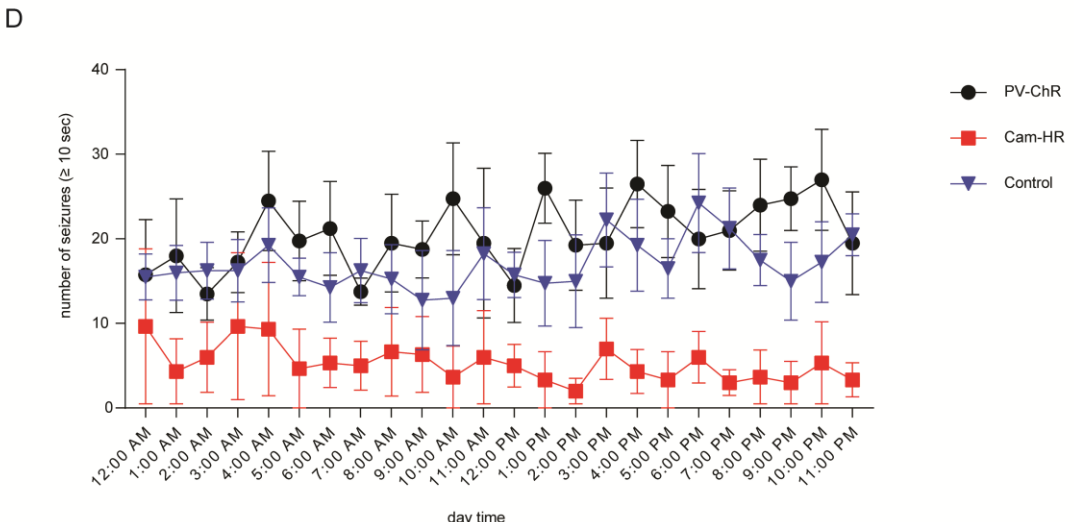
D
number of seizures (≥ 10 sec)
day time
PV-ChR
Cam-HR
Control

epilepsy, and the time window between a precipitating brain insult and the occurrence of the first clinical seizure should be considered for antiepileptogenic therapies. In addition, the inefficacy of a PV-mediated inhibition of short events could be explained by the time delay that arises using an indirect pathway for intervention. Krook-Magnuson et al. (2013) reported approximately 60% of seizures were stopped in Cam-HR mice within 1 s, while in PV-ChR mice within 5 s. Moreover, recent findings in a mouse model of optogenetically inducible seizures in the primary motor cortex showed that inhibition of PV+ (and SOM+) interneurons consistently reduced seizure duration, while inhibiting VIP+ interneurons disrupted both seizure initiation and maintenance (Khoshkhoo et al., 2017). While differences in the role of interneurons during seizures (i.e. beneficial inhibition vs. beneficial excitation) might be explained by differences in the epilepsy model and the fact that the preceding brain state affects the optogenetic curtailment of seizures (i.e. only non-theta state emerging hippocampal seizures can be curtailed by PV+ interneuron stimulation) (Sedigh-Sarvestani et al., 2014; Ewell et al., 2015), these findings by Khoshkhoo et al. (2017) suggest that other types of interneurons (than PV+ cell), which might not be secondarily recruited during epileptic discharges, are potentially more suitable targets for fast intervention.

Conclusions

We established a technique for fast closed-loop optogenetic intervention upon short epileptiform discharges and a program to analyze large data sets in order to study role of early epileptic discharges in acquired epileptogenesis. Preliminary results suggest that a closed-loop inhibition of epileptic activity during the latent period, through silencing of pyramidal cells, affect the seizure pathology later on. While these findings have to be confirmed using the analysis pipeline proposed and tested in this study, they might open new avenues to study the underlying mechanisms of epileptogenesis in TLE and define therapeutic windows for antiepileptogenic therapies.

IV. GENERAL DISCUSSION

The overall objective of this study was to investigate the mechanisms underlying epileptogenesis in TLE to unravel potential targets in order to prevent the epilepsy early on. Being listed among the nine top research priorities in the fourth edition of Jasper's Basic Mechanisms of the Epilepsies, we constrained this objective by focusing on three major topics employing the IHK model of TLE: the role of the monocytic immune response (study I), the effect of a comorbid AD-like pathology (study II) and the contribution of an early aberrant activity (study III) to the development of acquired epilepsy. While the first and the last study mainly focused on factors considered to be important in the ordinary course of epileptogenesis, the second study addressed the contribution of AD-like pathology on the development of a pro-epileptogenic environment. Although the clinical comorbidity of AD and epilepsy still remains underestimated, our observation of a curtailed latent period in AD transgenic mice turned out to be extremely fruitful to investigate the significance of the latent period prior to SRS onset.

In the first study, we confirmed previous reports that the innate and adaptive immune system tightly follows the course of neurodegeneration and the development of SRS (e.g. (Deprez et al., 2011; Zattoni et al., 2011)). However, we found no changes in the IHK-induced epileptogenesis after pre-exposure to the viral mimic PolyI:C (Figure 2-4), nor in a knockout model of NLRP3 inflammasomes (Figure 5) and in mice lacking infiltrating peripheral macrophages (Figure 6), contrary to our expectations based on previous findings (Vezzani et al., 1999c; Zattoni et al., 2011; Krstic et al., 2012). Different reasons (e.g. wildtype strain, non-canonical inflammasome pathway, epilepsy model) can potentially explain these discrepancies (see Discussion, study I). However, negative findings have to be interpreted with caution and our results should not be taken as evidence against a role for innate immune responses in the formation of an epileptic focus.

Investigations in the second study not only revealed an early onset of SRS in AD transgenic mice, but also showed, to our knowledge for the first time, that an early onset of SRS is not dependent on the severity of the preceding SE. While these mice were more susceptible to KA, application of diazepam reduced seizure severity and frequency during IHK-induced SE, however, without preventing seizure induced mortality during the latent period. In addition, we did not find any changes in innate (Figure 1, 5, and 8) or adaptive immune response (data not shown), axonal reorganization (Figure 7 and 9) or adult neurogenesis (Figure 6) in this AD mouse model that could explain differences in epileptogenesis. We revealed that NPY signaling

is affected early in AD mice (Figure 8). Most strikingly, we were able to alleviate the exacerbated seizure pathology seen in AD transgenics by neutralization of soluble Aβ species prior to the induction of epileptogenesis.

In the third study, we focussed on electrographic patterns appearing during early epileptogenesis, notably during the latent period. Previous studies have argued for early epileptiform activity being important for axonal reorganization (Sutula et al., 1988). Interfering with early epileptic discharges during the latent period using COI, our preliminary data show that early COI leads to reduced frequency of SRS four months after IHK injection (Figure 6). Although these findings have to be confirmed by further experiments, they suggest that early aberrant activity directly contribute to the emergence of spontaneous seizures later on.

Stages of epileptogenesis

In order to comprehend the mechanisms of epileptogenesis, the time course of events is crucial. Epileptogenesis in TLE is generally divided into consecutive stages, comprising a preclinical latent period after an insult and a clinical phase following the first seizure (Engel, 1996b, a). As a model of TLE, the IHK model shares not only many histopathological and electrographic features with TLE with hippocampal sclerosis (TLE-HS), but is also considered to be a valid representation of the progression of the disease in humans. The development of seizures in the IHK model is generally divided into three main stages, starting with the SE induced by KA, followed by the latent period that ends with the onset of SRS (Riban et al., 2002a). However, a study using a similar model, the "repeated low-dose kainate" model of TLE (Hellier et al., 1998; Hellier and Dudek, 1999), in which a SE is induced by multiple i.p. injections of kainic acid, emphasized that seizure frequency increases in a sigmoid function of time (Williams et al., 2009). Hence, four stages can be distinguished: the latent period, a slow growth phase, an exponential growth phase, and the plateau phase. Many other models of acquired epilepsy studied over several weeks report a similar course comprising a SE, a latent period, and a chronic period with a growth and a plateau phase, as for example in the pilocarpine model (Cavalheiro et al., 1991), the rat IHK model (Ledri et al., 2016), and models inducing a self-sustained status epilepticus (SSSE) by an electrical tetanic stimulation of the angular bundle (Gorter et al., 2001) or the lateral nucleus of the amygdala (Nissinen et al., 2000). As pointed out by Williams et al. (2009), the end of the latent period does, therefore, not coincide with the completion of epileptogenesis, and the therapeutic window to suppress acquired epilepsy potentially extends

beyond the first clinical seizure. In our third study, we recorded in two separate phases after surgery, continuously for three weeks following the SE and after four months again continuously for 2 weeks. Hence, we were able to confirm the three main periods (Figure 6, study III) previously reported in the first month of IHK-induced epileptogenesis (Riban et al., 2002a; Arabadzisz et al., 2005; Zattoni et al., 2011). Far from being the end of epileptogenesis, the latent period (also called silent or quiescent period) remains of particular importance when studying the development of epilepsy. The fact that no seizures occur during this period suggests that the generation of seizures only occurs after completion of an essential network reorganization or upon suppression of an inhibitory process that prevents prolonged epileptiform activity, for example the putative expression of an endogenous agent with anticonvulsant properties. We will discuss either possibility in the next paragraphs in detail.

Neuronal network reorganization

We were able to replicate in the first (Figure 1) and the second study (Figure 1, 5, 6, 8) a few of the many neuropathological alterations reported during the latent period. In the ipsilateral hippocampus, pyramidal cells in CA1, CA3c and hilar mossy cells start to degenerate after the IHK-induced SE (Suzuki et al., 1995b; Bouilleret et al., 1999). Moreover, within the first 24 hours of this initial insult follows a selective loss of PV-, CB-, SOM- and NPY-positive interneurons in the DG, CA1, and, to a lesser extent, in CA3, while CR-positive cells (except mossy cells) are largely spared (Bouilleret et al., 1999; Bouilleret et al., 2000b). Reelin-positive interneurons also disappear within 24 hours after IHK injection, while reelin- and CR-positive Cajal-Retzius cells located along the hippocampal fissure become gradually more visible due to an intracellular accumulation of truncated reelin (Duveau et al., 2011). This BDNF-mediated impairment in reelin secretion in the injected hemisphere causes a dispersion of GC (Bouilleret et al., 1999; Heinrich et al., 2006; Müller et al., 2009; Duveau et al., 2011). In the dentate gyrus, mossy fibers start to sprout aberrantly into the inner molecular layer (Buckmaster, 2012). In addition, SE causes an impairment of hippocampal adult neurogenesis (Kralic et al., 2005; Ledergerber et al., 2006; Sierra et al., 2015) after an initial, transient increase in cell proliferation (Parent et al., 1997; Jessberger et al., 2005). Notably, all these changes (or at least those which were tested) could be found after IHK injection in all the different animal models used in this study, apart from the GC dispersion, which was strongly reduced after i.c.v. injection of anti-Aβ antibody or control IgG in ArcticAβ mice (Figure 10, study II). However, it is unknown which of

these multiple alterations directly contribute to the development of SRS and which are concomitant sequelae. Based on the fact that in our second study we found a curtailment of the latent period in AD transgenic mice (Figure 4) without any difference in the gross neurodegenerative pattern (Figure 1), innate immune response (Figure 1 and 5), NPY-positive axonal sprouting (Figure 7) or adult neurogenesis (Figure 6), suggests that other alterations might be more important for the generation of SRS. Therefore, we will focus in the next two paragraphs on the dysfunction of interneurons and axonal reorganization, two potentially critical alterations during the latent period for the generation of SRS.

Dysfunction of interneurons

An important function of inhibitory GABAergic interneurons is to support network synchrony and oscillatory rhythmic activity (Buzsaki and Draguhn, 2004). Any dysfunction has supposedly a profound effect on the network performance, characterized by dysrhythmias and cognitive impairment. Previous studies reported that dysfunction of interneurons contribute to abnormalities in oscillatory rhythms and network synchronicity in both AD and epilepsy (reviewed in (Palop and Mucke, 2016)), thus affecting similar cognitive functions such as encoding of memory (Jokeit and Ebner, 1999; Sinforiani et al., 2003; Ito et al., 2009). In patients (Amatniek et al., 2006; Scarmeas et al., 2009; Vossel et al., 2013; Vossel et al., 2016) and animal models of AD (Busche et al., 2012; Kam et al., 2016; Schmid et al., 2016), aberrant activity and spontaneous seizures were found at an early stage of the pathogenesis. Similarly, we found in our second study that ArcticAβ mice are more susceptible to excitotoxicity (Figure 1-4), supposedly through the presence of Aβ oligomers. We have not tested if a pretreatment with the anti-Aβ antibody would reverse the hyperexcitable phenotype in ArcticAβ mice before and immediately after KA (in slice or in vivo). It has been shown, however, that neuronal hyperexcitability can be induced in wildtype mice by soluble Aβ (Busche et al., 2012) and that axons of CA1 O-LM interneurons are lost in young APP/PS1 mice (Schmid et al., 2016). We found decreased synaptic strength, increased KA-induced LTP and reduced frequency of sIPSCs (Figure 2-3, study II), assuming the inhibitory input is impaired or obstructed. We also discovered in these mice that the latent period was curtailed and the onset of SRS occurred within a few days (Figure 4, study II). One possible explanation could be that sudden local dysfunction in inhibition is sufficient to render the network susceptible to the generation of SRS. Interestingly, two recent studies support this assumption. Unilateral injection of an AAV containing DT receptors in dorsal CA1 of a Gad2-ires-Cre mice lead to a focal ablation of interneurons and the transient occurrence of regular SRS (with a mean duration of 45 seconds) for a few days, without the

appearance of an initial SE (Spampanato and Dudek, 2017). As SRS appeared within the timeframe required for a DT-mediated ablation, the authors assumed that there was no latent phase present. Another recent study showed that selectively silencing parvalbumin interneurons in the subiculum and hippocampal CA1 (irregularly inclusive in adjacent regions) injecting AAV expressing tetanus toxin light chain (TeLC) in PV-cre mice induced clusters of spike-wave discharges and regular SRS (with a mean duration of 25 seconds) (Drexel et al., 2017). The seizures occurred around 10 days after the AAV injection, however, at a low frequency (around 5 seizures per month). In addition, the attempt to induce SRS through a transient silencing of PV-positive interneurons (for about 1-2 hours) using DREADD (designer receptor exclusively activated by designer drugs) failed. Both studies reported on average below 10 seizures and in majority convulsive seizures (47% after CA1 ablation and 93-100% after subiculum/CA1 silencing) during the recording period of 1-2 months. In comparison, in the IHK model most seizures are non-convulsive with a frequency of around 9 per hour after 3 weeks (Zattoni et al., 2011), while convulsive seizures are rare and strongly vary between animals (Soltesz lab, personal communication). A possible explanation for this discrepancy could be that besides CA1 and the subiculum, the rest of the hippocampus is mostly unaffected in those two studies. In addition, a recent study showed that in the subiculum, depolarized GABAergic signaling caused by changes in chloride transporters mediates secondary generalized seizures in IHK model of TLE, with PV-positive interneurons being particularly vulnerable to become depolarized during secondary generalized seizures (Wang et al., 2017). Together, these findings suggest that although important, GABAergic and in particular PV-positive interneurons in CA1 or the subiculum are not solely responsible for the electrographic characteristics seen in the IHK model.

Different types of interneurons are affected in models of TLE while playing different roles for seizure generation. As in the IHK model, the number of SOM-, NPY- and PV-positive interneurons was found to be decreased in the first few days after pilocarpine injection (Lurton and Cavalheiro, 1997; Dinocourt et al., 2003). A lowered seizure-threshold was proposed to be mediated by a deficit in dendritic feedback inhibition, as for example by O-LM cells, while epileptiform activity is limited by somatic feed-forward inhibition (Cossart et al., 2001). A subset of NPY-positive cells in the hippocampus shows both dendritic feedforward and feedback inhibition, and belong to two related classes of interneurons, ivy and neurogliaform cells. Besides NPY, these cells of the neurogliaform family can express nitric oxide (NO) and high levels of $GABA_A$ receptor α1 subunits, but neither PV nor CCK (Fuentealba et al., 2008; Tricoire et al., 2010). Further, ivy cells can be distinguished from neurogliaform cells through

the lack of reelin (Fuentealba et al., 2010). Cells of the neurogliaform family are characterized by a dense local axonal plexus through which they mediate GABAergic non-synaptic volume transmission (Olah et al., 2009). As one of the most abundant types of interneurons in CA1 (Fuentealba et al., 2008) and known for their consistent firing rate across different behavioral states and network oscillations (Lapray et al., 2012), ivy cells provide a slow GABAergic input to principal cells, which was proposed to be important for maintaining network homeostasis and guarding against increased excitability. Thus, the firing rates of ivy cells increase upon enhanced network activity and synchrony, as for example seen during an increase in frequency and amplitude of field theta oscillations (Lapray et al., 2012). Similar properties were found in neurogliaform cells, and both ivy and neurogliaform cells provide potent feedforward inhibition to principal cells of the dentate gyrus, CA3 and CA1, while only ivy cells show direct feedback inhibition in CA1 and CA3 (Armstrong et al., 2012; Milstein et al., 2015). Moreover, both ivy and neurogliaform cells display persistent firing, a recently described phenomenon, where action potential firing in distal axons continues after cessation of depolarizing input (Krook-Magnuson et al., 2011; Sheffield et al., 2011). Whereas the physiological function of persistent firing is still a matter of open debate, a recent study emphasizes the potential of persistent firing for suppressing undesirable neuronal hyperactivity (Suzuki et al., 2014). These authors focused on neurogliaform cell-mediated feedback inhibition of pyramidal cells in the cerebral cortex, a conjunction only observed in ivy cells in the hippocampus (Price et al., 2005). However, hippocampal neurogliaform and ivy cells might provide a similar seizure alleviating effect by feedforward inhibition, interfering for example with the propagation speed of epileptic events (Trevelyan et al., 2007). Interestingly, in CA1, this feedforward inhibition can be abolished through activation of the Mu opioid receptors (μORs) (Krook-Magnuson et al., 2011). In a mouse model of AD, the endogenous μORs agonist enkephalin (ENK) was shown to be significantly upregulated already at an early age (2-4 months old), and contribute to neuronal and behavioral impairments in both young (3-5 months old) and old AD transgenic mice (9-10 months old) (Meilandt et al., 2008). Similarly, in a model of TLE, ENK-IR starts to increase in mossy fibers and in the inner molecular layer of the dentate gyrus 2-3 weeks after a single systemic injection of KA, during a the time when the first SRS occur, and ENK-IR was reported to remain elevated for at least 1 year (Bing et al., 1997). It would need to be determined if young ArcticAβ mice show elevated ENK-IR prior to IHK injection to assess if this pathway might serve as an explanation for the hyperexcitable phenotype and the early onset of SRS in our transgenic mice (Figure 4, study II). In our second study, we furthermore found a reduced expression of NPY in naïve adult ArcticAβ mice (Figure 8). Furthermore, we observed impaired

IHK-induced elevation in NPY-IR (Figure 7). Although we would first need to analyze whether levels of NPY are actually reduced in interneurons, it would be interesting to determine what implications a reduction has on the function of NPY-expressing interneurons, such as from the neurogliaform family, and consequently on the hippocampal network.

Axonal reorganization: loss of hilar mossy cell and mossy fiber sprouting

Mossy fiber sprouting, the synaptic innervation of GC axons (i.e. mossy fibers) with GC dendrites in the inner molecular layer, is initiated during SE and largely established still within the latent period (Figure 1, study I). Besides seizures, aberrant activity as chronic synchronous activation of the perforant path is reportedly capable of inducing mild mossy fiber sprouting, even in the absence of evoked epileptic discharges or neuronal loss (Sutula et al., 1988). Rapamycin was shown to abolish mossy fiber sprouting without affecting the frequency of seizures (Buckmaster and Lew, 2011). Unexpectedly, selective DT-mediated ablation of mossy cells does neither induce mossy fiber sprouting nor SRS (Jinde et al., 2012). Although the loss of hilar mossy cells is one of the first changes seen after IHK-induced SE (Figure 1, study I), the study by Jinde et al. (2012) revealed that a selective hilar mossy cell loss induces an acute GC hyperexcitability (4-11 days post-DT), which disappeared 6-8 weeks after DT, supposedly due to sprouting of GABAergic interneurons into the inner molecular layer of the dentate gyrus. However, it should be remembered that most TLE models show a simultaneous degeneration of mossy cells and of GABAergic interneurons, as for example of hilar NPY- and SOM-positive neurons.

The role of BDNF signaling in acquired epilepsy

At the same time, intrahippocampal BDNF was shown to induce seizures and mild mossy fiber sprouting (Scharfman et al., 2002), while IHK-induced SE increases BDNF expression in the dentate gyrus (Suzuki et al., 1995b). Interestingly, the inhibition of TrkB (Liu et al., 2013), or more specifically TrkB-mediated PLCγ1 signaling, by genetically uncoupling TrkB from adaptor proteins and enzymes (Gu et al., 2015) was shown to alleviate SE if applied in advance. Also, it massively reduces the number of SRS during chronic period if applied after SE. Together with recent findings from the same lab revealing that structural LTP induction involves NMDAR-CaMKII-dependent BDNF release and an autocrine activation of TrkB (Harward et al., 2016; Hedrick et al., 2016), aberrant activity during early stages of epileptogenesis become more important, while BDNF-TrkB signaling might serve as a link to explain mechanistically the results seen after early COI (Figure 6, study III). Antonucci et al. (2008) demonstrated that

intrahippocampal application of botulinum neurotoxin E (BoNT/E) after IHK injection reduced cell loss in CA1 and GC dispersion in the DG, while the latency to the first EEG seizure was prolonged and the frequency of spikes and sharp waves was reduced during the latent period. BoNT/E was injected to unleash its full potential several hours after IHK-induced SE until around 2 weeks later. It cleaves SNAP-25 within presynaptic terminals and therefore impairs vesicle fusion (Davletov et al., 2005). While BoNT/E treatment during the latent period had no effect on the frequency of SRS or the time spent in seizure during the early chronic period (Antonucci et al., 2008), a BoNT/E application during the chronic phase transiently reduced both SRS frequency and time spent in seizure (Antonucci et al., 2009). As BoNT/E during the latent period had no effect on SRS three weeks after IHK (Antonucci et al., 2008), it will have to be tested if our preliminary data in the third study (Figure 6) also holds true during the early chronic phase.

The importance of the BDNF-TrkB signaling during epileptogenesis was further highlighted by the effect of BoNT/E treatment in reducing the SE-induced elevation of TrkB-IR in Cajal-Retzius during the latent period, while simultaneously also reducing granule cell dispersion (Duveau et al., 2011). In this regard, innate and adaptive immune cells, as a source of BDNF (Kerschensteiner et al., 1999; Chan et al., 2015), might play a pivotal role. It would have to be determined if peripheral mononuclear phagocytes significantly contribute to BDNF in the DG, either by secretion or by stimulating BDNF expression in GC (Heinrich et al., 2011), and if a compensatory mechanism, substituting BDNF, can be hold responsible for the unexpected GC dispersion seen in CCR2-KO mice. Moreover, considering the importance of BDNF for LTP, BDNF from immune cells might contribute directly to early seizure-mediated plasticity. Parkhurst et al. (2013), for example, showed that a selective depletion of BDNF in microglia caused reduced levels of the NMDA receptor subunit NR2B and VGluT1, less improvement in rotarod performance after training, and impaired memory in the auditory fear-conditioning task, whereas it was not affecting performance in the novel object-recognition task nor synapse density in motor cortex or CA1. However, selective depletion of BDNF receptors in PV-positive interneurons lead to a desynchronization and reduced firing of PV-positive neurons and, in CA1, to decreased network activity in the gamma-frequency band (30-80 Hz) (Zheng et al., 2011). Interestingly, in our AD transgenic mouse model, the frequency of sIPSCs and the relative gamma power (90-100 Hz) in CA1 pyramidal cells were reduced after KA application, but not at baseline (Figure 3, study II). Balkowiec and Katz (2002) found that BDNF secretion in hippocampal neurons was significantly more effective upon 100 Hz tetanus and theta-burst

stimulation than upon lower-frequency stimulation. Although we found no difference in BDNF mRNA expression in naive ArcticAβ mice compared to wildtype littermates at 3 and 9 months of age (data not shown), it might be interesting to examine other members of the BDNF-TrkB signaling cascade.

Transient expression of anticonvulsants

Besides network alterations discussed in the former paragraph, which may or may not require time to establish an epileptic focus, several lines of evidence suggest that anticonvulsive agents transiently suppress epileptic discharges. In our second study, we report a transient bilateral increase in NPY in mossy fibers and GC within 24 hours after IHK-induced SE in wildtype mice, followed by a gradual decline over the next couple of days (Figure 7). Many studies found that NPY has anticonvulsive properties and alleviates seizures by either injecting it locally (Woldbye et al., 1996; Baraban et al., 1997; Woldbye et al., 1997; Vezzani et al., 1999a), or overexpressing NPY and its receptors, Y2R or Y5R (Richichi et al., 2004; Sorensen et al., 2009; Woldbye et al., 2010; Gotzsche et al., 2012). Interestingly, ArcticAβ mice showed a reduced seizure-induced activation of NPY signaling during the latent phase (Figure 7, study II), coinciding with the early onset of SRS. However, to test whether reduced levels of NPY are responsible for curtailment of the latent period, we would need to restore levels in ArcticAβ mice back to wildtypes, or vice versa. Another indirect approach to test the assumption would be to assess NPY signaling in other animal models with early onset of SRS. For example, in RAG1-KO mice lacking T- and B-cells, which show SRS already 2-3 days after IHK injection (Zattoni et al., 2011), it would be interesting to test if we see similar changes in NPY-IR as detected in ArcticAβ mice.

Animal models with an early onset of SRS or reduced dispersion

In two animal models of TLE, the pilocarpine and the IHK model, the contribution of T cells was emphasized for the development of SRS. By blocking the seizure-induced elevation of vascular cell adhesion molecules and thereby T cell extravasation, acute seizures and the development of SRS in response to pilocarpine-induced SE were markedly prevented (Fabene et al., 2008). The same study further reported that neutrophil depletion had the same effect and blood-brain barrier leakage could be prevented, suggesting a direct contribution of plasma proteins and K+ ions to

SRS (Marchi et al., 2007; Marchi et al., 2010). More relevant for a direct comparison to epileptogenesis was a study made with RAG1-KO mice injected with IHK. As assessed in Nissl-stained sections, neurodegeneration was exacerbated in CA1 and CA3 of mice lacking B and T cells, including a loss of dentate GC that start to become evident between 14 and 28 days (Deprez et al., 2011; Zattoni et al., 2011). The increased neurodegeneration was attributed to the occurrence of Gr-1-positive neutrophils in the ipsilateral hippocampus (except in the dentate gyrus), while GC survival and dispersion was supposed to be dependent on the presence of protective, infiltrating macrophages in the ipsilateral dentate gyrus (except in the hilus), an assumption that we could not confirm in mice lacking CCR2+ peripheral mononuclear phagocytes (Figure 6, study I). ArcticAβ mice did not show any difference in the overall neurodegeneration (e.g. CA1 or CA3), the GC survival or dispersion, and the number of infiltrating peripheral mononuclear phagocytes 21 days after injection (Figure 1, study II). Further, the number of infiltrating T cells was comparable between ArcticAβ mice and wildtype controls as revealed by a qualitative assessment of the number and distribution of CD3+ cells at 1, 3, 6, 14 dpi (data not shown). The lack of any abnormalities in the IHK-associated immune response in ArcticAβ mice (mentioned above) and RAG1-KO mice (Deprez et al., 2011; Zattoni et al., 2011; Bernhard, 2016) within the first few days when SRS start to occur suggests that the immune response (at least the elements described here) is not directly responsible for or capable of generating SRS. However, it cannot be excluded that the immune system contributes to the development of seizures by either promoting a pro-epileptic environment (e.g. lowering the seizure threshold) or by influencing anticonvulsive signaling.

In our second study, we cleared soluble Aβ species by injecting an Aβ-specific antibody or control immunoglobulin G (IgG) intracerebroventricularly in ArcticAβ mice (Figure 10). Interestingly, GC dispersion was not observed 18 days after injection in these two groups, albeit no GC loss was evident. Notably, the absence of T and B lymphocytes in RAG1-KO mice is associated with a lack of IgG production, revealed by the missing "background" in their IHC-stained tissue sections (Zattoni et al., 2011). Further, RAG1-KO mice showed a loss of GC at 28 dpi and peripheral mononuclear phagocytes were missing in mice with a severe degeneration at 14 dpi. Therefore, IgG might affect either granule cell dispersion directly, for example through BDNF-TrkB signaling (Duveau et al., 2011), or both peripheral and resident microglia in the DG by suppressing any putative contribution to GC dispersion and repressing the phagocytic activity, respectively. It will be interesting to determine how intraventricular IgG affects the innate immune response, in particular the infiltration of peripheral mononuclear phagocytes.

Discrepancies in AD mouse models: disease-stage dependent?

Aberrant network activity was reported in several animal models of AD. While 5-weeks-old Tg2576 mice (hAPPSwe) already showed a predisposition for interictal spikes during REM sleep, they only showed at an age of 7 months spontaneous seizures similar to 3- to 7-months-old J20 mice (hAPPSwe/Ind) or 3- to 4.5-months-old APdE9 mice (hAPPSwe/PS1dE9) (Palop et al., 2007; Minkeviciene et al., 2008; Kam et al., 2016). Although we assessed hippocampal LFP in untreated 3-months-old ArcticAβ mice only in three 3 hour recording sessions (data not shown), we did not find any spontaneous seizures in our mice. However, in the studies mentioned above, SRS were detected at an age in which most of these mice already suffer from a more advanced Aβ pathology, reporting already deposition of amyloid plaques (Mucke et al., 2000; Kawarabayashi et al., 2001; Minkeviciene et al., 2008). There are findings in some of these AD mouse models showing an early hyperexcitability and increased susceptibility to pro-convulsives (Roberson et al., 2007; Kam et al., 2016). While many studies related early hyperreactivity and neuronal network dysfunction to the presence of soluble or intraneuronal Aβ species (Billings et al., 2005; Busche et al., 2012), others attributed its effect to the Aβ composition (increased Aβ42/Aβ40 ratio) or its fibrillary or oligomeric conformation (Mucke et al., 2000; Minkeviciene et al., 2008). In line with these reports, we were able to alleviate the pro-epileptogenic phenotype in ArcticAβ mice by clearing Aβ species with an anti-Aβ-antibody prior to IHK-induced SE (Figure 11, study II). Several studies in J20 mice, showing SRS already at an age between 3 and 7 months, report an ectopic expression of NPY in mossy fibers, NPY axons in the molecular layer and a degeneration of CB-interneurons in the hippocampus (Palop et al., 2007; Roberson et al., 2007; Roberson et al., 2011). Similar observations were made by us in wildtype mice after SE-induced epileptogenesis (Figure 8, study II) and others (Vezzani et al., 1999a; Bouilleret et al., 2000b). Interestingly, the subset of APdE9 mice that did not show spontaneous seizures between 3 and 4.5 months did not exhibit any changes in NPY expression (Minkeviciene et al., 2008). We also did not find any changes in NPY-IR of 3-months-old ArcticAβ mice. However, as reported by Palop et al. (2007), we found an increased YR2 expression and first signs of NPY-IR in mossy fibers of our ArcticAβ mice (Figure 10, *study II*). Together with a body of literature highlighting anticonvulsive properties of NPY signaling (compare above), it suggests that these changes in NPY-IR reflect a compensatory mechanism to the earlier occurrence of SRS in APPJ20 mice. More recently, it was found that the same mice featured a reduced expression of the interneuron-specific and PV-cell-predominant voltage-gated sodium channel subunit Nav1.1 (also called SCN1A) in both hippocampus and parietal cortex, which through specific restorage

of Nav1.1in GABAergic neurons (primarily in PV interneurons) increased inhibitory synaptic currents and gamma activity, reducing thereby epileptiform discharges in the parietal cortex of hAPPJ20 mice (Verret et al., 2012). However, we did not detect any difference in hippocampal SCN1A expression in neither 3- nor 9-months-old ArcticAβ mice, suggesting that the reduced synaptic strength (Figure 2, *study II*), frequency of inhibitory activity and the trend towards a reduced gamma power (Figure 3, *study II*) are most likely affected by another mechanism.

Conclusion

In the IHK model of TLE, we aimed to reveal critical factors for the development of epilepsy by assessing morphological and functional alterations during early epileptogenesis. Several lines of evidence suggest that neuroinflammation following SE affects the formation of an epileptic focus and thereby the generation of seizures, through cytokines release and phagocytic activity. However, attempts to affect the innate immune response by prenatal priming with polyI:C, a lack of NLRP3 inflammasomes or peripheral mononuclear CCR2+ phagocytes had no effect on the development of IHK pathology. Although we cannot definitely exclude (e.g. strain-dependent) compensatory mechanisms interfering genetically or during development, our findings suggest that the innate immune response contributes indirectly to epileptogenesis and is not crucial for the chronic occurrence of SRS in this model of TLE. In line with this assumption, increased excitability and early onset of SRS in an AD mouse model after IHK-induced SE do not correlate with differences in neuroinflammation, which rather indicates that cellular hyperexcitability and impaired anticonvulsive NPY signaling are potentially affected early in AD pathology by Aβ oligomers. Although it still remains unknown what molecular or cellular alterations are ultimately responsible for the generation of seizures and the presence of a latent period, our preliminary data indicates that COI upon early aberrant activity of principal cells, but not PV interneurons, affects seizure pathology in the long-term. Hence, we assume that plasticity during epileptogenesis is activity-driven. Although epileptic discharges have an effect on many processes (compare e.g. kindling), we hope to untangle at least secondary sequelae of SE from mechanisms crucial for SRS generation by taking advantage of this reciprocal dependency between aberrant network activity of focal origin and activity-dependent structural plasticity in the epileptic focus. However, in particular concerning the controversy raised around the latent period, future studies will not be able to avoid research into endogenous seizure alleviating mechanisms (e.g. NPY signaling), which might camouflage the latent period as an

indispensability of the network to reorganize. Expanded effort into a holistic understanding of the etiology and pathogenesis of TLE might not only uncover new potential drug targets, but will also help to define treatment-specific therapeutic windows for more accurate intervention, thereby minimizing interference with normal brain activity.

REFERENCES

Alzheimer A, Stelzmann RA, Schnitzlein HN, Murtagh FR (1995) An English translation of Alzheimer's 1907 paper, "Uber eine eigenartige Erkankung der Hirnrinde". Clin Anat 8:429-431.

Amatniek JC, Hauser WA, DelCastillo-Castaneda C, Jacobs DM, Marder K, Bell K, Albert M, Brandt J, Stern Y (2006) Incidence and predictors of seizures in patients with Alzheimer's disease. Epilepsia 47:867-872.

Andersson PB, Perry VH, Gordon S (1991) The kinetics and morphological characteristics of the macrophage-microglial response to kainic acid-induced neuronal degeneration. Neuroscience 42:201-214.

Andre V, Marescaux C, Nehlig A, Fritschy JM (2001) Alterations of hippocampal GAbaergic system contribute to development of spontaneous recurrent seizures in the rat lithium-pilocarpine model of temporal lobe epilepsy. Hippocampus 11:452-468.

Antonucci F, Bozzi Y, Caleo M (2009) Intrahippocampal infusion of botulinum neurotoxin E (BoNT/E) reduces spontaneous recurrent seizures in a mouse model of mesial temporal lobe epilepsy. Epilepsia 50:963-966.

Antonucci F, Di Garbo A, Novelli E, Manno I, Sartucci F, Bozzi Y, Caleo M (2008) Botulinum neurotoxin E (BoNT/E) reduces CA1 neuron loss and granule cell dispersion, with no effects on chronic seizures, in a mouse model of temporal lobe epilepsy. Exp Neurol 210:388-401.

Antonucci F, Alpar A, Kacza J, Caleo M, Verderio C, Giani A, Martens H, Chaudhry FA, Allegra M, Grosche J, Michalski D, Erck C, Hoffmann A, Harkany T, Matteoli M, Hartig W (2012) Cracking down on inhibition: selective removal of GABAergic interneurons from hippocampal networks. J Neurosci 32:1989-2001.

Arabadzisz D, Antal K, Parpan F, Emri Z, Fritschy JM (2005) Epileptogenesis and chronic seizures in a mouse model of temporal lobe epilepsy are associated with distinct EEG patterns and selective neurochemical alterations in the contralateral hippocampus. Exp Neurol 194:76-90.

Arisi GM, Foresti ML, Katki K, Shapiro LA (2015) Increased CCL2, CCL3, CCL5, and IL-1β cytokine concentration in piriform cortex, hippocampus, and neocortex after pilocarpine-induced seizures. J Neuroinflammation 12:129.

Armstrong C, Krook-Magnuson E, Soltesz I (2012) Neurogliaform and Ivy Cells: A Major Family of nNOS Expressing GABAergic Neurons. Front Neural Circuits 6:23.

Armstrong C, Krook-Magnuson E, Oijala M, Soltesz I (2013) Closed-loop optogenetic intervention in mice. Nat Protoc 8:1475-1493.

Auvin S, Shin D, Mazarati A, Nakagawa J, Miyamoto J, Sankar R (2007) Inflammation exacerbates seizure-induced injury in the immature brain. Epilepsia 48 Suppl 5:27-34.

Balkowiec A, Katz DM (2002) Cellular mechanisms regulating activity-dependent release of native brain-derived neurotrophic factor from hippocampal neurons. J Neurosci 22:10399-10407.

Balosso S, Ravizza T, Aronica E, Vezzani A (2013) The dual role of TNF-α and its receptors in seizures. Exp Neurol 247:267-271.

Baraban SC (2002) Antiepileptic actions of neuropeptide Y in the mouse hippocampus require Y5 receptors. Epilepsia 43:9-13.

Baraban SC, Hollopeter G, Erickson JC, Schwartzkroin PA, Palmiter RD (1997) Knock-out mice reveal a critical antiepileptic role for neuropeptide Y. J Neurosci 17:8927-8936.

Beal MF, Mazurek MF, Chattha GK, Svendsen CN, Bird ED, Martin JB (1986) Neuropeptide Y immunoreactivity is reduced in cerebral cortex in Alzheimer's disease. Ann Neurol 20:282-288.

Ben-Ari Y, Crepel V, Represa A (2008) Seizures beget seizures in temporal lobe epilepsies: the boomerang effects of newly formed aberrant kainatergic synapses. Epilepsy Curr 8:68-72.

Benilova I, Karran E, De Strooper B (2012a) The toxic Aβ oligomer and Alzheimer's disease: an emperor in need of clothes. Nat Neurosci 15:349-357.

Benilova I, Karran E, De Strooper B (2012b) The toxic Abeta oligomer and Alzheimer's disease: an emperor in need of clothes. Nat Neurosci 15:349-357.

Benson MJ, Manzanero S, Borges K (2015) Complex alterations in microglial M1/M2 markers during the development of epilepsy in two mouse models. Epilepsia 56:895-905.

Bernhard FU (2016) Mechanisms of epileptogenesis in an immune-deficient mouse model of temporal lobe epilepsy.

Billings LM, Oddo S, Green KN, McGaugh JL, LaFerla FM (2005) Intraneuronal Abeta causes the onset of early Alzheimer's disease-related cognitive deficits in transgenic mice. Neuron 45:675-688.

Bing G, Wilson B, Hudson P, Jin L, Feng Z, Zhang W, Bing R, Hong JS (1997) A single dose of kainic acid elevates the levels of enkephalins and activator protein-1 transcription factors in the hippocampus for up to 1 year. Proc Natl Acad Sci U S A 94:9422-9427.

Blasco-Ibanez JM, Freund TF (1995) Synaptic input of horizontal interneurons in stratum oriens of the hippocampal CA1 subfield: structural basis of feed-back activation. Eur J Neurosci 7:2170-2180.

Boring L, Gosling J, Chensue SW, Kunkel SL, Farese RV, Broxmeyer HE, Charo IF (1997) Impaired monocyte migration and reduced type 1 (Th1) cytokine responses in C-C chemokine receptor 2 knockout mice. J Clin Invest 100:2552-2561.

Born HA, Kim JY, Savjani RR, Das P, Dabaghian YA, Guo Q, Yoo JW, Schuler DR, Cirrito JR, Zheng H, Golde TE, Noebels JL, Jankowsky JL (2014) Genetic suppression of transgenic APP rescues Hypersynchronous network activity in a mouse model of Alzeimer's disease. J Neurosci 34:3826-3840.

Bouilleret V, Schwaller B, Schurmans S, Celio MR, Fritschy JM (2000a) Neurodegenerative and morphogenic changes in a mouse model of temporal lobe epilepsy do not depend on the expression of the calcium-binding proteins parvalbumin, calbindin, or calretinin. Neuroscience 97:47-58.

Bouilleret V, Loup F, Kiener T, Marescaux C, Fritschy JM (2000b) Early loss of interneurons and delayed subunit-specific changes in GABA(A)-receptor expression in a mouse model of mesial temporal lobe epilepsy. Hippocampus 10:305-324.

Bouilleret V, Ridoux V, Depaulis A, Marescaux C, Nehlig A, Le Gal La Salle G (1999) Recurrent seizures and hippocampal sclerosis following intrahippocampal kainate injection in adult mice: electroencephalography, histopathology and synaptic reorganization similar to mesial temporal lobe epilepsy. Neuroscience 89:717-729.

Browne TR, Holmes GL (2001) Epilepsy. N Engl J Med 344:1145-1151.

Buckmaster PS (2012) Mossy Fiber Sprouting in the Dentate Gyrus. In: Jasper's Basic Mechanisms of the Epilepsies, 4th Edition (Noebels JL, Avoli M, Rogawski MA, Olsen RW, Delgado-Escueta AV, eds). Bethesda (MD).

Buckmaster PS, Lew FH (2011) Rapamycin suppresses mossy fiber sprouting but not seizure frequency in a mouse model of temporal lobe epilepsy. J Neurosci 31:2337-2347.

Buckmaster PS, Abrams E, Wen X (2017) Seizure frequency correlates with loss of dentate gyrus GABAergic neurons in a mouse model of temporal lobe epilepsy. J Comp Neurol 525:2592-2610.

Burré J, Sharma M, Tsetsenis T, Buchman V, Etherton MR, Südhof TC (2010) Alpha-synuclein promotes SNARE-complex assembly in vivo and in vitro. Science 329:1663-1667.

Busche MA, Chen X, Henning HA, Reichwald J, Staufenbiel M, Sakmann B, Konnerth A (2012) Critical role of soluble amyloid-beta for early hippocampal hyperactivity in a mouse model of Alzheimer's disease. Proc Natl Acad Sci U S A 109:8740-8745.

Buzsaki G (1989) Two-stage model of memory trace formation: a role for "noisy" brain states. Neuroscience 31:551-570.

Buzsaki G (1996) The hippocampo-neocortical dialogue. Cereb Cortex 6:81-92.

Buzsaki G, Horvath Z, Urioste R, Hetke J, Wise K (1992) High-frequency network oscillation in the hippocampus. Science 256:1025-1027.

Buzsaki G, Buhl DL, Harris KD, Csicsvari J, Czeh B, Morozov A (2003) Hippocampal network patterns of activity in the mouse. Neuroscience 116:201-211.

Buzsáki G (2015) Hippocampal sharp wave-ripple: A cognitive biomarker for episodic memory and planning. Hippocampus 25:1073-1188.

Carr MF, Karlsson MP, Frank LM (2012) Transient slow gamma synchrony underlies hippocampal memory replay. Neuron 75:700-713.

Castellani RJ, Rolston RK, Smith MA (2010) Alzheimer disease. Dis Mon 56:484-546.

Cavalheiro EA, Leite JP, Bortolotto ZA, Turski WA, Ikonomidou C, Turski L (1991) Long-term effects of pilocarpine in rats: structural damage of the brain triggers kindling and spontaneous recurrent seizures. Epilepsia 32:778-782.

Chan A, Yan J, Csurhes P, Greer J, McCombe P (2015) Circulating brain derived neurotrophic factor (BDNF) and frequency of BDNF positive T cells in peripheral blood in human ischemic stroke: Effect on outcome. J Neuroimmunol 286:42-47.

Chin J, Palop JJ, Yu GQ, Kojima N, Masliah E, Mucke L (2004) Fyn kinase modulates synaptotoxicity, but not aberrant sprouting, in human amyloid precursor protein transgenic mice. J Neurosci 24:4692-4697.

Cho KO, Lybrand ZR, Ito N, Brulet R, Tafacory F, Zhang L, Good L, Ure K, Kernie SG, Birnbaum SG, Scharfman HE, Eisch AJ, Hsieh J (2015) Aberrant hippocampal neurogenesis contributes to epilepsy and associated cognitive decline. Nat Commun 6:6606.

Choi J, Nordli DR, Jr., Alden TD, DiPatri A, Jr., Laux L, Kelley K, Rosenow J, Schuele SU, Rajaram V, Koh S (2009) Cellular injury and neuroinflammation in children with chronic intractable epilepsy. J Neuroinflammation 6:38.

Colgin LL (2012) Slow gamma takes the reins in replay. Neuron 75:549-550.

Colgin LL (2016) Rhythms of the hippocampal network. Nat Rev Neurosci 17:239-249.

Colonna M, Wang Y (2016) TREM2 variants: new keys to decipher Alzheimer disease pathogenesis. Nat Rev Neurosci 17:201-207.

Corder EH, Saunders AM, Strittmatter WJ, Schmechel DE, Gaskell PC, Small GW, Roses AD, Haines JL, Pericak-Vance MA (1993) Gene dose of apolipoprotein E type 4 allele and the risk of Alzheimer's disease in late onset families. Science 261:921-923.

Cossart R, Dinocourt C, Hirsch JC, Merchan-Perez A, De Felipe J, Ben-Ari Y, Esclapez M, Bernard C (2001) Dendritic but not somatic GABAergic inhibition is decreased in experimental epilepsy. Nat Neurosci 4:52-62.

Crespel A, Coubes P, Rousset MC, Brana C, Rougier A, Rondouin G, Bockaert J, Baldy-Moulinier M, Lerner-Natoli M (2002) Inflammatory reactions in human medial temporal lobe epilepsy with hippocampal sclerosis. Brain Res 952:159-169.

Curia G, Longo D, Biagini G, Jones RS, Avoli M (2008) The pilocarpine model of temporal lobe epilepsy. J Neurosci Methods 172:143-157.

Davletov B, Bajohrs M, Binz T (2005) Beyond BOTOX: advantages and limitations of individual botulinum neurotoxins. Trends Neurosci 28:446-452.

De Simoni MG, Perego C, Ravizza T, Moneta D, Conti M, Marchesi F, De Luigi A, Garattini S, Vezzani A (2000) Inflammatory cytokines and related genes are induced in the rat hippocampus by limbic status epilepticus. Eur J Neurosci 12:2623-2633.

De Strooper B, Karran E (2016) The Cellular Phase of Alzheimer's Disease. Cell 164:603-615.

Denes A, Coutts G, Lénárt N, Cruickshank SM, Pelegrin P, Skinner J, Rothwell N, Allan SM, Brough D (2015) AIM2 and NLRC4 inflammasomes contribute with ASC to acute brain injury independently of NLRP3. Proc Natl Acad Sci U S A 112:4050-4055.

Deprez F, Zattoni M, Mura ML, Frei K, Fritschy JM (2011) Adoptive transfer of T lymphocytes in immunodeficient mice influences epileptogenesis and neurodegeneration in a model of temporal lobe epilepsy. Neurobiol Dis 44:174-184.

Deprez F, Vogt F, Floriou-Servou A, Lafourcade C, Rudolph U, Tyagarajan S, Fritschy J (2016) Partial inactivation of $GABA_A$ receptors containing the α5 subunit affects the development of adult-born dentate gyrus granule cells. Eur J Neurosci doi: 10.1111/ejn.13329. [Epub ahead of print].

Diez M, Danner S, Frey P, Sommer B, Staufenbiel M, Wiederhold KH, Hokfelt T (2003) Neuropeptide alterations in the hippocampal formation and cortex of transgenic mice overexpressing beta-amyloid precursor protein (APP) with the Swedish double mutation (APP23). Neurobiol Dis 14:579-594.

Dinocourt C, Petanjek Z, Freund TF, Ben-Ari Y, Esclapez M (2003) Loss of interneurons innervating pyramidal cell dendrites and axon initial segments in the CA1 region of the hippocampus following pilocarpine-induced seizures. J Comp Neurol 459:407-425.

Donoho DL, Johnstone JM (1994) Ideal spatial adaptation by wavelet shrinkage. Biometrika 81:425-455.

Drexel M, Romanov RA, Wood J, Weger S, Heilbronn R, Wulff P, Tasan RO, Harkany T, Sperk G (2017) Selective silencing of hippocampal parvalbumin interneurons induces development of recurrent spontaneous limbic seizures in mice. J Neurosci.

Dugladze T, Vida I, Tort AB, Gross A, Otahal J, Heinemann U, Kopell NJ, Gloveli T (2007) Impaired hippocampal rhythmogenesis in a mouse model of mesial temporal lobe epilepsy. Proc Natl Acad Sci U S A 104:17530-17535.

Duveau V, Madhusudan A, Caleo M, Knuesel I, Fritschy JM (2011) Impaired reelin processing and secretion by Cajal-Retzius cells contributes to granule cell dispersion in a mouse model of temporal lobe epilepsy. Hippocampus 21:935-944.

El Bahh B, Balosso S, Hamilton T, Herzog H, Beck-Sickinger A, Sperk G, Gehlert D, Vezzani A, Colmers W (2005) The anti-epileptic actions of neuropeptide Y in the hippocampus are mediated by Y2 and not Y5 receptors.

. Eur J Neurosci 22:1417-1430.

Engel J (1998) Etiology as a risk factor for medically refractory epilepsy: a case for early surgical intervention. Neurology 51:1243-1244.

Engel J, Bragin A, Staba R, Mody I (2009) High-frequency oscillations: what is normal and what is not? Epilepsia 50:598-604.

Engel J, Jr. (1996a) Clinical evidence for the progressive nature of epilepsy. Epilepsy Res Suppl 12:9-20.

Engel J, Jr. (1996b) Introduction to temporal lobe epilepsy. Epilepsy Res 26:141-150.

England MJ, Liverman CT, Schultz AM, Strawbridge LM (2012) Epilepsy across the spectrum: promoting health and understanding. A summary of the Institute of Medicine report. Epilepsy Behav 25:266-276.

Erickson JC, Clegg KE, Palmiter RD (1996) Sensitivity to leptin and susceptibility to seizures of mice lacking neuropeptide Y. Nature 381:415-421.

Ewell LA, Liang L, Armstrong C, Soltesz I, Leutgeb S, Leutgeb JK (2015) Brain State Is a Major Factor in Preseizure Hippocampal Network Activity and Influences Success of Seizure Intervention. J Neurosci 35:15635-15648.

Fabene PF, Bramanti P, Constantin G (2010) The emerging role for chemokines in epilepsy. J Neuroimmunol 224:22-27.

Fabene PF et al. (2008) A role for leukocyte-endothelial adhesion mechanisms in epilepsy. Nat Med 14:1377-1383.

Fisher RS, Alger BE (1984) Electrophysiological mechanisms of kainic acid-induced epileptiform activity in the rat hippocampal slice. J Neurosci 4:1312-1323.

Fisher RS, Cross JH, French JA, Higurashi N, Hirsch E, Jansen FE, Lagae L, Moshe SL, Peltola J, Roulet Perez E, Scheffer IE, Zuberi SM (2017a) Operational classification of seizure types by the International League Against Epilepsy: Position Paper of the ILAE Commission for Classification and Terminology. Epilepsia 58:522-530.

Fisher RS, Cross JH, D'Souza C, French JA, Haut SR, Higurashi N, Hirsch E, Jansen FE, Lagae L, Moshe SL, Peltola J, Roulet Perez E, Scheffer IE, Schulze-Bonhage A, Somerville E, Sperling M, Yacubian EM, Zuberi SM (2017b) Instruction manual for the ILAE 2017 operational classification of seizure types. Epilepsia 58:531-542.

Fisher RS, Acevedo C, Arzimanoglou A, Bogacz A, Cross JH, Elger CE, Engel J, Jr., Forsgren L, French JA, Glynn M, Hesdorffer DC, Lee BI, Mathern GW, Moshe SL, Perucca E, Scheffer IE, Tomson T, Watanabe M, Wiebe S (2014) ILAE official report: a practical clinical definition of epilepsy. Epilepsia 55:475-482.

Fuentealba P, Begum R, Capogna M, Jinno S, Marton LF, Csicsvari J, Thomson A, Somogyi P, Klausberger T (2008) Ivy cells: a population of nitric-oxide-producing, slow-spiking GABAergic neurons and their involvement in hippocampal network activity. Neuron 57:917-929.

Fuentealba P, Klausberger T, Karayannis T, Suen WY, Huck J, Tomioka R, Rockland K, Capogna M, Studer M, Morales M, Somogyi P (2010) Expression of COUP-TFII nuclear receptor in restricted GABAergic neuronal populations in the adult rat hippocampus. J Neurosci 30:1595-1609.

Gage FH (2000) Mammalian neural stem cells. Science 287:1433-1438.

Galic MA, Riazi K, Pittman QJ (2012) Cytokines and brain excitability. Front Neuroendocrinol 33:116-125.

Galic MA, Riazi K, Heida JG, Mouihate A, Fournier NM, Spencer SJ, Kalynchuk LE, Teskey GC, Pittman QJ (2008) Postnatal inflammation increases seizure susceptibility in adult rats. J Neurosci 28:6904-6913.

Gan L, Qiao S, Lan X, Chi L, Luo C, Lien L, Yan Liu Q, Liu R (2008) Neurogenic responses to amyloid-beta plaques in the brain of Alzheimer's disease-like transgenic (pPDGF-APPSw,Ind) mice. Neurobiol Dis 29:71-80.

Gao B, Fritschy JM (1994) Selective allocation of GABAA receptors containing the alpha 1 subunit to neurochemically distinct subpopulations of rat hippocampal interneurons. Eur J Neurosci 6:837-853.

Gardoni F, Boraso M, Zianni E, Corsini E, Galli CL, Cattabeni F, Marinovich M, Di Luca M, Viviani B (2011a) Distribution of interleukin-1 receptor complex at the synaptic membrane driven by interleukin-1β and NMDA stimulation. J Neuroinflammation 8:14.

Gardoni F, Boraso M, Zianni E, Corsini E, Galli CL, Cattabeni F, Marinovich M, Di Luca M, Viviani B (2011b) Distribution of interleukin-1 receptor complex at the synaptic membrane driven by interleukin-1beta and NMDA stimulation. J Neuroinflammation 8:14.

Ge S, Goh EL, Sailor KA, Kitabatake Y, Ming GL, Song H (2006) GABA regulates synaptic integration of newly generated neurons in the adult brain. Nature 439:589-593.

Gfeller TP (2015a) Mechanisms of epileptogenesis in AD transgenic mice. Master thesis.

Gfeller TP (2015b) Mechanisms of epileptogenesis in AD transgenic mice. In: University of Zurich.

Gillespie AK, Jones EA, Lin YH, Karlsson MP, Kay K, Yoon SY, Tong LM, Nova P, Carr JS, Frank LM, Huang Y (2016) Apolipoprotein E4 Causes Age-Dependent Disruption of Slow Gamma Oscillations during Hippocampal Sharp-Wave Ripples. Neuron 90:740-751.

Glass CK, Saijo K, Winner B, Marchetto MC, Gage FH (2010) Mechanisms underlying inflammation in neurodegeneration. Cell 140:918-934.

Gorter JA, van Vliet EA, Aronica E, Lopes da Silva FH (2001) Progression of spontaneous seizures after status epilepticus is associated with mossy fibre sprouting and extensive bilateral loss of hilar parvalbumin and somatostatin-immunoreactive neurons. Eur J Neurosci 13:657-669.

Gotzsche CR, Nikitidou L, Sorensen AT, Olesen MV, Sorensen G, Christiansen SH, Angehagen M, Woldbye DP, Kokaia M (2012) Combined gene overexpression of neuropeptide Y and its receptor Y5 in the hippocampus suppresses seizures. Neurobiol Dis 45:288-296.

Gouder N, Scheurer L, Fritschy JM, Boison D (2004) Overexpression of adenosine kinase in epileptic hippocampus contributes to epileptogenesis. J Neurosci 24:692-701.

Gruber B, Greber S, Rupp E, Sperk G (1994) Differential NPY mRNA expression in granule cells and interneurons of the rat dentate gyrus after kainic acid injection. Hippocampus 4:474-482.

Gu B, Huang YZ, He XP, Joshi RB, Jang W, McNamara JO (2015) A Peptide Uncoupling BDNF Receptor TrkB from Phospholipase Cgamma1 Prevents Epilepsy Induced by Status Epilepticus. Neuron 88:484-491.

Guo H, Callaway JB, Ting JP (2015) Inflammasomes: mechanism of action, role in disease, and therapeutics. Nat Med 21:677-687.

Guo H, Castro PA, Palmiter RD, Baraban SC (2002) Y5 receptors mediate neuropeptide Y actions at excitatory synapses in area CA3 of the mouse hippocampus. J Neurophysiol 87:558-566.

Hardy JA, Higgins GA (1992) Alzheimer's disease: the amyloid cascade hypothesis. Science 256:184-185.

Harward SC, Hedrick NG, Hall CE, Parra-Bueno P, Milner TA, Pan E, Laviv T, Hempstead BL, Yasuda R, McNamara JO (2016) Autocrine BDNF-TrkB signalling within a single dendritic spine. Nature 538:99-103.

Hattiangady B, Rao MS, Shetty AK (2004) Chronic temporal lobe epilepsy is associated with severely declined dentate neurogenesis in the adult hippocampus. Neurobiol Dis 17:473-490.

Hedrick NG, Harward SC, Hall CE, Murakoshi H, McNamara JO, Yasuda R (2016) Rho GTPase complementation underlies BDNF-dependent homo- and heterosynaptic plasticity. Nature 538:104-108.

Heinrich C, Lahteinen S, Suzuki F, Anne-Marie L, Huber S, Haussler U, Haas C, Larmet Y, Castren E, Depaulis A (2011) Increase in BDNF-mediated TrkB signaling promotes epileptogenesis in a mouse model of mesial temporal lobe epilepsy. Neurobiol Dis 42:35-47.

Heinrich C, Nitta N, Flubacher A, Müller M, Fahrner A, Kirsch M, Freiman T, Suzuki F, Depaulis A, Frotscher M, Haas CA (2006) Reelin deficiency and displacement of mature neurons, but not neurogenesis, underlie the formation of granule cell dispersion in the epileptic hippocampus. J Neurosci 26:4701-4713.

Hellier JL, Dudek FE (1999) Spontaneous motor seizures of rats with kainate-induced epilepsy: effect of time of day and activity state. Epilepsy Res 35:47-57.

Hellier JL, Patrylo PR, Buckmaster PS, Dudek FE (1998) Recurrent spontaneous motor seizures after repeated low-dose systemic treatment with kainate: assessment of a rat model of temporal lobe epilepsy. Epilepsy Res 31:73-84.

Heneka MT, Kummer MP, Latz E (2014) Innate immune activation in neurodegenerative disease. Nat Rev Immunol 14:463-477.

Heneka MT, Golenbock DT, Latz E (2015) Innate immunity in Alzheimer's disease. Nat Immunol 16:229-236.

Heneka MT, Kummer MP, Stutz A, Delekate A, Schwartz S, Vieira-Saecker A, Griep A, Axt D, Remus A, Tzeng TC, Gelpi E, Halle A, Korte M, Latz E, Golenbock DT (2013) NLRP3 is activated in Alzheimer's disease and contributes to pathology in APP/PS1 mice. Nature 493:674-678.

Heppner FL, Ransohoff RM, Becher B (2015) Immune attack: the role of inflammation in Alzheimer disease. Nat Rev Neurosci 16:358-372.

Hesdorffer DC, Hauser WA, Annegers JF, Kokmen E, Rocca WA (1996) Dementia and adult-onset unprovoked seizures. Neurology 46:727-730.

Horvath A, Szucs A, Barcs G, Kamondi A (2017) Sleep EEG Detects Epileptiform Activity in Alzheimer's Disease with High Sensitivity. J Alzheimers Dis 56:1175-1183.

Houser CR (1990) Granule cell dispersion in the dentate gyrus of humans with temporal lobe epilepsy. Brain Res 535:195-204.

Huang Y, Mucke L (2012) Alzheimer mechanisms and therapeutic strategies. Cell 148:1204-1222.

Ito M, Echizenya N, Nemoto D, Kase M (2009) A case series of epilepsy-derived memory impairment resembling Alzheimer disease. Alzheimer Dis Assoc Disord 23:406-409.

Iyengar SS, LaFrancois JJ, Friedman D, Drew LJ, Denny CA, Burghardt NS, Wu MV, Hsieh J, Hen R, Scharfman HE (2015) Suppression of adult neurogenesis increases the acute effects of kainic acid. Exp Neurol 264:135-149.

Jessberger S, Romer B, Babu H, Kempermann G (2005) Seizures induce proliferation and dispersion of doublecortin-positive hippocampal progenitor cells. Exp Neurol 196:342-351.

Jiang W, Bell CW, Pisetsky DS (2007) The relationship between apoptosis and high-mobility group protein 1 release from murine macrophages stimulated with lipopolysaccharide or polyinosinic-polycytidylic acid. J Immunol 178:6495-6503.

Jin K, Galvan V, Xie L, Mao XO, Gorostiza OF, Bredesen DE, Greenberg DA (2004) Enhanced neurogenesis in Alzheimer's disease transgenic (PDGF-APPSw,Ind) mice. Proc Natl Acad Sci U S A 101:13363-13367.

Jinde S, Zsiros V, Jiang Z, Nakao K, Pickel J, Kohno K, Belforte JE, Nakazawa K (2012) Hilar mossy cell degeneration causes transient dentate granule cell hyperexcitability and impaired pattern separation. Neuron 76:1189-1200.

Jokeit H, Ebner A (1999) Long term effects of refractory temporal lobe epilepsy on cognitive abilities: a cross sectional study. J Neurol Neurosurg Psychiatry 67:44-50.

Jonsson T et al. (2012) A mutation in APP protects against Alzheimer's disease and age-related cognitive decline. Nature 488:96-99.

Kam K, Duffy AM, Moretto J, LaFrancois JJ, Scharfman HE (2016) Interictal spikes during sleep are an early defect in the Tg2576 mouse model of beta-amyloid neuropathology. Sci Rep 6:20119.

Karran E, Mercken M, De Strooper B (2011) The amyloid cascade hypothesis for Alzheimer's disease: an appraisal for the development of therapeutics. Nat Rev Drug Discov 10:698-712.

Kawarabayashi T, Younkin LH, Saido TC, Shoji M, Ashe KH, Younkin SG (2001) Age-dependent changes in brain, CSF, and plasma amyloid (beta) protein in the Tg2576 transgenic mouse model of Alzheimer's disease. J Neurosci 21:372-381.

Kerschensteiner M, Gallmeier E, Behrens L, Leal VV, Misgeld T, Klinkert WE, Kolbeck R, Hoppe E, Oropeza-Wekerle RL, Bartke I, Stadelmann C, Lassmann H, Wekerle H, Hohlfeld R (1999) Activated human T cells, B cells, and monocytes produce brain-derived neurotrophic factor in vitro and in inflammatory brain lesions: a neuroprotective role of inflammation? J Exp Med 189:865-870.

Khoshkhoo S, Vogt D, Sohal VS (2017) Dynamic, Cell-Type-Specific Roles for GABAergic Interneurons in a Mouse Model of Optogenetically Inducible Seizures. Neuron 93:291-298.

Kim S, Jeon BS, Heo C, Im PS, Ahn TB, Seo JH, Kim HS, Park CH, Choi SH, Cho SH, Lee WJ, Suh YH (2004) Alpha-synuclein induces apoptosis by altered expression in human peripheral lymphocyte in Parkinson's disease. FASEB J 18:1615-1617.

Kirschman LT, Borysiewicz E, Fil D, Konat GW (2011) Peripheral immune challenge with dsRNA enhances kainic acid-induced status epilepticus. Metab Brain Dis 26:91-93.

Knobloch M, Konietzko U, Krebs DC, Nitsch RM (2007) Intracellular Abeta and cognitive deficits precede beta-amyloid deposition in transgenic arcAbeta mice. Neurobiol Aging 28:1297-1306.

Knoferle J, Yoon SY, Walker D, Leung L, Gillespie AK, Tong LM, Bien-Ly N, Huang Y (2014) Apolipoprotein E4 produced in GABAergic interneurons causes learning and memory deficits in mice. J Neurosci 34:14069-14078.

Knuesel I, Chicha L, Britschgi M, Schobel SA, Bodmer M, Hellings JA, Toovey S, Prinssen EP (2014) Maternal immune activation and abnormal brain development across CNS disorders. Nat Rev Neurol 10:643-660.

Knuesel I, Nyffeler M, Mormède C, Muhia M, Meyer U, Pietropaolo S, Yee BK, Pryce CR, LaFerla FM, Marighetto A, Feldon J (2009) Age-related accumulation of Reelin in amyloid-like deposits. Neurobiol Aging 30:697-716.

Kralic JE, Ledergerber DA, Fritschy JM (2005) Disruption of the neurogenic potential of the dentate gyrus in a mouse model of temporal lobe epilepsy with focal seizures. Eur J Neurosci 22:1916-1927.

Krook-Magnuson E, Armstrong C, Oijala M, Soltesz I (2013) On-demand optogenetic control of spontaneous seizures in temporal lobe epilepsy. Nat Commun 4:1376.

Krook-Magnuson E, Luu L, Lee SH, Varga C, Soltesz I (2011) Ivy and neurogliaform interneurons are a major target of mu-opioid receptor modulation. J Neurosci 31:14861-14870.

Krook-Magnuson E, Szabo GG, Armstrong C, Oijala M, Soltesz I (2014) Cerebellar Directed Optogenetic Intervention Inhibits Spontaneous Hippocampal Seizures in a Mouse Model of Temporal Lobe Epilepsy. eNeuro 1.

Krook-Magnuson E, Armstrong C, Bui A, Lew S, Oijala M, Soltesz I (2015) In vivo evaluation of the dentate gate theory in epilepsy. J Physiol 593:2379-2388.

Krstic D, Knuesel I (2013) Deciphering the mechanism underlying late-onset Alzheimer disease. Nat Rev Neurol 9:25-34.

Krstic D, Madhusudan A, Doehner J, Vogel P, Notter T, Imhof C, Manalastas A, Hilfiker M, Pfister S, Schwerdel C, Riether C, Meyer U, Knuesel I (2012) Systemic immune challenges trigger and drive Alzheimer-like neuropathology in mice. J Neuroinflammation 9:151.

Kudrimoti HS, Barnes CA, McNaughton BL (1999) Reactivation of hippocampal cell assemblies: effects of behavioral state, experience, and EEG dynamics. J Neurosci 19:4090-4101.

Kwon MS, Seo YJ, Choi SM, Won MH, Lee JK, Park SH, Jung JS, Sim YB, Suh HW (2010) The time-dependent effect of lipopolysaccharide on kainic acid-induced neuronal death in hippocampal CA3 region: possible involvement of cytokines via glucocorticoid. Neuroscience 165:1333-1344.

Lam AD, Deck G, Goldman A, Eskandar EN, Noebels J, Cole AJ (2017) Silent hippocampal seizures and spikes identified by foramen ovale electrodes in Alzheimer's disease. Nat Med.

Lamkanfi M, Kanneganti TD (2010) Nlrp3: an immune sensor of cellular stress and infection. Int J Biochem Cell Biol 42:792-795.

Landi MS, Kreider JW, Lang CM, Bullock LP (1982) Effects of shipping on the immune function in mice. Am J Vet Res 43:1654-1657.

Lapray D, Lasztoczi B, Lagler M, Viney TJ, Katona L, Valenti O, Hartwich K, Borhegyi Z, Somogyi P, Klausberger T (2012) Behavior-dependent specialization of identified hippocampal interneurons. Nat Neurosci 15:1265-1271.

Lasarge CL, Danzer SC (2014) Mechanisms regulating neuronal excitability and seizure development following mTOR pathway hyperactivation. Front Mol Neurosci 7:18.

Latz E, Xiao TS, Stutz A (2013) Activation and regulation of the inflammasomes. Nat Rev Immunol 13:397-411.

Ledergerber D, Fritschy JM, Kralic JE (2006) Impairment of dentate gyrus neuronal progenitor cell differentiation in a mouse model of temporal lobe epilepsy. Exp Neurol 199:130-142.

Ledri LN, Melin E, Christiansen SH, Gotzsche CR, Cifra A, Woldbye DP, Kokaia M (2016) Translational approach for gene therapy in epilepsy: Model system and unilateral overexpression of neuropeptide Y and Y2 receptors. Neurobiol Dis 86:52-61.

Lee AK, Wilson MA (2002) Memory of sequential experience in the hippocampus during slow wave sleep. Neuron 36:1183-1194.

Lee SH, Kim BJ, Kim YB, Chung PW, Moon HS, Suh BC, Yoon WT, Jin DK, Park YS, Lee YT, Park KY (2012) IL-1β induction and IL-6 suppression are associated with aggravated neuronal damage in a lipopolysaccharide-pretreated kainic acid-induced rat pup seizure model. Neuroimmunomodulation 19:319-325.

Liimatainen S, Lehtimäki K, Kai L, Palmio J, Johanna P, Alapirtti T, Tiina A, Peltola J, Jukka P (2013) Immunological perspectives of temporal lobe seizures. J Neuroimmunol 263:1-7.

Liu G, Gu B, He XP, Joshi RB, Wackerle HD, Rodriguiz RM, Wetsel WC, McNamara JO (2013) Transient inhibition of TrkB kinase after status epilepticus prevents development of temporal lobe epilepsy. Neuron 79:31-38.

Lothman EW, Collins RC (1981) Kainic acid induced limbic seizures: metabolic, behavioral, electroencephalographic and neuropathological correlates. Brain Res 218:299-318.

Lu B, Nakamura T, Inouye K, Li J, Tang Y, Lundback P, Valdes-Ferrer SI, Olofsson PS, Kalb T, Roth J, Zou Y, Erlandsson-Harris H, Yang H, Ting JP, Wang H, Andersson U, Antoine DJ, Chavan SS, Hotamisligil GS, Tracey KJ (2012) Novel role of PKR in inflammasome activation and HMGB1 release. Nature 488:670-674.

Lurton D, Cavalheiro EA (1997) Neuropeptide-Y immunoreactivity in the pilocarpine model of temporal lobe epilepsy. Exp Brain Res 116:186-190.

Mack M, Cihak J, Simonis C, Luckow B, Proudfoot AE, Plachý J, Brühl H, Frink M, Anders HJ, Vielhauer V, Pfirstinger J, Stangassinger M, Schlöndorff D (2001) Expression and characterization of the chemokine receptors CCR2 and CCR5 in mice. J Immunol 166:4697-4704.

Madisen L et al. (2012) A toolbox of Cre-dependent optogenetic transgenic mice for light-induced activation and silencing. Nat Neurosci 15:793-802.

Mahar I, Albuquerque MS, Mondragon-Rodriguez S, Cavanagh C, Davoli MA, Chabot JG, Williams S, Mechawar N, Quirion R, Krantic S (2016) Phenotypic Alterations in Hippocampal NPY- and PV-Expressing Interneurons in a Presymptomatic Transgenic Mouse Model of Alzheimer's Disease. Front Aging Neurosci 8:327.

Makiura Y, Suzuki F, Chevalier E, Onteniente B (1999) Excitatory granule cells of the dentate gyrus exhibit a double inhibitory neurochemical content after intrahippocampal administration of kainate in adult mice. Exp Neurol 159:73-83.

Maloney JA, Bainbridge T, Gustafson A, Zhang S, Kyauk R, Steiner P, van der Brug M, Liu Y, Ernst JA, Watts RJ, Atwal JK (2014) Molecular mechanisms of Alzheimer disease protection by the A673T allele of amyloid precursor protein. J Biol Chem 289:30990-31000.

Manley NC, Bertrand AA, Kinney KS, Hing TC, Sapolsky RM (2007) Characterization of monocyte chemoattractant protein-1 expression following a kainate model of status epilepticus. Brain Res 1182:138-143.

Marchi N, Oby E, Batra A, Uva L, De Curtis M, Hernandez N, Van Boxel-Dezaire A, Najm I, Janigro D (2007) In vivo and in vitro effects of pilocarpine: relevance to ictogenesis. Epilepsia 48:1934-1946.

Marchi N, Teng Q, Ghosh C, Fan Q, Nguyen MT, Desai NK, Bawa H, Rasmussen P, Masaryk TK, Janigro D (2010) Blood-brain barrier damage, but not parenchymal white blood cells, is a hallmark of seizure activity. Brain Res 1353:176-186.

Marksteiner J, Ortler M, Bellmann R, Sperk G (1990) Neuropeptide Y biosynthesis is markedly induced in mossy fibers during temporal lobe epilepsy of the rat. Neurosci Lett 112:143-148.

Maroso M, Balosso S, Ravizza T, Liu J, Aronica E, Iyer AM, Rossetti C, Molteni M, Casalgrandi M, Manfredi AA, Bianchi ME, Vezzani A (2010) Toll-like receptor 4 and high-mobility group box-1 are involved in ictogenesis and can be targeted to reduce seizures. Nat Med 16:413-419.

Marsh DJ, Baraban SC, Hollopeter G, Palmiter RD (1999) Role of the Y5 neuropeptide Y receptor in limbic seizures. Proc Natl Acad Sci U S A 96:13518-13523.

McClelland S, Brennan GP, Dube C, Rajpara S, Iyer S, Richichi C, Bernard C, Baram TZ (2014) The transcription factor NRSF contributes to epileptogenesis by selective repression of a subset of target genes. Elife 3:e01267.

McKhann G, Drachman D, Folstein M, Katzman R, Price D, Stadlan EM (1984) Clinical diagnosis of Alzheimer's disease: report of the NINCDS-ADRDA Work Group under the auspices of Department of Health and Human Services Task Force on Alzheimer's Disease. Neurology 34:939-944.

McNamara JO, Scharfman HE (2012) Temporal Lobe Epilepsy and the BDNF Receptor, TrkB. In: Jasper's Basic Mechanisms of the Epilepsies, 4th Edition (Noebels JL, Avoli M, Rogawski MA, Olsen RW, Delgado-Escueta AV, eds). Bethesda (MD).

Meijering E, Jacob M, Sarria JC, Steiner P, Hirling H, Unser M (2004) Design and validation of a tool for neurite tracing and analysis in fluorescence microscopy images. Cytometry A 58:167-176.

Meilandt WJ, Yu GQ, Chin J, Roberson ED, Palop JJ, Wu T, Scearce-Levie K, Mucke L (2008) Enkephalin elevations contribute to neuronal and behavioral impairments in a transgenic mouse model of Alzheimer's disease. J Neurosci 28:5007-5017.

Meyer U (2014) Prenatal poly(i:C) exposure and other developmental immune activation models in rodent systems. Biol Psychiatry 75:307-315.

Meyer U, Nyffeler M, Engler A, Urwyler A, Schedlowski M, Knuesel I, Yee BK, Feldon J (2006) The time of prenatal immune challenge determines the specificity of inflammation-mediated brain and behavioral pathology. J Neurosci 26:4752-4762.

Meyer-Luehmann M, Spires-Jones TL, Prada C, Garcia-Alloza M, de Calignon A, Rozkalne A, Koenigsknecht-Talboo J, Holtzman DM, Bacskai BJ, Hyman BT (2008) Rapid appearance and local toxicity of amyloid-beta plaques in a mouse model of Alzheimer's disease. Nature 451:720-724.

Michalovicz LT, Konat GW (2014) Peripherally restricted acute phase response to a viral mimic alters hippocampal gene expression. Metab Brain Dis 29:75-86.

Milstein AD, Bloss EB, Apostolides PF, Vaidya SP, Dilly GA, Zemelman BV, Magee JC (2015) Inhibitory Gating of Input Comparison in the CA1 Microcircuit. Neuron 87:1274-1289.

Ming GL, Song H (2011) Adult neurogenesis in the mammalian brain: significant answers and significant questions. Neuron 70:687-702.

Minkeviciene R, Ihalainen J, Malm T, Matilainen O, Keksa-Goldsteine V, Goldsteins G, Iivonen H, Leguit N, Glennon J, Koistinaho J, Banerjee P, Tanila H (2008) Age-related decrease in stimulated glutamate release and vesicular glutamate transporters in APP/PS1 transgenic and wild-type mice. J Neurochem 105:584-594.

Minthon L, Edvinsson L, Ekman R, Gustafson L (1990) Neuropeptide levels in Alzheimer's disease and dementia with frontotemporal degeneration. J Neural Transm Suppl 30:57-67.

Mucke L, Masliah E, Yu GQ, Mallory M, Rockenstein EM, Tatsuno G, Hu K, Kholodenko D, Johnson-Wood K, McConlogue L (2000) High-level neuronal expression of abeta 1-42 in wild-type human amyloid protein precursor transgenic mice: synaptotoxicity without plaque formation. J Neurosci 20:4050-4058.

Müller MC, Osswald M, Tinnes S, Häussler U, Jacobi A, Förster E, Frotscher M, Haas CA (2009) Exogenous reelin prevents granule cell dispersion in experimental epilepsy. Exp Neurol 216:390-397.

Nadler JV, Perry BW, Cotman CW (1978) Intraventricular kainic acid preferentially destroys hippocampal pyramidal cells. Nature 271:676-677.

Nissinen J, Halonen T, Koivisto E, Pitkanen A (2000) A new model of chronic temporal lobe epilepsy induced by electrical stimulation of the amygdala in rat. Epilepsy Res 38:177-205.

Noè FM, Sørensen AT, Kokaia M, Vezzani A (2012) Gene therapy of focal onset epilepsy using adeno-associated virus vector-mediated overexpression of neuropeptide Y. In: Jasper's Basic Mechanisms of the Epilepsies, 4 Edition (Nobbles JL, Avoli M, Rogawski MA, Olsen RW, Delgado-Escueta AV, eds): Oxford University Press.

Notter T, Panzanelli P, Pfister S, Mircsof D, Fritschy JM (2014) A protocol for concurrent high-quality immunohistochemical and biochemical analyses in adult mouse central nervous system. Eur J Neurosci 39:165-175.

Notter TF (2015) Evaluation of three risk factors for sporadic Alzheimer's disease in human and in immune-challenged wild type mice. Zürich.

Okazaki MM, Evenson DA, Nadler JV (1995) Hippocampal mossy fiber sprouting and synapse formation after status epilepticus in rats: visualization after retrograde transport of biocytin. J Comp Neurol 352:515-534.

Olah S, Fule M, Komlosi G, Varga C, Baldi R, Barzo P, Tamas G (2009) Regulation of cortical microcircuits by unitary GABA-mediated volume transmission. Nature 461:1278-1281.

Oppenheim AV, Schafer RW, Buck JR (1999) Discrete-time signal processing (2nd ed.): Prentice-Hall, Inc.

Palchykova S, Winsky-Sommerer R, Shen HY, Boison D, Gerling A, Tobler I (2010) Manipulation of adenosine kinase affects sleep regulation in mice. J Neurosci 30:13157-13165.

Palop JJ, Mucke L (2009) Epilepsy and cognitive impairments in Alzheimer disease. Arch Neurol 66:435-440.

Palop JJ, Mucke L (2010) Amyloid-beta-induced neuronal dysfunction in Alzheimer's disease: from synapses toward neural networks. Nat Neurosci 13:812-818.

Palop JJ, Mucke L (2016) Network abnormalities and interneuron dysfunction in Alzheimer disease. Nat Rev Neurosci 17:777-792.

Palop JJ, Jones B, Kekonius L, Chin J, Yu GQ, Raber J, Masliah E, Mucke L (2003) Neuronal depletion of calcium-dependent proteins in the dentate gyrus is tightly linked to Alzheimer's disease-related cognitive deficits. Proc Natl Acad Sci U S A 100:9572-9577.

Palop JJ, Chin J, Roberson ED, Wang J, Thwin MT, Bien-Ly N, Yoo J, Ho KO, Yu GQ, Kreitzer A, Finkbeiner S, Noebels JL, Mucke L (2007) Aberrant excitatory neuronal activity and compensatory remodeling of inhibitory hippocampal circuits in mouse models of Alzheimer's disease. Neuron 55:697-711.

Parent JM, Yu TW, Leibowitz RT, Geschwind DH, Sloviter RS, Lowenstein DH (1997) Dentate granule cell neurogenesis is increased by seizures and contributes to aberrant network reorganization in the adult rat hippocampus. J Neurosci 17:3727-3738.

Parkhurst CN, Yang G, Ninan I, Savas JN, Yates JR, 3rd, Lafaille JJ, Hempstead BL, Littman DR, Gan WB (2013) Microglia promote learning-dependent synapse formation through brain-derived neurotrophic factor. Cell 155:1596-1609.

Paz JT, Davidson TJ, Frechette ES, Delord B, Parada I, Peng K, Deisseroth K, Huguenard JR (2013) Closed-loop optogenetic control of thalamus as a tool for interrupting seizures after cortical injury. Nat Neurosci 16:64-70.

Peng Z, Zhang N, Wei W, Huang CS, Cetina Y, Otis TS, Houser CR (2013) A reorganized GABAergic circuit in a model of epilepsy: evidence from optogenetic labeling and stimulation of somatostatin interneurons. J Neurosci 33:14392-14405.

Perry VH, Holmes C (2014) Microglial priming in neurodegenerative disease. Nat Rev Neurol 10:217-224.

Petrovic MM, Viana da Silva S, Clement JP, Vyklicky L, Mulle C, Gonzalez-Gonzalez IM, Henley JM (2017) Metabotropic action of postsynaptic kainate receptors triggers hippocampal long-term potentiation. Nat Neurosci 20:529-539.

Pineda E, Shin D, You SJ, Auvin S, Sankar R, Mazarati A (2013) Maternal immune activation promotes hippocampal kindling epileptogenesis in mice. Ann Neurol 74:11-19.

Pinel JP, Rovner LI (1978) Experimental epileptogenesis: kindling-induced epilepsy in rats. Exp Neurol 58:190-202.

Pitkänen A, Sutula TP (2002) Is epilepsy a progressive disorder? Prospects for new therapeutic approaches in temporal-lobe epilepsy. Lancet Neurol 1:173-181.

Price CJ, Cauli B, Kovacs ER, Kulik A, Lambolez B, Shigemoto R, Capogna M (2005) Neurogliaform neurons form a novel inhibitory network in the hippocampal CA1 area. J Neurosci 25:6775-6786.

Quiroga RQ, Nadasdy Z, Ben-Shaul Y (2004) Unsupervised spike detection and sorting with wavelets and superparamagnetic clustering. Neural Comput 16:1661-1687.

Qulu L, Daniels WM, Mabandla MV (2012) Exposure to prenatal stress enhances the development of seizures in young rats. Metab Brain Dis 27:399-404.

Racine RJ (1972) Modification of seizure activity by electrical stimulation. II. Motor seizure. Electroencephalogr Clin Neurophysiol 32:281-294.

Ramos B, Baglietto-Vargas D, del Rio JC, Moreno-Gonzalez I, Santa-Maria C, Jimenez S, Caballero C, Lopez-Tellez JF, Khan ZU, Ruano D, Gutierrez A, Vitorica J (2006) Early neuropathology of somatostatin/NPY GABAergic cells in the hippocampus of a PS1xAPP transgenic model of Alzheimer's disease. Neurobiol Aging 27:1658-1672.

Ravizza T, Noé F, Zardoni D, Vaghi V, Sifringer M, Vezzani A (2008a) Interleukin Converting Enzyme inhibition impairs kindling epileptogenesis in rats by blocking astrocytic IL-1beta production. Neurobiol Dis 31:327-333.

Ravizza T, Gagliardi B, Noé F, Boer K, Aronica E, Vezzani A (2008b) Innate and adaptive immunity during epileptogenesis and spontaneous seizures: evidence from experimental models and human temporal lobe epilepsy. Neurobiol Dis 29:142-160.

Reich CG, Karson MA, Karnup SV, Jones LM, Alger BE (2005) Regulation of IPSP theta rhythm by muscarinic receptors and endocannabinoids in hippocampus. J Neurophysiol 94:4290-4299.

Riazi K, Galic MA, Pittman QJ (2010) Contributions of peripheral inflammation to seizure susceptibility: cytokines and brain excitability. Epilepsy Res 89:34-42.

Riban V, Bouilleret V, Pham-Le BT, Fritschy JM, Marescaux C, Depaulis A (2002a) Evolution of hippocampal epileptic activity during the development of hippocampal sclerosis in a mouse model of temporal lobe epilepsy. Neuroscience 112:101-111.

Riban V, Bouilleret V, Pham-Lê BT, Fritschy JM, Marescaux C, Depaulis A (2002b) Evolution of hippocampal epileptic activity during the development of hippocampal sclerosis in a mouse model of temporal lobe epilepsy. Neuroscience 112:101-111.

Richichi C, Lin EJ, Stefanin D, Colella D, Ravizza T, Grignaschi G, Veglianese P, Sperk G, During MJ, Vezzani A (2004) Anticonvulsant and antiepileptogenic effects mediated by adeno-associated virus vector neuropeptide Y expression in the rat hippocampus. J Neurosci 24:3051-3059.

Roberson ED, Scearce-Levie K, Palop JJ, Yan F, Cheng IH, Wu T, Gerstein H, Yu GQ, Mucke L (2007) Reducing endogenous tau ameliorates amyloid beta-induced deficits in an Alzheimer's disease mouse model. Science 316:750-754.

Roberson ED, Halabisky B, Yoo JW, Yao J, Chin J, Yan F, Wu T, Hamto P, Devidze N, Yu GQ, Palop JJ, Noebels JL, Mucke L (2011) Amyloid-beta/Fyn-induced synaptic, network, and cognitive impairments depend on tau levels in multiple mouse models of Alzheimer's disease. J Neurosci 31:700-711.

Saijo K, Glass CK (2011) Microglial cell origin and phenotypes in health and disease. Nat Rev Immunol 11:775-787.

Sanchez PE, Zhu L, Verret L, Vossel KA, Orr AG, Cirrito JR, Devidze N, Ho K, Yu GQ, Palop JJ, Mucke L (2012) Levetiracetam suppresses neuronal network dysfunction and reverses synaptic and cognitive deficits in an Alzheimer's disease model. Proc Natl Acad Sci U S A 109:E2895-2903.

Santello M, Bezzi P, Volterra A (2011) TNFalpha controls glutamatergic gliotransmission in the hippocampal dentate gyrus. Neuron 69:988-1001.

Scarmeas N, Honig LS, Choi H, Cantero J, Brandt J, Blacker D, Albert M, Amatniek JC, Marder K, Bell K, Hauser WA, Stern Y (2009) Seizures in Alzheimer disease: who, when, and how common? Arch Neurol 66:992-997.

Scharfman HE, Goodman JH, Sollas AL, Croll SD (2002) Spontaneous limbic seizures after intrahippocampal infusion of brain-derived neurotrophic factor. Exp Neurol 174:201-214.

Scheibel ME, Crandall PH, Scheibel AB (1974) The hippocampal-dentate complex in temporal lobe epilepsy. A Golgi study. Epilepsia 15:55-80.

Schmid LC, Mittag M, Poll S, Steffen J, Wagner J, Geis HR, Schwarz I, Schmidt B, Schwarz MK, Remy S, Fuhrmann M (2016) Dysfunction of Somatostatin-Positive Interneurons Associated with Memory Deficits in an Alzheimer's Disease Model. Neuron 92:114-125.

Sedigh-Sarvestani M, Thuku GI, Sunderam S, Parkar A, Weinstein SL, Schiff SJ, Gluckman BJ (2014) Rapid eye movement sleep and hippocampal theta oscillations precede seizure onset in the tetanus toxin model of temporal lobe epilepsy. J Neurosci 34:1105-1114.

Semah F, Picot MC, Adam C, Broglin D, Arzimanoglou A, Bazin B, Cavalcanti D, Baulac M (1998) Is the underlying cause of epilepsy a major prognostic factor for recurrence? Neurology 51:1256-1262.

Serrano-Pozo A, Frosch MP, Masliah E, Hyman BT (2011) Neuropathological alterations in Alzheimer disease. Cold Spring Harb Perspect Med 1:a006189.

Sheffield ME, Best TK, Mensh BD, Kath WL, Spruston N (2011) Slow integration leads to persistent action potential firing in distal axons of coupled interneurons. Nat Neurosci 14:200-207.

Sholl DA (1953) Dendritic organization in the neurons of the visual and motor cortices of the cat. J Anat 87:387-406.

Sierra A, Martin-Suarez S, Valcarcel-Martin R, Pascual-Brazo J, Aelvoet SA, Abiega O, Deudero JJ, Brewster AL, Bernales I, Anderson AE, Baekelandt V, Maletic-Savatic M, Encinas JM (2015) Neuronal hyperactivity accelerates depletion of neural stem cells and impairs hippocampal neurogenesis. Cell Stem Cell 16:488-503.

Sinforiani E, Manni R, Bernasconi L, Banchieri LM, Zucchella C (2003) Memory disturbances and temporal lobe epilepsy simulating Alzheimer's disease: a case report. Funct Neurol 18:39-41.

Skaggs WE, McNaughton BL (1996) Replay of neuronal firing sequences in rat hippocampus during sleep following spatial experience. Science 271:1870-1873.

Song J, Zhong C, Bonaguidi MA, Sun GJ, Hsu D, Gu Y, Meletis K, Huang ZJ, Ge S, Enikolopov G, Deisseroth K, Luscher B, Christian KM, Ming GL, Song H (2012) Neuronal circuitry mechanism regulating adult quiescent neural stem-cell fate decision. Nature 489:150-154.

Sorensen G, Wegener G, Hasselstrom J, Hansen TV, Wortwein G, Fink-Jensen A, Woldbye DP (2009) Neuropeptide Y infusion into the shell region of the rat nucleus accumbens increases extracellular levels of dopamine. Neuroreport 20:1023-1026.

Spampanato J, Dudek FE (2017) Targeted Interneuron Ablation in the Mouse Hippocampus Can Cause Spontaneous Recurrent Seizures. eneuro.

Sperk G, Marksteiner J, Gruber B, Bellmann R, Mahata M, Ortler M (1992) Functional changes in neuropeptide Y- and somatostatin-containing neurons induced by limbic seizures in the rat. Neuroscience 50:831-846.

Stefanits H, Wesseling C, Kovacs GG (2014) Loss of Calbindin immunoreactivity in the dentate gyrus distinguishes Alzheimer's disease from other neurodegenerative dementias. Neurosci Lett 566:137-141.

Sudduth T, Greenstein A, Wilcock D (2013) Intracranial injection of Gammagard, a human IVIg, modulates the inflammatory response of the brain and lowers Aβ in APP/PS1 mice along a different time course than anti-Aβ antibodies. J Neurosci 33:9684-9692.

Sun B, Halabisky B, Zhou Y, Palop JJ, Yu G, Mucke L, Gan L (2009) Imbalance between GABAergic and Glutamatergic Transmission Impairs Adult Neurogenesis in an Animal Model of Alzheimer's Disease. Cell Stem Cell 5:624-633.

Sutula T, He XX, Cavazos J, Scott G (1988) Synaptic reorganization in the hippocampus induced by abnormal functional activity. Science 239:1147-1150.

Suzuki F, Junier MP, Guilhem D, Sørensen JC, Onteniente B (1995a) Morphogenetic effect of kainate on adult hippocampal neurons associated with a prolonged expression of brain-derived neurotrophic factor. Neuroscience 64:665-674.

Suzuki F, Junier MP, Guilhem D, Sorensen JC, Onteniente B (1995b) Morphogenetic effect of kainate on adult hippocampal neurons associated with a prolonged expression of brain-derived neurotrophic factor. Neuroscience 64:665-674.

Suzuki N, Tang CS, Bekkers JM (2014) Persistent barrage firing in cortical interneurons can be induced in vivo and may be important for the suppression of epileptiform activity. Front Cell Neurosci 8:76.

Tacke F, Alvarez D, Kaplan TJ, Jakubzick C, Spanbroek R, Llodra J, Garin A, Liu J, Mack M, van Rooijen N, Lira SA, Habenicht AJ, Randolph GJ (2007) Monocyte subsets differentially employ CCR2, CCR5, and CX3CR1 to accumulate within atherosclerotic plaques. J Clin Invest 117:185-194.

Tian DS, Peng J, Murugan M, Feng L, Liu JL, Eyo UB, Zhou LJ, Mogilevsky R, Wang W, Wu LJ (2017) Chemokine CCL2-CCR2 signaling induces neuronal cell death via STAT3 activation and IL-1beta production after status epilepticus. J Neurosci.

Tonder N, Kragh J, Finsen BR, Bolwig TG, Zimmer J (1994) Kindling induces transient changes in neuronal expression of somatostatin, neuropeptide Y, and calbindin in adult rat hippocampus and fascia dentata. Epilepsia 35:1299-1308.

Trevelyan AJ, Sussillo D, Yuste R (2007) Feedforward inhibition contributes to the control of epileptiform propagation speed. J Neurosci 27:3383-3387.

Tricoire L, Pelkey KA, Daw MI, Sousa VH, Miyoshi G, Jeffries B, Cauli B, Fishell G, McBain CJ (2010) Common origins of hippocampal Ivy and nitric oxide synthase expressing neurogliaform cells. J Neurosci 30:2165-2176.

Trinka E, Cock H, Hesdorffer D, Rossetti AO, Scheffer IE, Shinnar S, Shorvon S, Lowenstein DH (2015) A definition and classification of status epilepticus--Report of the ILAE Task Force on Classification of Status Epilepticus. Epilepsia 56:1515-1523.

Tsien JZ, Chen DF, Gerber D, Tom C, Mercer EH, Anderson DJ, Mayford M, Kandel ER, Tonegawa S (1996) Subregion- and cell type-restricted gene knockout in mouse brain. Cell 87:1317-1326.

Tu B, Timofeeva O, Jiao Y, Nadler JV (2005) Spontaneous release of neuropeptide Y tonically inhibits recurrent mossy fiber synaptic transmission in epileptic brain. J Neurosci 25:1718-1729.

Tuli JS, Smith JA, Morton DB (1995) Stress measurements in mice after transportation. Lab Anim 29:132-138.

Turski WA, Czuczwar SJ, Kleinrok Z, Turski L (1983) Cholinomimetics produce seizures and brain damage in rats. Experientia 39:1408-1411.

Van Rooijen N, Sanders A (1994) Liposome mediated depletion of macrophages: mechanism of action, preparation of liposomes and applications. J Immunol Methods 174:83-93.

Varella PP, Santiago JF, Carrete H, Jr., Higa EM, Yacubian EM, Centeno RS, Caboclo LO, Castro Neto EF, Canzian M, Amado D, Cavalheiro EA, Naffah-Mazzacoratti Mda G (2011) Relationship between fluid-attenuated inversion-recovery (FLAIR) signal intensity and inflammatory mediator's levels in the hippocampus of patients with temporal lobe epilepsy and mesial temporal sclerosis. Arq Neuropsiquiatr 69:91-99.

Varvel NH, Neher JJ, Bosch A, Wang W, Ransohoff RM, Miller RJ, Dingledine R (2016) Infiltrating monocytes promote brain inflammation and exacerbate neuronal damage after status epilepticus. Proc Natl Acad Sci U S A 113:E5665-5674.

Verret L, Jankowsky JL, Xu GM, Borchelt DR, Rampon C (2007) Alzheimer's-type amyloidosis in transgenic mice impairs survival of newborn neurons derived from adult hippocampal neurogenesis. J Neurosci 27:6771-6780.

Verret L, Mann EO, Hang GB, Barth AM, Cobos I, Ho K, Devidze N, Masliah E, Kreitzer AC, Mody I, Mucke L, Palop JJ (2012) Inhibitory interneuron deficit links altered network activity and cognitive dysfunction in Alzheimer model. Cell 149:708-721.

Vezzani A, Sperk G (2004) Overexpression of NPY and Y2 receptors in epileptic brain tissue: an endogenous neuroprotective mechanism in temporal lobe epilepsy? Neuropeptides 38:245-252.

Vezzani A, Viviani B (2015) Neuromodulatory properties of inflammatory cytokines and their impact on neuronal excitability. Neuropharmacology 96:70-82.

Vezzani A, Sperk G, Colmers WF (1999a) Neuropeptide Y: emerging evidence for a functional role in seizure modulation. Trends Neurosci 22:25-30.

Vezzani A, French J, Bartfai T, Baram TZ (2011) The role of inflammation in epilepsy. Nat Rev Neurol 7:31-40.

Vezzani A, Conti M, De Luigi A, Ravizza T, Moneta D, Marchesi F, De Simoni MG (1999b) Interleukin-1beta immunoreactivity and microglia are enhanced in the rat hippocampus by focal kainate application: functional evidence for enhancement of electrographic seizures. J Neurosci 19:5054-5065.

Vezzani A, Ravizza T, Moneta D, Conti M, Borroni A, Rizzi M, Samanin R, Maj R (1999c) Brain-derived neurotrophic factor immunoreactivity in the limbic system of rats after acute seizures and during spontaneous convulsions: temporal evolution of changes as compared to neuropeptide Y. Neuroscience 90:1445-1461.

Viviani B, Bartesaghi S, Gardoni F, Vezzani A, Behrens MM, Bartfai T, Binaglia M, Corsini E, Di Luca M, Galli CL, Marinovich M (2003) Interleukin-1beta enhances NMDA receptor-mediated intracellular calcium increase through activation of the Src family of kinases. J Neurosci 23:8692-8700.

Vossel KA, Beagle AJ, Rabinovici GD, Shu H, Lee SE, Naasan G, Hegde M, Cornes SB, Henry ML, Nelson AB, Seeley WW, Geschwind MD, Gorno-Tempini ML, Shih T, Kirsch HE, Garcia PA,

Miller BL, Mucke L (2013) Seizures and epileptiform activity in the early stages of Alzheimer disease. JAMA Neurol 70:1158-1166.

Vossel KA, Ranasinghe KG, Beagle AJ, Mizuiri D, Honma SM, Dowling AF, Darwish SM, Van Berlo V, Barnes DE, Mantle M, Karydas AM, Coppola G, Roberson ED, Miller BL, Garcia PA, Kirsch HE, Mucke L, Nagarajan SS (2016) Incidence and impact of subclinical epileptiform activity in Alzheimer's disease. Ann Neurol 80:858-870.

Voutsinos-Porche B, Koning E, Kaplan H, Ferrandon A, Guenounou M, Nehlig A, Motte J (2004) Temporal patterns of the cerebral inflammatory response in the rat lithium-pilocarpine model of temporal lobe epilepsy. Neurobiol Dis 17:385-402.

Walsh JG, Muruve DA, Power C (2014) Inflammasomes in the CNS. Nat Rev Neurosci 15:84-97.

Wang B, Wang Z, Sun L, Yang L, Li H, Cole AL, Rodriguez-Rivera J, Lu HC, Zheng H (2014) The amyloid precursor protein controls adult hippocampal neurogenesis through GABAergic interneurons. J Neurosci 34:13314-13325.

Wang Y, Cella M, Mallinson K, Ulrich JD, Young KL, Robinette ML, Gilfillan S, Krishnan GM, Sudhakar S, Zinselmeyer BH, Holtzman DM, Cirrito JR, Colonna M (2015) TREM2 lipid sensing sustains the microglial response in an Alzheimer's disease model. Cell 160:1061-1071.

Wang Y, Xu C, Xu Z, Ji C, Liang J, Wang Y, Chen B, Wu X, Gao F, Wang S, Guo Y, Li X, Luo J, Duan S, Chen Z (2017) Depolarized GABAergic Signaling in Subicular Microcircuits Mediates Generalized Seizure in Temporal Lobe Epilepsy. Neuron 95:92-105 e105.

Westmark CJ, Westmark PR, Beard AM, Hildebrandt SM, Malter JS (2008) Seizure susceptibility and mortality in mice that over-express amyloid precursor protein. Int J Clin Exp Pathol 1:157-168.

White AM, Williams PA, Ferraro DJ, Clark S, Kadam SD, Dudek FE, Staley KJ (2006) Efficient unsupervised algorithms for the detection of seizures in continuous EEG recordings from rats after brain injury. J Neurosci Methods 152:255-266.

White JD, Gall CM (1987) Differential regulation of neuropeptide and proto-oncogene mRNA content in the hippocampus following recurrent seizures. Brain Res 427:21-29.

Whittington MA, Traub RD, Kopell N, Ermentrout B, Buhl EH (2000) Inhibition-based rhythms: experimental and mathematical observations on network dynamics. Int J Psychophysiol 38:315-336.

Williams PA, White AM, Clark S, Ferraro DJ, Swiercz W, Staley KJ, Dudek FE (2009) Development of spontaneous recurrent seizures after kainate-induced status epilepticus. J Neurosci 29:2103-2112.

Woldbye DP, Madsen TM, Larsen PJ, Mikkelsen JD, Bolwig TG (1996) Neuropeptide Y inhibits hippocampal seizures and wet dog shakes. Brain Res 737:162-168.

Woldbye DP, Larsen PJ, Mikkelsen JD, Klemp K, Madsen TM, Bolwig TG (1997) Powerful inhibition of kainic acid seizures by neuropeptide Y via Y5-like receptors. Nat Med 3:761-764.

Woldbye DP, Angehagen M, Gotzsche CR, Elbrond-Bek H, Sorensen AT, Christiansen SH, Olesen MV, Nikitidou L, Hansen TV, Kanter-Schlifke I, Kokaia M (2010) Adeno-associated viral vector-induced overexpression of neuropeptide Y Y2 receptors in the hippocampus suppresses seizures. Brain 133:2778-2788.

Wu Y, Wang X, Mo X, Xi Z, Xiao F, Li J, Zhu X, Luan G, Wang Y, Li Y, Zhang J (2008) Expression of monocyte chemoattractant protein-1 in brain tissue of patients with intractable epilepsy. Clin Neuropathol 27:55-63.

Yang S, Liu ZW, Wen L, Qiao HF, Zhou WX, Zhang YX (2005) Interleukin-1beta enhances NMDA receptor-mediated current but inhibits excitatory synaptic transmission. Brain Res 1034:172-179.

Zattoni M, Mura ML, Deprez F, Schwendener RA, Engelhardt B, Frei K, Fritschy JM (2011) Brain infiltration of leukocytes contributes to the pathophysiology of temporal lobe epilepsy. J Neurosci 31:4037-4050.

Zheng K, An JJ, Yang F, Xu W, Xu ZQ, Wu J, Hokfelt TG, Fisahn A, Xu B, Lu B (2011) TrkB signaling in parvalbumin-positive interneurons is critical for gamma-band network synchronization in hippocampus. Proc Natl Acad Sci U S A 108:17201-17206.

ABBREVIATIONS

AAV	Adeno-associated virus
Aβ	amyloid-β
AD	Alzheimer's disease
AICD	APP intracellular domain
AIM2	absent in melanoma 2
ALR	absent in melanoma 2 (AIM2)-like receptors
apoE	apolipoprotein E
APP	amyloid precursor protein
AUC	area under the curve
BACE1	beta-secretase 1
BBB	blood brain barrier
BDNF	brain derived neurotrophic factor
BoNT/E	botulinum neurotoxin E
CA1	cornu ammonis area 1
CA3	cornu ammonis area 3
CB	calbindin
CCL2	chemokine (C-C motif) ligand 2
CCR2	chemokine (C-C motif) receptor type 2
CD68	cluster of differentiation 68
CNS	central nervous system
CR	calretinin
CSF	cerebrospinal fluid
dpi	days post injection
DAB	3,3-diaminobenzidine
DAMPS	damage-associated molecular pattern
DG	dentate gyrus
DREADD	designer receptors exclusively activated by designer drug
dsRNA	double-stranded ribonucleic acid
DT	diphtheria toxin
EC	entorhinal cortex
ENK	enkephalin

FAD	familial Alzheimer's disease
GABA	γ-aminobutyric acid
GD	gestational day
GFAP	glial fibrillary acidic protein
GL	granule layer (of the dentate gyrus)
hAPP	human amyloid precursor protein
HMGB1	high mobility group box 1
HS	hippocampal sclerosis
Iba1	ionized calcium-binding adapter molecule 1
ICAM-1	intercellular adhesion molecule 1
i.c.v.	intracerebroventricular
IgG	Immunoglobulin G
IHC	immunohistochemistry
IL	interleukin
ILAE	International League Against Epilepsy
IFN	interferon
IHK	intrahippocampal kainic acid
i.p.	intraperitoneal
IR	immunoreactivity
i.v.	intravenous
KA	kainic acid
LFP	local field potential
LOAD	late-onset Alzheimer's disease
LPS	lipopolysaccharides
LTD	long-term depression
LTLE	lateral temporal lobe epilepsy
LTP	long-term potentiation
mEPSC	miniature excitatory postsynaptic currents
mIPSC	miniature inhibitory postsynaptic currents
MIP	macrophage inflammatory protein
ML	molecular layer (of the dentate gyrus)
MTLE	medial temporal lobe epilepsy
μOR	Mu opioid receptor
NFT	neurofibrillary tangles

NLR	NOD-like receptors
NLRP	nucleotide-binding domain, leucine-rich repeat containing proteins
NPY	neuropeptide Y
NSC	neural stem cell
O-LM	oriens lacunosum-moleculare
PBS	phosphate-buffered saline
PolyI:C	polyriboinosinic-polyribocytidilic acid
PRR	pattern recognition receptor
PS1	presenilin 1
PSGL-1	P-selectin glycoprotein ligand-1
PV	parvalbumin
pTau	phosphorylated Tau
PTZ	pentylenetetrazol
RAG1	recombination activating gene 1
REM	rapid eye movement
ROI	region of interest
SE	status epilepticus
SEM	standard error of the mean
sEPSC	spontaneous excitatory postsynaptic currents
SGZ	subgranular zone
sIPSC	spontaneous inhibitory postsynaptic currents
SL	stratum lucidum
SLM	stratum lacunosum moleculare
SO	stratum oriens
SOM	somatostatin
SP	stratum pyramidale
SR	stratum radiatum
SRS	spontaneous recurrent seizures
ssf	optical fractionator sampling fraction
SSSE	self-sustained status epilepticus
SVZ	subventricular zone
SWR	sharp-wave ripples
TeLC	tetanus toxin light chain
TLE	temporal lobe epilepsy

TLR	Toll-like receptor
TNF	tumor necrosis factor
TrkB	tropomyosin receptor kinase B
VCAM-1	vascular cell adhesion molecule 1
vEEG	synchronous video and EEG recording

CURRICULUM VITAE

PERSONAL DETAILS

Last name	Gschwind
First name	Tilo
Middle name	Aurelio
Address	Winterthurerstrasse 190, CH-8057 Zurich
Date of Birth	6th of August 1986
Nationality	Swiss

Education

Since 2012	**Ph.D. student** at the University of Zurich; International Program of Neuroscience (ZNZ); Supervision Professor Dr. Jean-Marc Fritschy; Institute of Pharmacology and Toxicology, University of Zurich
2010 – 2012	**Degree: Master of Science UZH in Neuroscience** Preclinical Laboratory for Translational Research into Affective Disorders (PLaTRAD); Clinic for Affective Disorders and General Psychiatry; Psychiatric University Hospital Zurich; Switzerland Field of Master Thesis: Behavioral Neuroscience, Neuromorphology
2006 – 2009	**Degree: Bachelor of Science UZH in Biology** Faculty of Science; University of Zurich, Switzerland;
2002 – 2006	**Degree: Matura** (Major in: Biology and Chemistry); Kantonsschule Baden, Switzerland

PUBLICATIONS

Original Articles

Notter T*, Coughlin JM*, **Gschwind T**, Weber-Stadlbauer U, Wang Y, Kassiou M, Vernon AC, Benke D, Pomper MG, Sawa A, Meyer U (2017): Translational evaluation of translocator protein as a marker of neuroinflammation in schizophrenia. Molecular Psychiatry, Jan 17. doi: 10.1038/mp.2016.248. *shared first authorship

Labouesse MA, Lassalle O, Richetto J, Iafrati J, Weber-Stadlbauer U, Notter T, **Gschwind T**, Pujadas L, Soriano E, Reichelt AC, Labouesse C, Langhans W, Chavis P, Meyer U (2016): Hypervulnerability of the adolescent prefrontal cortex to nutritional stress via reelin deficiency. Molecular Psychiatry, Jul;22(7):961-971. doi: 10.1038/mp.2016.193. Epub 2016 Nov 15.

Pryce CR, Azzinnari D, Sigrist H, **Gschwind T**, Lesch KP, Seifritz E (2012): Establishing a learned-helplessness effect paradigm in C57BL/6 mice: behavioural evidence for emotional, motivational and cognitive effects of aversive uncontrollability per se. Neuropharmacology Jan;62(1):358-72. doi: 10.1016/j.neuropharm.2011.08.012. Epub 2011 Aug 16.

Abstracts for Posters

Gschwind T, Gfeller T, Zaichuk M, Knuesel I, Fritschy JM. "Mechanisms of increased seizure susceptibility in AD-mutant mice" Poster, ZNZ Symposium, Zurich, 11 September, 2015.

Gschwind T. "Mechanisms of increased seizure susceptibility in AD-mutant mice" Session talk, Spring Hippocampal Research Conference, Taormina, Italy, 5-9 June, 2015.

Gschwind T, Zaichuk M, Knuesel I, Fritschy JM. "The contribution of AD-like pathology to limbic seizures in rodents: Relevance of immune-mediated mechanisms" Poster, ZNZ Symposium, Zurich, 11 September, 2014.

Gschwind T, Zaichuk M., Knuesel I, Fritschy JM. "The contribution of AD-like pathology to limbic seizures in rodents: relevance of immune-mediated mechanisms." Poster, 9th FENS Forum, Milan, Italy, 5-9 July 2014

Gschwind T, Zaichuk M., Knuesel I, Fritschy JM. "The contribution of AD-like pathology to limbic seizures in rodents: Relevance of immune-mediated mechanisms". Swiss Society for Neuroscience, SSN Annual Meeting, Bern, Switzerland, January 24-25, 2014

APPENDIX

Declaration of originality

University of Zurich[UZH]

Institute of Pharmacology and Toxicology

Declaration of originality

The signed declaration of originality is a component of every Master's thesis, PhD thesis and any other degree paper undertaken during the course of studies, including the respective electronic versions.

Lecturers may also require a declaration of originality for other written papers compiled for their courses.

I hereby confirm that I am the sole author of the written work here enclosed and that I have compiled it in my own words. Parts excepted are corrections of form and content by the supervisor.

Title of work (in block letters):

Mechanisms of epileptogenesis in a mouse model of temporal lobe epilepsy

Authored by (in block letters):

For papers written by groups the names of all authors are required.

Name(s):	**First name(s):**
Gschwind	Tilo

With my signature I confirm that

- I have committed none of the forms of plagiarism described in the information sheet issued on 30 April 2007 by the Teaching Committee of the University of Zurich (http://www.lehre.uzh.ch/plagiate/20110314_LK_Plagiarism.pdf)
- I have documented all methods, data and processes truthfully.
- I have not manipulated any data.
- I have mentioned all persons who were significant facilitators of the work.

I am aware that the work may be screened electronically for plagiarism.

Place, date	**Signature(s)**
Zürich, 7.8.2017	

For papers written by groups the names of all authors are required. Their signatures collectively guarantee the entire content of the written paper.

Adapted from the Declaration of originality of the ETH Zürich